Equilibrium Melting Temperature Determination of Semicrystalline Polymers through Nonlinear Hoffman-Weeks Extrapolation and Secondary Crystallization of Ethylene/Styrene Copolymers

Jiannong Xu

Dissertation submitted to the Faculty of the
Virginia Polytechnic Institute and State University
in partial fulfillment of the requirement for the degree of

Doctor of Philosophy
in
Chemistry

Dr. Hervé Marand, Chair
Dr. James O. Glanville
Dr. Allan R. Shultz
Dr. Thomas C. Ward
Dr. Garth L. Wilkes

October 21, 1999
Blacksburg, Virginia

Keywords: Equilibrium Melting Temperature, Secondary Crystallization

Equilibrium Melting Temperature Determination of Semicrystalline Polymers through Nonlinear Hoffman-Weeks Extrapolation and Secondary Crystallization of Ethylene/Styrene Copolymers

Jiannong Xu

(**ABSTRACT**)

The applicability of the conventional Hoffman-Weeks (HW) linear extrapolation for the determination of the equilibrium melting temperatures of semicrystalline polymers is critically reviewed. It is shown that the linear extrapolation of observed melting temperatures cannot, in general, provide a reliable estimate of the equilibrium melting temperature. A more rigorous nonlinear HW analysis is proposed in this dissertation, which yields more accurate estimates of the equilibrium melting temperatures for semicrystalline polymers. The proposed nonlinear HW analysis is successfully applied to the cases of isotactic polypropylene and poly(ethylene oxide). The predicted initial lamellar thickness as a function of the crystallization temperature matches well with experimental results and/or literature values. Results based on the nonlinear HW analysis are consistent with those obtained from the analysis of the temperature dependence of the crystal growth rates. The general applicability of the Lauritzen Hoffman (LH) secondary nucleation theory is also addressed for isotactic polypropylene and poly(ethylene oxide). While the LH theory provides an excellent account of the temperature dependence of spherulitic growth rates and ratio of nucleation constants for different regimes, it appears not to yield a meaningful value for the substrate length, L, for poly(ethylene oxide).

In a second project, the effects of structural and topological constraints on the morphology, melting and crystallization behavior of ethylene/styrene copolymers are investigated. During cooling from the melt, the longest ethylene sequences crystallize into lamellae in the primary crystallization process, while the shorter ethylene sequences are suggested to form fringed

micelles in the secondary crystallization process. Kinetic studies indicate that secondary crystallization is characterized by an Avrami exponent of ½ which is consistent with a one dimensional, diffusion controlled growth. The increase in the melting temperature of secondary crystals with crystallization time is tentatively explained by a decrease in the molar conformational entropy of the remaining amorphous fraction as a result of secondary crystallization, although the possible role of an increase of crystal lateral dimensions with time cannot be rigorously ruled out.

To my wife, Qiong

Acknowledgements

I would like to take this opportunity to express my deepest appreciation to my advisor, Dr. Hervé Marand, for his guidance through the projects, for his helpful discussions and endless encouragement, for all the parties at his house and for his kindness in helping students from other countries. Special thanks go to those professors who have given inspirational courses and seminars that I attended through the years. I am also grateful for Dr. Glanville, Dr. Shultz, Dr. Ward and Dr. Wilkes who kindly served as my committee members.

I would like to thank Ms. Esther Brann for her help over the years. I also thank Mr. McCartney for training me in the AFM and TEM techniques. Special appreciation goes to Dr. Chad Snyder and Dr. Srivatsan Srinivas, who were post-doc fellows in our research group during my first year, for the assistance on equipments and the preliminary studies on the project of the nonlinear Hoffman-Weeks extrapolation, respectively. It has been a great experience to work over the last two years with Dr. Azar Alidadeh, who is a research assistant professor. I thank her for her friendship, encouragement and helpful discussions. My thanks go to all the members in Dr. Marand's research group, Sean Christian, Dr. Said Elkoun, Dr. Chitra Subramaniam, Robin Farmer, Seungman Sohn and Amit Kumar for providing their support and sharing ideas throughout the years. I wish them all to accomplish their goals successfully.

This work could never be finished without the continuous support from my beloved parents, Baoguo Xu and Chunling Tang. I was born in the northern part of Jiangsu, China, where one out of more than 100 young people could get the chance to enter college at that time. I became one of the luckiest because my parents knew from the beginning the importance of education to their children and because they educated me in the way they understood the importance. For this and their forever love, I appreciate them. I also thank my sister, Jianhua, for her encouragement over the years. My marriage in the second year of my program gave me much happiness and tremendous encouragement in the years. Appropriate words could not be found to express my

appreciation to my wife, Qiong He. It would not be an overstatement to say that this dissertation could never be finished without her love, patience and encouragement.

Finally, I thank the Dow Chemical Company for providing the ethylene/styrene samples and their financial support on the project, and Dr. Steve Chum, Dr. Martin Guest and Dr. Wilson Cheung for worthwhile discussions and their never-ending interest.

Table of Contents

List of Figures

List of Tables

Chapter 1. Introduction

1.1. General introduction to polymer crystallization

Polymer crystallization has been the subject of technical and scientific interest for decades. Morphology of polymer crystals is generally described in terms of chain folded lamellae,[1] which are thin along the chain direction (*l* in Figure 1.1, ca. 50 – 300 Å) and large in the other two directions (*X* and *Y* in Figure 1.1, in the magnitude of micrometers), when polymers crystallize from solution or from a quiescent melt. Crystallinity, which is defined as the fraction of crystals in the whole system, is invariably less than one hundred percent for polymeric materials with intermediate to high molecular weight. The observation of a semicrystalline state implies that polymer crystallization is controlled by kinetic rather than thermodynamic factors. Indeed, according to the Gibbs phase rule,[2] thermodynamic control of the crystallization process would imply the observation of a pure crystalline state below the equilibrium melting temperature. The morphology observed for semicrystalline polymers is the one which is associated with the fastest growth rate of crystallization. The melting temperature of polymer crystals in the most stable state, which is an infinite stack of fully extended chain crystals with chain ends in an equilibrium state of pairing, is defined as the equilibrium melting temperature for that polymer. This quantity is one of the most important thermodynamic properties of crystallizable chain polymers, as it is the reference temperature from which the driving force for crystallization is defined. Crystallization processes in polymers are generally thought to occur through a sequence of primary nucleation and crystal growth mechanisms, the rates of which, at a temperature T_x , are a function of the undercooling ΔT, $(T_m - T_x)$, where T_m is the equilibrium melting temperature. Knowledge of this quantity is essential for a proper understanding of the temperature dependence of bulk crystallization and linear crystal growth rates. More importantly, a precise determination of this thermodynamic quantity is necessary for evaluation and comparison of crystallization theories.[3-5]

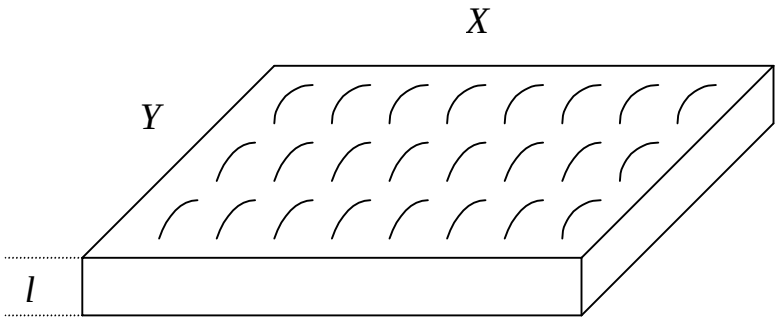

Figure 1.1. Schematic of a polymer lamellar crystal.

Since the morphology of semicrystalline polymers is controlled by kinetic factors rather than by thermodynamic ones, practitioners in this field are faced with the unfortunate fact that equilibrium crystals of even low to intermediate molecular weight polymers cannot be obtained experimentally. The equilibrium melting temperature for the crystalline form of a polymer can therefore only be obtained through extrapolative procedures. Four general methods have been devised for the assessment of equilibrium melting temperatures of semicrystalline polymers: the Gibbs-Thomson[2-6] and the Flory-Vrij[7-9] approaches, the Hoffman-Weeks (HW) linear extrapolation[10] and the fitting of growth rate data at sufficiently low undercooling with the classical theory of lamellar crystal growth.[11-12] The advantages and limitations of each method will be discussed in the next two chapters. Among the four methods, the HW linear extrapolation is the one most widely applied because of its straightforward experimental implementation and analytical simplicity. However, this method does not yield reliable equilibrium melting temperatures in most cases and a critical review of this method is given in the next chapter. One of the objectives of this dissertation is to propose a more rigorous method yielding a more accurate estimate of the equilibrium melting temperatures of semicrystalline polymers, and apply this method to isotactic polypropylene and poly(ethylene oxide).

When most homopolymers crystallize from a free, unconstrained melt, semicrystalline superstructures such as spherulites form and grow until they impinge upon one another. These

superstructures, which consist of radial arrays of periodically stacked lamellae, have dimensions ranging from micrometers to millimeters. However, even after the impingement of spherulites, the degree of crystallinity keeps increasing. It is therefore convenient to introduce here the concepts of primary and secondary crystallization, concepts which will be referred to very often in this work. The primary crystallization is defined as the fast sigmoidal increase in the degree of crystallinity at the early stage of the crystallization process. This stage is related to the formation and growth of lamellae from a free unconstrained melt. Secondary crystallization is then defined as any process leading to an increase in crystallinity through further crystallization within the superstructures generated by the primary crystallization process. Secondary crystallization generally takes place from the melt constrained by lamellae that resulted from the primary crystallization process. Superstructures like spherulites are lost when defects (such as short chain branches, regio or stereo defects) are introduced into polymer backbones because crystallization is highly prohibited by the existence of the noncrystallizable defects.[13] The effect of structural and topological constraints on the crystallization behavior of polymers is a topic of great importance and has received significant attention in industrial and academic research laboratories. In particular, many studies have focused on copolymer systems with one crystallizable unit (i.e. ethylene) and a noncrystallizable unit (e.g. 1-octene, 1-butene, etc.). If the content in the noncrystallizable unit increases, the length of ethylene sequences decreases, and the ability of the copolymer to form lamellar structures decreases. One of the fascinating questions for such systems is then what is the fate of ethylene sequences which are too short to form lamellae. Do they remain amorphous upon cooling? Can they crystallize by another mechanism? If they do, what is this mechanism? These questions will be addressed in this dissertation.

This dissertation is organized in such a way that each chapter (Chapter 2 to Chapter 5) is relatively independent from the others with its own introduction, experimental section, results, discussions and conclusions. Chapter 6 provides general conclusions and suggested future studies. To make it convenient for the readers, each chapter also has its own references listed at the end of it. The specific organization of this dissertation, which was motivated by the fact that

each chapter corresponds to a published or submitted paper, unfortunately leads to some repetitions, especially in the introduction for each chapter.

In Chapter 2,* the conventional HW linear extrapolation is critically reviewed and a more rigorous nonlinear HW analysis is proposed, which yields more accurate equilibrium melting temperatures for semicrystalline polymers.

In Chapter 3,* the new nonlinear HW analysis is applied to isotactic polypropylene. The results are compared with those obtained from the analysis of the temperature dependence of crystal growth rates. The general applicability of the Lauritzen-Hoffman (LH) secondary nucleation theory is also addressed. The effect of molecular weight on spherulitic growth rates and melting behavior is also addressed qualitatively. This latter part of the work was carried out after the publication of ref.15.

In Chapter 4,* the general applicability of the nonlinear HW analysis is further tested with poly(ethylene oxide) and the equilibrium melting temperature of PEO is determined. Results are compared to those from the analysis of the temperature dependence of crystal growth rates, and a rigorous test of the LH theory is carried out.

In Chapter 5,* the effect of the structural and topological constraints on the morphology, crystallization and melting behavior of ethylene/styrene copolymers is investigated. Specifically, secondary crystallization in this copolymer system is addressed and secondary crystals are suggested to be of fringed micellar type. Crystallization kinetics of these secondary crystals is also addressed.

1.2. Polymer crystallization theory

Several theories have been proposed to describe the kinetics of polymer crystallization, such as Sadler's rough surface model[16,17] and Lauritzen-Hoffman (LH) secondary nucleation theory.[1,2]

* Chapters 2 and 3 have been published.[14,15] Chapters 4 and 5 are being prepared for submission to Macromolecules.

The latter, which is the one most widely applied in literature, suggests that the rate of crystal growth is controlled by two elementary processes, the secondary nucleation process with rate i and subsequent lateral spreading with rate g. The LH theory then predicts that the polymer crystal growth can be categorized into three regimes. Let us first assume that the melt/crystal interface or the growth front can be described as a substrate with length L and thickness l (the lamellar thickness), shown in Figure 1.2. At high crystallization temperatures, i is much smaller than g, leading to the fact that once a nucleus deposits on the substrate, it grows in both directions to complete the total crystalline layer on the substrate before the next nucleation event occurs. This situation is denoted as regime I and the overall growth rate of polymer crystals, $G = b_o iL$, where b_o is the thickness of one crystalline layer. As temperature decreases, regime II mechanism sets in, where the magnitude of i and g are comparable. Thus, multiple nucleation occurs on the substrate and the nuclei spread laterally at the growth front but compete with each other to give rise to a new crystalline layer. In regime II, $G = b_o(2ig)^{1/2}$. Further decrease in the crystallization temperature results in a much larger i compared to g, and the secondary nucleation becomes the rate-determining step because there is no longer time for secondary nuclei to grow laterally. This regime is defined as regime III and $G = b_o iL'$, where L' is the average distance between niches, which is about 2 ~ 3 times the width of a stem. The detailed derivation of the expressions for i and g has been given in a review paper by Hoffman and Miller,[4] and will not be repeated here. The equation relating the overall growth rate, G, and the crystallization temperature, T_x, in the LH theory[4] is expressed as

$$G = G_j^{\,o} \exp\left(-\frac{U^*}{R(T_x - T_\infty)}\right)\exp\left(-\frac{K_{gj}}{T_x \Delta T}\right) \tag{1.1}$$

where U^* and T_∞ are the Vogel-Fulcher-Tamman-Hesse parameters describing the transport of polymer segments across the liquid/crystal interphase. $G_j^{\,0}$ is a prefactor assumed to be independent of temperature and K_{gj} is the secondary nucleation constant in a given regime. K_{gj} has been derived in the LH theory as

$$K_{gj} = \frac{j b_o \sigma \sigma_e T_m}{\Delta H_f k} \tag{1.2}$$

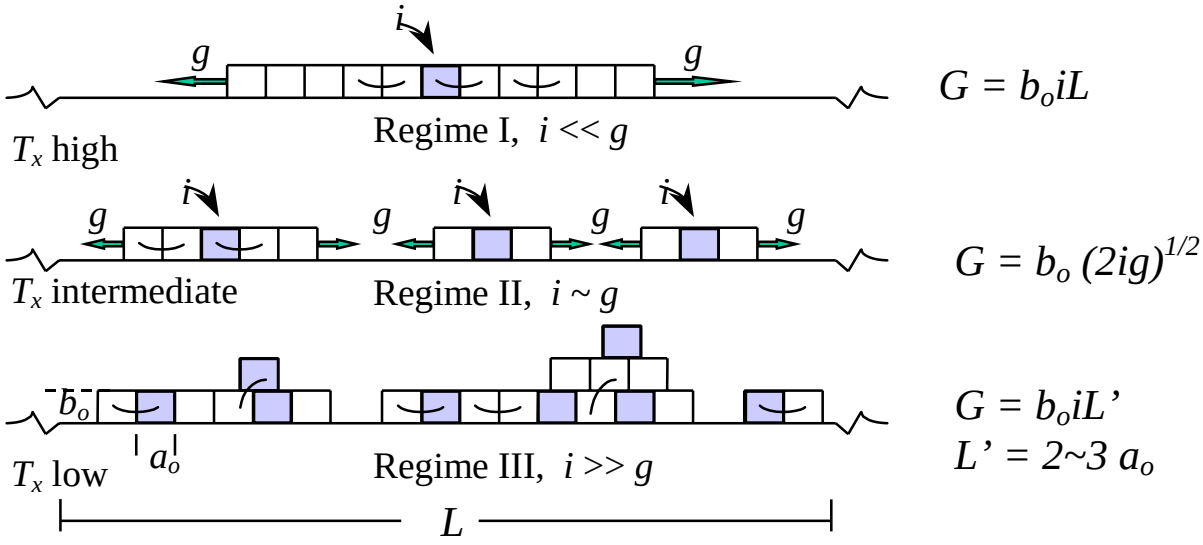

Figure 1.2. Schematic of the crystal growth in different regimes according to the LH theory.

where σ and σ_e are the lateral and fold surface free energy, respectively, ΔH_f is the theoretical heat of fusion and k is the Boltzmann constant. In the equation, $j = 4$ in regime I and III and $j = 2$ in regime II. Hence, the LH theory predicts that a plot of $\ln G + U^*/R(T_x - T_\infty)$ versus $1/T_x\Delta T$ yields K_{gj} as the slope and the slope in regime II is one half of those in regime I and III, namely, $K_{g\,I}/K_{g\,II} = K_{g\,III}/K_{g\,II} = 2$. The intercept of the plot in each regime provides the value of G_j^o for that regime. G_j^o is useful in the calculation of the substrate length, L, a value that has to be physically meaningful. When the temperature dependence of crystal or spherulitic growth rates is analyzed as discussed above, even small variations in the choice of the equilibrium melting temperature can lead to significant changes in the magnitude of the calculated secondary nucleation constants K_{gj}, and the surface free energy product $\sigma\sigma_e$. More importantly, it can lead to the artificial creation or disappearance of regime transitions when the raw spherulitic growth rate data are presented in a LH plot.

A more rigorous method is proposed in this dissertation to give a more accurate estimate of the equilibrium melting temperatures for semicrystalline polymers and is applied successfully to

isotactic polypropylene and poly(ethylene oxide). The general applicability of the LH theory is also tested in the systems of isotactic polypropylene and poly(ethylene oxide) in this work, using the value of the equilibrium melting temperatures obtained through the nonlinear HW analysis.

1.3. Copolymer crystallization theory

Copolymers usually exhibit the existing properties of both homopolymers as well as new properties by controlling the composition of the system. A good example is the ethylene/styrene copolymer system synthesized by metallocene-based catalysts.[18] A wide range of properties can be shown for these copolymers by controlling the styrene content. A low styrene content allows the copolymer to have a fairly high crystallinity, exhibiting typical plastic behavior of linear polyethylene, while a high styrene content copolymer shows typical glassy behavior of polystyrene. At an intermediate styrene content, the copolymer exhibits a typical elastomeric behavior due to the low crystallinity of the system.

Let us consider an A-B copolymer where A is a crystallizable unit (i.e. ethylene) and B acts as a defect in the polymer backbones (i.e. styrene). Properties of this copolymer largely depend on whether the defects can be included in the crystals or if they are completely excluded. Though investigations of the exclusion or inclusion of defects are not the main goals of this work, it is necessary to understand these concepts thoroughly. Flory[19] predicted the melting temperature and the crystallinity of the copolymer system as a function of temperature and sequence distribution length based on a phase equilibrium theory, assuming that B units are totally excluded from the crystals. The theory predicts a minimum stable crystallite length, ζ, which is determined by the crystallization temperature, T_x. At a given T_x, only those A sequences with a length larger than or equal to ζ will crystallize, while other A blocks with a length smaller than ζ will remain amorphous. ζ increases with an increase in T_x. During the cooling of copolymers from the melt to T_x, crystallization occurs in such an order that longer A sequences always crystallize earlier until the end of crystallization, where the lengths of the rest of the A blocks are smaller than $\zeta(T_x)$. Thus, the equilibrium crystallinity as a function of the

crystallization temperature can be calculated. The melting temperature depression of the copolymer system is predicted as,

$$1/T_m - 1/T_m{}^o = -(R/\Delta H_u)\ln p \qquad (5.3)$$

where T_m is the melting temperature of the copolymer, $T_m{}^o$ is the equilibrium melting temperature of the homopolymer, R is the gas constant, ΔH_u is the heat of fusion per unit of the homopolymer, and p is the sequence propagation probability. In a random copolymer system, $p = 1 - X_B$, where X_B is the content of the B unit. Since Flory's theory is based on the assumption that all the B units are excluded from the crystals, the melting temperature and the crystallinity of the system will not depend on the chemical nature of the B unit. This prediction is consistent with the experimental observations[13,20] that the melting temperature of homogeneous ethylene/α-olefin copolymers decrease with an increase in the comonomer unit content to an extent which does not depend on the chemical nature of the comonomer unit (assuming comonomers are larger than propylene). Quantitative comparisons of Flory's theory with experimental results are, however, not very satisfying, because the theory is based on a phase equilibrium assumption, while copolymer crystallization always occurs in a manner controlled by kinetics.

On the other hand, Sanchez and Eby[21,22] developed a theory based on the assumption that the comonomer units can be included into the crystal, and the extent of inclusion depends on the crystallization temperature employed. A faster crystallization rate results in a higher extent of inclusion. Sanchez and Eby predicted that the melting temperature of the copolymers decreases with increasing comonomer unit content due to the excess enthalpy caused by the introduction of the comonomer units (acting as defects) into the crystal. This differs from Flory's theory, which ascribes the melting temperature depression to an entropic effect.

The size of the comonomer units decides whether they can be included or not. Methyl branches can be included in the polyethylene crystals,[23] thus ethylene/propylene copolymers can be described by Sanchez and Eby's inclusion model. However, for comonomer units larger than propylene, diverse opinions exist. Experimental results show that the melting temperature and crystallinity of homogeneous ethylene/α-olefin copolymers (comonomer unit: 1-butene, 1-

pentene, 1-hexene, 1-octene) do not depend on the chemical nature of the comonomers while they strongly depend on the comonomer content.[13,20] These results strongly support the application of the exclusion model. Theoretical work by Helfand and Lauritzen[24] insists that the inclusion of comonomer units in the crystals is universal, the difference is only the degree of inclusion.

In this work, we will show that the extent of the inclusion of comonomer units is too small to affect the materials' properties, thus the exclusion model will be applied. The objective of this project is to study the effect of the structural and topological constraints on the morphology, crystallization and melting behavior of ethylene/styrene copolymers. This work will specifically focus on the secondary crystallization behavior of ethylene/styrene copolymers. A detailed literature review about the previous studies of other authors in this field is given in Chapter 5. This subject is also motivated by understanding the very practical phenomenon that the properties of many polyolefins, including ethylene copolymers and polypropylene, change dramatically at room temperature after their solidification. Such a phenomenon is likely to be related to the secondary crystallization process of these materials. The introduction of styrene units into the polymer backbones results in a large amount of ethylene blocks that are not long enough to form chain-folded lamellae. The role of these ethylene blocks in the crystallization process is investigated when the copolymers are cooled from the melt. They are likely to crystallize into another type of crystals (i.e. fringed micelle) without chain folding at low temperatures in the secondary crystallization process. The kinetics of the secondary crystallization is studied and the formation of the secondary crystals is found to be consistent with a one-dimensional, diffusion controlled growth.

1.4. References

1. Keller, A. *Philos. Mag*. **1957**, *2*, 1171.
2. Wunderlich, B. Crystal Melting, *Macromolecular Physics*, Academic Press: New York, **1980**, *Vol. 3*.
3. Hoffman, J. D.; Davis, G. T.; Lauritzen, J.I. In *Treatise on Solid State Chemistry*; Hannay, N.B. Ed.; Plenum Press: New York, **1976**; *Vol. 3*, Chapter 7.
4. Hoffman, J. D.; Miller, R. L. *Polymer* **1997**, *38*, 3151.
5. Armitstead, K.; Goldbeck-Wood, G. *Adv. Polym. Sci*. **1992**, *100*, 218.
6. Marand, H.; Hoffman, J. D. *Macromolecules* **1990**, *23*, 3682.
7. Broadhurst, M. G. *J. Chem. Phys*. **1962**, *36*, 2578.
8. Flory, P. J.; Vrij, A. *J. Am. Chem. Soc*. **1963**, *85*, 3548.
9. Mandelkern, L.; Stack, G. M. *Macromolecules* **1984**, *17*, 871.
10. Hoffman, J. D.; Weeks, J. J. *J. Res. Natl. Bur. Stand. (U.S.)* **1962**, *A66*, 13.
11. Huang, J.; Marand, H. *Polymer* **1994**, *35*, 1896.
12. Huang, J.; Prasad, A.; Marand, H. *Macromolecules* **1997**, *30*, 1069.
13. Alidazeh, A.; Richardson, L.; Xu, J.; McCartney, S.; Marand, H.; Cheung, W.; Chum, S. *Macromolecules* **1999**, *32*, 6221.
14. Marand, H.; Xu, J.; Srinivas, S. *Macromolecules* **1998**, *31*, 8219.
15. Xu, J.; Srinivas, S.; Marand, H.; Agarwal, P. *Macromolecules* **1998**, *31*, 8230.
16. Sadler, D. M.; Gilmer, G. H. *Polymer* **1984**, *25*, 1446.
17. Sadler, D. M. *Polymer* **1983**, *24*, 1401.
18. Chen, H.; Guest, M.; Chum, S.; Hiltner, A.; Baer, E. *J. Appl. Polym. Sci.* **1988**, *70*, 109.
19. Flory, P. *J. Trans. Faraday, Soc*. **1955**, *51*, 848.
20. Alamo, R.; Mandelkern, L. *Thermochimica Acta* **1994**, *238*, 155.
21. Sanchez, I. C.; Eby, R. K. *J. Res. Natl. Bur. Std. -- A. Phys. & Chem*. **1973**, *77A*, 353.
22. Sanchez, I. C.; Eby, R. K. *Macromolecules* **1975**, *8*, 638.
23. Cham, P. Ph.D. Dissertation, Virginia Polytechnic Institute and Sate University, **1996**.
24. Helfand, E.; Lauritzen Jr.; J. *Macromolecules* **1973**, *6*, 631.

Chapter 2. Determination of the Equilibrium Melting Temperature of Semicrystalline Polymers by Non-linear Hoffman-Weeks Extrapolation

2.1. Introduction

The equilibrium melting temperature, T_m , of a polymer crystal is defined as the melting temperature of an infinite stack of extended chain crystals, large in directions perpendicular to the chain axis and where the chain ends have established an equilibrium state of pairing. This quantity is one of the most important thermodynamic properties of crystallizable chain polymers, as it is the reference temperature from which the driving force for crystallization is defined. Within the current paradigm of crystallization theories,[1-4] knowledge of this quantity is essential for a proper understanding of the temperature dependence of bulk crystallization and lineal crystal growth rates. More importantly, a precise determination of this thermodynamic quantity is necessary for evaluation and comparison of crystallization theories. Crystallization processes in polymers are generally thought to occur through a sequence of primary nucleation and crystal 4growth mechanisms, the rates of which, at a temperature T_x , are a function of the undercooling ΔT (T_m -T_x), where T_m is the equilibrium melting temperature. When the temperature dependence of crystal or spherulitic growth rates is analyzed in the context of the Lauritzen-Hoffman (LH) secondary nucleation theory,[1,2] even small variations in the choice of the equilibrium melting temperature can lead to significant changes in the magnitude of the calculated nucleation constant K_g, and surface free energy product $\sigma\sigma_e$. More importantly, it can lead to the artificial creation or disappearance of regime transitions when the raw spherulitic growth rate data are presented in a LH plot.[5]

Since the morphology of semicrystalline polymers is controlled by kinetic factors rather than by thermodynamic ones, practitioners in this field are faced with the unfortunate fact that equilibrium crystals of even low to intermediate molecular weight polymers cannot be obtained experimentally.[6,7] The equilibrium melting temperature for the crystalline form of a polymer can therefore only be obtained through extrapolative procedures. Four general methods have been devised for the assessment of equilibrium melting temperatures of semicrystalline polymers: the

Gibbs-Thomson[1-3,8,9] and the Flory-Vrij approaches,[10,11,12] the Hoffman-Weeks procedure[13] and the fitting of growth rate data at sufficiently low undercooling with the classical theory of lamellar crystal growth.[14,15] The applicability of the latter two methods relies on the assumption of a specific crystal growth model. The former two methods are based solely on thermodynamic arguments and should be a priori more reliable, although they have limitations of their own.

The Flory-Vrij formalism was developed to determine the equilibrium melting temperature of polyethylene in the long chain limit and is based on the availability of equilibrium melting temperature data for a series of pure short chain paraffins, which are homologues of polyethylene. The equilibrium melting temperature of an extended chain crystal of linear polyethylene having n CH_2 groups and two methyl end groups can then be calculated from the latent heat and entropy of fusion per methylene group, the methyl end groups contribution to the enthalpy and entropy of fusion and the localization entropy associated with the pairing of chain ends. These thermodynamic input parameters are obtained through refinement of paraffin melting and heat capacity data. As this approach requires the availability of a homologous series of strictly monodisperse materials and an inordinate amount of thermodynamic data, it has not been widely applied to other semicrystalline polymers.[12]

The Gibbs-Thomson approach is based on the thermodynamic argument, that the melting temperature of a crystal of finite size is depressed below that of an infinite size crystal, the result of an increase in free energy of the crystal with a decrease in its dimensions. In the case of polymer lamellar crystals, it is generally but not universally observed, that the lamellar thickness is much smaller than the other two dimensions, in which case, the melting temperature depression is proportional to the ratio of the crystal basal surface free energy to the theoretical enthalpy of fusion (*i.e.* to the reciprocal of the lamellar thickness, see below). Limitations of this thermodynamic treatment have been discussed in the literature[3,16] and are not of particular concern for relatively high molecular weight flexible linear polymers, for which the equilibrium melting temperature becomes approximately independent of chain length. A plot of the observed melting temperature as a function of the reciprocal of the lamellar thickness, if linear, would

therefore yield the equilibrium melting temperature as the intercept. This method, which appears at first sight very straightforward, is only suitable if a number of experimental conditions are satisfied. First, lamellar crystals should be large enough along directions parallel to their basal plane for the lateral surface free energy contribution to the melting point depression to be negligible. Second, the crystal lamellar thickness should be measured just prior to the onset of their melting. If the crystal thickness is recorded at the crystallization temperature or at ambient conditions, the crystals may reorganize, melt and recrystallize or thicken during the heating scan required to record their melting temperature.[9] In most instances, the lamellar thickness is actually determined at room temperature from either small angle X-ray scattering measurements, electron microscopy observations or from the longitudinal acoustic modes (LAM) observed by Raman spectroscopy. It must be emphasized that in the case of Raman LAM studies the correction for chain tilt with respect to the normal of the basal crystal planes must be carried out to determine the actual lamellar thickness. Furthermore, as a result of the finite crystal-melt interfacial thickness at the crystal basal plane, it is anticipated that both the SAXS and the LAM analyses lead to a slight overestimation of the core lamellar thickness. In the SAXS analysis this arises from the equal apportionment of the interphase thickness to the crystal and amorphous phases. In the Raman LAM analysis of polyethylene, overestimation results from the variable persistence of trans sequences into the interfacial region. In any case, for linear polyethylene, estimates of the interfacial thickness through SAXS and Raman spectroscopy suggest that this overestimation should be of magnitude *ca* 5 Å per interphase. Unless the above issues are rigorously addressed, one should not expect the Gibbs-Thomson method to provide an accurate estimate of the equilibrium melting temperature.

The best possible approach may consist in following simultaneously the evolution of the SAXS and WAXD patterns of a semicrystalline polymer during heating using a synchrotron radiation source.[17] The latter assertion obviously assumes that the semicrystalline polymer morphology can be reasonably approximated by the lamellar stack model, so that the correlation or interface distribution function approach can be reliably used to determine the length scales associated with spatially periodic electron density fluctuations.[18,19] It is therefore doubtful that

such a technique could be rigorously applied to polymers such as poly(ethylene terephthalate), poly(ether ether ketone) or poly(phenylene sulfide), since morphological studies carried out by transmission electron microscopy have unambiguously revealed that, over most of their practical crystallization temperature range, these polymers display thin lamellae of relatively narrow width.[20-22]

The determination of the equilibrium melting temperature through the analysis of the temperature dependence of spherulitic growth rates was first proposed by Marand et al.[14,15] and will be addressed for the case of isotactic poly(propylene) in the next chapter.

The Hoffman-Weeks (HW) method involves the extrapolation of a linear regression of experimentally observed melting temperatures, T_m' , for various crystallization temperatures, T_x , to the equilibrium line $T_m' = T_x$. The associated HW equation results from a combination of the Gibbs-Thomson equation and an expression derived from the LH secondary nucleation theory,[1,2] which relates the initial stem length to the undercooling. It is also based on the assumption that the difference between crystallization and observed melting temperatures is solely due to the thickening of lamellae formed at the crystallization temperature. The thickening coefficient, γ_{HW}, which is calculated as the reciprocal of the slope of the T_m' versus T_x regression line, should account, in principle, for the thickening process occurring during isothermal crystallization.[13] Because of its straightforward experimental implementation and its analytical simplicity, this method has been widely used for the determination of the equilibrium melting temperatures of semicrystalline polymers. It should be noted, however, that this procedure was not developed to provide the best estimate of equilibrium melting temperatures, but merely to explain the observed increase in melting temperature with crystallization temperature.[2,5] It has been reported that in some cases this approach fails as a result of enhanced lamellar thickening for samples crystallized at the lowest undercoolings.[2,23] It is also commonly but incorrectly accepted (see below) that the observation of a linear T_m' versus T_x behavior is an indication that the lamellar thickening coefficient is constant. At this stage, it is important to realize that a necessary prerequisite for the isothermal lamellar thickening process is the existence of some molecular

mechanism for segmental motion within the lamellar crystal. It is generally agreed that the observation of a crystalline α relaxation (through dielectric, dynamic mechanical and NMR spectroscopic measurements), provides compelling evidence for the existence of segmental motion within the lamellar crystals.[24] However, one should note that the existence of such a relaxation is a necessary, but not sufficient, prerequisite for the lamellar thickening process. Other factors such as the presence of non-crystallizable units along the polymer backbone (branches, comonomer, etc..), a high entanglement density in the interlamellar regions and the nature of the lamellar morphology (for example the cross hatched morphology[19,25,26] in isotactic polypropylene) may affect the kinetics of this process in such a way that lamellae do not thicken considerably after their formation. Furthermore, a number of polymers such as PEEK, PPS, PET, nylons, it-PS, and so forth show no sign of a distinct crystalline α relaxation in the temperature range where their crystallization/melting behavior has been investigated.[24] These materials are therefore not expected to exhibit lamellar thickening under isothermal crystallization conditions. Time resolved SAXS studies have actually suggested that for this latter class of materials, the average lamellar thickness does not increase during primary or secondary crystallization but appears to decrease, most likely the result of secondary crystallization.[27-30] In light of the above discussion, it is rather puzzling to note that the linear HW analysis almost invariably yields thickening coefficients between 2 and 3, regardless of the polymer under consideration, its molecular weight, and the existence or absence of a crystalline α relaxation.

The goals of this work are then to examine the assumptions involved in the linear HW extrapolation and to investigate the applicability of this method to the determination of the equilibrium melting temperature and thickening coefficient of a given polymer crystal. Firstly, the general relationship between observed melting and crystallization temperatures is recalled, expected on the basis of the LH theory, and the validity of the various approximations involved in the HW linear extrapolation are discussed. Secondly, the conditions are examined under which the linear extrapolation is expected to provide a reliable estimate of the equilibrium melting temperature, the effect of lamellar thickening is investigated in the temperature range where experimental data are accessible. Thirdly, a number of model calculations are carried out

using different values of the thickening coefficient (γ = 1 and 2). The case γ =1 is elaborated upon to provide insight into the behavior of polymers whose crystals do not exhibit isothermal lamellar thickening or for which the melting temperature of non-thickened crystals can be either recorded experimentally or inferred from experimental data. Finally, the case of a hypothetical linear polyethylene material of sufficiently high molecular weight (the equilibrium melting temperature is independent of chain length) is considered. The choice of this polymer is dictated by the a-priori reliable estimate of its equilibrium melting temperature (upper bound) through the Flory-Vrij treatment, and by the availability of thermodynamic and crystallographic parameters[2,23,31] Pertinent molecular characteristics and thermodynamic properties for this material are listed in Table 2.1.

2.2. Linear and non-linear Hoffman-Weeks extrapolation

This section starts with the conventional Hoffman-Weeks treatment, followed by the discussion why this method is not valid in most cases. The strict conditions for using the conventional Hoffman-Weeks extrapolation are derived. Finally, a non-linear Hoffman-Weeks extrapolation is introduced, both its advantage over the conventional Hoffman-Week linear treatment and its limitations are discussed.

Table 2.1. Thermodynamic constants for high molecular weight linear polyethylene.

T_m (°C)	145.5[a]
ΔH_f (J.cm^{-3})	283[b]
$\sigma_{em} = \sigma_e^1$ (erg/cm^2)	90.4[c]
C_2 (Å)	43.25[c]

[a] Flory-Vrij extrapolation (see ref. 2), [b] calculated using a density of 0.968 g.cm^{-3} at 145.5°C (ref. 45), [c] (ref. 2)

2.2.1. The conventional Hoffman-Weeks linear treatment

The HW approach assumes that the initial lamellar thickness, l^*, of a polymer crystal growing under isothermal and quiescent conditions is appropriately described by the LH secondary nucleation theory. It is also assumed that the Gibbs-Thomson equation, in its standard form, provides an accurate estimate of the melting temperature depression associated with the finite thickness of lamellar crystals. This latter assertion has been rigorously verified for polymers in the long chain length limit.[2,16] We recall that a rigorous use of the Gibbs-Thomson equation requires recording both the melting temperature and the lamellar thickness for the same crystals (minimize reorganization, pre-melting or thickening of the crystals during heating or measure the lamellar thickness just before the onset of melting). According to the LH theory, the average initial lamellar thickness observed at the temperature of crystallization, T_x, is given by

$$l^* = \frac{2\sigma_{ex}}{\Delta G_{fx}} + \delta l_x \tag{2.1}$$

where σ_{ex} and ΔG_{fx} are, respectively, the basal plane crystal/melt interfacial free energy and the bulk free energy of fusion at T_x, and δl_x is the thickness increment above the minimum lamellar thickness, which enables the secondary surface nucleus to enter a region of thermodynamic stability at the fastest rate at T_x.[1,2] The importance of δl_x is generally recognized by noting that it prevents a crystal formed at T_x to melt at its own crystallization temperature. In the $\psi = 0$ version of this theory,[2] δl_x is expressed by

$$\delta l_x = \left(\frac{kT_x}{2b_0\sigma_x}\right)\left(\frac{4\sigma_x + a_0\Delta G_{fx}}{2\sigma_x + a_0\Delta G_{fx}}\right) \tag{2.2}$$

where σ_x is the lateral crystal/melt interfacial free energy at the crystallization temperature, k is the Boltzmann constant, b_0 is the thickness of the secondary nucleus in the direction normal to the growth front and a_0 is the width of the stem in the direction parallel to the long dimension of the growth plane. It should be noted that Equation 2.1 has been criticized as being invalid for some polymers (such as isotactic polystyrene[32]) at large undercoolings, where apparently the lamellar thickness becomes independent of crystallization temperature. However, inspection of this earlier experimental study indicates that it is the long spacing and not the actual lamellar thickness, which becomes independent of T_x. This criticism is not rigorously warranted for

flexible chain polymers with small repeat units, as the LH theory only addresses isothermal growth rates and stem lengths of isolated crystals and cannot provide any information on the thickness of the interlamellar amorphous region, except, however, for low molecular weight polymers, where chain folds and cilia are the only amorphous constituents of these regions.[2] For other polymers, such as polyamides,[33] the maximization of interchain hydrogen bonded interactions may prevent the lamellar thickness from varying smoothly with crystallization temperature. Such specific cases need to be recognized but are beyond the focus of this work and will not be discussed here.

The bulk free energy of fusion at the crystallization temperature can be expressed in terms of the undercooling, ($\Delta T = T_m - T_x$), the latent heat of fusion at the equilibrium melting temperature, ΔH_f and a correction factor f_x accounting for the temperature dependence of both the latent heat and entropy of fusion.

$$\Delta G_{fx} = \frac{f_x \Delta H_f (T_m - T_x)}{T_m} \tag{2.3}$$

The term f_x can be rigorously determined by carrying out a Taylor series expansion of the Gibbs free energy of fusion around T_m.[10-12]

Let us consider a lamellar crystal of thickness, l, with lateral dimensions, X and Y. Setting the free energy of fusion of the finite size crystal at the observed melting temperature, T_m', to be zero, we obtain

$$XYl\Delta G_{fm'} - 2XY\sigma_{em'} - 2l(X+Y)\sigma_{m'} = 0 \tag{2.4}$$

where $\Delta G_{fm'}$, $\sigma_{em'}$ and $\sigma_{m'}$ are the bulk free energy of fusion, and the basal and lateral interfacial free energies at the observed melting temperature T_m', respectively. Expressing $\Delta G_{fm'}$ in terms of the melting temperature depression $T_m - T_m$' in a similar manner as shown in Equation 2.3 leads to the classical Gibbs-Thomson equation

$$T_m' = T_m\left(1 - \frac{2\sigma_{em'}}{lf_{m'}\Delta H_f}\right) \tag{2.5}$$

when the conditions $\sigma_{m'}/X$ and $\sigma_{m'}/Y << \sigma_{em'}/l$ are satisfied.

Since a number of polymer crystals thicken[34] either isothermally at T_x or upon heating to the melting temperature, the lamellar thickness at the time of melting, l, may be greater than the initial lamellar thickness, l^*. An average thickening coefficient, γ_{xm}, is introduced and defined by

$$\gamma_{xm} = \frac{l}{l^*} \tag{2.6}$$

It should be noted that γ_{xm} is generally a function of crystallization temperature, time and possibly heating conditions up to the melting temperature.[23,34,35]

At this juncture, we can combine Equations 2.1, 2.3, 2.5 and 2.6 to obtain the general form of the relation between the observed melting temperature and the crystallization temperature.[23,36]

$$T_m' = T_m \left\{ 1 - \frac{1}{\gamma_{xm}} \left(\frac{T_m - T_x}{T_m} \right) \left(\frac{\sigma_{em'}}{\sigma_{ex}} \right) \left(\frac{f_x}{f_{m'}} \right) \left(\frac{1}{1 + \frac{\delta l_x \Delta H_f f_x (T_m - T_x)}{2\sigma_{ex} T_m}} \right) \right\} \tag{2.7}$$

A number of approximations are generally made to render this approach tractable. First, it is assumed that both the ratio of the fold surface free energies and that of the f_T terms are close to unity. Under these conditions, the expression relating T_m' and T_x becomes

$$T_m' = T_m \left(1 - \frac{\Theta_x}{\gamma_{xm}} \right) + T_x \frac{\Theta_x}{\gamma_{xm}} \tag{2.8}$$

where

$$\Theta_x = \frac{1}{1 + \frac{\delta l_x \Delta H_f f_x (T_m - T_x)}{2\sigma_{ex} T_m}} \tag{2.9}$$

Second, if we consider crystallization processes carried out at low undercoolings, such that the term $\delta l_x \, \Delta H_f f_x \, (T_m - T_x)$ is significantly smaller than $2\sigma_{ex} \, T_m$, then we may neglect the contribution from the δl_x containing term to the melting depression below the equilibrium melting temperature and assume that Θ_x is unity. This consideration, combined with the assumption that

the thickening coefficient γ_{xm} is constant, constitutes the various approximations which are at the origin of the classic linear Hoffman-Weeks approach.[13] This approach, therefore, implicitly assumes that T_m' is greater than T_x solely due to crystal thickening effects and yields a linear relationship between observed melting and crystallization temperatures

$$T_m' = T_m^{HW}\left(1 - \frac{1}{\gamma_{HW}}\right) + \frac{T_x}{\gamma_{HW}} \tag{2.10}$$

where T_m^{HW} and γ_{HW} are the "equilibrium melting temperature" and the thickening coefficient obtained from the intercept with the equilibrium line and the reciprocal of the slope of the T_m' versus T_x regression line, respectively. One of the goals of this manuscript is therefore concerned with the determination of the conditions under which $T_m^{HW} = T_m$ and $\gamma_{HW} = \gamma$.

It is apparent in the conventional HW treatment, that the δl_x term, which is of prime importance when considering the rate of substrate completion,[2] plays no role in relating the melting temperature to the crystallization conditions. On cursory examination, this assumption seems justified in the case of polyethylene and a few additional polymers such as PEO, which display relatively large lamellar thicknesses (l >> 100 Å). Indeed, the δl_x value, calculated from Equation 2.2 to be 13 ± 1 Å for polyethylene in the practical isothermal crystallization range, would make a negligible contribution to l, especially at low undercooling.

Rather than assuming that the initial lamellar thickness is given by Equation 2.1, a prediction of the LH theory, it appears safer to express l^* by

$$l^* = \frac{C_1}{\Delta T} + C_2 \tag{2.11}$$

where C_1 and C_2 are constants, obtained experimentally. It has been previously suggested for polyethylene [2,17,31] that the quantity C_1 is approximately equal to $2\sigma_{em}T_m/\Delta H_{fm}$. On the other hand, C_2 is found to be ca. 43 Å, which is about three to four times larger than the δl_x value calculated from Equation 2.2. The origin of this discrepancy between the magnitude of C_2 and δl_x is discussed below. Since large values of C_2 are also found for other semicrystalline polymers,[37] it would follow that the approximation $C_2 << l^*$ is generally unjustified.

Furthermore, if we exclude polyethylene and poly(ethylene oxide), which can crystallize fairly rapidly at low undercooling to yield thick lamellae, most polymers crystallize sufficiently rapidly under isothermal conditions only at fairly large undercoolings. Under these conditions, their lamellar thickness is expected to be much lower than observed for PEO or even PE (i.e. $l \sim 100$ Å). Consequently, the above approximation ($C_2 << l^*$) will be more inaccurate for these polymers than for PE and PEO.

Another important consequence of the above approximation is that the linear HW treatment, in the conventional form (Equation 2.10), cannot describe the melting of polymer crystals which do not thicken isothermally or upon heating ($\gamma_{xm} = 1$), as this yields the erroneous conclusion that $T_m' = T_x$. If lamellar crystals formed at a crystallization temperature T_x, melt and recrystallize into thicker crystals during the heating process, the basic premise of the HW treatment, that we can correlate the crystallization temperature to the resulting observed melting temperature, is not satisfied and this treatment should not be used without further modification.

2.2.2. A more rigorous relationship between observed melting and crystallization temperatures

We noted in the previous section a discrepancy between the magnitude of C_2 and δl_x. This discrepancy can be qualitatively accounted for on the basis of stem length fluctuations during the chain folding process. Lauritzen and Passaglia[38] proposed a stem length fluctuation model in which they computed the "kinetic" fold surface energy, σ_{ex}, accounting for the extra lateral surface energy due to fold protrusion and for the mixing entropy associated with stems of different lengths. The kinetic roughening of the fold surface leads to an increase in the basal plane interfacial free energy with increasing undercooling, which is approximated by:

$$\sigma_{ex} = \sigma_e^1(1 + y\Delta T) \tag{2.12}$$

where y is a small positive constant and σ_e^1 is the fold surface free energy estimated from the slope of l^* versus $1/\Delta T$.[1,2] Under these conditions, the undercooling dependence of the initial lamellar thickness can be recast as

$$l^* = \frac{2\sigma_e^1 T_m}{\Delta H_f \Delta T} + \frac{2\sigma_e^1 y T_m}{\Delta H_f} + \delta l_x \qquad (2.13)$$

The sum of the last two terms on the R.H.S. of Equation 2.13 can be taken as constant (i.e. independent of undercooling), which we associate with the term C_2. The constant y has been evaluated[1,2,39-41] from the experimental value of C_2 and the estimate of δl_x, defined by Equation 2.2, and has been quoted in the range from 0.0025 to 0.05 K^{-1}. We will however not indulge here in such calculations, which we feel are unlikely to shed new light on this problem, as (1) the quantity δl_x , given in Equation 2.2, actually depends on the magnitude of ψ,[1] which, although thought to be small, is not known accurately and may differ for substrate completion and first stem deposition processes,[42] (2) the exact temperature dependence of σ_{ex} is unlikely to be rigorously linear.[1,38] In any case, examination of a number of studies lends support to the applicability of Equation 2.11 and to the need to account for the temperature dependence of the kinetic fold surface free energy. In recent treatments,[1,2] it has been implicitly assumed that the fold surface free energy, σ_e^1 which appears in the term C_1 is approximately equal to that appearing in the Gibbs-Thomson equation. Although one should expect the quantities σ_e^1 and σ_{em} to be slightly different,[38,39] experimental results in the literature are not accurate enough to allow us to differentiate these quantities. The linearity, universally observed in Gibbs-Thomson plots, indeed, suggests that σ_{em} can be assumed constant, in agreement with the prediction that the equilibrium roughness of the fold surface is only very weakly temperature dependent.[38,39] The use of σ_{em} rather than σ_{ex} in the Gibbs-Thomson equation implies that either subsequent to the folding process at T_x or during heating to the melting temperature, the fold surface has enough mobility to reach a state of equilibrium roughness. If we nevertheless assume, for the sake of completeness, that the magnitude of σ_e^1 and σ_{em} may differ slightly, combination of Equation 2.5, 2.6, 2.11-2.13 leads to the following relationship between T_m' and T_x

$$T_m' = T_m\left(1-\frac{1}{\gamma_{xm}}\left(\frac{T_m-T_x}{T_m}\right)\left(\frac{f_x}{f_{m'}}\right)\left(\frac{\sigma_{em}}{\sigma_e^1}\right)\left(\frac{1}{1+\frac{C_2\Delta H_f}{2\sigma_e^1}\frac{(T_m-T_x)}{T_m}}\right)\right) \tag{2.14}$$

We note that Equation 2.14 differs from similar relationships given in the literature in two respects. First, and most significantly, δl_x has been replaced by C_2, which, as will be shown below, renders the approximation $\Theta(T_x) = 1$ very inaccurate. Second, a new term (σ_{em}/σ_e^1) is introduced in the T_m' versus T_x relation, which may or may not be significant, but whose value should be obtained experimentally for a more rigorous estimation of T_m.

2.2.3. Conditions when the linear extrapolation is rigorously valid

Focusing on polymer crystals which may exhibit isothermal lamellar thickening and/or lamellar thickening during heating, without melting-recrystallization, we investigate the conditions under which the $C_2 = 0$ approximation is justified. To do so, we calculate the difference between the observed melting temperature predicted by the linear HW equation (Equation 2.10) and that derived from the more general relation (Equation2.14) and determine the conditions under which this difference is less than some fixed error, ε. This procedure allows us to define a range of undercoolings up to which the linear extrapolation is a good approximation of the non-linear one. As justified above, we emphasize that, from here on, we describe the undercooling dependence of the initial lamellar thickness using the term C_2 rather than δl_x. Subtracting Equation 2.10 from Equation 2.14 and setting the absolute value of the difference to be less than ε leads to

$$\left|\left(\frac{T_m-T_x}{\gamma_{xm}}\right)\left(1-\frac{1}{1+\frac{C_2\Delta H_f(T_m-T_x)}{2\sigma_e^1 T_m}}\right)\right| \le \varepsilon \tag{2.15}$$

which, assuming σ_{xm} to be constant and σ_e^1 to be equal to σ_{em}, is recast as

$$a\left(T_m - T_x\right)^2 - a\varepsilon\gamma_{xm}\left(T_m - T_x\right) - \varepsilon\gamma_{xm}T_m \leq 0 \tag{2.16}$$

where a is defined as

$$a = \frac{C_2 \Delta H_f}{2\sigma_e^1} \tag{2.17}$$

The only physically meaningful solution of Equation 2.16 is

$$T_m - T_x \leq \frac{\varepsilon\gamma_{xm}}{2}\left(1 + \sqrt{1 + \frac{8\sigma_e^1 T_m}{\varepsilon\gamma_{xm} C_2 \Delta H_f}}\right) \tag{2.18}$$

This derivation implies that for a given set of T_m, σ_e^1 , ΔH_f , σ_{xm} and C_2 values, the observed melting temperature predicted by the HW equation (Equation 2.10) differs by at most ε from the melting temperature predicted by the more rigorous approach (Equation 2.14), if the undercooling is less than that given by Equation 2.18. In Table 2.2, these maximum undercoolings are given for various choices of the thickening coefficient and of the allowable error, ε, in the case of polyethylene. The input material parameters for polyethylene are given in Table 2.1. Considering the results shown in Table 2.2, it is immediately apparent that the linear extrapolation is only valid at very small undercoolings, where crystallization would not occur on

Table 2.2. Undercooling ΔT_{max} up to which the linear (Equation 2.10) and the non-linear (Equation 2.14) expressions of $T_m' = f(T_x)$ differ by less than ε for γ_{xm} =1 and 2.

	$\gamma_{xm} = 1$	$\gamma_{xm} = 2$
ε (°C)	ΔT_{max} (°C)	ΔT_{max} (°C)
0.1	2.5	3.6
0.5	5.8	8.4
1	8.4	12.1
2	12.1	17.8
5	20.2	30.3

any practical time scale. These calculations also indicate that for a larger but constant thickening coefficient, there is a larger temperature range below the equilibrium melting temperature, where the linear extrapolation is accurate. Recalling that among all known polymers, polyethylene exhibits one of the highest crystallization rates at a given undercooling, one can conclude that other polymers will generally crystallize at a finite rate only at larger undercoolings. Thus, their observed melting temperature will be more significantly depressed below the equilibrium melting temperature than for the case of polyethylene, and systematic deviations between the linear approximation and the non-linear form of $T_m' = f(T_x)$ will become more significant. This simple calculation therefore indicates that, if the linear extrapolation is used, accurate values of the equilibrium melting temperature should not be expected in general.

2.2.4. Practical consequences of the linear T_m' versus T_x extrapolation

To examine the implications of using the linear LH treatment in a temperature range where it is not rigorously applicable, we first generate a set of T_m' versus T_x data using Equation 2.14, assuming a constant thickening coefficient. To generate this data for polyethylene, we make use of the thermodynamic constants listed in Table 2.1. Theoretical plots of T_m' versus T_x for different values of the thickening coefficient (γ_{xm} = 1 and γ_{xm} = 2) are then constructed using Equation 2.14, where, as indicated above, we assume $\sigma_{em} = \sigma_e$[1] and take f_T to be unity, and σ_{xm} to be independent of temperature. The latter approximations are of no consequence here. The results of these calculations are shown in Figure 2.1, where predicted melting temperatures are plotted as a function of crystallization temperature for γ_{xm} = 1 and γ_{xm} = 2. It is clear that these plots exhibit significant curvature in the hypothetical crystallization temperature range between 100°C and 140°C. Linear extrapolations, carried out from different data sets selected over a 10°C crystallization temperature interval lead to different intercepts with the $T_m' = T_x$ line, the worst case being when the extrapolation is carried out far from the true equilibrium melting temperature and the thickening coefficient is low. We now apply the HW procedure to the T_m' versus T_x generated data for the experimental range of crystallization temperatures that is appropriate for linear polyethylene (*i.e.* from T_x = 120 to 130 °C). Below 120 °C, isothermal crystallization may not be achieved with bulk samples, as primary nucleation and growth process

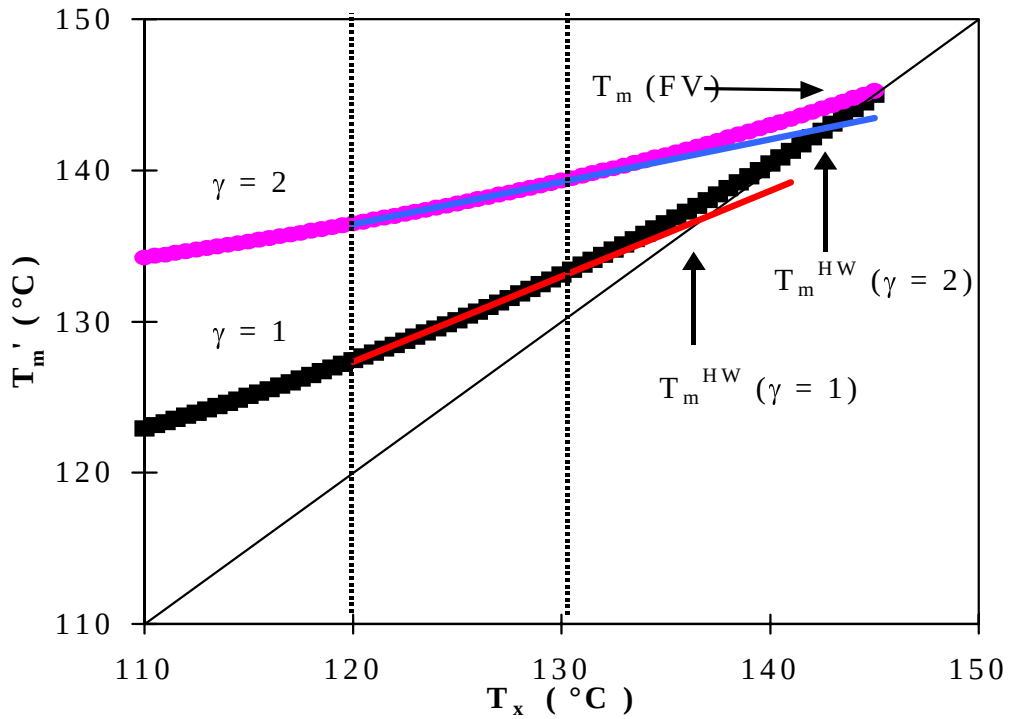

Figure 2.1. Dependence of the observed melting temperature on crystallization temperature as calculated from Equation 2.14 for γ_{xm} = 1 (■) and 2 (●). The full lines are the corresponding HW linear regressions and extrapolations from the 120 - 130°C crystallization temperature range. T_m (FV) is the equilibrium melting temperature calculated from the Flory-Vrij equation. T_m^{HW} ($\gamma = 1$) and T_m^{HW} ($\gamma = 2$) are the "equilibrium melting temperatures" determined by the linear HW extrapolation for the indicated thickening coefficients.

could occur during cooling. Above 130 °C, isothermal thickening becomes very significant, leading unavoidably to a non-constant thickening factor.[23,37] Linear regressions of the predicted melting points in the 120 - 130 °C crystallization temperature range for the cases γ_{xm} = 1 and γ_{xm} = 2 are also shown in Figure 2.1. Intersection of these linear extrapolations with the $T_m' = T_x$ line leads to apparent equilibrium melting temperatures of 136.9 °C and 142.9 °C for γ_{xm} = 1 and γ_{xm} = 2, respectively. These values are 8.6 °C and 2.6 °C lower than the Flory-Vrij estimate (T_m = 145.5 °C), which was used to generate the theoretical T_m' versus T_x data.

It is also worth noting that the apparent thickening coefficient, which is calculated from the slope of the HW linear extrapolation, overestimates the value chosen in the calculation of the T_m' versus T_x data. The data generated with γ_{xm} = 1, when fitted by a straight line in the T_x range from 120 to 130 °C, leads to an apparent thickening coefficient of γ_{HW} = 1.77. For the data generated with γ_{xm} = 2, γ_{HW} is equal to 3.54. The results of HW extrapolations carried out over various temperature intervals in the 100 to 140°C are shown in Table 2.3.

This exercise allows us to draw a number of conclusions. First, the linear extrapolation is not justified on theoretical grounds, as it is shown to hold only at exceedingly low undercoolings, which are not experimentally accessible. Second, the linear extrapolation leads to an underestimation of the equilibrium melting temperature and an overestimation of the thickening coefficient. The extent of this underestimation decreases as the thickening coefficient increases, but could become extremely significant if the range of undercoolings, over which the linear extrapolation is carried out, is far removed from the equilibrium melting temperature. We assert that the principal reason for the inaccuracy of the HW procedure lies in the neglect of the C_2. It

Table 2.3. Hoffman-Weeks analysis of theoretical T_m' versus T_x data generated using C_2 = 43.25 Å, σ_e^1 = 90.4 mJ/m^2, T_m = 145.5°C, for γ = 1 and γ = 2. The HW linear extrapolation is carried out over different temperature ranges from 100 to 140 °C.

		Temperature Range Considered			
		100°C-110°C	110°C-120°C	120°C-130°C	130°C-140°C
γ = 1	T_m (HW) (°C)	130.3	133.4	136.9	141.1
	γ_{HW}	2.74	2.23	1.77	1.36
γ = 2	T_m (HW) (°C)	139.6	141.2	142.9	144.6
	γ_{HW}	5.48	4.46	3.54	2.73

is noted that the linear extrapolation does not appear to lead to a large error in the case of PE, since this polymer crystallizes at relatively low undercoolings. However, the constant thickening coefficient assumption made here in the analysis of T_m', T_x data is not appropriate, as was clearly pointed by Alamo *et al*..[23] These authors clearly showed that, as a result of the temperature dependence of the lamellar thickening coefficient, it is actually very difficult to define rigorously a temperature region over which to carry out the extrapolation. These authors furthermore demonstrated that linear extrapolations lead to different "equilibrium melting temperatures" when carried out with series of samples exhibiting different degrees of crystallinity. Similar results were obtained by Hoffman and Weeks for poly(chlorotrifluoroethylene).[13] The origin of such discrepancies can now be understood as arising from (1) the fact that linear extrapolations are not justifiable even for samples crystallized at different temperatures but exhibiting the same lamellar thickening coefficient and (2) isothermal crystallization at different temperatures to the same level of crystallinity invariably leads to systematic variations in the lamellar thickening coefficient.

The above exercise also suggests that one should anticipate even larger errors for slower "crystallizers", such as isotactic poly(propylene) (it-PP), where the practical range of crystallization temperatures is further removed from the equilibrium melting temperature, and where, consequently, the average lamellar thicknesses are smaller than for PE. The case of it-PP will be discussed in detail in the next chapter. Finally, polymers such as it-PS, PEEK and PPS, whose crystals do not exhibit any isothermal lamellar thickening, deserve particular attention, as in this case, the difference between observed melting and crystallization temperatures cannot be accounted for by the magnitude of γ_{xm}, since it must be unity. If the use of the LH theory is still justified for these semi-flexible chain polymers, and if melting-recrystallization-remelting effects can be ignored, one would have to face the fact that the simple application of the HW procedure would lead to a very significant underestimation of their equilibrium melting temperatures (tens of degrees). For these materials, the assumption that the melting temperature depression is only associated with the thickness of the crystals and not with their width (Gibbs-Thomson equation)

may not even be valid, except possibly at the highest crystallization temperatures. This specific issue will be dealt with in future works.

2.2.5. New nonlinear analysis of experimental T_m', T_x data

We now consider another method for the analysis of experimental T_m' versus T_x data. Defining the quantities M and X (scaled melting and crystallization temperatures) by $M = T_m / (T_m - T_m')$ and $X = T_m / (T_m - T_x)$, respectively, and using the definition of the term a given in Equation 2.17, we can rearrange Equation 2.14 as

$$M = \gamma_{xm} \frac{\sigma_e^1}{\sigma_{em}} (X + a) \tag{2.19}$$

This simple equation seems to provide a means to assess whether the thickening coefficient, γ_{xm}, is constant or not. On the basis of linearity of an M versus X plot, one may be tempted to conclude that the quantities γ_{xm} and a are independent of temperature and can be obtained in a straightforward manner from the slope and intercept. In principle, this procedure provides access to the quantity C_2, if σ_e^1, σ_{em} and ΔH_f are known from independent measurements (in the absence of l^* versus ΔT data, we noted earlier that $\sigma_e^1 = \sigma_{em}$ may be a good approximation). Conversely, for a polymer crystal of unknown T_m, if the magnitude of γ_{xm} can be determined experimentally (*e.g.* SAXS, LAM Raman), then varying the equilibrium melting temperature until the correct value of γ_{xm} is obtained, would enable the determination of the equilibrium melting temperature. It is important to note that an observed non-linearity in an M versus X plot can arise for a variety of reasons, such as a significant but unrecognized temperature dependence of γ_{xm} or simply an inadequate choice of T_m. It should be recalled, in contrast, that the linearity in a T_m' versus T_x plot is not expected on theoretical grounds, nor should its observation prove γ_{xm} to be constant. Let us consider again the T_m' versus T_x data (shown in Figure 2.1), where we chose γ_{xm} to be either 1 or 2. Recalling that T_m' was calculated using the Flory-Vrij estimate of T_m (145.5°C), we can plot M versus X for different choices of T_m and attempt to infer from the linearity of these plots whether the appropriate value of T_m was selected. Such plots are shown on Figures 2.2a and 2.2b for T_m values of 138 °C, 145.5°C and 150°C for the cases $\gamma_{xm} = 1$ and $\gamma_{xm} = 2$, respectively.

For the case γ_{xm} = 2, it is clear that, except when the correct equilibrium melting temperature is used, the plots *M* versus *X* are no longer linear and the apparent slopes differ from the initially chosen γ_{xm} values.

In the case γ_{xm} = 1, these theoretical plots exhibit only minor curvature. This curvature would most likely not be observed due to data scatter, if experimental, instead of theoretical, values of the observed melting temperature were used. In this case, the artificial observation of linearity in the *M* versus *X* plot cannot guarantee that the correct equilibrium melting temperature was used. Recalling that the curvature in a *M* versus *X* plot increases with the magnitude of the thickening coefficient, we can state that an equilibrium melting temperature determination will be most accurate for crystals that exhibit large but constant thickening coefficients! This result is obviously discouraging as it is difficult, if not impossible, to crystallize samples at different temperatures with a-priori the same lamellar thickening coefficient. Historical considerations of the widespread use of the HW linear approach lead us to believe that one might be tempted to apply "blindly" the *M* versus *X* procedure to determine the equilibrium melting temperature for any polymer. Therefore, it is necessary to emphasize that scatter in the data and slight but unrecognized variations of γ_{xm} with temperature may prevent the optimum equilibrium melting temperature to be determined by this simple procedure, unless further assumptions are made, as will be discussed below.

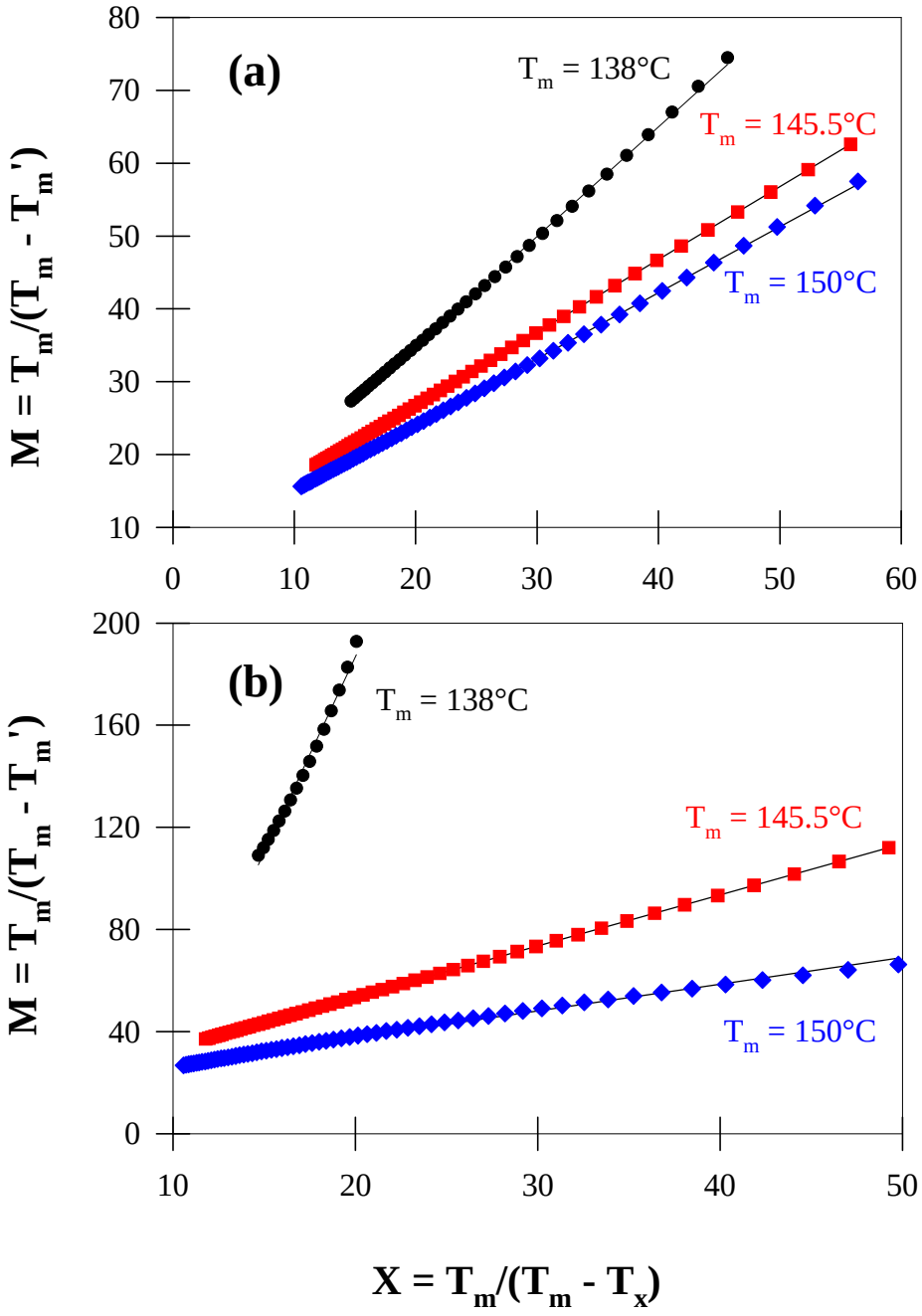

Figure 2.2. *M* versus *X* plot assuming T_m = 138°C (●), 145.5°C (■) or 150°C (♦). T_m' was calculated for each T_x using thermodynamic data in Table 2.1. Regression lines are shown to highlight the departure from linearity when T_m differs from the Flory-Vrij value used to calculate T_m' for each T_x. *M* and *X* were calculated using the above values of T_m. (a) for γ_{xm} = 1, (b) for γ_{xm} = 2.

2.2.6. Practical use and limitations of the *M-X* method

Having noted in the previous section that the temperature dependence of the lamellar thickening coefficient prevents an accurate determination of the equilibrium melting temperature through an optimization of an *M* versus *X* regression, we consider the case where the thickening coefficient is assumed to be constant and a-priori known and where the experimental data exhibit a certain amount of random scatter. This is equivalent to treating the case where polymer crystals formed at different temperatures exhibit slight and random variations in the thickening coefficient about a known average. We first generate a set of theoretical T_x, T_m' data points in the T_x range from 120°C to 130°C using the thermodynamic input parameters in Table 2.1 and an a-priori thickening coefficient γ. We then impart a certain amount of random scatter to the various T_m' values (maximum scatter was ± 0.3°C, which is considered an absolute upper bound rarely encountered by a careful experimentalist). Since we attempt to deal with practical situations, we only consider the analysis of a rather small number of data points. However, we "chose" the random scatter in such a way that the sum of the deviations between theoretical observed melting temperatures, T_m' and scattered observed melting temperatures, $T_{m\ scatt}$' is small (*ca.* 0.03°C). We then assume an equilibrium melting temperature T_m and calculate for this choice of T_m the magnitude of *X* and *M* associated with each T_x and $T_{m\ scatt}$'. A linear regression of the *M* versus *X* generated data allows us to derive values of a_{fit}, γ_{fit} . From these two values, we can calculate the fitted values of *M*, denoted M_{fit}, and the fitted observed melting temperature, $T_{m\ fit}$'. The sum of the squares of the deviations between the fitted observed melting temperatures and the scattered observed melting temperatures is then calculated and denoted by the quantity S^2. The process is repeated for different choices of the equilibrium melting temperature. These calculations are carried out for a number of initial sets of scattered observed melting temperatures. Typical results are shown in Figures 2.3 and 2.4 for the case $\gamma = 1$ and in Figures 2.5 and 2.6 for the case $\gamma = 2$. Focusing first on Figure 2.3, we note that the equilibrium melting temperature estimated from the first minimum in the variance S^2 for $\gamma = 1$ is 137.0°C, which is significantly lower than the expected value of 145.5°C. Furthermore, if this value of 137.0°C is chosen for the equilibrium melting temperature of polyethylene, the thickening coefficient derived from this analysis is estimated to be $\gamma_{fit} = 1.7$ as opposed to the expected value of 1.0.

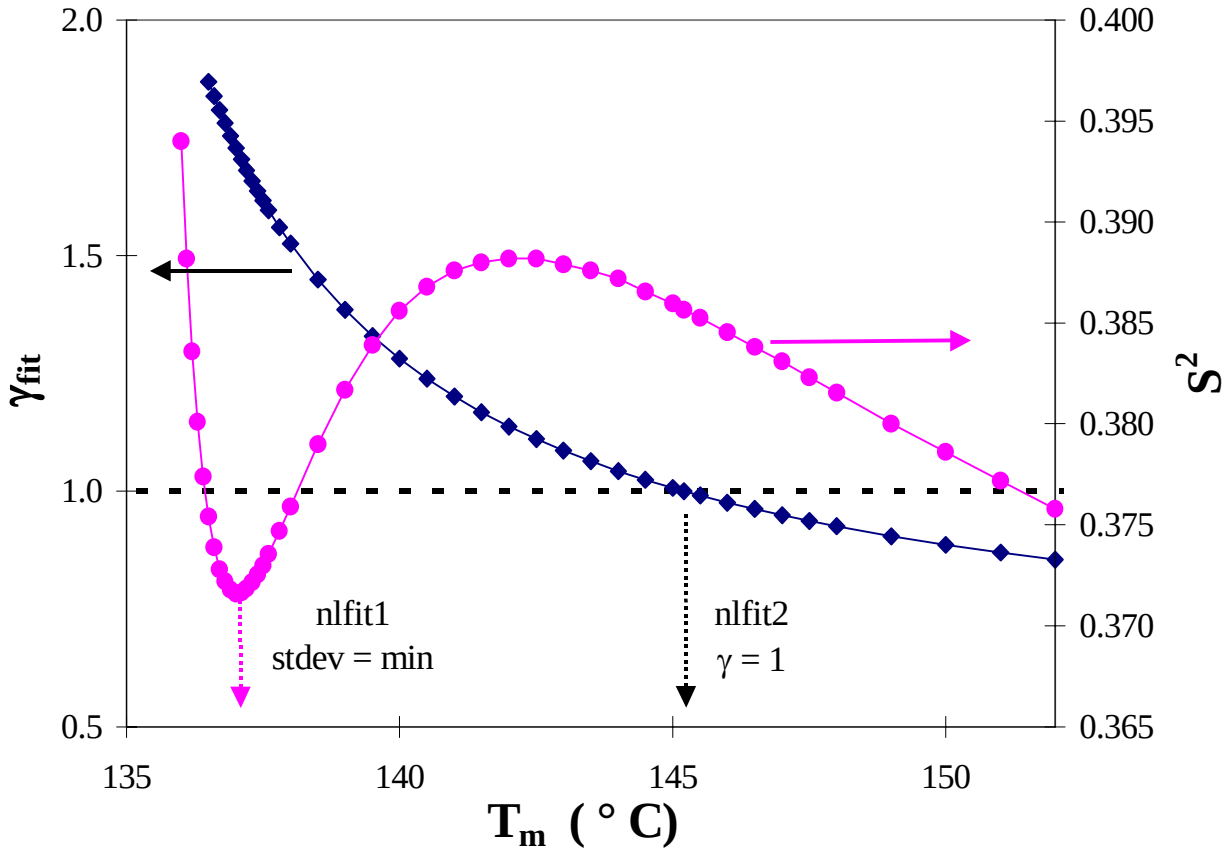

Figure 2.3. Dependence of the thickening coefficient, γ_{fit}, and of the variance, S^2, on the choice of the equilibrium melting temperature, T_m, used to generate the M versus X plot (see text for details). Case $\gamma = 1$.

Similarly, the C_2 value inferred from the quantity a_{fit} is estimated to be 4 Å instead of the expected 43.3 Å. If, on the other hand, we assume a-priori knowledge of the thickening coefficient (in this case $\gamma = \gamma_{fit} = 1$), we infer from the plot shown in Figure 2.3, that the equilibrium melting temperature is 145.2°C, which is an acceptable estimate of the theoretical equilibrium melting temperature (145.5°C). Under these conditions, the C_2 value inferred from the quantity a_{fit} is estimated to be 44.8 Å instead of the expected 43.3 Å.

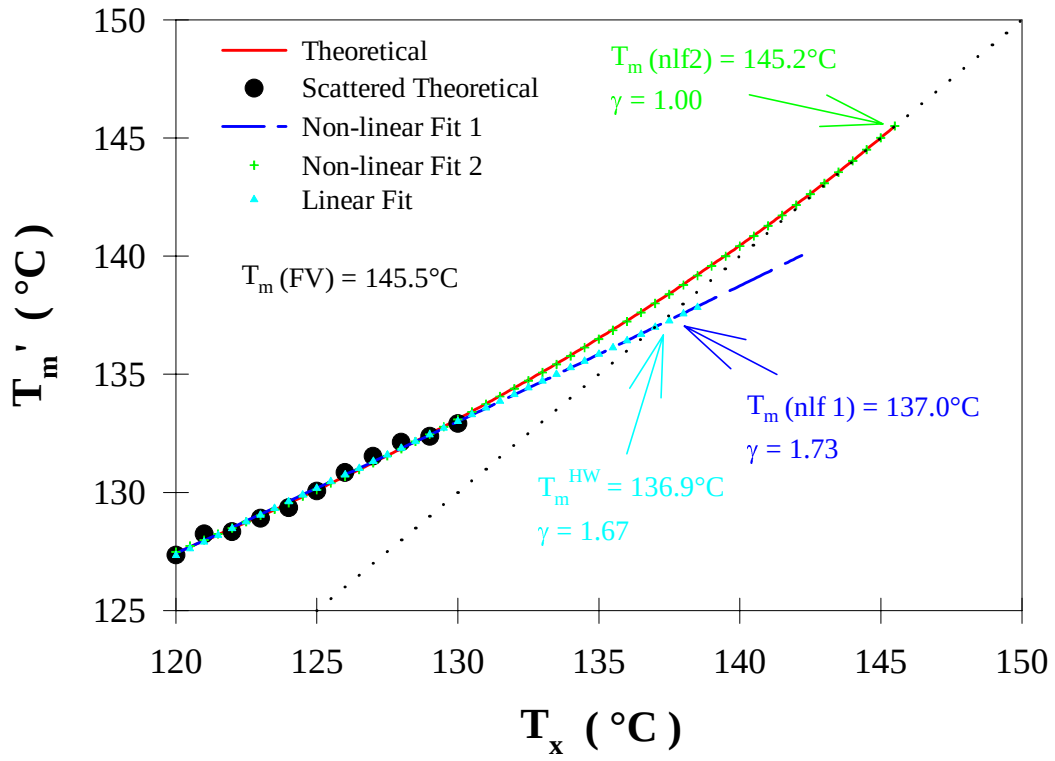

Figure 2.4. Variation of T_m' with T_x. Theoretical (Equation 2.14, full curve), Scattered theoretical in the 120 - 130°C temperature range (●), Non-linear fit 1 (T_m defined by the minimum of S^2, short dash curve), Non-linear fit 2 (T_m defined by γ = 1, +), HW linear regression and extrapolation (Equation 2.10). Case γ = 1.

On Figure 2.4, we show the theoretical variation of T_m' with T_x, the variation of $T_{m\ scat}$' with T_x, the linear HW extrapolation of the scattered data and the non-linear extrapolations of $T_{m\ scat}$' versus T_x for cases where T_m is chosen as 137.0°C (nlf1) or where γ is chosen as 1.0 (nlf2). Note that the non-linear fit nlf2 (γ = 1.0) cannot be discerned from the theoretical data and that the HW linear extrapolation significantly underestimates the equilibrium melting temperature and overestimates the thickening coefficient. Similar results are obtained for the case where we initially calculate T_m' from T_x for γ = 2. Minimization of the variance through changes of T_m

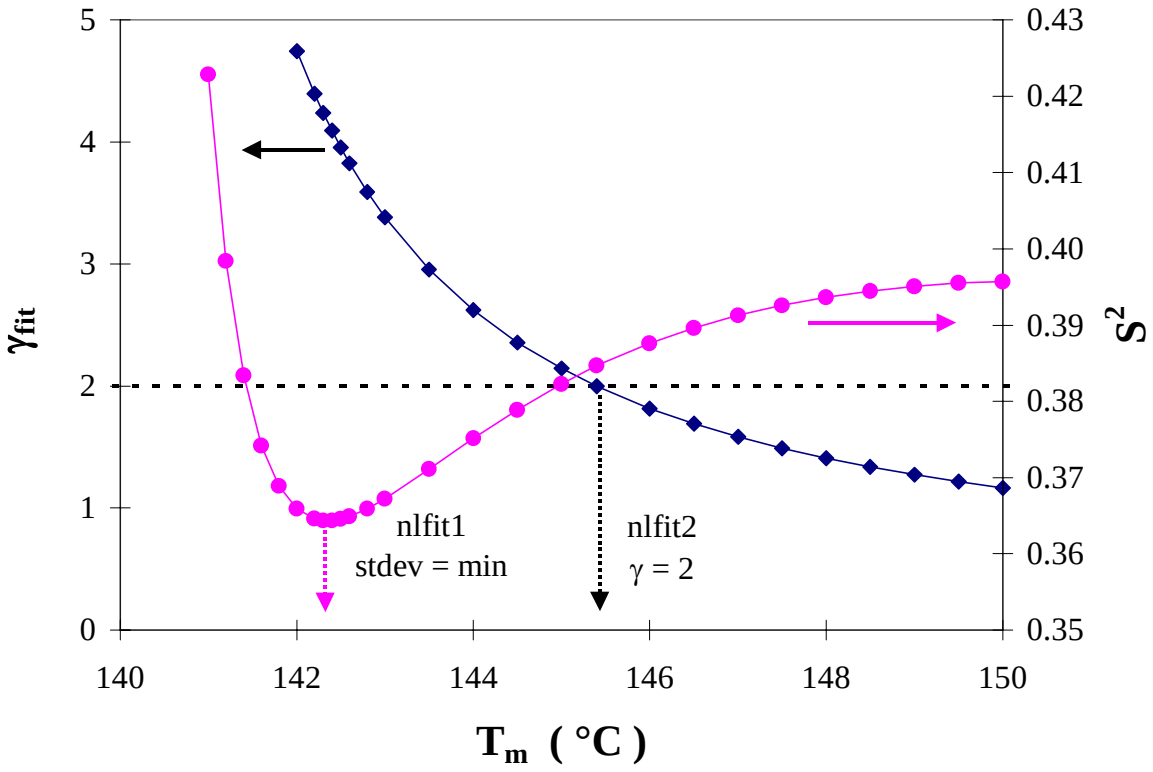

Figure 2.5. Dependence of the thickening coefficient, γ_{fit}, and of the variance, S^2, on the choice of the equilibrium melting temperature, T_m, used to generate the M versus X plot (see text for details). Case $\gamma = 2$.

leads to a more accurate estimation of the equilibrium melting temperature in the case $\gamma = 2$ than for $\gamma = 1$ (T_m = 142.3°C for $\gamma = 2$ nlfit1 on Figure 2.5). Again, assuming a-priori knowledge that $\gamma = 2$, leads to a further increase in the accuracy of the estimation of the equilibrium melting temperature (T_m = 145.4°C for nlfit2 on Figure 2.5). In this case, C_2 is estimated to be 45.2Å. In Figure 2.6, we show the theoretical variation of T_m' with T_x, the variation of $T_{m\ scat}$' with T_x, the HW linear extrapolation of the scattered data and the non-linear extrapolations of $T_{m\ scat}$' versus T_x for cases where T_m is chosen as 142.3°C (nlf1) or where γ is chosen as 2.0 (nlf2). Note again that the non-linear fit nlf2 ($\gamma = 2.0$) cannot be discerned from the theoretical data and that the HW linear extrapolation underestimates the equilibrium melting temperature and

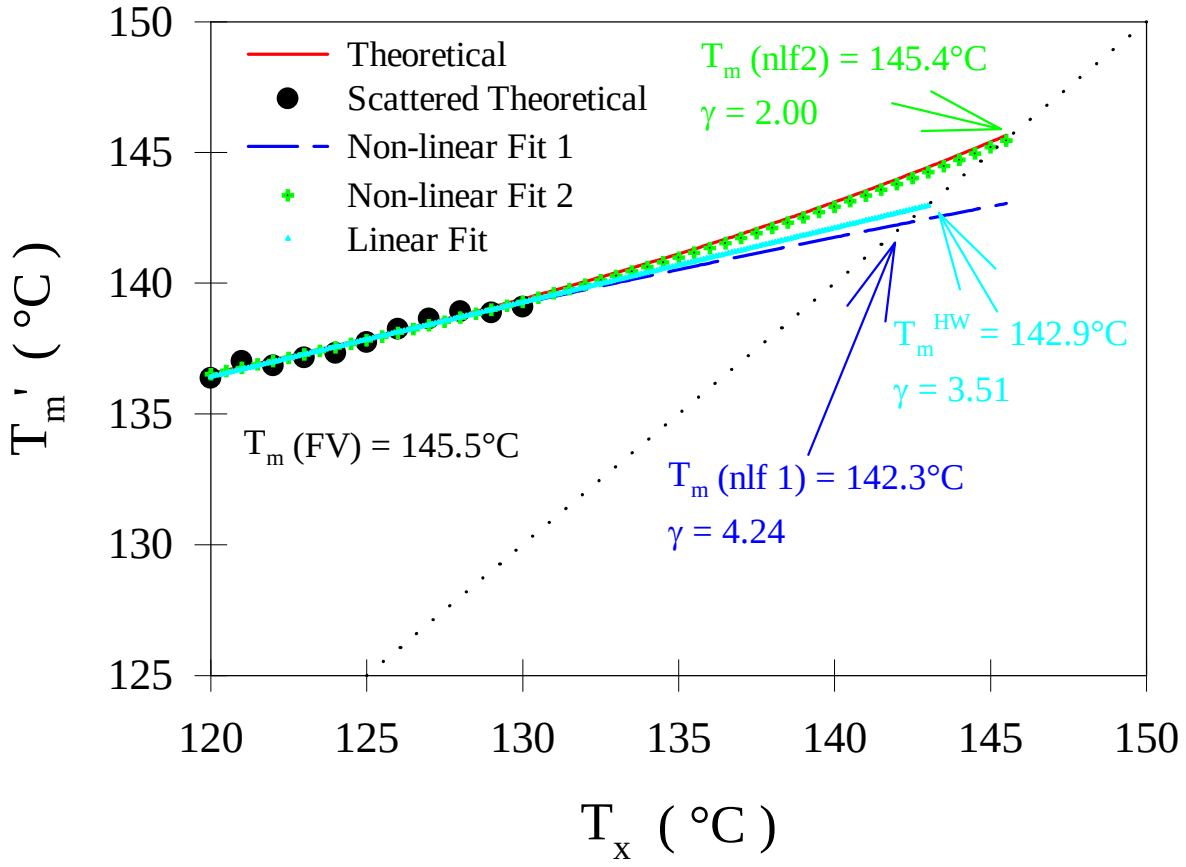

Figure 2.6. Variation of T_m' with T_x: Theoretical (Equation 2.14, full curve), Scattered theoretical in the 120 - 130°C temperature range (●), Non-linear fit 1 (T_m defined by the minimum of S^2, short dash curve), Non-linear fit 2 (T_m defined by $\gamma = 2$, +), HW linear regression and extrapolation (Equation 2.10). Case $\gamma = 2$.

overestimates the thickening coefficient. These results allow us to conclude that the *M* versus *X* approach can only provide an accurate estimation of the equilibrium melting temperature in two situations: (1) when the thickening coefficient is constant and much larger than unity, in which case an a-priori knowledge of the thickening constant is not required and an acceptable estimate (within a few degrees) of the equilibrium melting temperature can be obtained by minimizing the

variance of the fit (see above) and (2) when the thickening coefficient is known to be unity and the equilibrium melting temperature is determined using the constraint $\gamma = 1$. It is worth pointing out that the latter method appears to be significantly more accurate. We will show in the next chapter that the melting temperature of unthickened lamellar crystals ($\gamma = 1$) can indeed be inferred by extrapolation of the melting behavior of samples isothermally crystallized for different times.

In connection with the former method, it is noted that when γ is constant, two minima are generally observed in plots of the variance versus the equilibrium melting temperature (a hint for the existence of a second minimum at higher T_m values is apparent upon examination of Figures 2.3 and 2.5). This should be expected on the basis of the relationship between T_m' and T_x. Using Equation 2.14 and assuming $\sigma_{em} = \sigma_e$[1], we can express the quantity T_m' - T_x as a function of T_x.

$$T_m' - T_x = (T_m - T_x) - \left(\frac{T_m}{\gamma}\right)\left(\frac{T_m - T_x}{T_m + a(T_m - T_x)}\right) \tag{2.20}$$

The function T_m' - T_x = f(T_x) = 0 has two roots, T_m and T_m (1+ (1/a).(1-1/γ)). At each of these values, the theoretical T_m' = f(T_x) curve crosses the T_m' = T_x line. Obviously, the equilibrium melting temperature should correspond to the smaller of these two solutions since the quantity a must be positive and γ must be larger or equal to unity. Note that for $\gamma = 1$, the two roots are equal to each other and the theoretical T_m' = f(T_x) curve is tangential to the T_m' = T_x line at the equilibrium melting temperature. It is therefore important when using the above M versus X approach for large and constant γ to ensure that the non-linear regression analysis only yields the melting temperature associated with the first minimum of the variance versus temperature plot.

2.3. Conclusions

We have shown through an examination of the various assumptions inherent to the Hoffman-Weeks linear extrapolation that the increase in melting temperature with crystallization temperature cannot be solely attributed to the existence of lamellar thickening during crystallization or upon heating to the melting temperature. A significant contribution to the

difference between melting and crystallization temperatures arises from the C_2 term, which, in the LP secondary nucleation theory, accounts for both the temperature dependence of the fold surface free energy and the thickness increment δl above the minimum (thermodynamic) lamellar thickness. When the value chosen for C_2 for polyethylene is appropriately taken from experimental LAM or SAXS data (C_2 = 43.3 Å), it makes a significant contribution to the elevation of the melting temperature above the crystallization temperature. The contribution of the term C_2 leads to a non-linear relationship between observed melting temperature and crystallization temperature. Not accounting for this term (HW linear approach) leads to an underestimation of the equilibrium melting temperature and overestimation of the thickening coefficient. The inaccuracy of the HW linear extrapolation was shown to worsen for polymer crystals which do not thicken and have a relatively large value of C_2 and when it is carried out in the temperature range far from the true equilibrium melting temperature. The experimental observation of a linear T_m' - T_x behavior is shown to be inconsistent with a constant thickening coefficient. Finally, a new method is proposed for a more accurate estimation of equilibrium melting temperatures. This method should only be used to analyze T_m', T_x data, when T_m' values refer to real or hypothetical lamellar crystals exhibiting a temperature independent lamellar thickening coefficient. It is important to note that this new approach relies on a specific relationship between initial lamellar thickness and undercooling. This method is applied in the next two chapters to the cases of isotactic poly(propylene) and poly(ethylene oxide), where it is shown that the use of the linear HW extrapolation leads to an underestimation of the equilibrium melting temperature by as much as 25 - 30 °C for it-PP. The non-linear M versus X approach, when applied to the melting of unthickened crystals (γ = 1), yields an estimate of the equilibrium melting temperature which is consistent with that obtained from the analysis of the temperature dependence of spherulitic growth rate data, as will be shown in the next two chapters.

2.4. References

1. Hoffman, J.D.; Davis, G.T.; Lauritzen, J.I. In *Treatise on Solid State Chemistry*; Hannay, N.B. Ed.; Plenum Press: New York, **1976**; Vol. 3, Chapter 7.
2. Hoffman J.D.; Miller, R.L. *Polymer* **1997**, *38*, 3151
3. Armitstead, K.; Goldbeck-Wood, G. *Adv. Polym. Sci.* **1992**, *100*, 219
4. Point, J.J. *Disc. Faraday Soc.* **1979**, *68*, 167
5. Hoffman, J.D. Marand, H. personal communication
6. Stack, G.M.; Mandelkern, L.; Kröhnke, C.; Wegner, G. *Macromolecules* **1989**, *22*, 4351
7. Hoffman, J.D. *Polymer* **1991**, *32*, 2828
8. Marand, H.; Hoffman, J.D. *Macromolecules* **1990**, *23*, 3682
9. Wunderlich, B. *Macromolecular Physics*, Vol 3, "Crystal Melting", Academic Press, New York, **1980**.
10. Broadhurst, M.G. *J. Chem. Phys.* **1962**,*36*, 2578
11. Flory, P.J.; Vrij, A. *J. Am. Chem. Soc.* **1963**, *85*, 3548
12. Mandelkern, L.; Stack, G.M. *Macromolecules* **1984**, *17*, 871
13. Hoffman, J.D.; Weeks, J.J. *J. Res. Natl. Bur. Stand. U.S.A.* **1962**, *A66*, 13
14. Huang, J.; Prasad, A.; Marand, H. *Polymer* **199**4, *35*, 1896
15. Huang, J.; Marand, H. *Macromolecules* **1997**, *30*, 1069
16. Buckley, C.P.; Kovacs A.J. *Colloid Polym. Sci.* **1976**, *254*, 695
17. Marand, H.; Barham, P.J., in preparation
18. Ruland, W. *Colloid Polym. Sci.* **1977**, *255*, 417
19. Albrecht, T.; Strobl, G. *Macromolecules* **1995**, *28*, 5267
20. Lovinger, A.J.; Hudson, S.D.; Davis, D.D. *Macromolecules* **1992**, *25*, 1752
21. Lovinger, A.J. *Bull. Am. Phys. Soc.* **1988**, *33*, 718
22. Groeninckx, G.; Reynaers, H.; Berghmans, H.; Smets, G. *J. Polym. Sci., Polym. Phys. Ed.* **1980**, *18*, 1311
23. Alamo, R.G.; Viers, B.D.; Mandelkern, L. *Macromolecules* **1995**, *28*, 3205
24. Boyd, R. *Polymer* 1985, *26*, 323; *ibid* **1985**, *26*, 1123
25. Khoury, F. *J. Res. Natl. Bur. Stand.* **1966**, *70A(1)*, 29

26. Lotz, B.; Wittmann, J.C. *J. Polym. Sci., Polym. Phys. Ed.* **1986**, *24*, 1541
27. Verma, R.K.; Velikov, V.; Kander, R.G.; Marand, H.; Chu, B.;Hsiao, B.S. *Polymer* **1996**, *37*, 5357
28. Verma, R.K.; Marand, B.S.; Hsiao, B. *Macromolecules* **1996**, *29*, 7767
29. Blais, J. J. B.P.; St. John Manley, R. *J. Macromol. Sci.-Phys.* **1967**, *B1(3)*, 525
30. Hsiao, B.S. *Bull. Am. Phys. Soc.* **1997**, *42(1)*, 146
31. Barham, P.J.; Chivers, R.A.; Keller, A.; Martinez-Salazar, J.; Organ, S.J. *J. Mat. Sci.* **1985**, *20*, 1625
32. Jones, D.H.; Latham, A.J.; Keller, A.; Girolamo, M. *J. Polym. Sci., Polym. Phys. Ed.* **1973**, *11*, 1759
33. Magill, J.H.; Girolamo, M.; Keller, A. *Polymer* **1981**, *22*, 43
34. Barham *et al.* (*J. Polym. Sci., Polym. Phys. Ed.* **1989**, *27*, 1029) have suggested a very rapid doubling of the initial lamellar thickness in linear PE at early crystallization time. However, these observations were not substantiated in subsequent work by Bark *et al.* (*Makromol. Chem.* **1992**, *193*, 2363) and Albrecht et al. (*Macromolecules* **1996**, *29*, 783.
35. Stack, G.M.; Mandelkern, L.; Voigt-Martin, I.G. *Polym. Bull.* **1982**, *8*, 421
36. Morra, B.S.; Stein, R.S. *J. Polym. Sci., Polym. Phys. Ed.* **1982**, *20*, 2243
37. Linear relationship between initial lamellar thickness and undercooling have also been observed for poly(ethylene oxide) (Cheng *et al*. *Macromolecules* **1992**, *25*, 1453) and poly(oxymethylene) (Korenaga *et al*. *Polymer J*. **1972**, *3*, 21). In both cases experimentally dertermined C_2 is much larger than δl_x.
38. Lauritzen, J.I.; Passaglia, E. *J. Res. Natl. Bur. Stand.* **1960**, *A64*, 73
39. Hoffman, J.D.; Lauritzen, J.I.Jr.; Passaglia, E.; Ross, G.S.; Frolen, L.J.; Weeks, J.J. *Kolloid Z. u. Z. Polym.* **1969**, *231*, 566
40. Miller, R.L. *Kolloid Z. u. Z. Polym.* **1968**, *2225*, 62
41. Richardson, M.J. *Trans. Faraday Soc.* **1965**, *61*, 1876
42. Snyder, C.R.; Marand, H. *Macromolecules* **1997**, *37*, 2759
43. Xu, J.; Srinivas, S.; Marand, H. Agarwal, P. *Macromolecules* **1998**, 31, 8230.
44. Xu, J., Srinivas, S., Subramaniam, C., Marand, H. *Bull. Am. Phys. Soc.* **1998**, *43*, 596

45. Davis, G.T.; Eby, R.K.; Colson, J.P. *J. Appl. Phys.* **1970**, *41*, 4316

Chapter 3. Equilibrium Melting Temperature and Temperature Dependence of the Spherulitic Growth Rate of isotactic Poly(propylene)

3.1. Introduction

In the last chapter, it is suggested that in the absence of isothermal lamellar thickening effects, the equilibrium melting temperature of a crystallizable polymer can be obtained through consideration of the non linear dependence of the observed melting temperature on crystallization temperature.[1] Studies to be discussed in the present paper indicate that such concepts can be successfully applied to the case of isotactic poly(propylene) synthesized with Ziegler-Natta catalysts. Specifically, our results indicate that the equilibrium melting temperature for the α–phase of it-PP derived from the non-linear Hoffman-Weeks (HW) analysis is in good agreement with that derived from a study of the temperature dependence of isothermal spherulitic growth rates.

It-PP is specifically chosen for this study for three reasons: first, there appear to be considerable discrepancies in the literature between values reported for both the equilibrium melting temperature[2-18] and the secondary nucleation constants;[7-10,20-33] second, some claims have been made[9,12] that there is agreement between the evaluation of the equilibrium melting temperature by the linear HW and the Gibbs-Thomson (GT) approaches, which, if verified, would contradict the assertion from the last chapter that the linear HW extrapolation[34] is not justified on theoretical grounds and third, the recent synthesis of isotactic poly(propylene) of controlled defect content and type, using metallocene catalysts, has led to a renewed interest in this polymer in academic and industrial circles and comparison of these polymers to their Ziegler-Natta counterpart requires the knowledge of the effect of defects on the equilibrium melting temperature.

Another important issue addressed in this manuscript is concerned with the general applicability of the Lauritzen-Hoffman (LH) secondary nucleation theory.[35,36] Although the LH concepts seem to successfully account for a large number of experimental observations in the

case of linear polyethylene, criticism of the concept of regimes continues to appear in the literature.[37] It has been stated before and is important to realize that a proper test of the LH secondary nucleation theory cannot be carried out in the absence of an accurate estimate of the equilibrium melting temperature for that polymer. Critics of the regime theory have emphasized that experimentally observed regime transitions are too sharp to be associated with a change in the surface nucleation rate.[37] Such criticism can be considered meaningful only if the experimental data are evaluated with an acceptable estimate of the equilibrium melting temperature and with knowledge of the uncertainty associated with the experimental growth rates. Similarly, evaluation of secondary nucleation constants for regimes II and III and comparison of their ratio to the LH theoretical predictions[34, 35] demand that the correct equilibrium melting temperature be used, as it is known that their magnitude depends sharply on the equilibrium melting temperature adopted in the analysis.

Finally, it is shown that a careful analysis of both the temperature dependence of the spherulitic growth rate and the relationship between crystallization and observed melting temperatures provide some stringent conditions on possible values for the equilibrium melting temperature, basal plane interfacial free energy and C_2 parameter. These constraints allow one to predict not only the temperature dependence of the initial lamellar thickness ($l^* = C_1/\Delta T + C_2$), but also the crystallization time dependence of the average lamellar thickness when experimental data on the evolution of the melting behavior with crystallization time is available. Comparison of these theoretical predictions with actual experimental morphological data would then constitute a final and necessary check as to the self-consistency of the parameters derived from the spherulitic growth rate analysis. It is only under such conditions that secondary nucleation parameters obtained for different polymers can be compared and correlation between chain structure and crystallization behavior can be drawn.

3.2. Experimental procedures

Three narrow molecular weight distribution isotactic poly(propylene) fractions of relatively high isotactic content, from the Exxon Chemical Company were used in this study. Sample characteristics are listed in Table 3.1. Thin films (*ca.* 50 μm) were prepared by melt pressing at *ca.* 200 psi in a hot press at 210°C under dry nitrogen purging and subsequent quenching in an ice-water mixture. Prior to carrying out the isothermal crystallization studies, it-PP films were melted at 200 °C for 5 minutes under nitrogen in a Linkam heating stage whose temperature scale was calibrated with benzoic acid, indium and tin. The samples were crystallized isothermally at temperatures in the range from 123 to 155°C and the spherulitic growth was recorded using a Zeiss polarized light optical microscope equipped with a Javelin video camera and Hitachi videotape recorder. The diameter of the spherulites was recorded as a function of crystallization time using a calibrated video caliper. As expected, the spherulite radius was observed to increase linearly with crystallization time until impingement. Under isothermal conditions, spherulitic growth rates are then calculated from the slope of the spherulite radius versus time plots. For each crystallization temperature, an average spherulitic growth rate was estimated from a minimum of 5 individual experiments, each being carried out with a fresh film. The uncertainty on these average growth rates was invariably less than 5% of the magnitude of *G*. The spherulitic growth rates were shown to be independent of film thickness for thicknesses larger than 15 μm. The uncertainty associated with temperature fluctuations in the heating stage was estimated to be ± 0.1°C.

Table 3.1. Sample characteristics of it-PP provided by the manufacturer.

Sample ID	M_n (g/mol)	M_w/M_n	Regio defect	Stereo-defect
it-PP1	26 700	2.38	0	1.17
it-PP2	41 800	2.09	0	1.11
it-PP3	78 300	3.56	0	1.14

It-PP samples were also crystallized under isothermal conditions in the temperature range from 126 to 146°C in a Perkin Elmer differential scanning calorimeter model 2 operated under nitrogen flow and calibrated at different heating rates with high purity standards from Perkin Elmer Co.. Crystallization temperatures were calibrated by extrapolation of the melting temperature of the standard to zero heating rate. The melting behavior of isothermally crystallized samples was recorded by heating these samples from their crystallization temperature up to 220°C at a rate of 10°C/min. The observed melting temperature was taken as the peak temperature, corrected for thermal lag.

Morphological studies were carried out for it-PP samples after being isothermally crystallized for a given time in the temperature range 126 - 150°C in the heating stage under the protection of the dry nitrogen. For each crystallization temperature, enough time (available from the DSC studies) was given for the it-PP sample to finish the primary crystallization. Then the it-PP samples were quenched to room temperature. Morphological measurements were conducted in a NanoScope III SPM instrument (Digital Instrument) operating in a tapping mode at room temperature. In the tapping mode of AFM, an etched single crystal silicon probe is mounted at the end of a cantilever, which vibrates at or near its resonance frequency. The detected signal is the deflection of this lever caused by a force due to the interaction between the tip and the specimen. Height and phase images of the specimen surface are achieved by recording the amplitude and the phase changes of the cantilever during the interaction with the specimen. Phase image was used to measure the lamellar thickness, and a large amount of measurements were completed for each sample with the average taken as the lamellar thickness specific to a given crystallization temperature.

3.3. Results

This section is organized into four parts. The first three parts are results of the it-PP fraction 2 with M_n = 41 800g/mol and the results of other two it-PP fractions are presented in the last part. The first three parts are arranged as: first, the non-linear HW analysis based on the data

from the DSC studies, second, the analysis of the temperature dependence of the spherulitic growth rates and third, the temperature dependence of the lamellar thickness measured by AFM.

3.3.1. Non-linear Hoffman-Weeks analysis

The equilibrium melting temperature of it-PP was determined following the method described in the last chapter. As was discussed in the last chapter, for any T_m' versus T_x type analysis to be meaningful and reliable, it is imperative that the lamellar thickening coefficient be the same for samples crystallized at different temperatures. When isothermal lamellar thickening occurs, its rate increases with crystallization temperature. On the other hand, in the usual temperature range where crystallization proceeds isothermally from the melt state, the rate of crystallization decreases with increasing temperature. It is then generally an impossible task to crystallize a given polymer over a wide range of crystallization temperatures, while ensuring a constant thickening coefficient. Rather than adjusting the crystallization time at a given crystallization temperature to control the extent of thickening, it appears more practical to obtain the observed melting temperature of non-thickened crystals (γ = 1) by extrapolation of the melting temperature of thickened lamellae to zero crystallinity.

To determine the observed melting temperature of original lamellar crystals, we follow simultaneously the evolution of the crystallinity and the observed melting temperature with crystallization time during primary crystallization for various crystallization temperatures. The expected melting temperature of initial lamellar crystals, T_m', is then estimated by extrapolation to the time where crystallinity is first detected. An example of the above analysis is shown in Figure 3.1 for a crystallization temperature T_x = 136°C for it-PP2. The crystallinity at time t_x is determined from the heat of fusion recorded by calorimetry during a heating run initiated at T_x after crystallization for time t_x. Fitting the evolution of the crystallinity with time at early crystallization times allows one to determine t_o, the induction time at this crystallization temperature. For a given crystallization temperature, the observed melting temperature, T_m', increases linearly with the logarithm of crystallization time during the primary crystallization

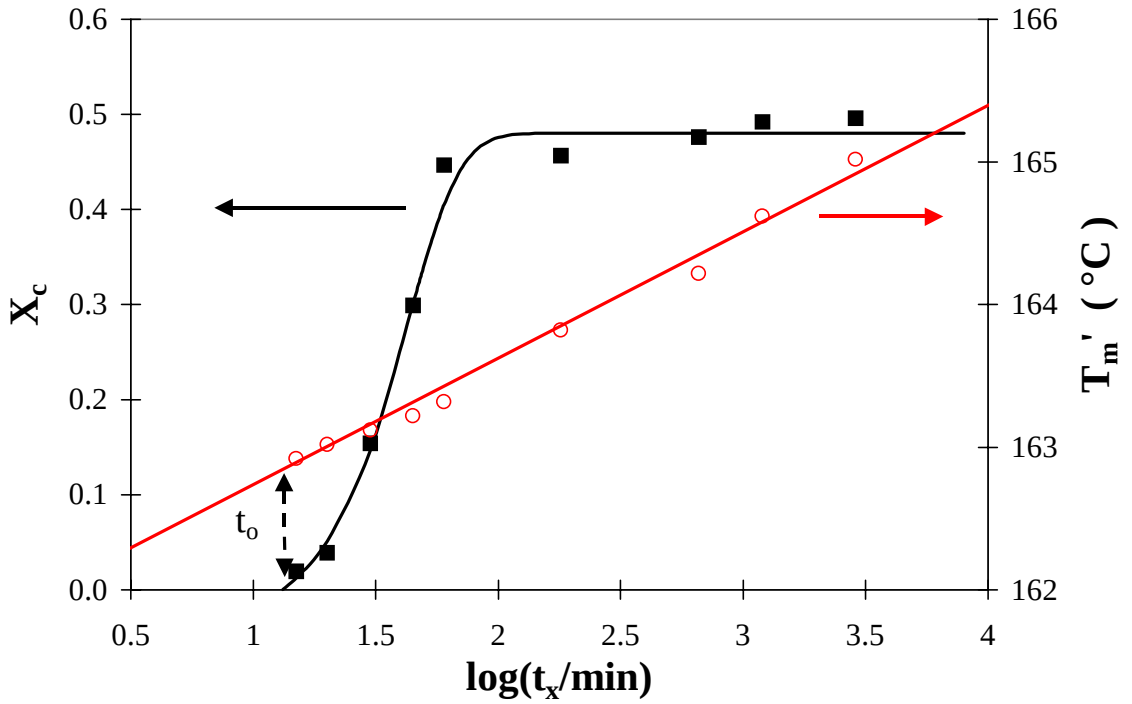

Figure 3.1. Evolution of the degree of crystallinity, X_c, and the observed peak melting temperature with crystallization time at 136.0°C for it-PP2, M_n = 41 800 g/mol.

stage. We can then define parameters $A(T_x)$ and $B(T_x)$ for each crystallization temperature such that:

$$T_m'[T_x,t_x] = A[T_x] + B[T_x] \log [t_x] \tag{3.1}$$

The observed melting temperature of original crystals at T_x is then estimated as

$$T_m'[T_x,t_o] = A[T_x] + B[T_x] \log [t_o] \tag{3.2}$$

A similar behavior for the evolution of the melting temperature with crystallization time is observed for different crystallization temperatures (Figure 2.2, data for it-PP2). Combining data shown in Figure 2.2 with the corresponding evolution of the degree of crystallinity with time allows one to derive the parameters $A[T_x]$, $B[T_x]$ for each crystallization temperature, the induction $t_o(T_x)$ and $T_m'[T_x, t_o]$, the melting temperature of initial lamellar crystals at $t_o(T_x)$ (Table 3.2).

Let us define the quantities M and X by[1] $M = T_m / (T_m - T_m')$ and $X = T_m / (T_m - T_x)$, where T_m is the equilibrium melting temperature, T_m' is the observed melting temperature of original crystals formed at T_x. For a set of T_m', T_x values, corresponding sets of M, X values can be calculated for a given choice of the equilibrium melting temperature. It has been shown in the previous chapter that if the initial lamellar thickness is given by $l_g^* = C_1/\Delta T + C_2$, where C_1 is equal to $2\sigma_e^1 T_m/\Delta H_f$ and C_2 is a constant accounting for both the term δl_x and the temperature dependence of the kinetic fold surface free energy σ_{ex}, then the crystallization temperature dependence of the observed melting temperature can be rewritten as[1]

Table 3.2. Parameters describing the crystallization time dependence of the observed melting temperature and the induction time for the primary stage of isothermal crystallization at different temperatures for it-PP2, M_n = 41 800 g/mol. Also shown are the observed melting temperatures of the initial lamellar crystals (at the induction time or zero crystallinity).

T_x (°C)	$A[T_x]$ (°C)	$B[T_x]$ (°C)	$t_o(T_x)$ (min)	$T_m'[T_x,t_o]$
126.0	158.72	0.63	0.2	158.3
129.0	160.06	0.76	1.5	160.2
131.0	160.33	0.82	4.6	160.9
134.0	161.33	0.86	7.3	162.1
136.0	161.85	0.89	11.7	162.8
139.0	161.73	1.49	27.9	163.9
141.0	162.18	1.71	36.5	164.9
146.0	163.83	1.97	50.0	167.2

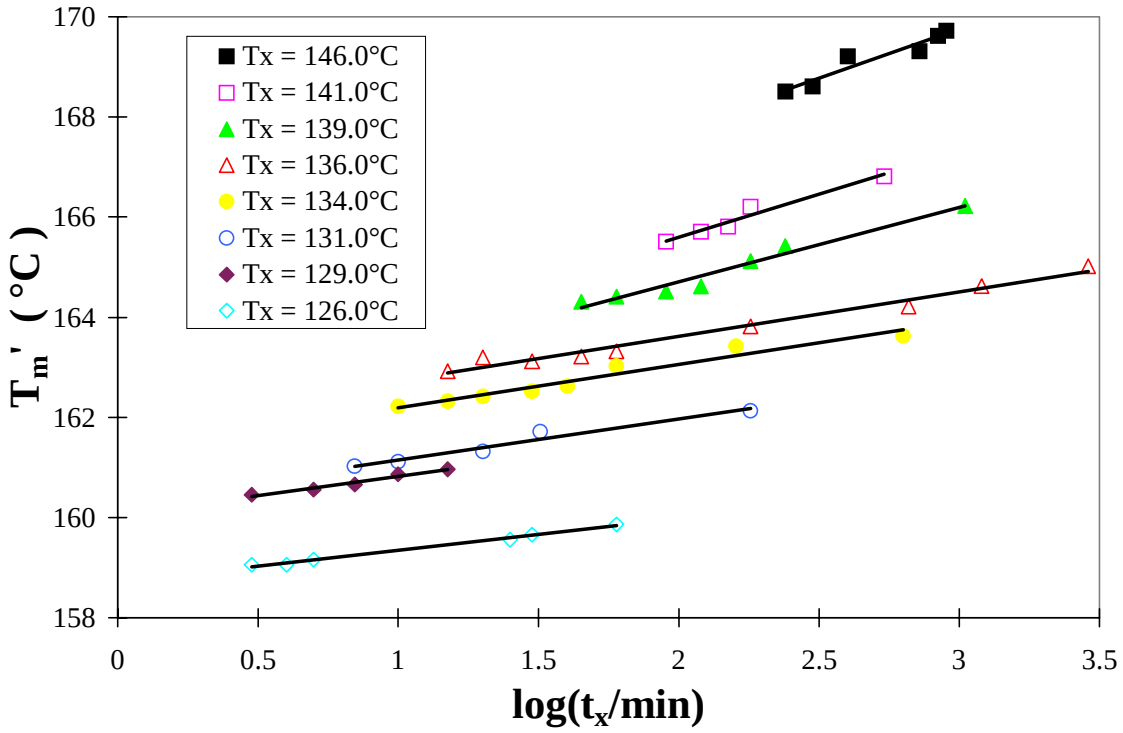

Figure 3.2. Evolution of the observed peak melting temperature with crystallization time at various crystallization temperatures for it-PP2, M_n = 41 800 g/mol.

$$M = \gamma\left(\frac{\sigma_e^{\,1}}{\sigma_{em}}\right)(X + a) \tag{3.3}$$

where σ_{em} is the fold surface free energy appearing in the Gibbs-Thomson equation, $a = \Delta H_f C_2 / 2\sigma_e^{\,1}$. It has been discussed in the last chapter that σ_{em} may a prior differ slightly from $\sigma_e^{\,1}$. However, studies of linear polyethylene suggest that, within experimental uncertainty (ca. 5 – 10%), these quantities cannot be unambiguously differentiated. ΔH_f is the theoretical heat of fusion and C_2, as noted in the last chapter, is a function of δl_x, the lamellar thickness increment above the minimum lamellar thickness necessary for crystal growth to proceed at a finite rate. When this method is applied to the melting of "original" crystals ($\gamma = 1$), a plot of M versus X for the "true" equilibrium melting temperature should yield a straight line of slope unity (if $\sigma_e^{\,1}$ =

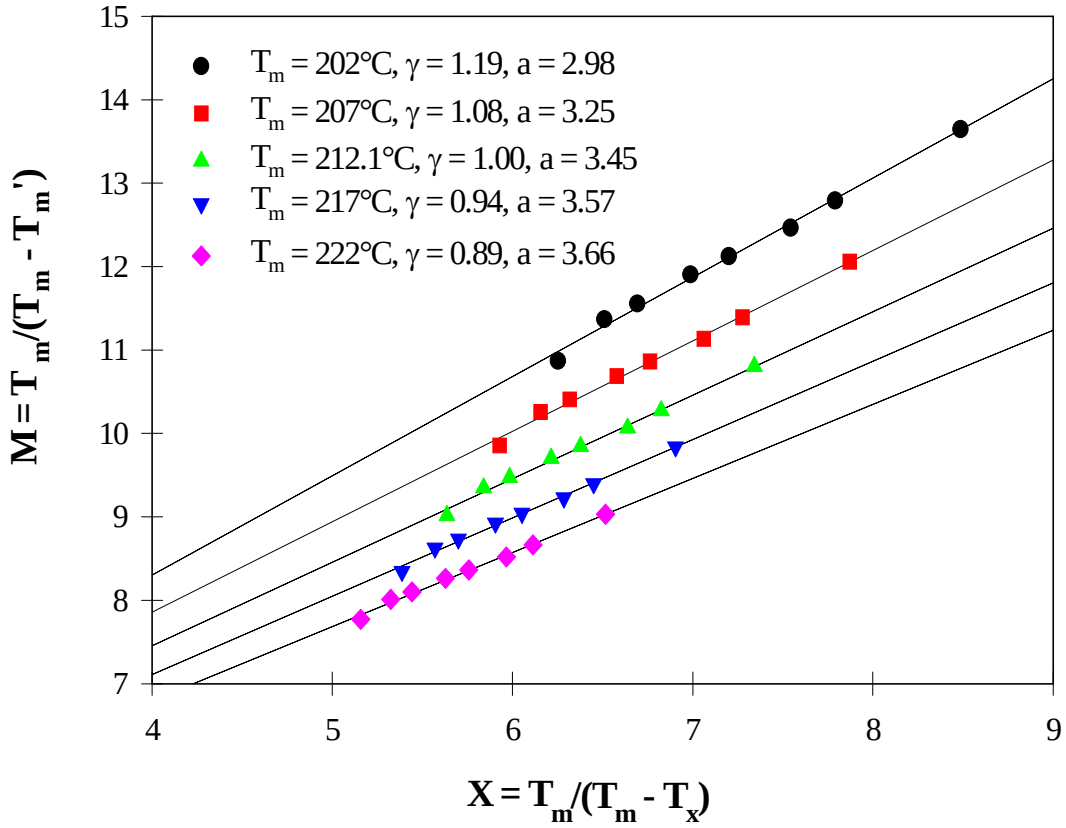

Figure 3.3. Plot of the scaled observed melting temperature $M = T_m/(T_m-T_m')$ versus scaled crystallization temperature $X = T_m/(T_m-T_x)$ for various choices of the equilibrium melting temperature, T_m, for it-PP2, M_n = 41 800 g/mol.

σ_{em}) and intercept equal to a. Figure 3.3 shows the evolution of M versus X plots for different choices of the equilibrium melting temperature in the case of it-PP2. Figure 3.4 shows the variation in the slope of M versus X plots with the value adopted for the equilibrium melting temperature for it-PP2. The equilibrium melting temperature of it-PP2 obtained by this method (γ =1) is found to be T_m = 212.1°C. The value of a associated with this equilibrium melting temperature is then obtained from the intercept of M versus X with the M axis (a = 3.45). Figure 3.5 shows the evolution of the extrapolated melting temperature of initial crystals with crystallization temperature for it-PP2. Also shown are the HW linear and non-linear extrapolations constructed as described in the last chapter. It is quite clear that the linear and non-linear extrapolations lead to significantly different estimates of the equilibrium

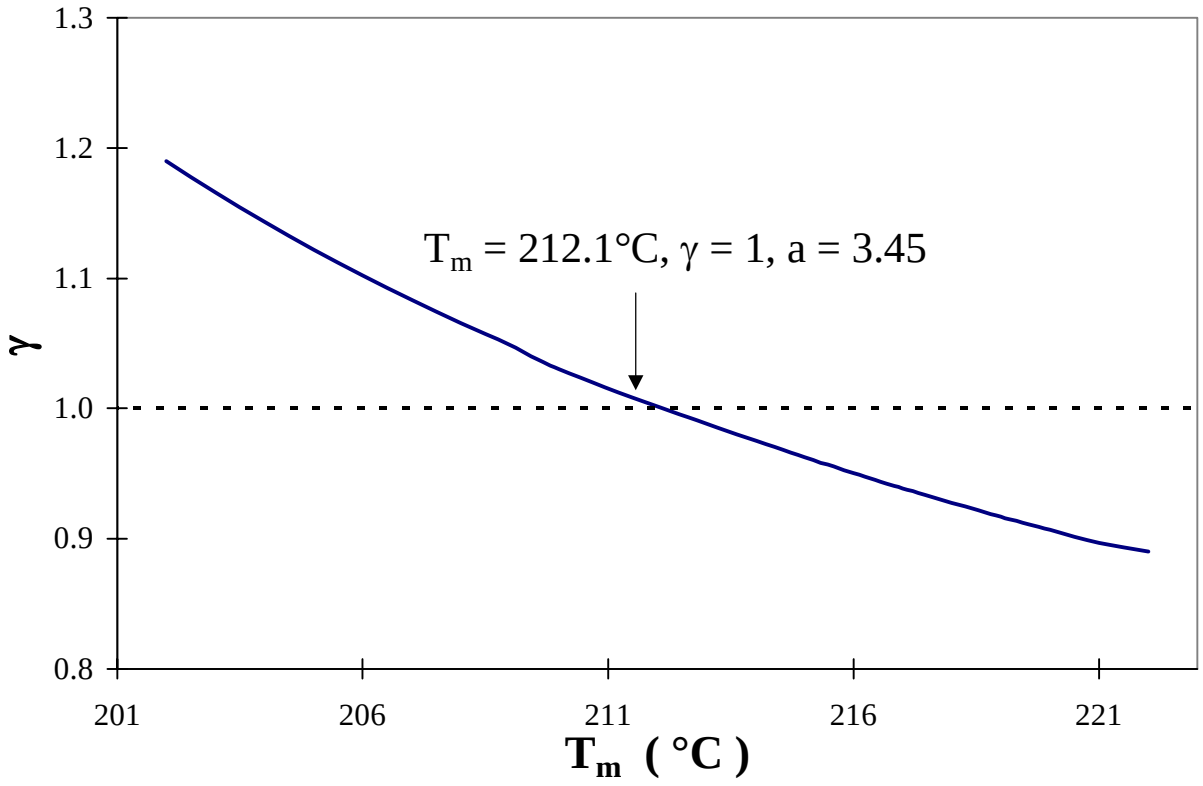

Figure 3.4. Plot of the thickening coefficient, γ, as a function of the chosen equilibrium melting temperature for it-PP2, M_n = 41 800g/mol.

melting temperature, the non-linear estimate being higher by about 30°C. Furthermore, the apparent thickening coefficient inferred from the linear HW analysis is estimated to be $\gamma = 2.4$ for it-PP2, a value which is physically meaningless, as it would imply instantaneous and significant thickening of polymer lamellae at very short times after their formation. The constant apparent thickening coefficient suggested by the linear HW analysis[34] is furthermore inconsistent with the increase in thickening rate with crystallization temperature which can be inferred from Figure 3.2 (data in Table 3.2) and from the literature.[12,38,39]

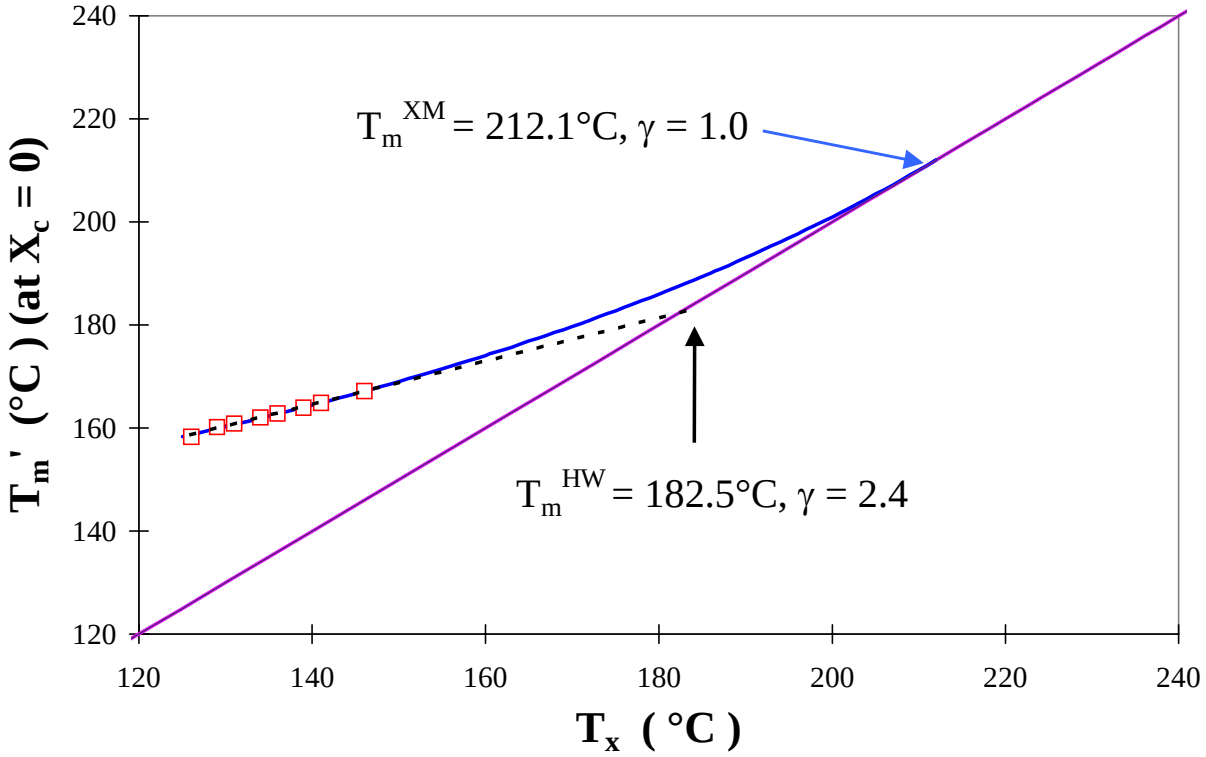

Figure 3.5. Plot of the observed melting temperature of initial lamellar crystals versus crystallization temperature for it-PP2, M_n = 41 800 g/mol. The solid curve is the non-linear HW extrapolation calculated using a = 3.45, γ =1 and T_m = 212.1°C. The dotted curve is the linear HW extrapolation based on experimental data points (□).

3.3.2. Temperature dependence of spherulitic growth rates

Spherulitic growth rates for the α-phase of it-PP measured at temperatures between 123 and 154°C are plotted as a function of crystallization temperature in Figure 3.6. A barely visible discontinuity in the temperature dependence of the curvature of ln G versus T_x is observed around 139°C - 140°C. This discontinuity has been observed by previous investigators in the same temperature range and has been interpreted as a regime II - III transition.[8-10,27-33] To analyze these data in the context of the Lauritzen-Hoffman secondary nucleation theory,[35,36] the growth rate is plotted as a function of the undercooling according to the classical equation:

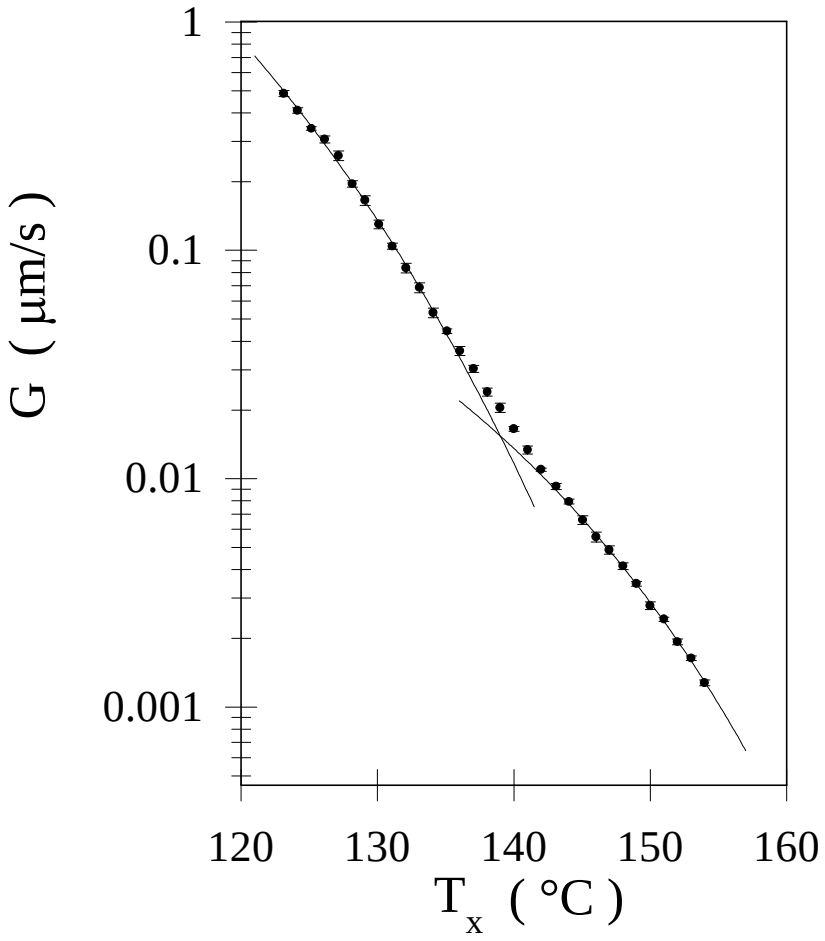

Figure 3.6. Plot of experimental spherulitic growth rate versus crystallization temperature for it-PP2, M_n = 41 800g/mol. Error bars for the magnitude of the growth rate at each crystallization temperature are shown. The solid curves represent the theoretical expressions of G versus T_x in each regime calculated using Equation 3.4 and data in Table 3.8 for T_m = 212.1°C.

$$\ln G_j + \frac{U^*}{R(T_x - T_\infty)} = \ln G_j^0 - \frac{K_{gj}}{T_x(T_m - T_x)} \tag{3.4}$$

where U^* and T_∞ are the Vogel-Fulcher-Tamman-Hesse parameters describing the transport of polymer segments across the liquid/crystal interphase and K_{gj} is the secondary nucleation constant in a given regime and G_j^0 is a prefactor assumed to be independent of temperature. Although we initially chose for the VFTH parameters the universal values recommended

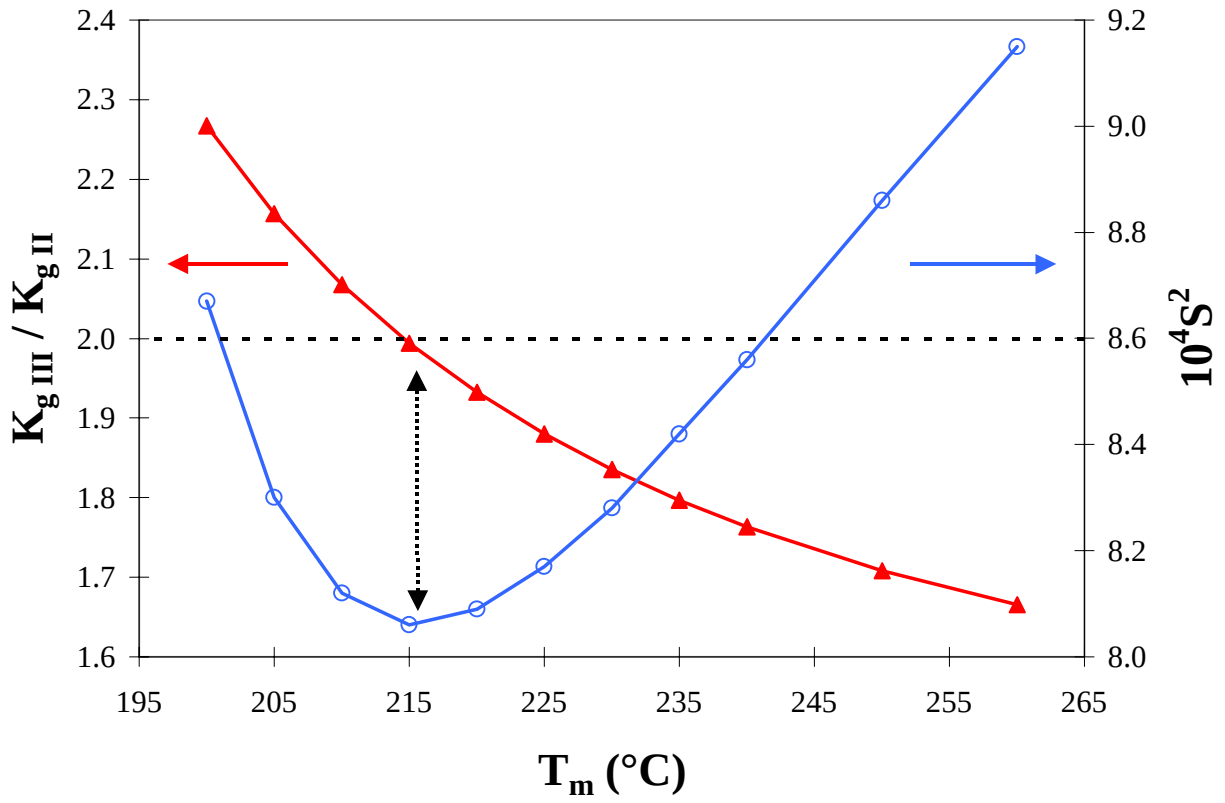

Figure 3.7. Ratio of secondary nucleation constants in regimes III and II, $K_{g\,III} / K_{g\,II}$, and overall variance of the fit, S^2, as a function of the chosen equilibrium melting temperature, T_m, for it-PP2, M_n = 41 800 g/mol.

by Hoffman *et al.*[35, 36] (*i.e.* U^* = 1500 cal/mol and $T_\infty = T_g$ -30K), similar analyses were also carried out using different pairs of U^* and T_∞, inferred from viscoelastic measurements on at-PP melts by Plazek *et al.*[40] and by Pearson *et al.*[41] Since we do not know a-priori the equilibrium melting temperature, T_m, for the α-phase of it-PP, we use a technique developed earlier for spherulitic growth studies on poly(pivalolactone)[42,43] by Huang et al. and calculate, for a given choice of T_m , the variance of the fit of the growth rate data to Equation 3.4. The equilibrium melting temperature appropriate for the polymer of interest can then be defined as that leading to a minimization of the variance of this fit. In the case of it-PP spherulitic growth, this process has to be carried out separately for crystallization temperatures below and above 139.5°C to investigate the possibility of a regime II to III transition at that temperature. Furthermore, it is expected on theoretical grounds that regime transitions are not sharp but develop over

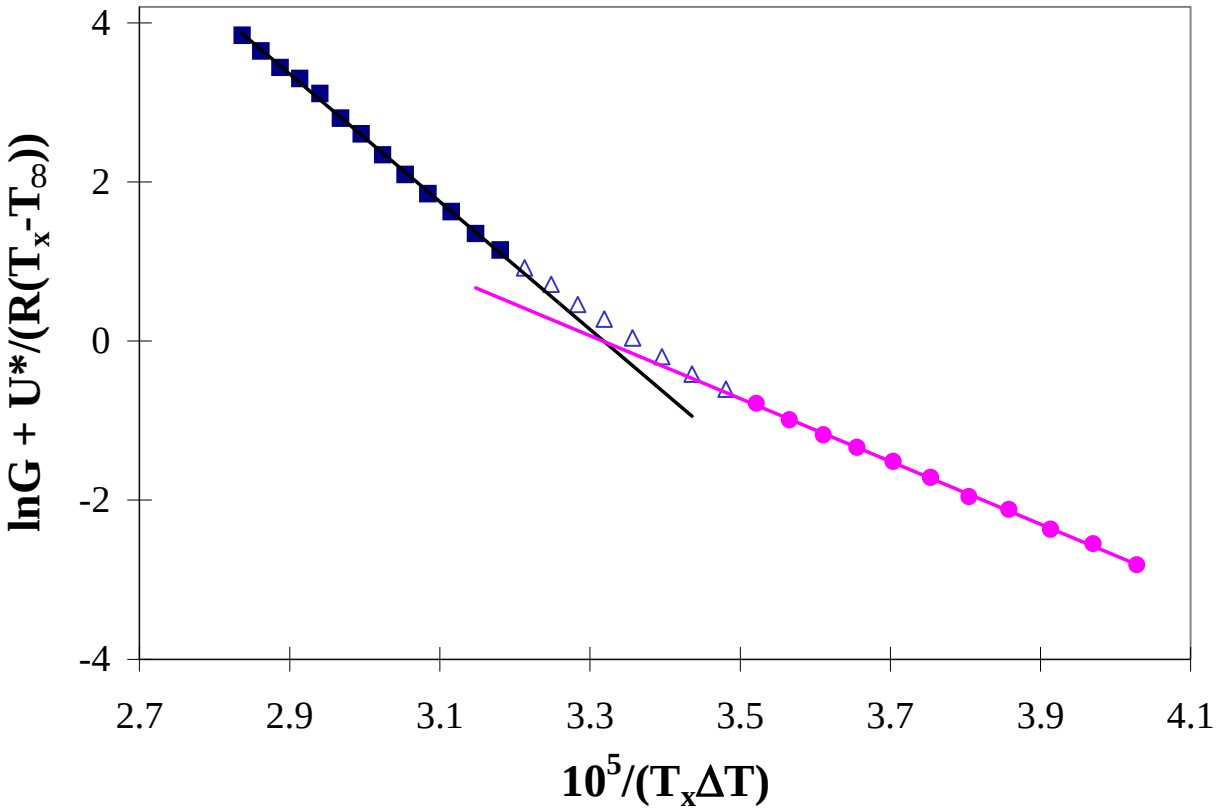

Figure 3.8. LH plot of it-PP2, M_n = 41 800 g/mol using T_m = 212.1°C, U^* = 1500 cal.mol^{-1}, T_∞ = T_g - 30 K. Regime III data used in the analysis (■). Regime II data used in the analysis (●). Data in the transition region ignored in the analysis (Δ).

some finite temperature range.[37] So the linear regression over the experimental data is conducted in such a way as to ignore data points in the direct vicinity of the hypothetical transition (i.e. between 135 and 143°C). Alternatively, if it is established that the polymer of interest exhibits a II/III regime transition, we could define the equilibrium melting temperature as that leading to a ratio of the secondary nucleation constants in regimes III and II equal to 2.0.[35, 36] The results of these analyses (using U^* = 1500 cal/mol and $T_\infty = T_g$ - 30K) are shown in Figure 3.7 for it-PP2 where the overall variance, S^2 and the ratio of secondary nucleation constants in the two hypothetical regimes, $K_{g\ II}$ and $K_{g\ III}$ are plotted as a function of the equilibrium melting temperature, T_m, chosen in the analysis. Examination of Figure 3.7 allows one to conclude that the best fit of experimental spherulitic growth rate data above and below T = 139.5°C

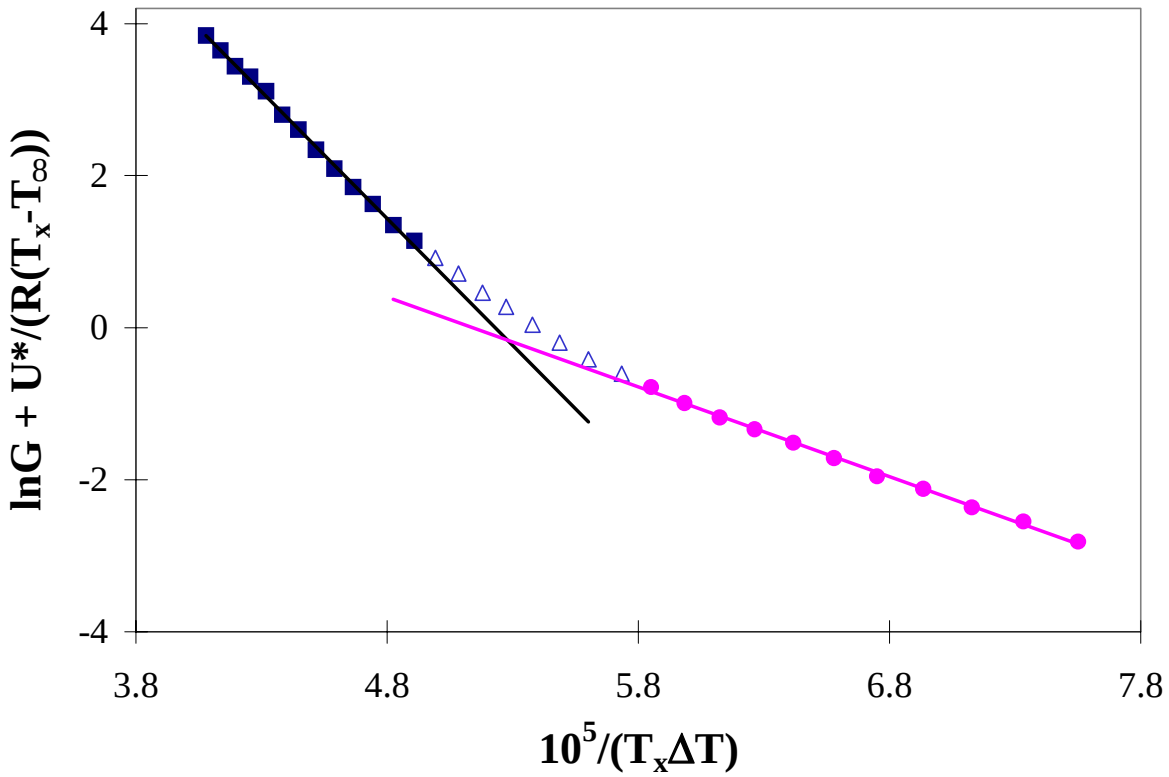

Figure 3.9. LH plot of it-PP2 for T_m = 185°C, U^* = 1500 cal.mol^{-1}, $T_\infty = T_g$ - 30 K. Regime III data used in the analysis (■). Regime II data used in the analysis (●). Data in the transition region ignored in the analysis (Δ).

is obtained for a value of the equilibrium melting temperature T_m = 215.5°C. For this choice of the equilibrium melting temperature, the ratio of the two secondary nucleation constants is 1.99, in good accord with predictions from the LH theory. Alternatively, for the ratio of secondary nucleation constants to be equal to 2.0, the equilibrium melting temperature should be 214.5°C. The results of similar analyses carried out with different sets of U^* and T_∞ are given in Table 3.3 for it-PP2. In this table, enclosed are the values of T_m, $K_{g\ II}$, $K_{g\ III}$ and $K_{g\ III}/K_{g\ II}$ determined using four different criteria (A-D). For criterion A, the "best" equilibrium melting temperature is that leading to the minimization of the variance in Regime II. Similarly, criterion B defines the best choice of T_m from the minimization of the variance in regime III. Criterion C uses a minimization of the overall variance (sum of variances in regimes II and III) to define the best

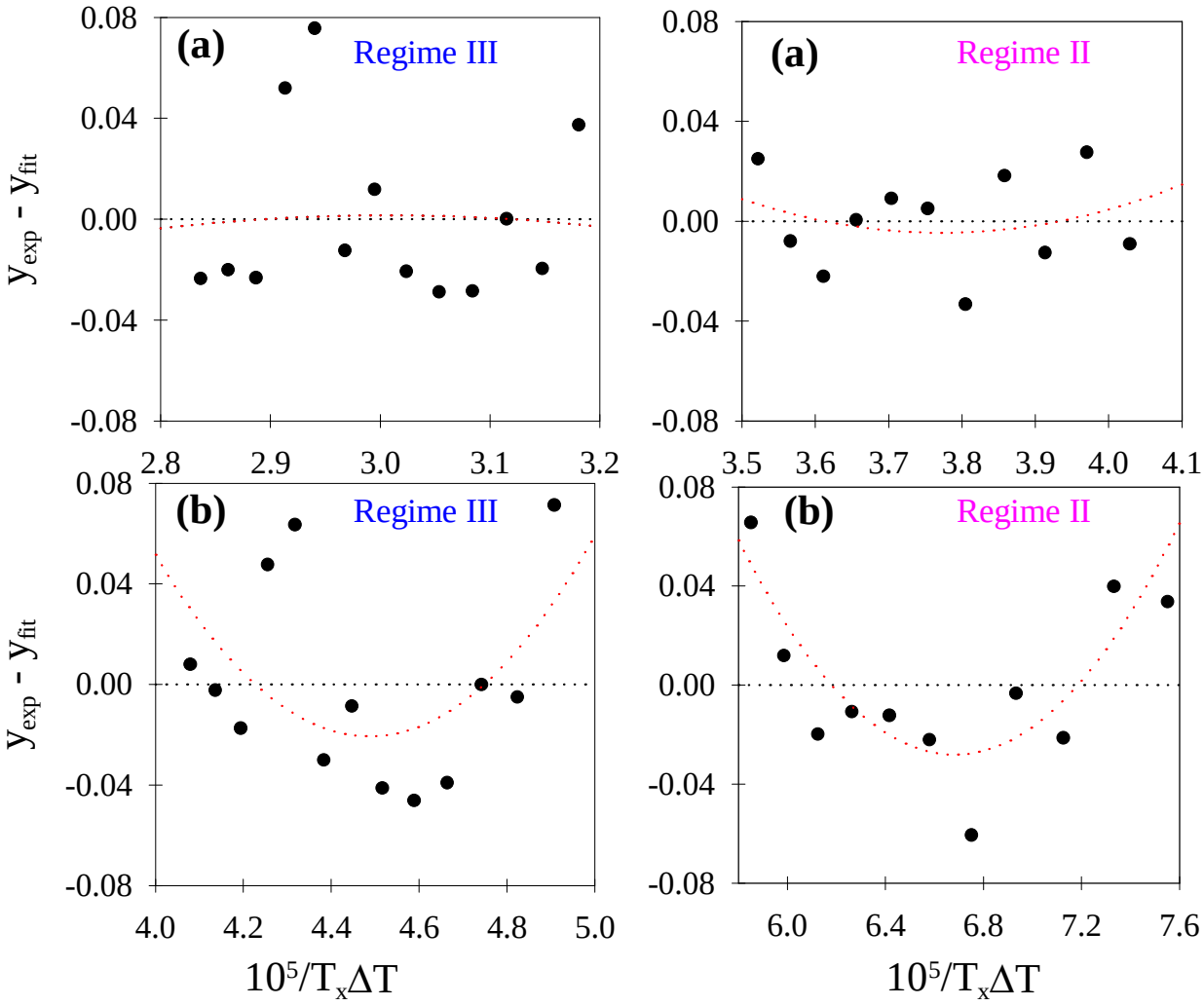

Figure 3.10. Difference between experimental and fitted spherulitic growth rates of it-PP2 as a function of $1/T_x\Delta T$ for regimes II and III for LH plot based on (a) T_m = 212.1°C, (b) T_m = 185°C.

T_m, whereas criterion D determines T_m as the value leading to a ratio of two for the secondary nucleation constants in regime III and II. We have also analyzed the temperature dependence of spherulitic growth rates using U^* = 1500 cal/mol and $T_\infty = T_g$ - 30 K and assuming either T_m = 185°C the most widely reported equilibrium temperature for α-phase it-PP[2-12,27] or T_m = 212.1°C, the equilibrium melting temperature predicted by the non-linear HW analysis. The results of

these analyses are given in Table 3.4. Plots of $\ln G + U^*/R(T_x - T_\infty)$ versus $1/T_x\Delta T$ for T_m = 212.1°C and T_m = 185°C are shown in Figures 3.8 and 3.9, respectively. Note that, in both cases, the data "appears" to be linearized. However, if one calculates the difference between the

Table 3.3. Equilibrium melting temperature and secondary nucleation constants determined through the analysis of the temperature dependence of the spherulitic growth rate assuming specific values of U^* and T_∞ and specific criteria (A through D, see text). Results are for it-PP2, M_n = 41 800 g/mol

Criteria	U^* (cal/mol)	0	1500[27]	2043[40]	2684[41]	2932[40]
	T_∞ (K)		231.2[27]	233.2[40]	224.2[41]	213.2[40]
A	T_m (°C)	212.6	223.6	228.4	231.5	230.8
	$10^{-5}\ K_{g\,II}$ (K^2)	3.60	5.70	6.82	7.63	7.46
	$10^{-5}\ K_{g\,III}$ (K^2)	7.23	10.8	12.7	14.0	13.7
	$K_{g\,III}\ /\ K_{g\,II}$	2.00	1.89	1.86	1.83	1.83
B	T_m (°C)	196.6	209.2	214.9	218.3	217.1
	$10^{-5}\ K_{g\,II}$ (K^2)	1.92	3.56	4.51	5.18	4.97
	$10^{-5}\ K_{g\,III}$ (K^2)	4.49	7.40	9.03	10.14	9.78
	$K_{g\,III}\ /\ K_{g\,II}$	2.34	2.08	2.00	1.96	1.97
C	T_m (°C)	204.0	215.5	220.6	223.9	222.9
	$10^{-5}\ K_{g\,II}$ (K^2)	2.62	4.42	5.42	6.15	5.95
	$10^{-5}\ K_{g\,III}$ (K^2)	5.66	8.79	10.5	11.7	11.3
	$K_{g\,III}\ /\ K_{g\,II}$	2.16	1.99	1.93	1.90	1.90
D	T_m (°C)	213.1	214.5	215.1	215.2	214.7
	$10^{-5}\ K_{g\,II}$ (K^2)	3.66	4.28	4.54	4.68	4.59
	$10^{-5}\ K_{g\,III}$ (K^2)	7.33	8.56	9.08	9.36	9.18
	$K_{g\,III}\ /\ K_{g\,II}$	2.00	2.00	2.00	2.00	2.00

experimental values of $\ln G + U^*/R(T_x - T_\infty)$ and the calculated values of $\ln G_0^j - K_{gj}/T_x\Delta T$ for both T_m = 212.1°C and T_m = 185°C, systematic deviations are observed between fitted and experimental values only for the lower equilibrium melting temperature (Figures 3.10 (a) and (b), respectively). This is a clear indication that the curvature of ln G versus T_x is much better accounted for by choosing T_m = 212.1°C as the appropriate equilibrium melting temperature for this polymer. Examination of Figures 2.6 and 2.8 suggests that the transition between regimes II and III for it-PP occurs gradually over a temperature range of approximately 9°C. The criticism[37] that the observed II/III Regime transition is too sharp is therefore not supported by the current study.

Table 3.4. Secondary nucleation constants and basal plane interfacial free energy of it-PP2 determined through the analysis of the temperature dependence of the spherulitic growth rate assuming U^* = 1500 cal/mol, $T_\infty = T_g$ - 30 K and different values of T_m.

	T_m = 185°C	T_m = 212.1°C
$10^{-5} K_{g\,II}$ (K^2)	1.01	3.94 ± 0.41
$10^{-5} K_{g\,III}$ (K^2)	3.02	8.03 ± 0.67
$K_{g\,III} / K_{g\,II}$	2.99	2.04 ± 0.05
σ_e (erg.cm^{-2}) *	50.9	152 ± 48

* A (110) growth plane was assumed[67] and the value of σ was calculated using the Thomas-Staveley empirical equation.[49] The uncertainties are calculated very conservatively assuming separate uncertainties of ±3°C on T_m and ±2 erg.cm^{-2} on σ.

3.3.3. Temperature dependence of the crystal thickness

The dependence of the observed melting temperature on the crystallization temperature is derived through (1) the correlation between the crystallization temperature and the initial lamellar thickness ($l^* = C_1/\Delta T + C_2$), (2) the relation between the lamellar thickness, l, and the observed melting temperature (Gibbs-Thomson equation) and, (3) the ratio between the lamellar thickness and the initial lamellar thickness ($\gamma = l / l^*$). Having established the values of T_m, σ_e, and C_2 (the calculation of C_2 will be shown in the Discussion section), the correlation between the initial lamellar thickness and the crystallization temperature can be predicted (see Discussion). It is thus very important to carry out morphological studies to check the consistency between the predicted and the experimental crystal thicknesses as a function of the

Table 3.5. The induction time and the observed melting temperature of the initial lamellar crystals (at the induction time) at different crystallization temperatures for it-PP1 and it-PP3.

it-PP1, M_n = 26 700 g/mol			it-PP3, M_n = 78 300 g/mol		
T_x (°C)	$t_o(T_x)$ (min)	$T_m'[T_x,t_o]$ (°C)	T_x (°C)	$t_o(T_x)$ (min)	$T_m'[T_x,t_o]$ (°C)
127.5	1.1	155.51	126.5	1.2	161.19
128.5	1.2	155.95	127.5	1.6	161.54
129.5	1.8	156.40	128.5	2.7	162.06
130.5	2.4	156.79	129.5	3.5	162.47
131.5	3.1	157.11	130.5	3.8	162.80
132.5	4.6	157.54	131.5	4.5	163.20
135.6	9.9	158.89	132.5	5.5	163.60
137.6	16.4	159.63	133.5	7.2	163.88
140.6	29.9	161.73			

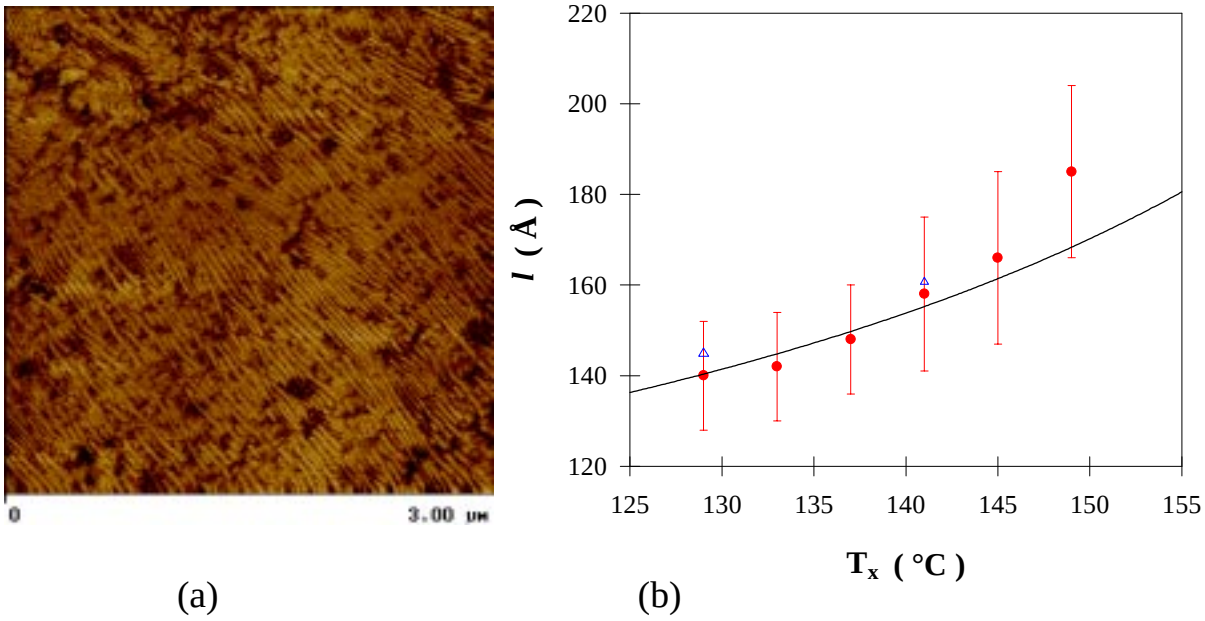

Figure 3.11. (a) the micrograph of it-PP2 after isothermal crystallization at149°C for 20 hours. (b) The lamellar thickness versus the crystallization temperature for it-PP2, M_n = 41 800 g/mol. Samples were isothermally crystallized at each T_x for a given time, which allows the primary crystallization to finish. Solid symbols: measured lamellar thickness, solid curve: predicted initial lamellar thickness using Equation 3.5, open symbols: predicted lamellar thickness after the samples were isothermally crystallized 60 min @ 129.0°C and 300 min @ 141°C.

crystallization temperature. Figure 3.11(b) shows the temperature dependence of the lamellar thickness measured by AFM for it-PP2 (solid symbols). Figure 3.11(a) is a AFM micrograph of it-PP2 after isothermal crystallization at 149°C for 20 hours. The lamellar thickness at each temperature is the average value of more than 50 measurements. Large error bars are shown to indicate the limitation of the technique employed. One must note that the lamellar thickness measured is not the initial lamellar thickness because the samples were isothermally crystallized for a given time until the primary crystallization was over. On the other hand, if the

crystallization time dependence of the observed melting temperature at a certain crystallization temperature is experimentally available, the lamellar thickness can be predicted through the Gibbs-Thomson equation (see Discussion). Thus, predicted lamellar thickness can be compared to experimental thickness after the sample is isothermally crystallized for a given time at a temperature for which the observed melting temperature data is available.

3.3.4 Results of it-PP1 and it-PP3

Similar experiments except morphological studies were carried out for the other two it-PP fractions. Results of the induction time and the observed melting temperature of the original crystals as a function of the crystallization temperature are given in Table 3.5. The equilibrium melting temperatures determined by the nonlinear HW analysis are given in Table 3.6. Also given are the "equilibrium melting temperatures" extrapolated by the linear HW procedure for comparison. Raw spherulitic growth rates were plotted against the crystallization temperature in Figure 3.12(a) for the three it-PP fractions. A barely observable transition was found at ca. 140°C for all three it-PP fractions. Similar regime analyses as discussed in the second part were performed on the crystal growth rates of it-PP1 and it-PP3, all leading to the confirmation of a regime III/II transition. Values of the equilibrium melting temperature and the ratio of the nucleation constants in regime III and II are listed in Table 3.7, using U^* = 1500 cal/mol and $T_\infty = T_g$ - 30 K, according to the criterion A through D, defined in the second part.

Table 3.6. Equilibrium melting temperatures determined by the linear and the nonlinear HW extrapolations for the three it-PP fractions. Also enclosed are the thickening coefficient, γ, the value of a from the nonlinear HW analysis, σ_e and C_2 (see discussion).

	linear HW analysis		nonlinear HW analysis				
Sample	T_m (°C)	γ	T_m (°C)	γ	a	σ_e^1 (erg.cm^{-2})	C_2 (Å)
it-PP1	176.8	2.31	205.2	1.00	3.48	117	42
it-PP2	182.5	2.40	212.1	1.00	3.45	146	52
it-PP3	183.6	2.55	216.8	1.00	3.39	154	54

A number of conclusions can be drawn based on the results of the three it-PP fractions from studies of the melting behavior using the nonlinear HW analysis and from investigations of the temperature dependence of spherulitic growth rates. First, the linear HW extrapolation significantly underestimates the equilibrium melting temperatures (ca. 30 K lower than those determined by the nonlinear HW analysis) and overestimates the thickening coefficient. Although the observed melting temperatures used in the analysis are the values extrapolated to zero crystallinity, the thickening coefficients obtained from the linear HW analysis are ca. 2.4. These values are physically meaningless because they reflect a fast and significant thickening of the original crystals right after their formation, which does not have any experimental support in

Table 3.7. The equilibrium melting temperature and the ratio of the secondary nucleation constants in regime III and II obtained from the analysis of the temperature dependence of the crystal growth rates, using U^* = 1500 cal/mol and $T_\infty = T_g$ - 30 K, according to the criteria A through D, defined in the second part of this section.

Criteria		it-PP1	it-PP2	it-PP3
A	T_m (°C)	196.1	223.6	333.0
	$K_{g\,III} / K_{g\,II}$	2.06	1.89	1.56
B	T_m (°C)	239.0	209.2	267.1
	$K_{g\,III} / K_{g\,II}$	1.64	2.08	1.67
C	T_m (°C)	211.1	215.5	330.9
	$K_{g\,III} / K_{g\,II}$	1.84	1.99	1.57
D	T_m (°C)	199.5	214.5	217.3
	$K_{g\,III} / K_{g\,II}$	2.00	2.00	2.00

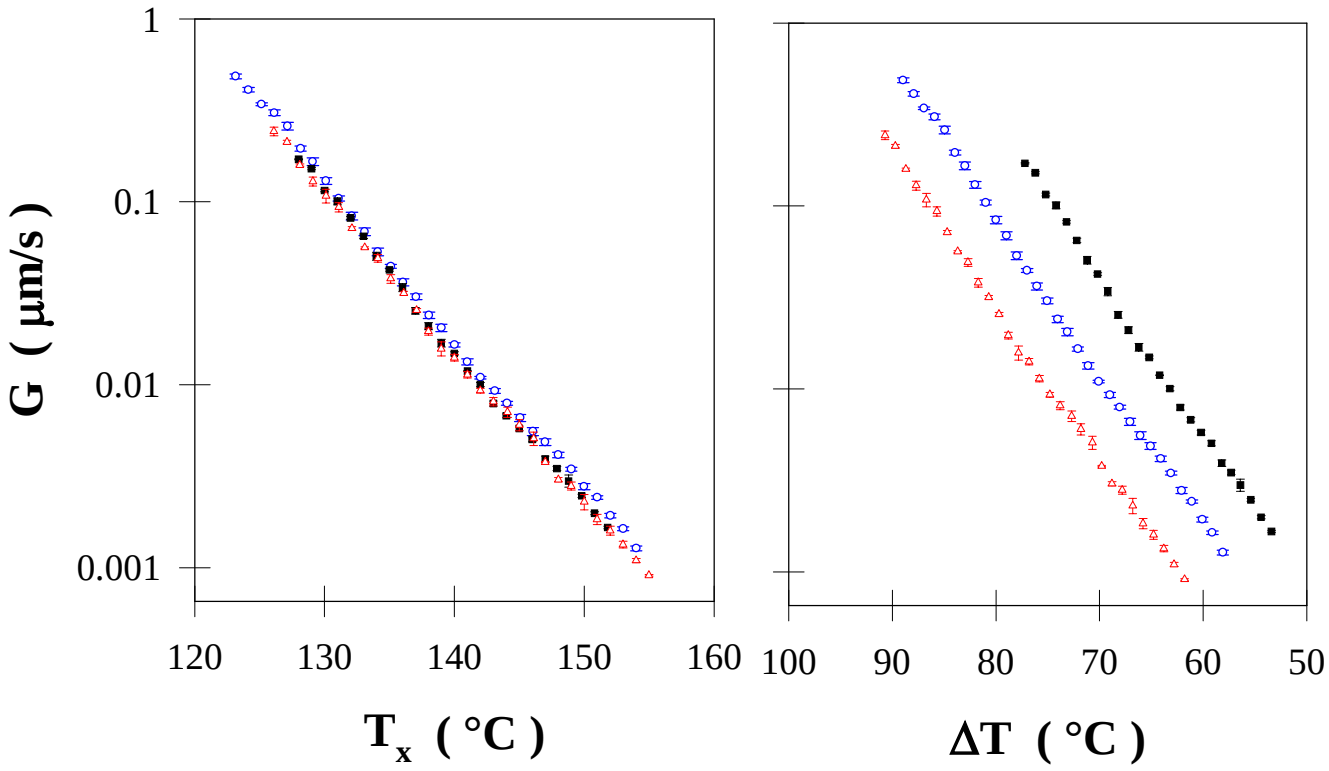

Figure 3.12. The raw crystal growth rate data of the three it-PP fractions versus the crystallization temperature (left) and the undercooling (right) (T_m values in Table 3.6 are used). (■) it-PP1, M_n = 26 700 g/mol, (○) it-PP2, M_n = 41 800 g/mol and (△), it-PP3, M_n = 78 300 g/mol.

the case of it-PP. Second, the equilibrium melting temperatures determined by the nonlinear HW analysis for the three it-PP fractions are located in the same temperature range (ca. 210°C), and the equilibrium melting temperature increases with the increase in molecular weight. But the quantitative evaluation of the molecular weight dependence of equilibrium melting temperature will not be further discussed here due to the very limited molecular weight range probed. Furthermore, the high stereo defects of it-PP1 and high polydispersity of it-PP3 may lead to a certain uncertainty in the determination of the equilibrium melting temperature. Third, independent criteria yield very close equilibrium melting temperatures for it-PP2, the fraction with the lowest polydispersity and the highest isotacticity. The nonlinear HW analysis yields 212.1°C and the criteria C and D in Table 3.7 yields 215.5 and 214.5°C, respectively. For it-

PP1, criteria C and D, and the nonlinear HW analysis also yield close equilibrium melting temperatures (211.1, 199.5, 205.2°C), the result based on the nonlinear HW analysis, which is also identical to the average value (205.3°C), is taken as the final equilibrium melting temperature for it-PP1. For it-PP3, only criteria D and the nonlinear HW analysis give close equilibrium melting temperatures (216.8 and 217.3°C), and the value from the nonlinear HW analysis is taken as the true equilibrium melting temperature for it-PP3. Criteria C yields unreasonable T_m value for it-PP3, which possibly results from the high polydispersity of the sample. Experimental work is necessary to address the polydispersity dependence of the crystal growth rate at a given temperature, thus, the equilibrium melting temperature determined from criterion C. This issue is beyond the goal of this thesis and will not be further discussed. Having established the equilibrium melting temperatures for the three it-PP fractions (values from the nonlinear HW analysis), crystal growth rates were plotted against the undercooling in Figure 3.12(b) for a clean observation of the crystal growth rates at various undercoolings/crystallization temperatures.

3.4 Discussions

3.4.1. Analysis of the temperature dependence of spherulitic growth rates

The criterion C used in the last section for estimation of the equilibrium melting temperature of α-phase it-PP was used successfully in the crystallization studies of poly(pivalolactone) and blends of poly(pivalolactone) with vinylidene fluoride homo and copolymers by Huang and Marand.[42-44] This method is based on the assumption that the spherulitic growth rate, G, of high enough molecular weight polymers (*i.e.* non-oligomeric) can be well represented far above the glass transition temperature by the expression $\ln G \alpha 1/ T_x\Delta T$, where ΔT is the undercooling (T_m - T_x) below the equilibrium melting temperature. A reliable estimate of T_m can then be obtained through linearization and refinement of the fit of experimental G data using results of secondary nucleation theories. As long as the analysis is restricted to growth rate data obtained on the right hand side of the G versus T_x curve, the estimate thereby obtained should be fairly independent of the choice of functional form or specific parameters used to describe the effect of chain transport on the crystal growth rate. Examination of Table 3.3 indicates that regardless of the choice of

the U^*, T_∞ pair used in the analysis, the equilibrium melting temperature is always significantly higher than 185°C and more likely in the vicinity of 212°C. The best results (*i.e.* these simultaneously yielding the lowest value of S^2 and a ratio of $K_{g\ III}$ to $K_{g\ II}$ equal to 2.0) are obtained when the values U^* = 1500 cal/mol and $T_\infty = T_g$ - 30K are used. One should ascertain, whether this result is an indication that the segmental dynamics in the direct vicinity of a crystal growth front indeed differs from that in the bulk melt or whether the LH secondary nucleation theory is only capable of capturing the essential features of the growth kinetics at low undercoolings, where the supercooled melt is not too far from equilibrium. Incidentally, at low undercoolings, the kinetics of the crystal growth process is largely dominated by secondary nucleation effects (*i.e.* the second exponential term in Equation 3.4) and independent of the details associated with the segmental dynamics. Although this should not be a surprise to those who use the LH theory, the classical growth rate expression (Equation 3.4) is actually the result of a number of approximations that are only justifiable at low undercoolings. Indeed, the major goal of Hoffman and coworkers has been to provide a physically meaningful account of linear polyethylene crystallization (*i.e.* at undercoolings less than 30 K).[36] Although an exhaustive listing of the assumptions necessary to reach Equation 3.4. is beyond the scope of the current work, the reader is reminded that the LH theory assumes, for the sake of mathematical tractability, that the segmental dynamics associated with first stem deposition is identical to that associated with subsequent stem depositions. That this is inadequate can be anticipated by stating that first stem deposition is viewed as a local segmental process (Rouse like), while substrate completion may involve significant reeling in effects and therefore the friction coefficient of a whole chain (for chain lengths low enough that multiple pinning at different sites is not likely).[45,46] Second, and more closely related to the choice of the specific values to be used for U^* and T_∞, the friction coefficient used in the transport term, β, should be viewed as an apparent friction coefficient and not as the true friction coefficient associated with the reptative motion of polymer chains in an equilibrium melt. As was discussed by Snyder et al.[45,46] the friction coefficient, which is defined through the equality between the nucleation based substrate completion rate and the forced-reptation based substrate completion rate, must also reflect the multitude of unsuccessful conformational transitions involved in the process of chain folding.

As was proposed by Snyder et al., the apparent friction coefficient may be a complicated function of the apportionment factors for first and subsequent stem placement and of the work of chain folding. One should therefore not expect a priori to obtain a best fit of the temperature dependence of crystal growth rates by simply combining the "secondary nucleation" exponential with the Vogel or Arrhenius transport term obtained from viscoelastic studies of the bulk melt. This should be especially true at large undercoolings near and below the growth rate maximum, where the segmental dynamics becomes more important. It was actually showed in the case of isotactic polystyrene, which can be crystallized isothermally at temperatures in the vicinity of the glass transition that consideration of a third exponential term, involving the work of chain folding allows to reconcile the values of the Vogel-Fulcher-Tamman-Hesse parameters obtained from growth rate and viscoelastic measurements.[47,48] Such an approach cannot however be rigorously attempted here, since growth rate measurements are only available on the high temperature side of the growth rate curve for it-PP.

With this proviso in mind, we can nevertheless state that the equilibrium melting temperature derived from the non-linear HW analysis is consistent with that obtained through the growth rate

Table 3.8. Thermodynamic and crystallographic parameters for the monoclinic α-crystal phase of it-PP

		ref no., comments
ΔH_f (J/g)	207	ref 81
ρ_c (g/cm^3)	0.934	ref 75
a_o (cm)	5.49×10^{-8}	ref 57 assuming (110) growth front[67]
b_o (cm)	6.26×10^{-8}	ref 57 assuming (110) growth front[67]

analysis, when U^* = 1500 cal/mol and $T_\infty = T_g$ - 30K. It is also comforting to note in Table 3.3, that the ratio of the secondary nucleation constants in regimes II and III does not depend significantly on the choice of U^* and T_∞. Examination of Table 3.3 further shows that, although the equilibrium melting temperature predicted by the analysis of spherulitic growth rates is significantly higher than currently accepted value of 185°C, variation in the parameters U^* and T_∞ may lead to a somewhat significant uncertainty in the value of T_m, when variance-based criteria are used. These results further indicate that different equilibrium melting temperatures are predicted depending on which regime is considered in the minimization of the variance. Although resolution of this issue must await 1) a better understanding of the exact temperature dependence of segmental dynamics during crystallization (see above) and 2) a more rigorous extension of Equation 3.4 for high undercoolings, it appears, at least for it-PP, that criterion D ($K_{g\ III}/K_{g\ II}$ = 2) leads to a much narrower spread in the estimated T_m values. Obviously, use of this criterion relies on the assumption that regime transition concepts are physically meaningful.

Examination of Tables 3.3 and 3.4 also allows one to confirm the earlier statement that reliable secondary nucleation constants can only be obtained if the estimate of the equilibrium melting temperature is sufficiently accurate. In Figure 3.13, the average secondary nucleation constant ($0.5\ K_{g\ III} + K_{g\ II}$) is plotted as a function of equilibrium melting temperature (data from Tables 3.3 and 3.4). A clear correlation between the equilibrium melting temperature chosen for the analysis and the resulting secondary nucleation constant derived from the LH plot can be observed. Note the large difference between nucleation constants for the lowest T_m values (182.8 and 185°C) and for the T_m value extracted from the non-linear HW analysis (T_m = 212.1°C).

Knowledge of the secondary nucleation constants $K_{g\ II}$ and $K_{g\ III}$ (see Table 3.4) and of the various thermodynamic and crystallographic parameters for it-PP (Table 3.8) allows one further to determine the magnitude of the basal plane interfacial free energy, σ_e^1, if the lateral melt/crystal interfacial free energy, σ, is known (Equation 1.2). This later quantity can be calculated either from the Thomas-Staveley equation[49] (σ_{TS} = 11.3 erg.cm^{-2}) or from the recently

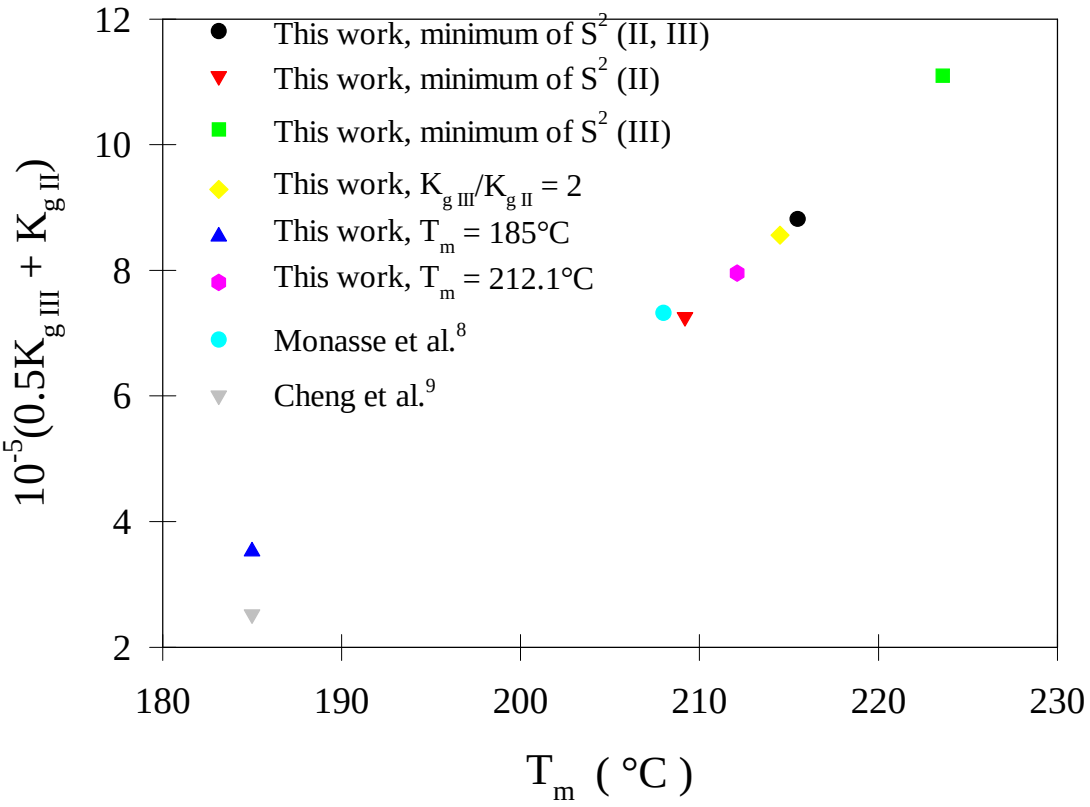

Figure 3.13 Average secondary nucleation constant (0.5 $K_{g\,III}$ + $K_{g\,II}$) versus the equilibrium melting temperature, T_m, chosen in the LH analysis.

proposed correlation between σ and C_∞, the chain characteristic ratio ($\sigma_{C\infty}$ = 12.6 erg.cm^{-2}).[50] Taking the average of these two values for σ, the value of σ_e^1 is determined to be 146 erg.cm^{-2} for it-PP2, values of σ_e^1 for the other two it-PP fractions are also calculated and all the results are included in Table 3.6.

3.4.1 Correlations between crystallization temperature, melting temperature and lamellar thickness

Using the value obtained for σ_e^1, we can now perform an estimate of the C_2 parameter for α-phase it-PP from the intercept a of the M versus X plot shown in Figure 3.3 for γ=1. Assuming T_m = 212.1°C, the value obtained for it-PP2 is C_2 = 52Å, which appears reasonable, when considered in light of that estimated for linear polyethylene (C_2 (PE) = 43.3 Å).[1] Values of C_2

for the other two it-PP fractions were calculated using T_m from the nonlinear HW analysis and they are 42 and 54 Å for it-PP1 and it-PP3, respectively, shown in Table 3.6. Note that the value of C_2 so estimated is larger than δl_x calculated using the LH theory with $\psi = 0$ (δl = 6 Å), a result which was discussed previously in the case of linear polyethylene.[1] Knowledge of σ_e^1 C_2 and of the theoretical enthalpy of fusion of α-phase it-PP (Table 3.8) enables the estimation of the temperature dependence of the initial lamellar thickness for it-PP, and an example is given below for it-PP2,

$$l^* = \frac{7{,}342}{212.1 - T_x} + 52 \tag{3.5}$$

where l^* is given in Å and T_x in °C. The accuracy of this relationship is dependent on the validity of the assumption that σ is appropriately given either by the Thomas-Staveley empirical equation or by the C_∞ - σ correlation, since the magnitude of σ_e^1 (146 erg.cm^{-2}) was calculated from the ratio of $\sigma\sigma_e$ (derived from K_g's) to that of σ. Furthermore, one must bear in mind that the proposed relationship depends on the ability to extract the melting temperature associated with the initial lamellar thickness through an extrapolation to short times of the melting temperature of annealed crystals. Finally, this relationship only pertains to the thickness of the leading radial lamellae and not to the subsidiary lamellae which nucleate epitaxially, initially on leading lamellae and subsequently on daughter lamellae and which give rise to the well documented cross-hatched morphology.[51-58] Despite all the limitations discussed above about Equation 3.5, the predicted initial lamellar thickness matches well at low crystallization temperatures with the experimentally measured lamellar thickness, as both are plotted against the crystallization temperature in Figure 3.11. The deviation at high crystallization temperatures is because the experimental lamellar thickness is not the initial lamellar thickness, it was measured after the samples had been isothermally crystallized for a given time that is enough to accomplish the primary crystallization. Apparently, it takes much longer time to finish the primary crystallization process at high crystallization temperatures, furthermore, high temperatures give rise to a faster thickening rate of the lamellae. As a result, the experimental lamellar thickness matches well with the predicted initial lamellar thickness at low crystallization temperatures within experimental uncertainty, but becomes larger than the predicted value with

the increase in the crystallization temperature, and the amount of difference increases at higher crystallization temperatures. One must note that large error bars are presented with the measured lamellar thickness, which is due to the limited resolution (ca. 10Å) of the instrument used to carry out the experiments. Thought AFM has become a technique widely used to measure the lamellar thickness, a careful calibration at the magnitude of ca. 100Å (lamellar thickness is about 50 – 300 Å) has seldom been reported. It is safer to add a larger error bar (20 Å) to Figure 3.11, since no calibration has been done in the current work. The purpose of the morphological work is to prove the prediction of the initial lamellar thickness as a function of the crystallization temperature is correct within an acceptable uncertainty. A more accurate measurement of the lamellar thickness as a function of the crystallization temperature for it-PP, thus, becomes one of the future works.

Having established new values for the equilibrium melting temperature, the C_2 parameter, and the basal plane interfacial free energy for the α-phase of it-PP, we can now discuss the extent of lamellar thickening to be expected for isothermally crystallized it-PP. Equation 3.5 provides an estimate of the undercooling dependence of the initial lamellar thickness, l^*. The Gibbs-Thomson equation[35] (Equation 3.6, below), on the other hand, yields a relationship between observed melting temperature and the lamellar thickness, l.

$$T_m' = T_m\left(1 - \frac{2\sigma_{em}}{\Delta H_f l}\right) \tag{3.6}$$

Combination of Equations 3.5 and 3.6 with the definition of the thickening coefficient $\gamma = l/l^*$, allows one to predict the crystallization time and temperature dependence of the thickening coefficient and the lamellar thickness:

$$\gamma(t) = \frac{l(t)}{l^*} = \frac{\dfrac{2\sigma_{em}T_m}{\Delta H_f\left(T_m - T_m'\right)}}{\dfrac{2\sigma_e{}^1 T_m}{\Delta H_f\left(T_m - T_x\right)} + C_2} = \left(\frac{\sigma_{em}}{\sigma_e{}^1}\right)\frac{M(t)}{(X+a)} \cong \frac{M(t)}{(X+a)} \tag{3.7}$$

From the data presented in Figure 2.2, a plot of l(t) versus the crystallization time at various temperatures is shown in Figure 3.14. This plot clearly suggests that the thickening coefficient for the α-phase of it-PP increases with increasing crystallization temperature but remains very minimal in the temperature range investigated. The predicted lamellar thickness ranges from 145 Å at 126°C to nearly 170 Å at 146°C for a crystallization time of approximately four hours. These predictions appear to be in good agreement, especially at low crystallization temperatures, with recent morphological studies by White *et al*..[57] Also the predictions are consistent with the measurements of the lamellar thickness at low temperatures in the current work, according to Figure 3.11. Also included in Figure 3.11 are the calculated lamellar thickness of it-PP2 after the samples were isothermally crystallized (1) 60 minutes @ 129.0°C and (2) 300 minutes @ 141.0°C, shown by open triangles. These calculations can be done because the relationship between the observed melting temperature and the crystallization time at these two temperatures is available (Figure 3.2 and Table 3.2). It is also worth noting that a significant increase in the thickening rate is observed at the onset of regime II. This is obviously expected from a higher probability for adjacent reentry folding in regime II than in regime III.[36] A similar conclusion was reached by Mezghani *et al.*[12] Lamellar thickening for it-PP is certainly expected on the basis of the existence of a crystal α relaxation[59-62] for this polymer, relaxation associated with helical jump motions in the crystal phase which allows a net transport of segments from the metastable amorphous fraction into the more stable crystal phase. We may speculate that the small extent of lamellar thickening for it-PP, as compared to polyethylene, may be related to the combination of a significantly higher activation energy for the α-process of it-PP,[59-63] and the crystallization in regimes III and II for it-PP as opposed to II and I for PE. Raising the crystallization temperature of PE through the I/II regime transition has already been shown to lead to a significant enhancement in the rate of lamellar thickening.[36]

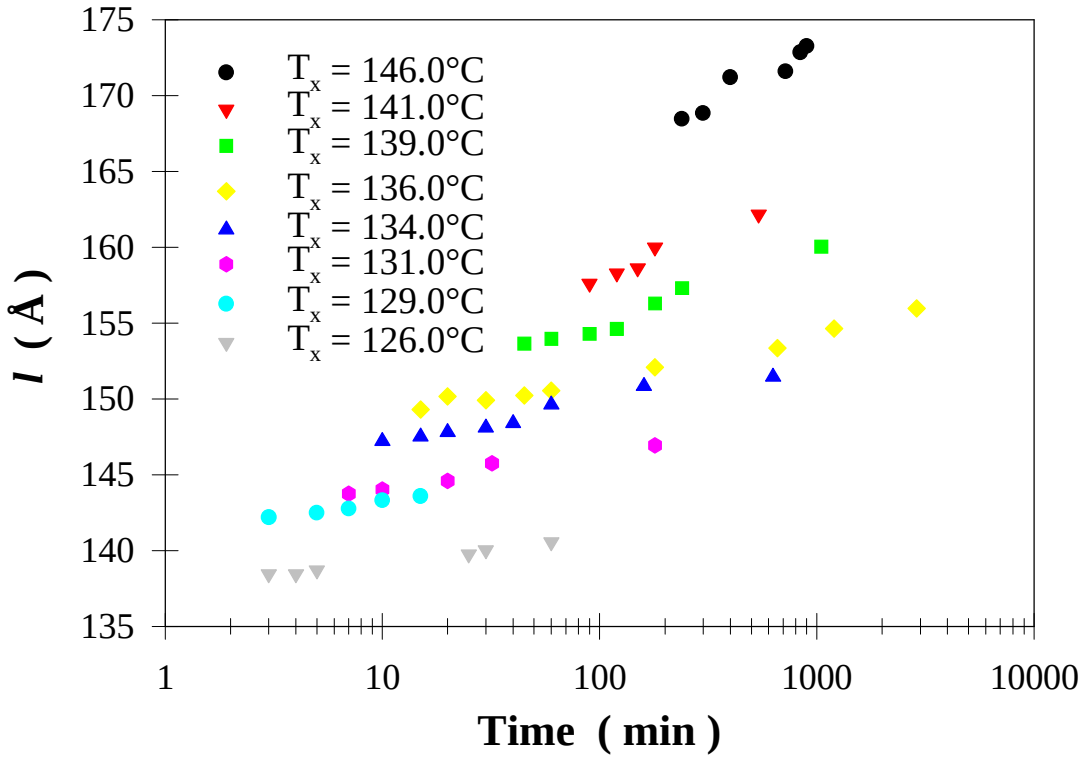

Figure 3.14 Estimated lamellar thickness as a function of crystallization time and temperature. Calculation based on T_m = 212.1°C, C_2 = 52Å, σ_e = 146 erg.cm^{-2} and ΔH_f = 193 J.cm^{-3}.

3.4.2. Self-consistency of the analysis and comparison with previous results

At this juncture, it is worth comparing the results presented in this manuscript with those from previous investigations. We will first address the evaluation of the equilibrium melting temperature through the linear HW and the Gibbs-Thomson analyses. The discussion will obviously be restricted to the analysis of the thermodynamic parameters describing the crystal growth and melting processes for the α-phase of it-PP.

Equilibrium melting temperatures obtained by the HW linear extrapolation generally fall into two widely different ranges 185-190°C[2-12] and 208-220°C[4,8,13-19]. Certainly a range of equilibrium melting temperatures is expected a-priori on the basis of tacticity and molecular weight differences between samples studied.[9,10] Furthermore, recent studies by VanderHart *et*

al.[64] indicate that different defect types are included to different extents in it-PP α-phase crystals. Specifically, the regio defects found in metallocene based isotactic poly(propylene) are thought to be for the most part excluded from the lamellar structures (*ca.* 10% inclusion), whereas the stereo defects found in both metallocene and Ziegler-Natta it-PP are much more significantly incorporated (*ca.* 50-60% inclusion). The level of defect incorporation obviously also depends on crystallization temperature (the lower the undercooling, the lower the expected level of defect inclusion). The fact of that stereo defects can be at least partially included in the lamellar crystals furthermore provides some justification for the use of the Gibbs-Thomson and LH theories for it-PP. It is noted that such theories should not rigorously apply for statistical copolymers or stereo-irregular homopolymers where defects are not included in the crystalline lattice, since in these cases, the average lamellar thickness is not solely controlled by the undercooling but is also strongly influenced by the defect distribution along the polymer backbone.

Since most of the early studies focused on Ziegler-Natta it-PP but did not report the tacticity of the materials investigated, we only consider the two most recent studies by Cheng *et al.*[9] and Mezghani *et al.*[12] where the stereo defect content was less than 1%. Clearly, for these latter materials, the highest possible value of the equilibrium melting temperature for the α-phase of it-PP should be obtained. Both studies concluded through a combination of linear HW extrapolation and the Gibbs-Thomson (GT) analysis that the equilibrium melting temperature in the high chain length limit should be *ca.* 185°C. In the above studies, the observed melting temperature used in the linear HW analyses was either that recorded visually at the disappearance of birefringence of very small spherulites during heating in an optical microscope hot stage[12] or that taken as the onset of the melting endotherm.[9] Examination of results obtained in the current study confirms that, indeed, a linear extrapolation of T_m' versus T_x in the limit of very short crystallization times yields a similar value for the apparent equilibrium melting temperature. From the studies in the last chapter, it has been, however, established that such a linear extrapolation is without physical basis and that the extrapolation must indeed be non-linear, if it is to be consistent with the theory it is based on.[1] Furthermore, from the examination

of the T_m' versus T_x data from Mezghani *et al.*,[12] we can infer that the apparent thickening coefficient (reciprocal of the slope of the T_m' versus T_x regression) is in the range 2.4 - 2.7 even for samples that were crystallized for extremely short times at crystallization temperatures in the range 116 to 145°C. The thickening coefficient inferred from samples crystallized for short times is actually predicted to be higher than for samples crystallized for long times. Such a value of the apparent thickening coefficient is clearly inconsistent with the expectation of insignificant isothermal lamellar thickening in very small spherulites and with an increase in the magnitude of γ with crystallization time. Further examination of these data confirms the prediction from the previous chapter that as the range of crystallization temperatures, where the linear extrapolation is carried out, is shifted down, the linearly extrapolated value of the apparent equilibrium melting temperature is more significantly underestimated (T_m^{app} = 184.5°C for T_x in the range 116 - 136°C versus T_m^{app} = 188.5°C for T_x in the range 126 - 145°C). In this work,[12] the linear extrapolation of observed melting temperature versus crystallization temperature data for impinged spherulites leads to an apparent equilibrium melting temperature of 210.1°C. The situation appears here very similar to that encountered in the last chapter for the melting of linear polyethylene. An apparently correct value of the equilibrium melting temperature is obtained for fortuitous reasons associated with the effect of crystallization temperature and crystallization time on the magnitude of the thickening coefficient. The larger scatter in the data for long crystallization times than for short ones is again a hint that samples crystallized at different temperatures and for different durations exhibit a non-constant thickening coefficient. Similar conclusions can be drawn from the data published by Cheng *et al.*[9]

Let us now turn our attention to the Gibbs-Thomson analyses of it-PP published in the literature and specifically to these by Cheng *et al.*[9] and Mezghani *et al.*[12] which appear to present the most complete data sets. In all cases, the GT analysis was carried out through a combination of differential scanning calorimetry to measure observed melting temperatures and small angle X-ray scattering to estimate lamellar thicknesses. In one case,[9] the lamellar thickness was obtained at the crystallization temperature using the correlation function approach, whereas in the other case,[12] it was estimated at room temperature from the Lorentz corrected long period and

the bulk crystallinity measured through wide angle X-ray diffraction. Plots of T_m' versus 1/l are then constructed to obtain the equilibrium melting temperature from the intercept at 1/l = 0 and the basal plane interfacial free energy, σ_e from the slope. Focusing first on Mezghani *et al.*'s data,[12] the equilibrium melting temperature is found to be 186.1°C in good agreement with the values of 184.5 and 188.8°C obtained from the linear HW analysis. The magnitude of σ_e was not reported but can be estimated to be 45 erg.cm^{-2} , if a value of 193 J/cm^3 is used for the theoretical heat of fusion. From this value of the fold interfacial free energy, one can infer a work of chain folding, q = 4.4 kcal/mol, if a (110) growth plane is assumed. Turning now to Cheng *et al.*'s data,[9] the inferred equilibrium melting temperature is 185°C, again in agreement with the linear HW extrapolation. The fold interfacial free energy value is calculated to be 31 erg.cm^{-2} leading to a work of chain folding, q = 3 kcal/mol. The values reported above for the work of chain folding are obviously significantly different from one another (*ca.* 50%), but more surprisingly are lower than that of linear polyethylene (q = 4.9 kcal/mol).[36] Furthermore, these values appear to be inconsistent with those obtained from the analysis of the temperature dependence of spherulitic growth rates (52 -70 erg.cm^{-2})[9,27] when one assumes T_m = 185°C and σ = 11.5 erg.cm^{-2}. It is also important to realize, as was pointed out by Monasse *et al.*,[8] that if a higher equilibrium melting temperature is used (*i.e.* T_m = 208°C), the estimate of the fold surface free energy value is significantly higher. Using the secondary nucleation constants given by Monasse *et al.*[8] and the thermodynamic and crystallographic parameters in Table 3.8, σ_e^1 is estimated to be 141 erg.cm^{-2} (q = 13.9 kcal/mol), consistent with the results in the current work.

Having addressed above and in the last chapter the reasons for the lack of applicability of the linear HW extrapolation, it is a necessity now to discuss why the GT analysis also generally leads to erroneous results in the case of it-PP. To shed some light on this issue, it is worth examining again Mezghani *et al.*[12] and Cheng *et al.*[9] SAXS data. From the GT plots published by these authors, it is possible to determine the range of lamellar thicknesses and observed melting temperatures investigated. In the former study,[12] calculated lamellar thicknesses range from 98 Å (T_m' = 164°C) to 166 Å (T_m' = 173.5°C), whereas in the latter study,[9] they range from 27 Å (T_m' = 131.9°C) to 98 Å (T_m' = 171.9°C). Some inconsistency between these two data sets

is already apparent in the fact that for it-PP samples of identical stereo defect content (less than 1%) and of identical lamellar thickness (98 Å), a difference of 8°C in the observed melting temperature is reported. This discrepancy cannot be explained by differences in the definition adopted for the melting temperature (the endotherm peak in one case[12] and the endothmeric peak onset in the other case[9]), and is inconsistent with the observation that both studies yield the same extrapolated equilibrium melting temperature. One could argue that the correlation function approach cannot be employed to analyze SAXS data for it-PP after cooling below the isothermal crystallization temperature. According to Strobl *et al.*,[65] the lack of applicability of the correlation function approach stems from the significant increase in crystallinity observed during cooling, the associated change in the specific inner surface and the departure of the morphology from the lamellar stack model. Indeed, in one case,[9] lamellar thicknesses were estimated using the correlation function approach with scattering data recorded at each crystallization temperature, whereas in the second case,[12] they were determined at room temperature by multiplying the Lorentz-corrected long period, L_B, by the WAXD crystallinity, X_c^W. Strobl *et al.*[65] point out that the significant increase in crystallinity observed in it-PP upon cooling below the crystallization temperature is not accompanied by a change in long spacing. One would therefore expect that the it-PP lamellar thicknesses estimated through a combination of room temperature SAXS and WAXD measurements are overestimated. This conclusion is however neither supported by a comparison of the two sets of SAXS/DSC data,[9, 12] nor is it supported by comparison of SAXS[9,12] and TEM[57] data.

To show the general failure of the SAXS technique to provide reliable morphological details for isotactic poly(propylene), let us briefly review the pertinent literature. First, it is established that, when it-PP crystallizes in the form of α-phase spherulites, the spherulites exhibit a birefringence whose sign and magnitude depend on crystallization temperature.[53,55] The birefringence continuously decreases from positive values at low crystallization temperatures to negative values at higher temperatures. The temperature where the changes in the birefringence sign is observed, is dependent on molecular weight and on the content in stereo and other defects along the chains. Second, it is equally well established that the change in spherulite

birefringence with crystallization temperature is associated with the corresponding change in the relative fraction of radial and nearly tangential lamellae within the spherulites.[51-53,55] Following the nomenclature of Bassett, the dominant lamellae within the spherulites are obviously always radial but subsidiary lamellae can be either radial or tangential. Tangential lamellae are initiated by homoepitaxy on radial lamellae and subsidiary radial lamellae are initiated by similar epitaxy on tangential lamellae. This crystallographic lamellar branching, apparently unique to the α-phase of it-PP, is triggered by the similarity in the unit cell a and c axis dimensions and the presence of helices of the same hand in two successive ac layers of the parent lamella.[54,58] This cross-hatching morphology manifests itself for most melt crystallization conditions (*i.e.* between 90 and 160°C).[58] Examination of the cross-hatched morphology by TEM suggests that leading radial lamellae are thicker than the daughter tangential lamellae and do not pack in stacks, except possibly at the highest crystallization temperatures (150°C and above) in the outer regions of spherulites.[57] Lamellar stacking, when observed by transmission electron microscopy at intermediate crystallization temperatures (120-150°C), appears to be limited to daughter tangential lamellae, and is generally spatially restricted. In view of the difference between daughter and parent lamellae and the difference in their stacking behavior, one should not expect to find a simple correlation between the peak melting temperature (characteristic of the thicker radial lamellae) and the lamellar thickness calculated from the SAXS data (most likely dominated by periodic density fluctuations within the stacks of thinner lamellae). Qualitatively, it appears that lamellar thicknesses inferred from the SAXS analysis are much lower than those estimated by transmission electron microscopy.[9,12,57]

Further inconsistencies in the results obtained by SAXS are uncovered when considering recent studies by Ryan *et al.*.[66] Using, simultaneously, calorimetry and synchrotron SAXS and WAXD techniques, they followed the evolution of the invariant, correlation function, and degree of crystallinity of it-PP during isothermal melt crystallization at 133°C. During primary crystallization, the long spacing obtained either from the correlation function (L_γ) or the Bragg maximum in the Lorentz corrected scattering profile (L_B) is constant. However, in contrast with the SAXS analysis at room temperature by Mezghani *et al.*[12] where L_B was systematically larger

than L_γ by ca. 20%, study by Ryan *et al.*[66] yields the opposite conclusion (*i.e.* L_B is lower than L_γ by ca. 20%), suggesting apparent but unexplained differences in long spacing distributions. In the latter study, the lamellar thickness estimated from the correlation function appears to be independent of crystallization time during the primary crystallization stage.[66] This is apparently inconsistent with the suggestion by Mezghani *et al.*[12] that significant lamellar thickening occurs even during primary crystallization and is at the origin of the increase in observed melting temperature. For a quantitative assessment of the relationship between lamellar thickness and increase in observed melting temperature, we have plotted on Figure 3.15 T_m' versus l data generated with the T_m, σ_e values reported by Cheng *et al.*,[9] Mezghani *et al.*[12] and these estimated in this chapter. We have shown in Figure 3.2 that for all crystallization temperatures investigated in the current study, the observed melting temperature increases linearly with the logarithm of crystallization time during primary crystallization. For crystallization temperatures in the range 129 to 136°C, the increase in observed melting temperature during the primary crystallization stage is approximately 1.0 to 1.5 °C, in agreement with data reported with Mezghani *et al.*.[12] For a crystallization temperature of 133°C, the long spacing and lamellar thickness estimated by Ryan *et al.*[66] are approximately ca. 200 Å and 135 Å, respectively, in qualitative agreement (within 20% or so, see above) with estimates by Mezghani *et al.*[12] Focusing now on Figure 3.15, a 1.0 - 1.5 °C change in observed melting temperature can arise from a change in lamellar thickness, the magnitude of which depends only on the magnitude of the σ_e, T_m parameters for α-phase it-PP. If our parameters are used, the predicted change in lamellar thickness is relatively small (3.5 to 5Å or so). On the other hand, whether Mezghani *et al.* or Cheng *et al.*'s values are used, a measurable change in lamellar thickness is expected (Δl = 10 or 25 Å). Since such changes are not observed in Ryan *et al.*' s data,[66] it suggests an inconsistency in the SAXS/DSC approach. Morphological studies of the evolution of the lamellar thickness with crystallization time will be one of the future works to confirm the relatively small change in lamellar thickness with crystallization time. The fact that lamellar thicknesses obtained by SAXS are underestimated has been verified in the current work (Figure 3.11) and is also confirmed in recent work by White *et al.*.[57]

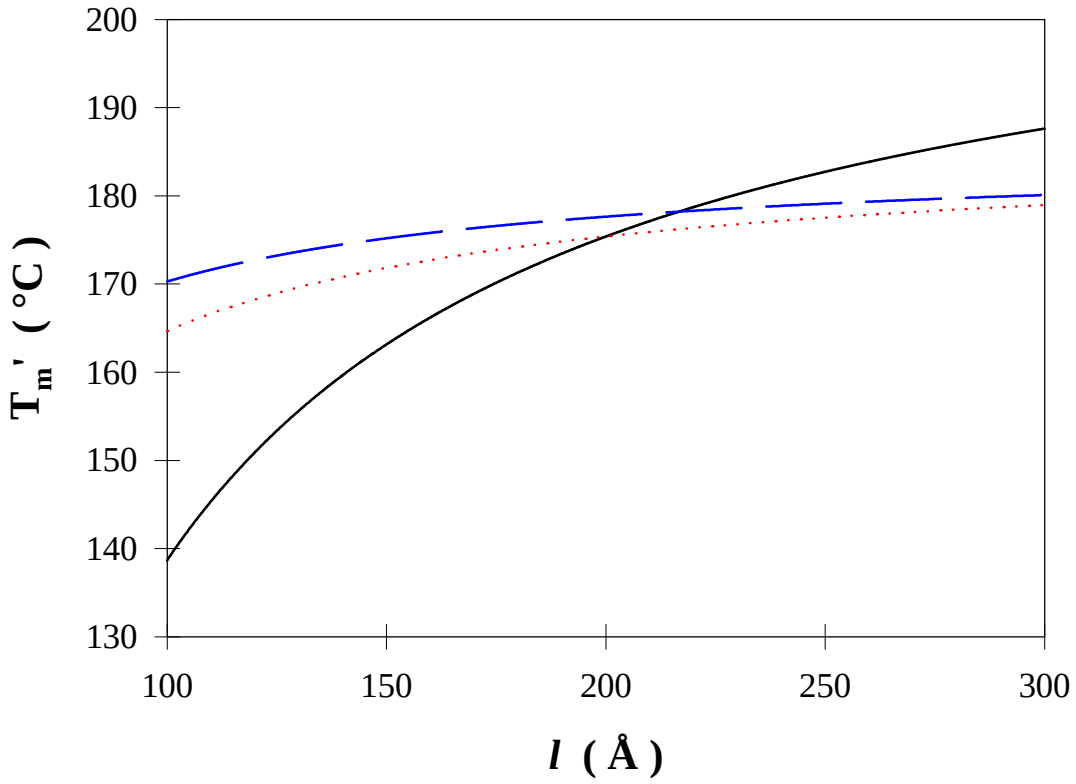

Figure 3.15 Correlation between observed melting temperature and lamellar thickness. Full curve (this work), long-dash curve (Cheng *et al.*[9]), dotted curve (Mezghani *et al.*[12]).

A final issue related to the use of SAXS to determine lamellar thickness, pertains to the possibility that samples crystallized at extremely large undercoolings (as in Cheng *et al.* studies[9]), may contain a non negligible fraction of smectic or even β phase it-PP. These two different phases would contribute in some unpredictable fashion to the SAXS profile but are ignored in the calorimetric analysis if one focuses on the endotherm peak position.

It should therefore be apparent from the above discussion that use of the Gibbs-Thomson analysis to infer the equilibrium melting temperature of it-PP has very serious limitations, when it is based on SAXS data. These limitations could obviously be overcome if the thickness of leading radial lamellae is measured through a direct technique such as transmission electron microscopy.

Having established a rationale for the lack of accuracy in previous estimates of T_m and σ_e obtained from a combination of SAXS and DSC and for the problems associated with the linear HW approach, a different strategy has been proposed for the evaluation of these thermodynamic quantities. The value of T_m = 212 ± 5°C appears to be well established on the basis of the non-linear HW approach and is consistent with results from the analysis of the temperature dependence of spherulitic growth rates. The new values proposed in this work for the basal plane interfacial free energy, σ_e^1, and the C_2 parameter depend critically on the choice of both T_m and σ. Note that similar estimates of σ were obtained from the Thomas-Staveley empirical relation and the σ - C_∞ correlation. It would be however more satisfying to obtain independent estimates of σ_e^1 through measurements of initial lamellar thickness as a function of crystallization temperature and through correlation between lamellar thickness and observed melting temperature, using electron or atomic force microscopy.

For the sake of completeness and rigor, it is also important to note a number of unresolved issues for it-PP crystallization, which are clearly pertinent to the above discussion. First, there is still some uncertainty as to the nature of the growth plane for the α-phase of it-PP. All previous analyses of the temperature dependence of it-PP spherulitic growth rates have universally adopted (110) as the growth plane for this crystal phase. The appropriateness of this choice appears to be supported by electron microscopy studies by Lotz, Wittmann and coworkers using the decoration method.[67] On the other hand, Petraccone *et al.*[68] suggest on the basis of tacticity and crystallographic considerations that folding must occur in a direction parallel to the (010) plane. If this suggestions is indeed correct, then the folding process would take place along the long axis of it-PP lath-like crystals (i.e. folds would not be parallel to the growth front but perpendicular to it and into the melt). This situation obviously differs dramatically from that addressed by the LH secondary nucleation model[35,36] and one should not expect the growth rate data to be accounted for by that model. It is however fairly difficult to envision how such process could indeed take place. In a more recent study, Petraccone *et al.*[69] calculated fold conformational energies for possible folds in it-PP, assuming folding parallel to the (010) plane.

The corresponding fold interfacial free energies are found to be in the range of 50 - 70 erg.cm^{-2}, in accord with estimates derived from the analysis of the temperature dependence of spherulitic growth rates for α-phase it-PP assuming T_m = 185°C. However, as indicated above, the LH theory should not apply for folding in directions normal to the growth front and a melting temperature of 185°C is not justifiable.

A second unresolved issue pertains to the multiple melting behavior observed for Ziegler-Natta it-PP in two different ranges of crystallization temperature (T < 120°C and 135°C < T < 150°C).[4,38, 9,70-74] The most complete studies suggest that, in both cases, this phenomenon is associated with a melting-recrystallization-remelting process.[71,72] This assertion can certainly be understood for the lowest crystallization temperature range, where, indeed, initial melting occurs in a temperature range where recrystallization could take place on a short time scale. It is however difficult to understand why this process would reappear at relatively high temperatures (135°C - 150°C), where rates of crystallization appear to be increasingly slower, whereas it is not present in the intermediate temperature range (120°C < T < 135°C). It appears more appealing to rationalize the onset of the double melting behavior for samples crystallized in the higher temperature range in terms of a bimodal distribution of lamellar thicknesses (thicker dominant radial lamellae and thinner tangential or radial daughter lamellae). Indeed, as shown by White *et al.*,[57] for crystallization temperatures below *ca*. 130°C, the difference in thickness between dominant and cross-hatching lamellae becomes vanishingly small, whereas at higher temperature (*ca*. 140°C) the thickness of these lamellae differ more significantly, thus leading to separate and easily resolvable melting endotherms. As the temperature of crystallization is raised further (*ca*. 150 - 160°C) the population of cross-hatching lamellae decreases significantly leading again to a single melting endotherm, as observed experimentally.[72-74] It is likely that melting-recrystallization occurs to a limited extent upon heating, especially at the lowest heating rates. It is however unlikely, especially in view of the recrystallization rates reported in the literature[72] and the known existence of a bimodal distribution of lamellar thicknesses,[57] that the double melting behavior be entirely attributed to a melting-recrystallization process. The most recent work by Mandelkern et al.[82] assigns the two melting peaks of it-PP to the existence of the mother

and the daughter lamellae. The thickness of the radial lamellar is only slightly above that of the tangential lamellae at low crystallization temperatures and become much thicker than that at high crystallization temperatures. Studies of optical microscopy verified that the tangential lamellae melt earlier than the radial lamellae (the birefringence become negatively enhanced at the point where the tangential lamellae have melted while the radial lamellae have not.). The work by Mandelkern et al.[82] is not out of question, the area of the lower melting peak, which is assigned to the melting of the tangential lamellae, becomes larger at higher temperatures, indicating that more tangential lamellae are formed at higher crystallization temperatures. This issue, certainly, deserves further attention.

On a related matter, the existence of two limiting structures have been proposed for the α-form.[75-77] The α_2 structure is an ordered limiting structure (crystallographic symmetry $P2_1/c$) with well defined arrangement of up and down 3_1 helices, whereas the α_1 structure is a disordered limiting structure (crystallographic symmetry C2/c) with a random distribution of up and down helices. Guerra *et al.*[78] showed on the basis of diffraction studies that structures more akin to the α_2 form are favored at high annealing temperatures (T_a >> 153°C). Using complementary calorimetric studies they inferred from the observation of single endotherms in the thermogram of annealed samples that the annealing process at high temperature leads to a "continuum" of structures intermediate between the α_1 and the α_2 forms. It is concluded from their study that annealing below 153°C should not yield wildly different crystal structures. From this observation, it would be tempting to conclude that the spherulitic growth rates reported in the current study (measured from 123 to 154°C) can be safely analyzed in the context of a single crystalline phase. It is however not known at this time how the result of these annealing studies can be applied to the case of isothermal crystallization. Recent studies by Awya[79] suggest that isothermal melt crystallization at 155°C of a low molecular weight it-PP results in a predominantly α_2 crystal form. Furthermore, significant melting-recrystallization effects would hamper our ability to correlate crystallization and melting temperatures. Recrystallization during heating would lead to the formation of the more ordered structure, which is likely to have a slightly different equilibrium melting temperature than the initial disordered limiting structure.[80]

While these issues cannot be resolved with currently available information, they certainly place some limitations on the claims that are made in the present manuscript. It is nevertheless anticipated that future and more accurate examinations of the correlation between crystallization temperature, melting temperature and lamellar thickness can shed some light on the validity of the assumptions used in this manuscript and on how serious the above limitations truly are.

3.5. Conclusions

In this chapter, a new strategy has been applied for the evaluation of the thermodynamic parameters relevant for the crystal growth and the melting processes in the case of isotactic-polypropylene prepared by Ziegler-Natta catalysts. The reliability of the method is strictly dependent on (1) the applicability of the classical relationship between the initial lamellar thickness and the undercooling ($l = 2\sigma_e^1/\Delta G_f + C_2$), (2) the assumption that σ_e^1 can be equated to σ_{em}, and (3) the appropriateness of the method used to estimate melting temperatures of initial (*i.e.* non-thickened) lamellae. It can be concluded that, for it-PP, $T_m = 212 \pm 5$°C, $\sigma_e = 146 \pm 48$ erg.cm^{-2} and $\delta l = 52 \pm 17$ Å. These values are more consistent with the limited direct morphological data available in the literature than those previously reported on the basis of a linear HW approach or of the SAXS based Gibbs-Thomson analysis. Predictions of the initial lamellar thickness as a function of crystallization temperature based on these quantities are consistent with the morphological studies accomplished in this lab. It has been emphasized in this chapter that an accurate estimation of the equilibrium melting temperature is of center importance in the analysis of crystal growth rate data and in a rigorous test of the Lauritzen-Hoffman surface nucleation model. Possible limitations of the current approach for the case of isotactic poly(propylene) have been discussed. Further possible refinement of the magnitude of the basal plane interfacial free energy, σ_e^1, and the C_2 parameter must await more complete morphological studies of it-PP. The results of such studies can in turn provide an evaluation of the self-consistency of the LH theory.

3.6. References

1. Marand, H.; Xu, J.; Srivatsan, S. *Macromolecules* **1998**, *31*, 8219.
2. Wyckoff, H.W. *J. Polym. Sci.* **1962**, *62*, 83.
3. Danusso, F.; Gianotti, G. *Makromol. Chem.* **1964**, *80*, 1.
4. Samuels, R.J. *J. Polym. Sci. Polym. Phys. Ed.* **1975**, *13*, 1417.
5. Martuscelli, E.; Pracella, M.; Zambelli, A. *J. Polym. Sci., Polym. Phys. Ed.* **1980**, *18*, 619.
6. Miller, R.L.; Seeley, E.G. *J. Polym. Sci., Polym. Phys. Ed.* **1982**, *20*, 2297.
7. Martuscelli, E.; Pracella, M.; Crispino, L. *Polymer* **1983**, *24*, 693.
8. Monasse, B.; Haudin, J.M. *Colloid Polym. Sci.* **1985**, *263*, 822.
9. Cheng, S.Z.D., Janimak, J.J.; Zhang, A.; Cheng, H.N. *Macromolecules* **1990**, *23*, 298.
10. Cheng, S.Z.D.; Janimak, J.J.; Zhang, A.; Hsieh, E.T. *Polymer* **1991**, *32*, 648.
11. Mezhgani, K.; Phillips, P.J. *Macromolecules* **1994**, *27*, 6145.
12. Mezghani, K.; Campbell, R.A.; Phillips, P.J. *Macromolecules* **1994**, *27*, 997.
13. Falkai, B.V. *Makromol.Chem.* **1960**, *41*, 86.
14. Rybnikar, F. *Collect. Czech. Chem. Commun.* **1962**, *28*, 320.
15. Cox, W.W.; Duswalt, A.A. *Polym. Eng. Sci.* **1967**, *10*, 309.
16. Kamide, K,.; Toyama, K. *Kobunshi Kagaku* **1969**, *25*, 49.
17. Fatou, J.G. *Eur. Polym. J.* **1971**, *7*, 1057.
18. Mucha, M. *J. Polym. Sci. Polym. Symp.* **1981**, *69*, 79.
19. Yadav, Y.S.; Jain, P.C. *Polymer* **1986**, *27*, 721.
20. Falkai, B.V.; Stuart, H.A. *Kolloid Z.* **1959**, *162*, 309.
21. Falkai, B.V.; Stuart, H.A. *Makromol. Chem.* **1960**, *41*, 86.
22. Binsbergen, F.L.; DeLange, B.G.M. *Polymer* **1970**, *11*, 309.
23. Lovinger, A.J.; Chua, J.Q.; Gryte, C.C. *J. Polym. Sci., Polym. Phys.Ed.* **1977**, *15*, 641.
24. Goldfarb, L.; *Makromol.Chem.* **1978**, *179*, 2297.
25. Wlochowicz, A.; Eder, M. *Polymer* **1981**, 22, 1285.
26. Martuscelli, E.; Silvestre, C.; Abate, G. *Polymer* **1982**, *23*, 229.
27. Clark, E.J.; Hoffman, J.D. *Macromolecules* **1984**, *17*, 878.
28. Janimak, J.J.; Cheng, S.Z.D. *Polym. Bull.* **1989**, *22*, 95.

29. Pospisil, L.; Rybnikar, F. *Polymer* **1990**, *31*, 477.
30. Okada, T.; Saito, H.; Inoue, T. *Macromolecules* **1992**, *25*, 1908.
31. Celli, A.; Fichera, A.; Marega, C.; Marigo, A.; Paganetto, G.; Zannetti, R. *Eur. Polym. J.* **1993**, *29*, 1037.
32. Wang, Y.F.; Lloyd, D.R. *Polymer* **1993**, *34*, 2324.
33. Ding, Z.; Spruiell, J.E. *J. Polym. Sci. Polym. Phys. Ed.* **1997**, *35*, 1077.
34. Hoffman, J.D.; Weeks, J.J. *J. Res. Natl. Bur. Stand. U.S.A.* **1962,** *A66*, 13.
35. Hoffman, J.D.; Davis, G.T., Lauritzen, J.I. In *Treatise on Solid State Chemistry*; Hannay N.B. Ed.; Plenum Press: New York, **1976**; Vol. 3, Chap. 7.
36. Hoffman, J.D.; Miller, R.L. *Polymer* **1997**, *38*, 3151.
37. Point, J.-J.; Janimak, J.J. *J. Cryst. Growth* **1993**, *131*, 501.
38. Kamide, K.; Yamaguchi, K. *Makromol. Chem.* **1972**, *162*, 205.
39. Kamide, K.; Yamaguchi, K. *Makromol. Chem.* **1972**, *162*, 219.
40. Plazek, D.L.; Plazek, D.J. *Macromolecules* **1983**, *16*, 1469.
41. Pearson, D.S.; Fetters, L.J.; Younghouse, L.B.; Mays, J.W. *Macromolecules* **1988**, *21*, 478.
42. Huang, J.; Prasad, A.; Marand, H. *Polymer* **1994**, *35*, 1896.
43. Huang, J.; Marand, H. *Macromolecules* **1997**, *30*, 1069.
44. Marand, H.; Hoffman, J.D. *Macromolecules* **1990**, *23*, 3682.
45. Snyder, C.R.; Marand, H.; Mansfield, M. *Macromolecules* **1996**, *29*, 7508.
46. Snyder, C.R.; Marand, H. *Macromolecules* **1997**, *30*, 2759.
47. Iler, H.D. Ph.D. Dissertation, Virginia Polytechnic Institute and State University, **1996**.
48. Marand, H; Iler, H.D.; Snyder, C.R. *Bull. Am. Phys. Soc.* **1996**, *41(1)*, 394.
49. Thomas, D.G.; Staveley, L.A.K. *J. Chem. Soc.* **1952**, 4569.
50. Hoffman, J.D.; Miller, R.L.; Marand, H.; Roitman, D.B. *Macromolecules* **1992**, *25*, 2221.
51. Khoury, F.A. *J. Res. Natl. Bur. Std.* **1966**, *70A*, 29.
52. Binsbergen, F.L.; de Lange, B.G.M. *Polymer* **1968**, *9*, 23.
53. Padden, F.; Keith, H.D. *J. Appl. Phys.* **1973**, *44*, 1217.
54. Wittmann, J.C.; Lotz, B. *J. Polym. Sci., Polym. Phys. Ed.* **1985**, *23*, 205.
55. Norton, D.R.; Keller, A. *Polymer* **1985**, *26*, 704.

56. Olley, R.H.; Bassett, D.C. *Polymer* **1989**, *30*, 399.
57. White, H.M.; Bassett, D.C. *Polymer* **1997**, *38*, 5515.
58. Lotz, B.; Wittmann, J.C.; Lovinger, A.J. *Polymer* **1996**, *37*, 4979.
59. McCrum, N.G. *Polymer* **1984**, *25*, 299.
60. Boyd, R.H. *Polymer* **1985**, *26*, 1123.
61. Syi, J.-L.; Mansfield, M. *Polymer* **1988**, *29*, 987.
62. Schaefer, D.; Spiess, H.W.; Suter, U.W.; Fleming, W.W. *Macromolecules* **1990**, *23*, 3431.
63. Skinner, J.L.; Park, Y.H. *Macromolecules* **1984**, *17*, 1735.
64. VanderHart, D. L.; Alamo, R.G.; Kim, M.H.; Mandelkern, L.; Perez, E., Mansel, S. *Bull. Am. Phys. Soc.* **1998**, *43*, 270.
65. Albrecht, T.; Strobl, G. *Macromolecules* **1995**, *28*, 5267.
66. Ryan, A.J.; Stanford, J.L.; Bras, W. Nye, T.M.W. *Polymer* **1997**, *38*, 759.
67. Lotz, B.; Graff, S.; Wittmann, J.C.; *J. Polym. Sci., Polym. Phys. Ed.* **1985**, *24*, 2017.
68. Petraccone, V.; Pirozzi, B.; Meille, S.V. *Polymer* **1986**, *27*, 1665.
69. Petraccone, V.; Pirozzi, B.; Meille, S.V. *Eur. Polym. J.* **1989**, *25*, 43.
70. Corradini, P.; Napolitano, R.; Oliva, L.; Petraccone, V.; Pirozzi, B. *Makromol. Chem., Rapid Commun.* **1982**, *3*, 753.
71. Carfagna, C.; De Rosa, C.; Guerra, G.; Petraccone, V. *Polymer* **1984**, *25*, 1462.
72. Petraccone, V.; De Rosa, C.; Guerra, G.; Tuzi, A. *Makromol. Chem., Rapid, commun.* **1984**, *5*, 631.
73. Petraccone, V.; Guerra, G.; DeRosa, C.; Tuzi, A. *Macromolecules* **1985**, *18*, 813.
74. Passingham, C.; Hendra, P.J.; Cudby, M.E.A.; Zichy, V.; Weller, M. *Eur. Polym. J.* **1990**, *26*, 631.
75. Natta, G.; Pino, P.; Corradini, P.;Danusso, F.; Mantica, E.; Mazzanti, G.; Moraglio, G. *J. Am. Chem. Soc.* **1952**, *77*, 1708.
76. Mencik, Z. *J. Macromol. Sci. Phys.* **1972**, *B6*, 101.
77. Hikosaka, M.; Seto, T. *Polym. J.* **1973**, *5*, 111.
78. Guerra, G.; Petraccone, V.; Corradini, P.; De Rosa, C.; Napolitano, R.; Pirozzi, B.; Giunchi, G. *J. Polym. Sci., Polym. Phys. Ed.* **1984**, *22*, 1029.

79. Awaya, H. *Polymer* **1988**, *29*, 591.
80. Based on energy calculations, the $P2_1/c$ structure appears slightly more stable than the C2/c structure (Corradini, P.; Petraccone, V.; Pirozzi, B. *Eur. Polym. J.* **1983**, *19*, 299).
81. Bu, H.-S.; Cheng, S.Z.D., Wunderlich, B. *Makromol. Chem. Rapid Commun.* **1988**, *9*, 76.
82. Alamo, R. G.; Brown, G. M.; Mandelkern, L.; Lehtinen, A.; Paukkeri, R. *Polymer*, **1999**, *40*, 3933.

Chapter 4. Equilibrium Melting temperature and temperature dependence of crystal growth rate of poly(ethylene oxide)

4.1. Introduction

The crystalline morphology and crystallization kinetics of poly(ethylene oxide) (PEO) have commanded much attention during the past three decades.[1-13] A wide range of values for the equilibrium melting temperature, T_m, have been quoted in the literature and applied in the analysis of the temperature dependence of crystal growth rates.[3,13-18] Three major methods have been adopted in literature to obtain extrapolated values of T_m for PEO. Buckley and Kovacs[3] extended the theoretical treatment developed by Flory and Vrij[19] to PEO, and obtained a value of ca. 69°C for the equilibrium melting temperature. The same treatment was also employed by Beech and Booth[14] and Afifi-Effat and Hay,[18] but a slightly different extrapolation procedure was used, which resulted in the value of T_m ca. 76°C. However, the extended application of the Flory and Vrij treatment to PEO was criticized on theoretical grounds by Mandelkern and Stack[17] on the basis that nearly monodisperse low molecular weight PEO fractions are not molecular species and cannot form molecular crystals. According to the studies by Beech and Booth[14] and Marentette and Brown,[13] experimentally recorded melting temperatures of high molecular weight PEO fractions can exceed 69°C, thus casting some doubts on the low T_m value estimated by Kovacs et al.[3] The second method is based on the Gibbs-Thomson equation and involves a linear extrapolation of the observed melting temperature of lamellar crystals as a function of the reciprocal of their thickness.[20] Results from this treatment also lead to a T_m value in the vicinity of 69°C,[3,21] which according to Beech and Booth[14] is incorrect. These authors indicate that the fold surface free energy of PEO fractions is highly molecular weight dependent in the low molecular weight range.[14] It is important to note that lamellar thicknesses and melting temperatures must be measured simultaneously in a rigorous application of the Gibbs-Thomson method for intermediate to high molecular weight fractions to ensure that these two parameters are associated with the same crystal. According to Alfonso and Russell,[15] evaluation of lamellar thicknesses by X-ray scattering or diffraction techniques is not feasible due to the intrinsically large thickness of PEO crystals. Hence, great efforts (i.e. the use of

ultra small angle X-ray scattering) may be required to apply the Gibbs-Thomson method to the determination of PEO's equilibrium melting temperature.

The third method is the Hoffman-Weeks (HW) linear extrapolation.[22] This method which is easy to implement experimentally and involves a relative simple data analysis has been widely used in the literature. The HW treatment is based on a linear regression of the observed melting temperatures, T_m', for various crystallization temperatures, T_x, and extrapolation to the equilibrium line, $T_m' = T_x$. As pointed out in two earlier publications from this group,[20,23] results from HW linear extrapolations greatly depend on the chosen crystallization temperature range and residence time at each temperature. It is thus not surprising that values of T_m obtained from this method range from 70 to 80°C[6,13-16] Therefore, at this time the equilibrium melting temperature for PEO is not firmly established. Furthermore, as demonstrated in the last two chapters, analyses of the temperature dependence of spherulitic growth rates are strongly dependent on the choice of T_m. An incorrect T_m could lead to the artificial creation or disappearance of regime transitions when the temperature dependence of crystal growth rates is analyzed in the context of Lauritzen-Hoffman (LH) secondary nucleation theory.[20]

Validity of the conventional HW linear extrapolation has been re-evaluated and the specific conditions for the validity of HW linear extrapolation were discussed in Chapter 2. It was found that the HW linear extrapolation invariably underestimates the equilibrium melting temperature and overestimates the thickening coefficient of semicrystalline polymers in the practical crystallization temperature range.[20] Such deviations are the result of a crucial approximation in the derivation of the HW equation, which has been discussed in detail in the second chapter. A more rigorous nonlinear HW extrapolation was proposed, which reveals that the dependence of T_m' on T_x is nonlinear in nature. In the second chapter of this dissertation, a strategy was designed for a more rigorous analysis of the nonlinear dependence of T_m' on T_x, under conditions where the thickening coefficient is independent of crystallization temperature and known a priori. The proposed nonlinear HW analysis was successfully applied to Ziegler-Natta isotactic polypropylene in the preceding chapter, and the conditions of a constant thickening coefficient were achieved by extrapolating the observed melting temperatures of thickened lamellae as a function of crystallization time to

zero crystallinity (γ = 1) for each crystallization temperature. The equilibrium melting temperature of it-PP was thus determined to be ca. 212°C, about 25 K above the most widely reported value of 186°C.[23] Consistency between the result obtained by the nonlinear HW extrapolation (T_m = 212°C) and those obtained through the analysis of the temperature dependence of spherulitic growth rates (T_m = 215°C) is very satisfactory. Furthermore, as discussed in the last chapter, the predicted initial lamellar thickness of it-PP matches well the measured value at a certain crystallization temperature.

In this chapter, the nonlinear HW analysis is applied to PEO to determine its equilibrium melting temperature. PEO was specifically chosen as a model system for three reasons. First, PEO has only one crystal phase.[1] Second, issues of tacticity and polydispersity which could be raised in the case of it-PP are avoided in the case of PEO. Narrow molecular weight PEO fractions with polydispersity as low as 1.03, can be readily obtained. Third, PEO appears to show similarities to polyethylene in the sense that three crystallization regimes have been reported in literature.[11] If this is confirmed, one should be able to estimate some important fundamental parameters such as the substrate length, L. Thus, one may be able to check quantitatively the validity of the LH theory in the case of PEO. Finally, as discussed in the second chapter, the degree to which the T_m value is underestimated by the linear HW extrapolation is predicted to decrease when the crystallization temperature range over which the HW technique is applied corresponds to lower undercoolings. Such a prediction can be tested in the case of PEO because PEO appears to crystallize at much lower undercoolings than it-PP.

In addition to determining the equilibrium melting temperature for PEO, the applicability of the LH secondary nucleation theory to PEO is also addressed in this chapter. Although the LH theory appears to successfully account for a large number of experimental observations,[24] criticism of the concept of regimes and the LH theory in general continues to make its way into the literature.[12] Since knowledge of an accurate estimate of T_m is crucial for regime analysis, most criticisms of the theory cannot be taken seriously until the issue of equilibrium melting temperature has been resolved. In the previous chapter, confusions in the case of it-PP have been clarified and a regime II/III transition has been confirmed at ca. 140°C.[23] An important issue in the case of PEO relates to the report of a change in crystallographic growth

face by Point et al.[12] at a temperature very close to the regime II/III transition temperature reported by Cheng et al.[11] Conclusions drawn by Point et al. were later confirmed by Marentette and Brown.[13] and cast some doubts as to the meaning of regime transitions reported by Cheng et al. In this chapter, crystal growth rate data as a function of temperature and molecular weight from Cheng et al.[11] are re-analyzed using the LH theory.

4.2. Experimental procedures

Three poly(ethylene oxide) fractions with narrow molecular weight distributions purchased from Polymer Laboratory Inc. were used in this study. The molecular characteristics of these fractions are shown in Table 4.1. The PEO samples were stored in vacuum before experiments to prevent absorption of moisture and degradation.

PEO samples were isothermally crystallized in the temperature range from 50 to 60°C in a Pyris differential scanning calorimeter from Perkin Elmer, operated under dry nitrogen flow and with an ice-water bath. The temperature scale was calibrated using the high purity indium from Perkin Elmer, sandwiched between two polymeric films to account for differences in thermal conductivity between metals and polymers. Crystallization temperatures were calibrated by extrapolation of the melting temperature of the standard to zero heating rate. The melting traces of isothermally crystallized samples were recorded at 10 K/min from their crystallization temperatures to 85°C. The observed melting temperature was taken as the peak melting temperature, corrected for thermal lag. A small mass of PEO samples (ca. 2 mg) was used in all the DSC studies to minimize thermal lag effects.

Table 4.1. Molecular Characteristics of PEO Fractions.

Sample	M_n ($g.mol^{-1}$)	M_w/M_n
PEO1	72 555	1.03
PEO2	112 080	1.02
PEO3	217 776	1.03

4.3. Results

The heating rate dependence of the peak melting temperature of PEO was first investigated to ascertain whether melting-recrystallization-remelting or crystal thickening processes take place during the heating scans at 10 K/min. PEO samples were kept at 90°C for 3 minutes to erase prior thermal history and were subsequently quenched to 30°C. Then, heating scans from 30 to 85°C were recorded at different rates. Results for PEO1 are shown in Figure 4.1 after thermal lag correction. The peak melting temperature is plotted as a function of heating rate in Figure 4.2 for PEO1. Crystal reorganization during heating is observed only when the heating rate is less than 5 K/min. We note that the heating rate dependence of the peak melting temperature of PEO is quite similar to that of linear polyethylene, which is known to exhibit lamellar thickening during heating at low rates.[25]

In order to successfully apply the nonlinear HW analysis, the thickening coefficient, γ, has to remain constant in the whole crystallization temperature range.[20] For polymers which exhibit crystal thickening during the isothermal crystallization process, a practical technique was proposed in the last chapter to ensure that the thickening coefficient is constant prior to the analysis of T_m', T_x data. The technique is through the extrapolation of T_m' at various t_x (thickened lamellae) for a given T_x to the induction time, yielding the observed melting temperature of the original crystals at T_x (γ = 1). The induction time at each T_x can be obtained by extrapolating the crystallinity at various t_x to zero crystallinity. This technique allows one to obtain for various crystallization temperatures the observed melting temperatures of initial crystals, thus, ensuring that the thickening coefficient has the same value (γ = 1) for all crystallization temperatures.

Isothermal crystallization of PEO fractions was carried out at various T_x for different times. The evolution of the degree of crystallinity, X_c, with crystallization time, t_x at 56.06°C is given in Figure 4.3 for the three PEO fractions. A fast sigmoidal increase of the crystallinity in the primary crystallization region is observed, followed by a slower increase of the crystallinity in the secondary crystallization region. Though the total degree of crystallinity decreases with increasing molecular weight, the fraction of the crystallinity developed in the secondary crystallization region increases with increasing molecular weight.

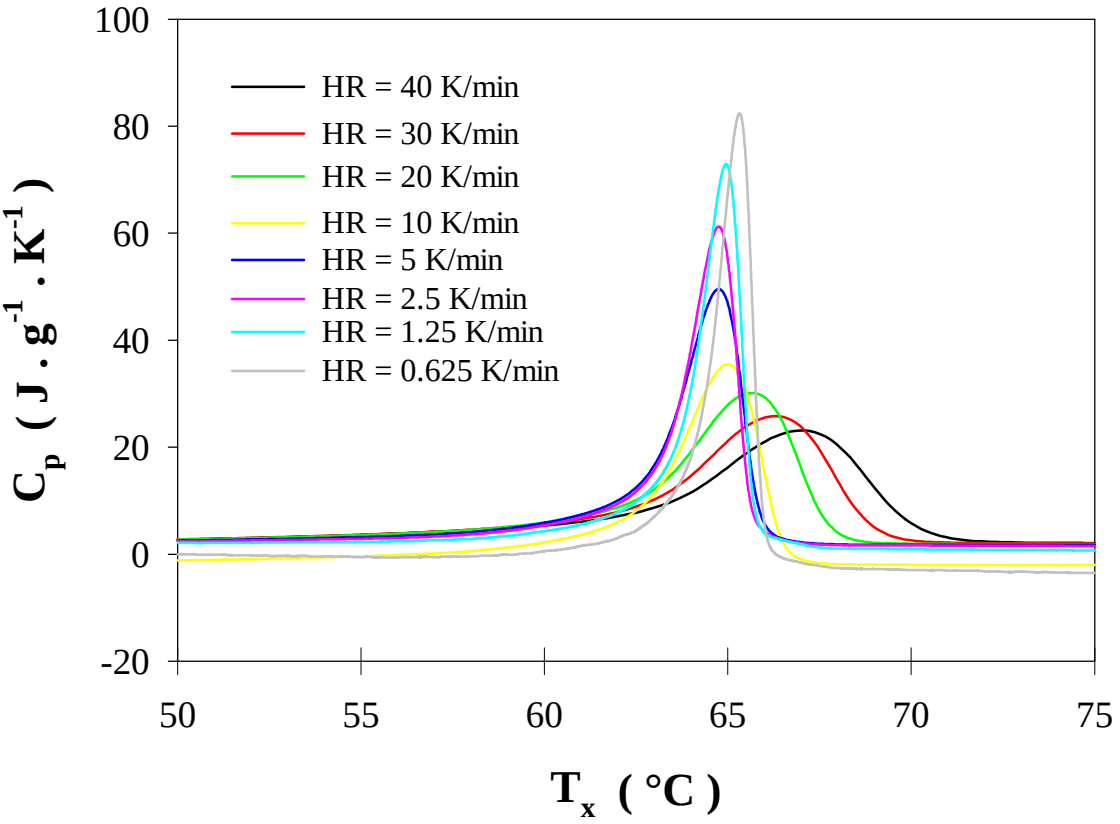

Figure 4.1. The heating scans at various rates for PEO1 after the samples were quenched from the melt.

This implies that the higher molecular weight PEO fraction tends to thicken more in the secondary crystallization region due to the lower crystallinity developed during primary crystallization. Figure 4.4a shows the evolution of the peak melting temperature, T_m', with logt_x for the three PEO fractions. T_m' is observed to increase sharply in the primary crystallization region, and much more slowly in the secondary crystallization region. The leveling off of T_m' is likely due to the extremely high crystallinity of PEO fractions (ca. 80%) developed in the primary crystallization region. In other words, very narrow amorphous layers resulted from the primary crystallization give rises to the dramatic decrease of lamellar thickening, thus, the shifting rate of T_m' with logt_x in the secondary crystallization region.

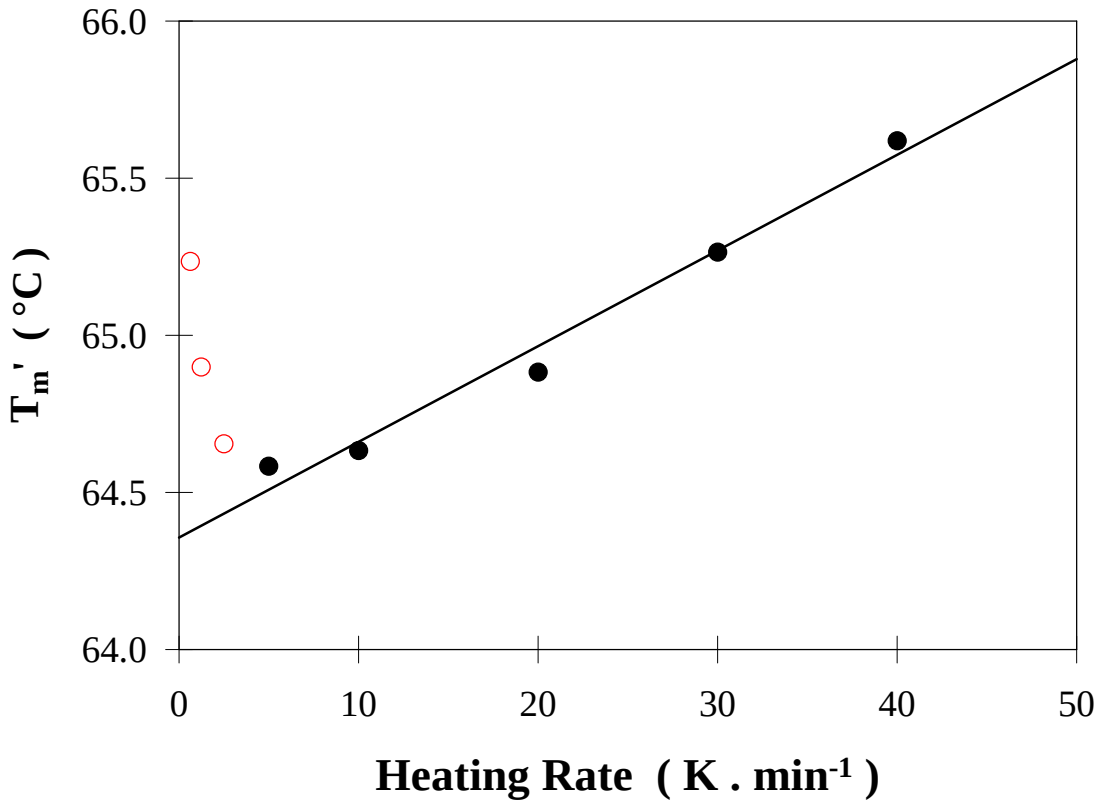

Figure 4.2. The peak melting temperature versus the heating rate for PEO1.

Such a phenomenon was not observed in the case of it-PP whose crystallinity is greatly less than PEO (ca. 50%). Furthermore, the rate of shift of T_m' with time during secondary crystallization increases with molecular weight, suggesting that crystals thicken more in higher molecular weight (lower total crystallinity) fractions. This is consistent with the fact that the crystallinity fraction developed during secondary crystallization increases with increasing molecular weight as shown from Figure 4.3. It is also important to note from Figure 4.4a that the rate of shift T_m' of with time during primary crystallization decreases with increasing molecular weight, suggesting that the larger number of entanglements present in the interlamellar amorphous phase of higher molecular weight samples impedes more significantly the crystal thickening process.

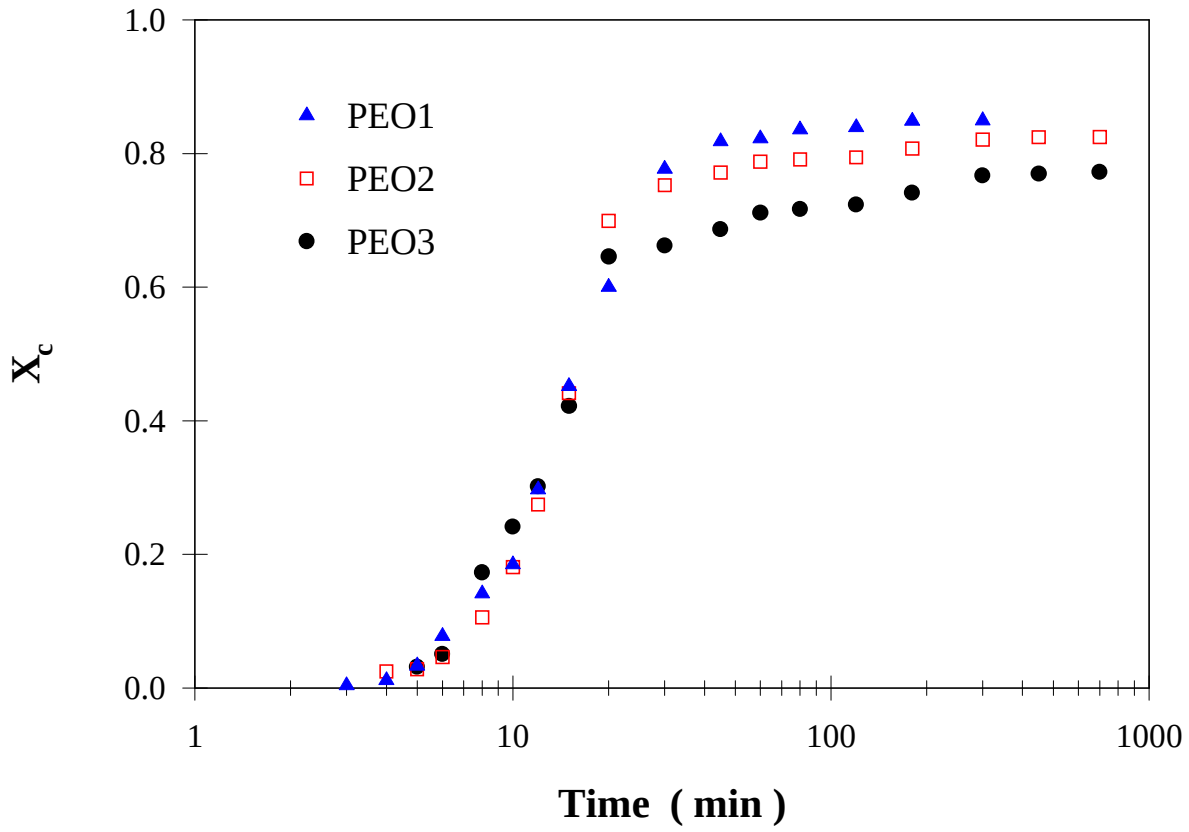

Figure 4.3. Evolution of the crystallinity with the logarithm of the crystallization time at 56.06°C for PEO fractions. The theoretical heat of fusion used in the calculation, 198 J/g, was obtained from ref.1.

The induction time, t_o, for the three PEO fractions was obtained by extrapolating the crystallinity (using a sigmoidal function) at various t_x to zero crystallinity, and the results are listed in Table 4.2. Two extrapolative procedures were used to achieve the observed melting temperature at the induction time. First, we could approximate the evolution of T_m' with time by assuming a linear variation of T_m' with logt_x in the primary crystallization range (Figure 4.4a). Alternatively, we could fit the evolution of $T_m'(t_x)$ with logt_x by a sigmoidal function (Figure 4.4b). The latter extrapolation yields a slightly higher $T_m'[T_x, t_o]$ value than the former one, and the differences are 0.14°C and 0.30°C for PEO2 and PEO1, respectively

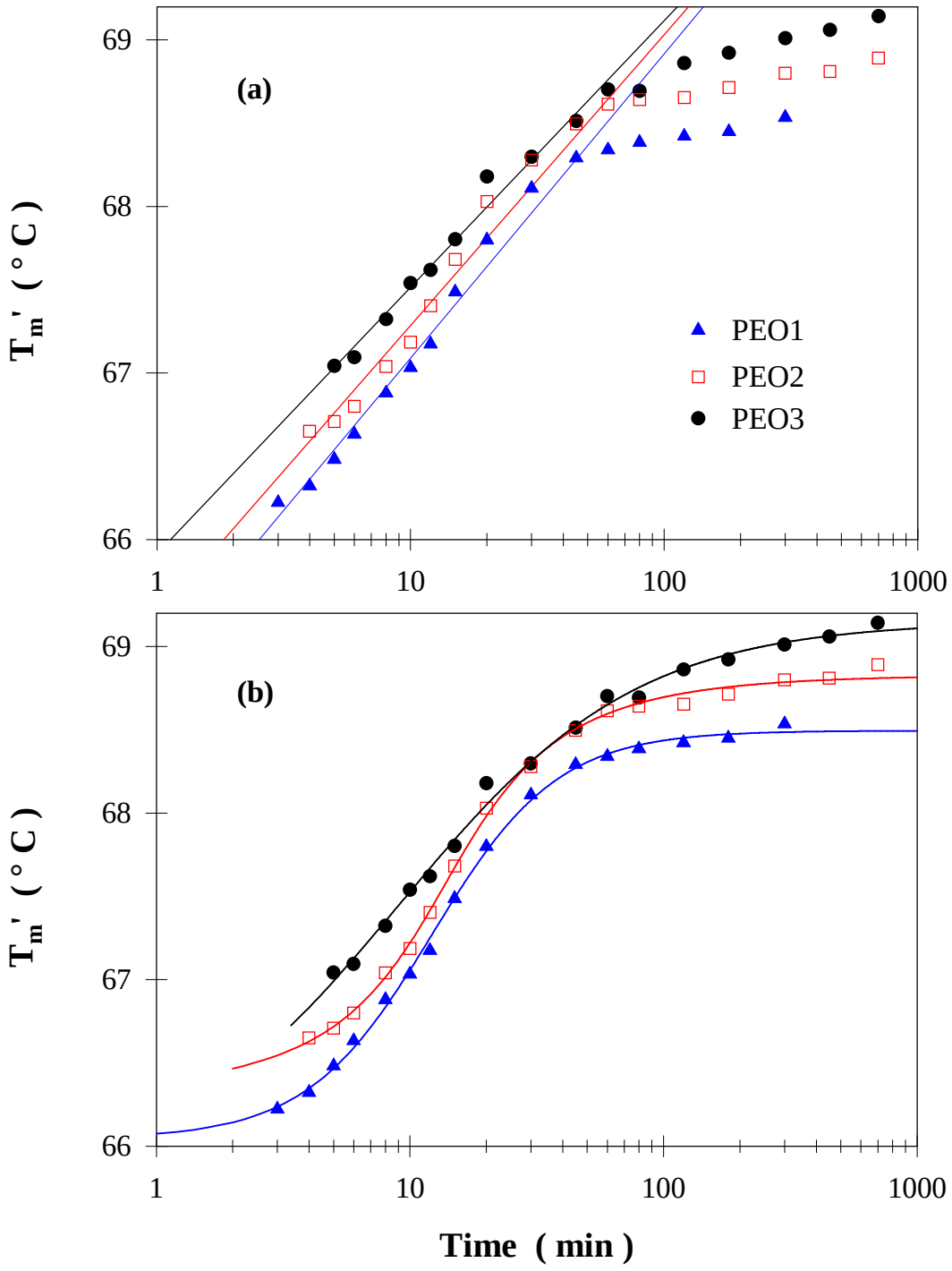

Figure 4.4. The evolution of the peak melting temperature versus the crystallization time for PEO fractions at 56.06°C. (a) Linear extrapolation in the primary crystallization region, (b) sigmoidal fitting in the whole temperature range.

(no difference in case of PEO3). The results obtained from the former method will be used below and the difference between the two methods is taken as an uncertainty of $T_m'[T_x, t_o]$.

The results of $T_m'[T_x, t_o]$ for three PEO fractions are given in Table 4.2 for various T_x. If the conventional HW linear extrapolation is performed, as depicted in Figure 4.5, values ca. T_m = 72°C are obtained for PEO, which are similar to those reported by Alfonso and Russell.[15]

In the second chapter, the derivation of the non-linear equation relating T_m' and T_x (Equation 2.14) was given. If the initial lamellar thickness is given by $l^* = C_1/\Delta T + C_2$, where C_1 is equal to $2\sigma_e^1 T_m/\Delta H_f$, C_2 is a constant accounting for both the δl term and the temperature dependence of the kinetic fold interfacial free energy, σ_{ex}, then Equation 2.14 can be rearranged into:[20]

$$M = \gamma \frac{\sigma_e^{\,1}}{\sigma_{em}} (X + a) \tag{4.1}$$

In this equation, $M = T_m/(T_m - T_m')$, $X = T_m/(T_m - T_x)$, σ_{em} is the fold interfacial free energy appearing in the Gibbs-Thomson Equation, and $a = \Delta H_f C_2/2\sigma_e^1$, where ΔH_f is the theoretical

Table 4.2. Induction time and the observed melting temperature of initial lamellar crystals as a function of crystallization temperature for PEO fractions.

T_x (°C)	PEO1		PEO2		PEO3	
	t_o (min)	$T_m'[T_x, t_o]$ (°C)	t_o (min)	$T_m'[T_x, t_o]$ (°C)	t_o (min)	$T_m'[T_x, t_o]$ (°C)
52.06					0.7	65.57
53.06			1.1	65.35	1.1	65.87
54.06	0.7	65.24	1.8	65.77	2.0	66.20
55.06	1.4	65.53	2.1	66.05	2.6	66.56
56.06	2.1	65.87	3.2	66.37	4.7	66.86
57.06	3.0	66.24	4.4	66.79	8.1	67.40
58.06	3.8	66.68	6.3	67.13	14.1	67.68
59.06	4.7	67.02	9.2	67.62		
60.06	9.3	67.45				

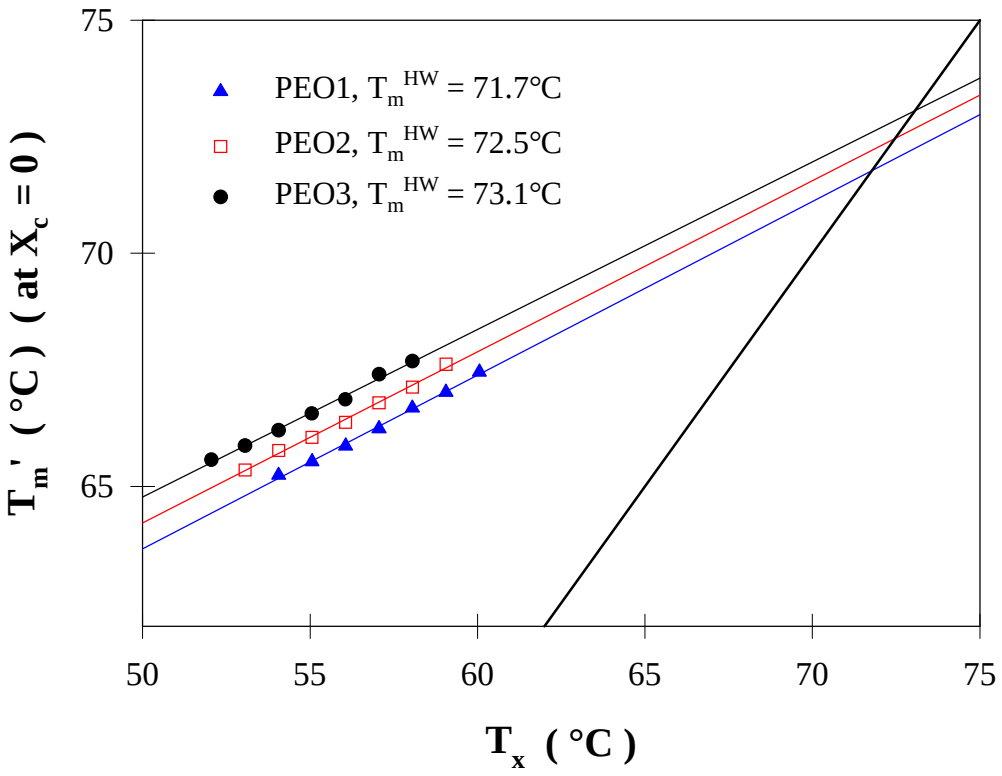

Figure 4.5. The conventional HW linear extrapolations for PEO fractions, results are listed on the plot.

heat of fusion. For a set of T_m', T_x values, a corresponding set of M, X values can be calculated for a given choice of the equilibrium melting temperature. The slope of a M versus X plot yields the thickening coefficient, provided that $\sigma_e^1 = \sigma_{em}$, which is a reasonable assumption based on the study of linear polyethylene. As a result, the thickening coefficient, γ, can be obtained as a function of the chosen T_m value (see Figure 4.6 for PEO1). Since T_m' values used in the analysis are the observed melting temperatures of initial lamellar crystals, a plot of M versus X for the true equilibrium melting temperature should yield a straight line of the slope unity ($\gamma = 1$) and intercept equal to a. The equilibrium melting temperature obtained by this method for PEO1 is therefore found to be 80.6°C. The same method was used for PEO2 and PEO3, resulting in equilibrium melting temperatures of 82.3 and 83.7°C, respectively. If the uncertainty of $T_m'[T_x, t_o]$ is taken into account, the results of the equilibrium melting temperature are 81.4, 82.7 and 83.7°C for PEO1, PEO2 and PEO3,

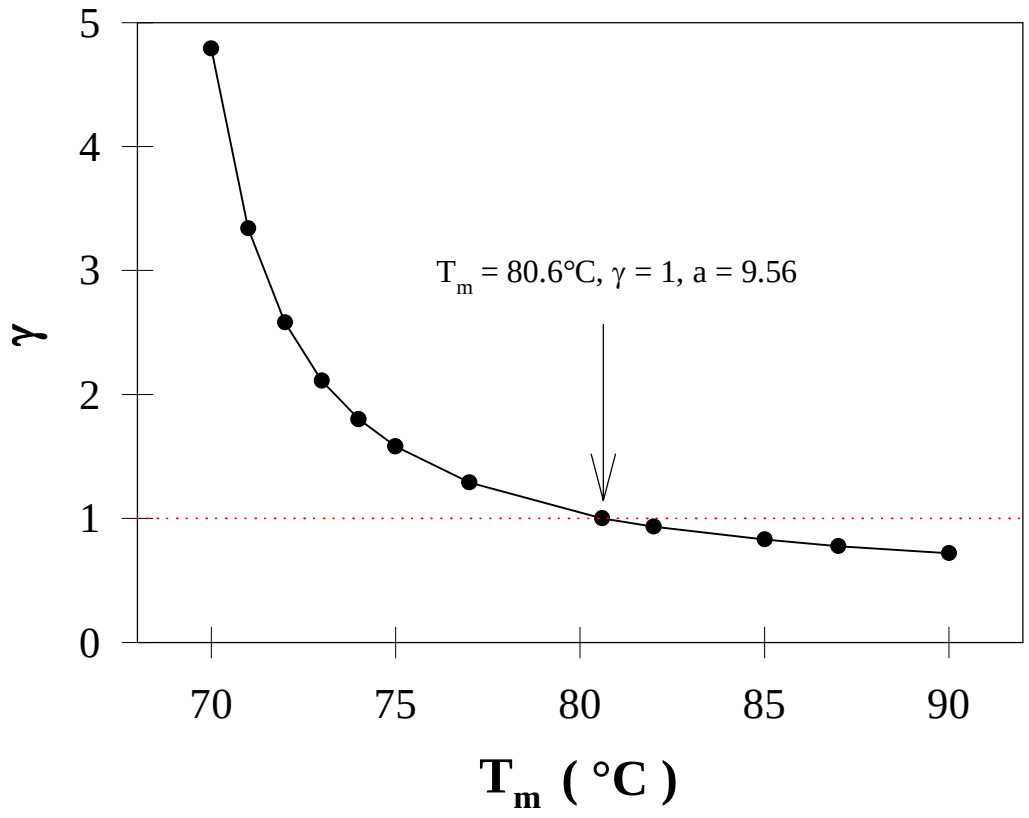

Figure 4.6. Plot of the thickening coefficient, γ, as a function of chosen equilibrium melting temperature for PEO1.

respectively. As expected, the magnitude of T_m increases with molecular weight. A quantitative analysis of the molecular weight dependence of the equilibrium melting temperature is however not carried out due to 1) the very limited molecular weight range employed in the current study and 2) the uncertainty associated with $T_m'[T_x, t_o]$ through the extrapolation methods. Figure 4.7 shows the plot of M versus X for each of the three PEO fractions investigated here using the equilibrium melting temperatures derived from the $\gamma = 1$ condition. Figure 4.8 shows the HW linear and nonlinear extrapolations based on the set of T_m', T_x data for PEO1, where T_m' is the extrapolated melting temperature of initial lamellar crystals and T_x is the crystallization temperature. Linear and nonlinear extrapolations lead to estimates of the equilibrium melting temperature, which differ by ca. 10K. The underestimation of the equilibrium melting temperature by the linear Hoffman-Weeks

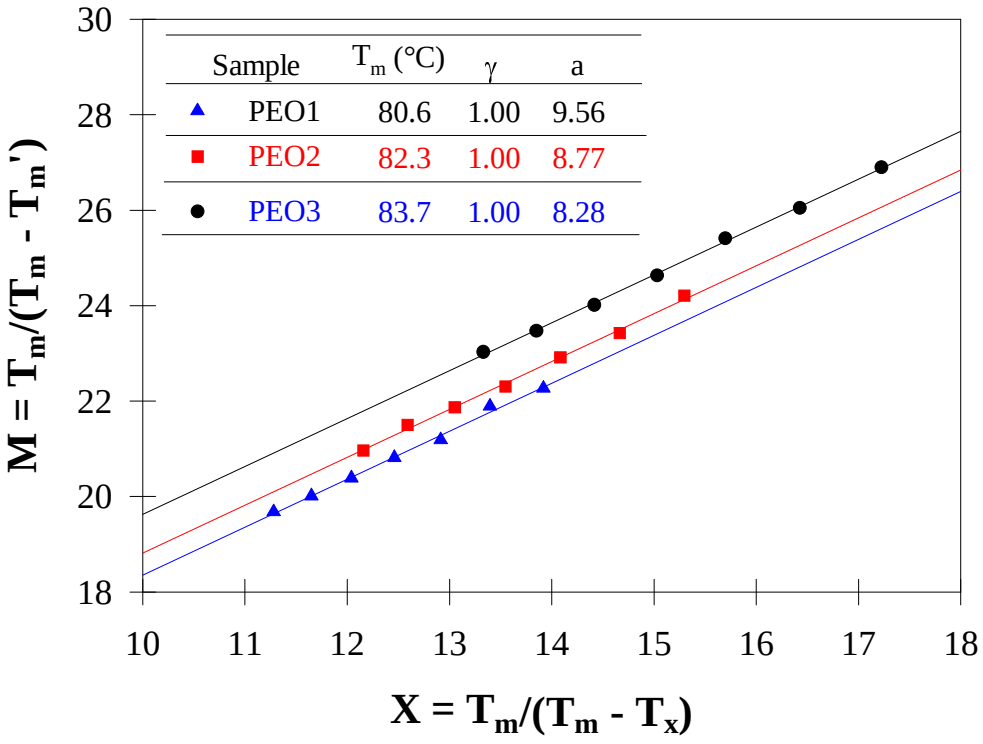

Figure 4.7. *M* versus *X* plot for PEO fractions, T_m used for each PEO fraction is the value which yields $\gamma = 1$. Values of T_m and *a* are tabulated on the plot.

extrapolation is much smaller in the case of PEO (10 K) than in the case of it-PP (25 K). This result is consistent with the prediction that the extent to which T_m is underestimated by the linear analysis decreases if isothermal crystallization is carried out at very low undercoolings and if the crystals are more susceptible to thickening. Furthermore, the thickening coefficient inferred from the linear HW analysis in Figure 4.8 is having a magnitude of 2.7, which is not supported by recent time resolved synchrotron SAXS studies for PEO.[31]

4.4. Discussion

One expects on theoretical grounds the nonlinear HW analysis to yield a more accurate equilibrium melting temperature than the conventional linear HW extrapolation. However, the results obtained through this nonlinear extrapolation must also be consistent with those

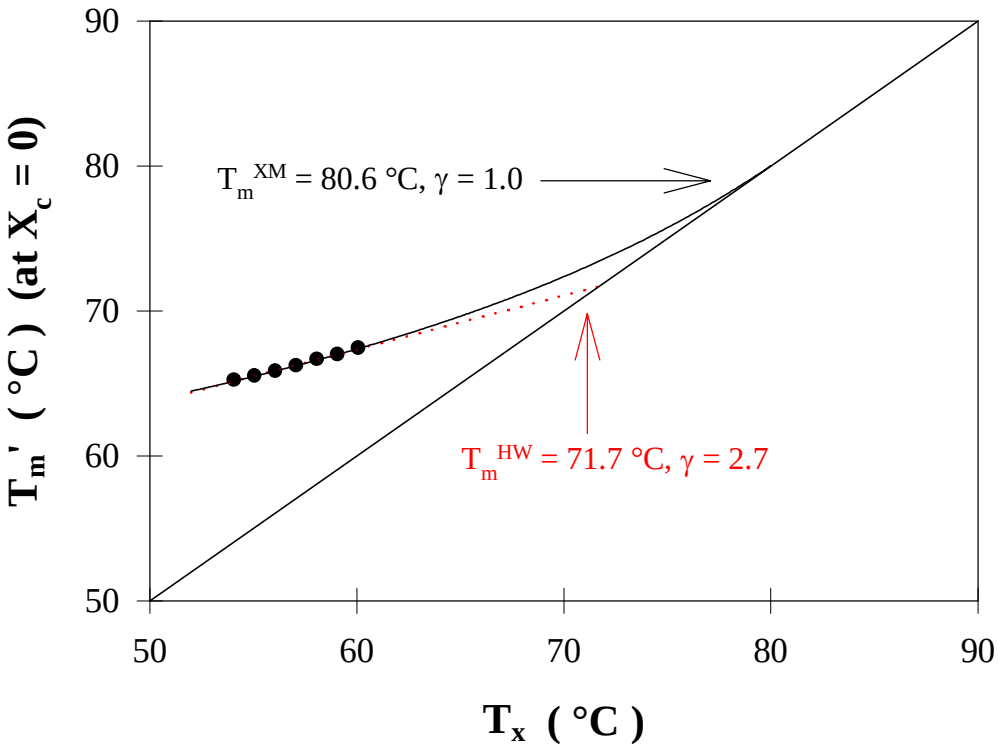

Figure 4.8. Plot of the observed melting temperature of initial lamellar crystals versus the crystallization temperature for PEO1. The solid curve is the nonlinear HW analysis calculated using T_m = 80.6°C, γ = 1 and a = 9.56. The dotted line is the linear HW extrapolation based on T_m', T_x data.

obtained from the analysis of the temperature dependence of spherulitic growth rates. Thus spherulitic growth rate data from the literature are analyzed in the context of the LH secondary nucleation theory, following an approach similar to that discussed for it-PP. Then, the temperature dependence of the initial lamellar thickness predicted using the thermodynamic parameters calculated in this work is compared to experimental data published recently by Talibuddin et al.[31]

4.4.1. Analysis of the temperature dependence of the spherulitic growth rates

Figure 4.9 shows spherulitic growth rate data for three PEO fractions (defined as PEO4, PEO5, PEO6) as a function of the crystallization temperature. These data were scanned from

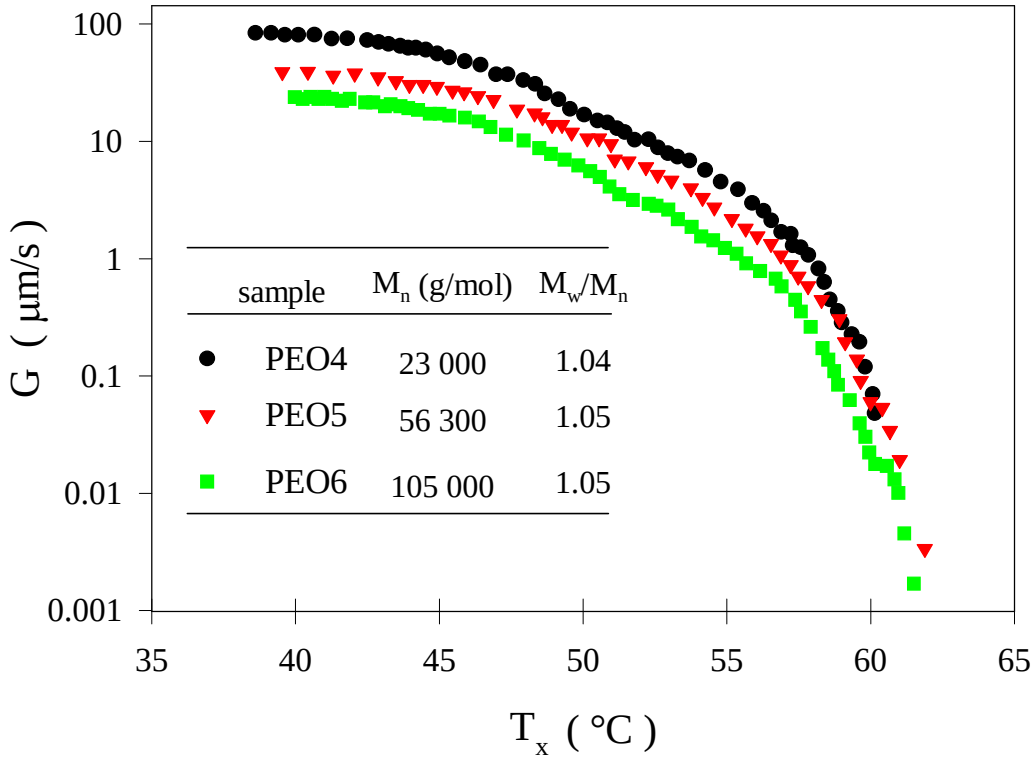

Figure 4.9. The raw crystal growth rates versus the crystallization temperature for three PEO fractions with the characteristics listed on the plot. Data scanned from ref.11.

a recent publication of Cheng et al.[11] and constitute the only data set providing growth rates up to very high crystallization temperatures. The molecular characteristics of these three PEO fractions are shown on Figure 4.9. PEO5 (M_n = 56 300 g.mol^{-1}, M_w/M_n = 1.05) is taken as an example to discuss the regime analysis. The results shown below are all concerned with this fraction unless otherwise noted. A dip is observed at ca. 50°C in each of the growth rate curves shown in Figure 4.9. This dip was taken as a regime II/III transition in the original paper by Cheng et al.[11] when T_m = 69°C was used in the regime analysis. However, Point et al. reported a crystal growth face transformation at ca. 50°C, changing from (120) at temperature above 50°C to (010) at lower temperatures.[12] This change of the growth front was subsequently confirmed by Marentette and Brown.[13] It is also important to note that crystal growth rates below 50°C are close to or exceed 10 μm/s. As a result of the fast

crystallization, a large amount of heat is released at the growth front, and the local temperature at the growth front is altered. Therefore, the crystallization temperature differs from that set in the hot-stage and the growth rates are underestimated. Hence, the crystal growth rate data below 51°C will not be included in the analysis.

The LH secondary nucleation theory predicts the following relation between the spherulitic growth rate, G, and the crystallization temperature, T_x,[24]

$$\ln G_j + \frac{U^*}{R(T_x - T_\infty)} = \ln G_j^{\,o} - \frac{K_{gj}}{T_x(T_m - T_x)} \tag{4.2}$$

where U^* and T_∞ are the Vogel-Fulcher-Tamman-Hesse (VFTH) parameters describing the temperature dependence of the transport of polymer segments across the liquid/crystal interphase, K_{gj} is the secondary nucleation constant in a given regime, and G_j^o is the prefactor assumed to be independent of temperature. The VFTH parameters recommended by Hoffman et al.[24] are U^* = 6270 J/mol and $T_\infty = T_g$ - 30K. A plot of the left hand side of Equation (4.2) versus $1/T_x\Delta T$ yields K_{gj} as the slope. According to the LH theory, the ratio of the secondary nucleation constants in regime I and regime II, $K_{g\,I}/K_{g\,II}$, should be equal to 2.[24] Previous studies showed that the choice of an equilibrium melting temperature has a profound effect on the magnitude of K_{gj} and on their ratios. Figure 4.10 shows the results of the LH analysis of crystal growth rates for PEO5 using T_m = 81.5°C, a value close to that obtained from the nonlinear HW extrapolation. A slope change is observed at ca. 57°C, and the nucleation constant at temperatures below 57°C is found to be one half of that at temperatures above 57°C, suggesting that a regime I/II transition exists at ca. 57°C. A gradual transition, over ca. 3 K, is observed at ca. 57°C, so the data in the transition zone (open triangles) are excluded from the analysis. Figure 4.11 shows the evolution of the ratio of $K_{g\,I}$ to $K_{g\,II}$ as a function of the value chosen for T_m in the analysis. The ratio of $K_{g\,I}$ to $K_{g\,II}$ is equal to 2 for T_m = 81.5°C. Therefore, choosing 81.5°C for the equilibrium melting temperature satisfies the criterion D defined in the previous chapter for it-PP. As discussed in the previous chapter, values of T_m obtained through other criteria (A - C) are significantly affected by the quality of the data. Therefore, analyses based on criteria A through C will not be carried out in the case of PEO since the scatter in the growth rate data of Cheng et al. appears significant.

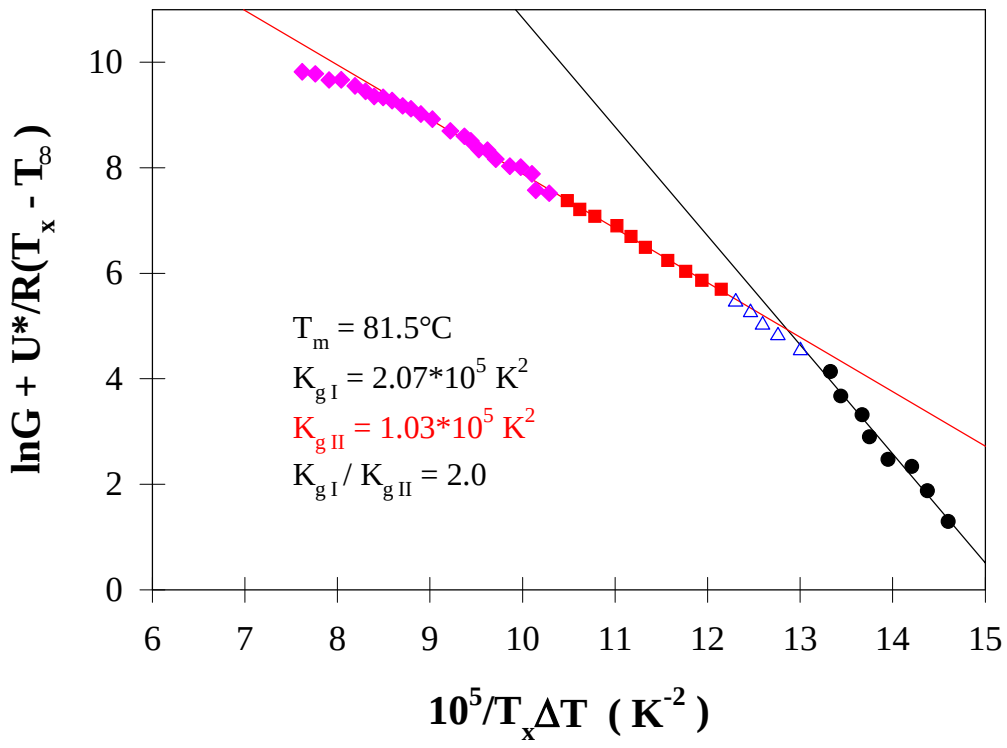

Figure 4.10. LH plot for PEO5 using U* = 6270 J/mol and T_∞ = 190.2 K. Solid circle: regime I; solid square: regime II; open triangle: data in the transition zone and they are not included in calculating K_g values; solid diamond: data below 51°C where the growth face has changed and they are not included in the analysis.

A similar analysis based on criterion D is carried out with U^* = 29.3 kJ/mol, a value used by Buckley and Kovacs,[4] Cheng et al.[11] and Marentette and Brown.[13] Unreasonably high estimates of T_m (102.9°C) and of the secondary nucleation constants are obtained in this case, as shown in Table 4.3. However, choosing U^* = 29.3 kJ/mol appears to be unreasonable since this value is actually the activation energy associated with self-diffusion in low molecular weight PEO.[4] Thus, this value should be used in the Arrhenius rather than the VFTH formulation of the transport term. If an Arrhenius form is used for the transport term, equation (4.2) becomes:

$$\ln G_j + \frac{Q_d^*}{RT_x} = \ln G_j^{\,o} - \frac{K_{gj}}{T_x(T_m - T_x)} \tag{4.3}$$

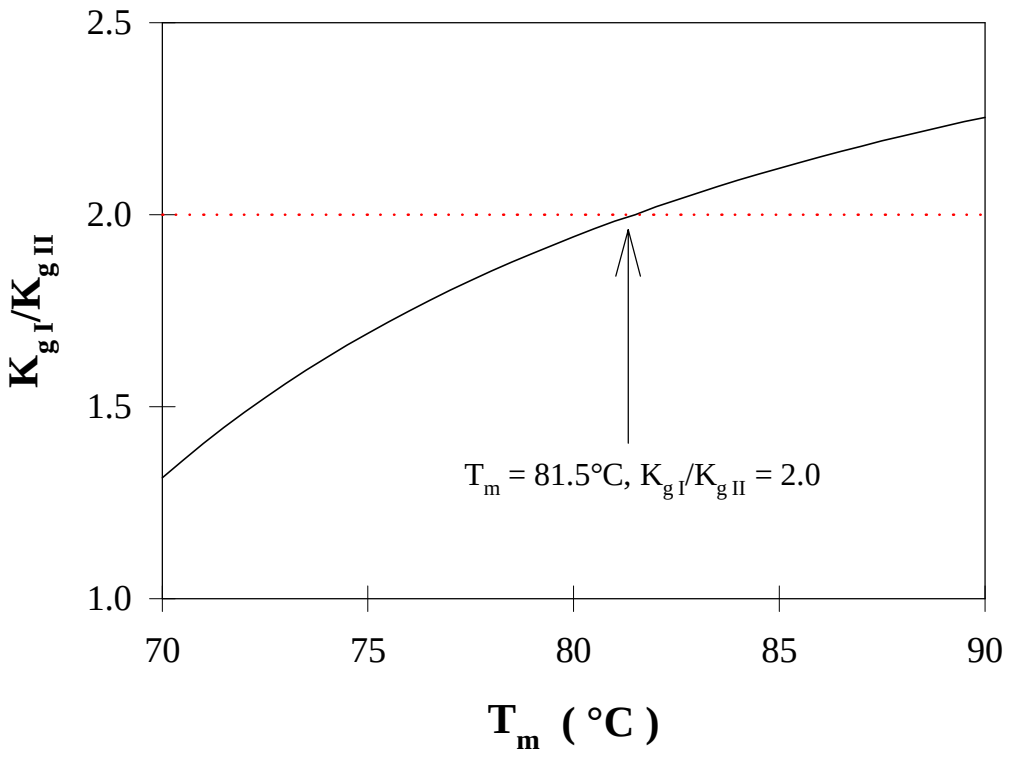

Figure 4.11. Evolution of the ratio of the secondary nucleation constant in regime I to that in regime II as a function of chosen equilibrium melting temperature. At T_m = 81.5°C, the ratio is equal 2.

where Q_d* is the activation energy for diffusion.[24] The results of the regime analysis based on Equation 4.3, using Q_d* = 29.3 kJ/mol and criterion D are also listed in Table 4.3. It is reassuring to observe that these latter results are very similar to those obtained using Equation 4.2 and U* = 6270 J/mol. As pointed out by Hoffman and Miller,[24] both Equation 4.2 and Equation 4.3 can be used when the crystallization temperatures are in excess of T_g + 100K, and only Equation 4.2 should be used when crystallization is carried out at temperatures below T_g + 100K. Since the crystallization temperature range for PEO is located above T_g + 100K, the crystal growth process is fairly independent of the details of the transport mechanism and either equation is appropriate.

An activation energy of 29.3 kJ/mol however appears to be inappropriate for the analysis of spherulitic growth rates of intermediate to high molecular weight PEO fractions.

According to Cheng et al.[26] and Appel et al.,[27] the activation energy for diffusion decreases sharply with molecular weight at molecular weights above ca. 20,000 g/mol. An activation energy of 16 kJ/mol, reported by Appel et al., for molecular weights above 20,000 g/mol, was also used in the analysis of the temperature dependence of spherulitic growth rates (Table 4.3). Only slight differences in the values of T_m (ca. 1.5 °C) and of the nucleation constants result from changing Q_d* from 29.3 to 16 kJ/mol.

Similar calculations are also performed for PEO4 and PEO6, and the results are given in Table 4.3 for comparison. Values of T_m obtained using U* = 6270 J/mol for Equation 4.2 or using Q_d* = 16 kJ/mol for Equation 4.3 are located in a very narrow temperature range (78.2°C - 83.8°C) for each of the three PEO fractions. T_m values in all cases increase as expected with molecular weight and are found to be slightly larger (2 K) when derived from Equation 4.2 (U* = 6270 J/mol) than from Equation 4.3 (Q_d* = 16 kJ/mol).

Table 4.3. Results from the LH analysis using criterion D ($K_{g\ I}/K_{g\ II}$ = 2.0). Different U* values (Equation 4.2) and Q_d* values (Equation 4.3) were adopted in the analyses.

Sample		U* = 6270 J/mol T_∞ = 190.2 K	U* = 29.3 kJ/mol T_∞ = 190.2 K	Q_d* = 29.3 kJ/mol	Q_d* = 16 kJ/mol
PEO4	T_m (°C)	80.5	109.5	79.7	78.2
	$10^{-5}K_{g\ I}$ (K^2)	1.83	12.49	1.69	1.42
	$10^{-5}K_{g\ II}$ (K^2)	0.92	6.25	0.84	0.71
PEO5	T_m (°C)	81.5	102.9	80.8	79.5
	$10^{-5}K_{g\ I}$ (K^2)	2.07	9.80	1.92	1.66
	$10^{-5}K_{g\ II}$ (K^2)	1.03	4.90	0.96	0.83
PEO6	T_m (°C)	83.8	115.9	82.9	81.2
	$10^{-5}K_{g\ I}$ (K^2)	2.34	15.88	2.15	1.82
	$10^{-5}K_{g\ II}$ (K^2)	1.17	7.94	1.08	0.91

The equilibrium melting temperatures obtained from the analysis of the temperature dependence of spherulitic growth rates (79.3°C to 83.8°C) are very similar to these obtained from the nonlinear HW analysis (80.6°C - 83.7°C). Such an agreement supports the general applicability of both the nonlinear HW extrapolation and the LH secondary nucleation theory for the determination of equilibrium melting temperatures. While a regime I/II transition was clearly observed at ca. 57°C in the LH plot (Figure 4.10), it is reassuring that this transition is also visible in the original growth rate data (Figure 4.9). Data below 51°C were not included in the regime analysis, but are also presented in Figure 4.10 to show that there is no change of slope at ca. 50°C. The slope shift at ca. 50°C in the original paper by Cheng et al.[11] was solely due to the use of an incorrect T_m value (69°C). The same conclusion was reached by Marentette and Brown[13] based on their analysis of the temperature dependence of the crystal growth rates. A change in slope of the LH plot is observed at ca. 50°C if T_m is chosen to be 69.0°C but disappears when T_m is chosen to be 76.0°C. It is clear that the choice of T_m is crucial for a rigorous regime analysis. An incorrect T_m value (only 7°C lower in this case) easily leads to the artificial appearance or disappearance of a regime transition. In the analysis of the original data by Cheng et al.,[11] in addition to regime II/III transition at ca. 50°C, a regime I/II transition was observed at ca. 57°C, in the vicinity of the regime I/II transition temperature reported in this work. In Cheng's work, however, the K_g ratio (1.63) was significantly smaller than the theoretical value (2.0). More surprisingly, a reversal of regime I back to regime II was reported at still higher temeperatures.[11] In the analysis presented, this unusual transition from regime I to regime II upon increasing the crystallization temperature does not appear at all. As a result, all data points above 57.0°C are in regime I. Although the data are slightly scattered, they are distributed randomly along the linear regression line (Figure 4.10).

Knowledge of the equilibrium melting temperature, the secondary nucleation constants and the theoretical heat of fusion of PEO enables one to calculate the product of the surface free energy, $\sigma\sigma_e^{\,1}$, using predictions of the LH theory:

$$K_{gI} = 2K_{gII} = \frac{4b_o\sigma\sigma_e T_m}{\Delta H_f k} \tag{4.6}$$

where b_o is monomolecular layer thickness in the direction normal to the growth front.[24] For the (120) growth face, b_o = 0.462 nm.[15] T_m is taken as *81.5*°C for U^* = 6270 J/mol (Equation

4.2) and ΔH_f = 231 J.cm^{-3}.[1] $\sigma\sigma_e^1$ is then calculated to be 1006 erg^2.cm^{-4}. Two methods have been proposed in literature to estimate the value of σ. The first method is the empirical correlation between heat of fusion and lateral interfacial free energy by Thomas and Staveley,[28]

$$\sigma_{TS} = \alpha(a_o b_o)^{1/2} \Delta H_f \tag{4.5}$$

where α = 0.1 for polyethylene.[27] Though the physical meaning of the α parameter is not well understood, a value of 0.1 has been widely used in the literature. This low value of α (0.1) was found appropriate for a class of polymers including polyethylene and isotactic poly(propylene), while a higher value (0.25) was proposed for high melting aliphatic polyesters, such as poly(pivalolactone).[29] Considering that PEO and PE are fairly similar in structure, we assume α = 0.1 and obtain a value of 10.2 erg.cm^{-2} for σ. The second method is based on the theory developed by Hoffman et al.[30] which relates σ to the chain characteristic ratio, C_∞. This theory proposes that σ is given by:

$$\sigma_{C_\infty} = \Delta H_f \left(\frac{a_o}{2}\right)\frac{1}{C_\infty} \tag{4.6}$$

where a_o is the width of polymer chains along the growth front. Taking a_o = 0.462 nm for the (120) growth face of PEO and C_∞ = 4.0,[15] $\sigma_{C\infty}$ was determined to be 12.7 erg.cm^{-2}. These two methods yield very similar values of the lateral surface free energy, indicating that α = 0.1 is a reasonable assumption for PEO. The average of the two values (11.4 erg.cm^{-2}) is then used to calculate the fold interfacial free energy, σ_e^1 (88.3 erg.cm^{-2}). This value is only slightly higher than that reported by Alfonso and Russell (76 erg.cm^{-2}),[15] but is much higher than that reported by Kovacs and Gonthier (22.4 erg.cm^{-2}) based on studies of low molecular weight PEO fractions.[2]

4.4.2. Correlations between crystallization temperature, melting temperature and lamellar thickness.

As discussed in the Results section, when a good estimate of the equilibrium melting temperature is used to generate a *M-X* plot, the slope is equal to the thickening coefficient and the intercept *a*, is given by $a = \Delta H_f C_2/2\sigma_e^1$. The value of C_2 is available from previous studies by Cheng et al.[10] These authors found that C_2 = 76Å and is approximately

independent of molecular weight. Taking C_2 = 76Å, a = 9.56 for PEO1 (Figure 4.6), σ_e^1 was calculated to be 91.8 erg.cm^{-2}. The nonlinear HW extrapolation and the analysis of the temperature dependence of the spherulitic growth rates yield similar values of T_m values (80.6 - 83.7°C and 81.5 - 83.8°C) and nearly identical values of σ_e^1 (91.8 erg.cm^{-2} for PEO1 and 88.3 erg.cm^{-2} for PEO5). All the input values and results of calculations are listed in Table 4.4.

The correlation between the initial lamellar thickness and the crystallization temperature can be expressed as[20],

$$l^* = \frac{C_1}{\Delta T} + C_2 = \frac{2\sigma_e^1 T_m}{\Delta H_f \Delta T} + C_2 \tag{4.7}$$

Having established estimates for the equilibrium melting temperature and the fold surface free energy, it is now straightforward to predict the crystallization temperature dependence of the initial lamellar thickness for PEO1,

$$l^* = \frac{2811}{(80.6 - T_x)} + 76 \tag{4.8}$$

where l^* is given in Å, and T_x is in °C. Figure 4.12 shows the plot of the predicted initial lamellar thickness against crystallization temperature for PEO1. Also shown are two data

Table 4.4. Comparison of the results from the nonlinear HW extrapolation (PEO1) and from the regime analysis of the temperature dependence of the crystal growth rates using Equation 4.2 and U^* = 6270 J/mol (PEO5).

Nonlinear HW Extrapolation		Lauritzen-Hoffman Theory	
T_m (°C)	80.6	T_m (°C)	81.5
a	9.56	b_o (nm)	0.462
C_2 (Å)	76	σ (erg/cm^2)	11.4
ΔH_f (J/cm^3)	231	ΔH_f (J/cm^3)	231
σ_e^1 (erg/cm^2)	91.8	σ_e^1 (erg/cm^2)	88.3

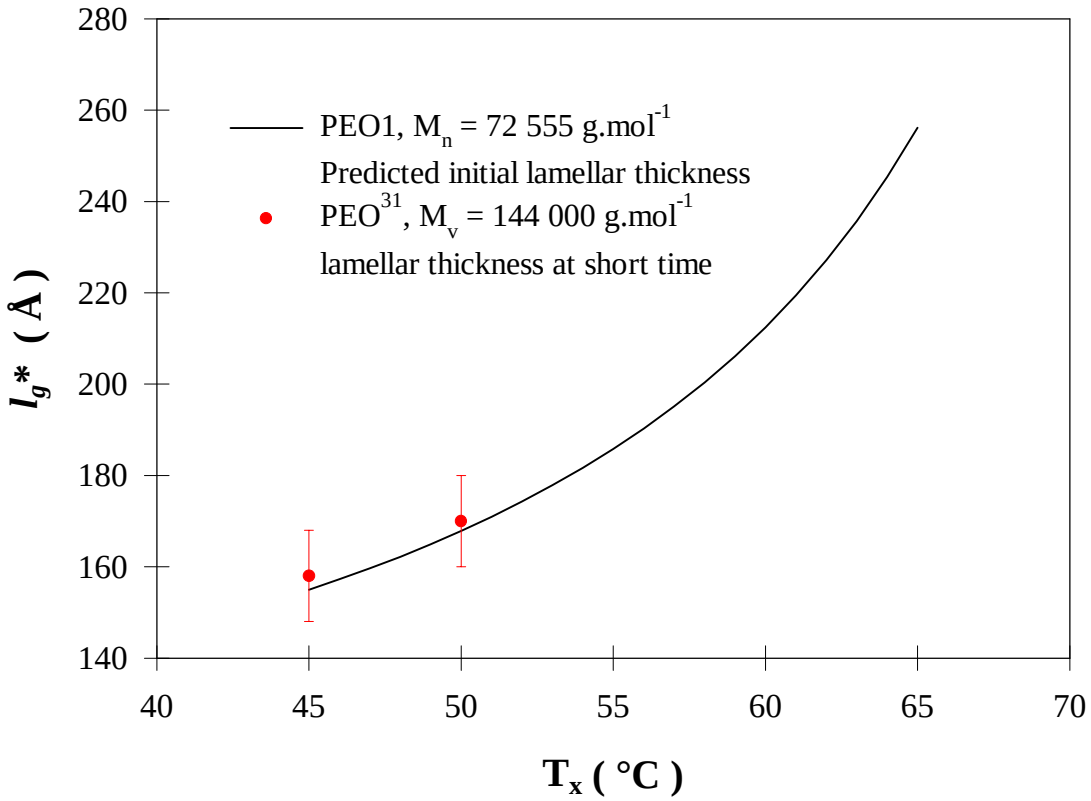

Figure 4.12. Plot of predicted initial lamellar thickness versus crystallization temperature for PEO. Also shown are the two data points obtained through real time small angle X-ray measurements reported by Talibuddin et al.[31]

points obtained from Talibuddin et al.,[31] using real time small angle X-ray scattering measurements. In this study, since PEO samples were isothermally crystallized at 45 and 50°C for very short times (7 minutes and 10 minutes, respectively), the measured lamellar thicknesses must be very close to those characteristic of initial lamellae. In further support for the validity of the M-X approach, we note that the agreement between theoretical predictions and experiments is well within the experimental uncertainty. We note that very limited information on the temperature dependence of initial lamellar thicknesses is available in literature, especially at high crystallization temperatures. One possible reason, as pointed out by Alfonso and Russell, is that at higher crystallization temperatures, the thicknesses of PEO lamellar crystals are too large to be detected by conventional X-ray scattering or diffraction.[15]

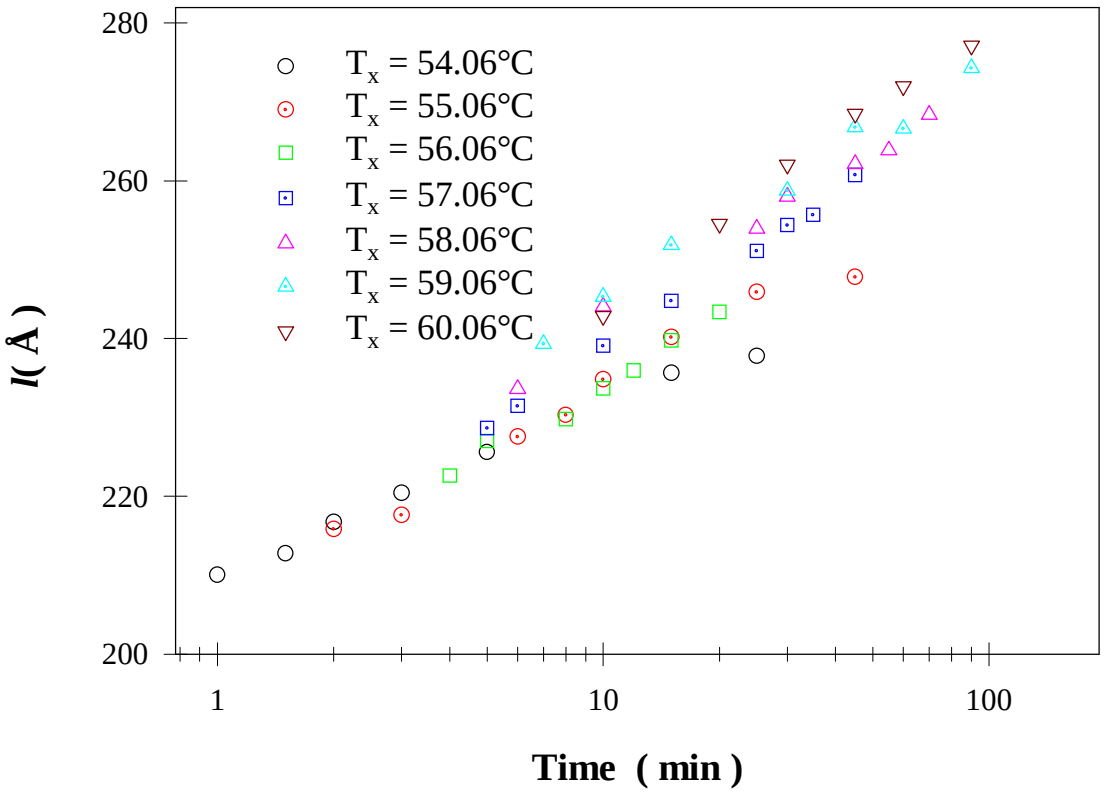

Figure 4.13. Calculated lamellar thickness of PEO1 versus the crystallization time at various T_x. Gibbs-Thomson equation was used in the calculations of the lamellar thickness.

The correlation between the observed melting temperature and the lamellar thickness, l, is expressed by the Gibbs-Thomson equation,

$$T_m' = T_m\left(1-\frac{2\sigma_{em}}{\Delta H_f l}\right) \tag{4.9}$$

Since the values for T_m and σ_{em} are known and the observed melting temperature is measured experimentally (a function of t_x and T_x), it is possible to calculate the evolution of the lamellar thickness of PEO crystals as a function of the crystallization time for different crystallization temperatures (Figure 4.13). This plot suggests that the PEO lamellar thickness increases more rapidly with the logarithm of the crystallization time at higher temperatures, an expected result because thickening is a thermally activated process. To determine the extent of lamellar thickening after isothermal crystallization at each T_x for a given period,

Equation 4.9 and 4.10 were combined, resulting in an equation relating the thickening coefficient and the crystallization time at various temperatures,

$$\gamma = \frac{l}{l^*} = \frac{2\sigma_{em}/(\Delta H_f (T_m - T_m'))}{2\sigma_e^{\,1} T_m/(\Delta H_f (T_m - T_x)) + C_2} = \left(\frac{\sigma_{em}}{\sigma_e^{\,1}}\right)\frac{M(t)}{X+a} \cong \frac{M(t)}{X+a} \qquad (4.10)$$

Though the absolute amount of thickening increases with increasing temperature, the relative percentage of thickening remains the same for various temperatures at the longest crystallization times and the value is ca. 20%. For example, the lamellar thickness of PEO1 increases from 242Å (10 minutes' isothermal crystallization at 60.0°C) to 282Å for a residence time of 150 minutes at 60.0°C. The relative increase in lamellar thickness during secondary crystallization is therefore much higher for PEO (20%) than for it-PP (5%). This observation is likely to be the result of the much higher flexibility of the PEO chains as compared to it-PP.

4.4.3. A rigorous test of the Lauritzen-Hoffman secondary nucleation theory

The LH secondary nucleation theory has been applied to a large number of semicrystalline polymers in literature, and appears to successfully account for a large number of experimental observations, such as the undercooling dependence of both the initial lamellar thickness and the crystal growth rates, and the existence and origin of breaks in growth rate curves.[24,32-38] However, except for polyethylene which has been studied extensively by Hoffman and Miller,[24] no other polymers have ever been tested rigorously. By a rigorous test, one refers to rigorously estimating fundamental parameters in the theory such as the substrate length. The Z-test proposed by Lauritzen[39] can only give a very rough estimate of the substrate length.[33,34,37] The substrate length for polyethylene lamellar crystals was found to be 865 Å within a factor of about 1.5. This value is believed to be associated with the range of the lattice coherence, which can be inferred from a careful analysis of the diffraction pattern. For a rigorous calculation of the substrate length, *L*, to be possible, it is necessary that the particular polymer under consideration exhibits a transition between regimes I and II. PLLA and cis-polyisoprene are among the very few polymers which exhibit regime I and II crystallization behavior, as reported by Vasanthakumari et al.[33] and Phillips et al.[32]. However, no estimate of the substrate length was given in the latter, and the Z-test was used to estimate the substrate length in the former and the result was claimed to be

reasonable. PEO is known to show regimes I and II crystallization behavior, though no estimate was given of the substrate length in the original paper.[11] A rigorous calculation of the substrate length is carried out for PEO in the remainder of this section.

According to the LH theory,[24] the substrate length is given by $L = n_L a_o$, where n_L is the number of chain stems on the substrate and a_o, is the width of the stem along the growth front. The explicit expressions for the prefactors in regime I and II are given in the LH theory by

$$G_I^{\,o} = \left(\frac{C_o \kappa n_L}{n}\right)\left(\frac{b_o k_B T}{h}\right)\left(\frac{k_B T a_o \Delta H \Delta T}{4 b_o l_u \sigma^2 T_m}\right) \tag{4.11}$$

and

$$G_{II}^{\,o} = \left(\frac{C_o^{\,1/2} \kappa}{n}\right)\left(\frac{b_o k_B T}{h}\right)\left(\frac{a_o \Delta H \Delta T}{\sigma T_m}\right)\left(\frac{k_B T}{2 b_o \sigma l_u}\right)^{1/2} \exp\left(-q / 2 k_B T\right) \tag{4.12}$$

In the above two equations, G_j^o is the prefactor for a given regime and is obtained from the intercept of the LH plot, C_o is the configurational path degeneracy, κ is a numerical constant and its determination is discussed below, n is the average number of repeat units in the polymer chain feeling the force of reptation during substrate completion and $n = (2/3)(M_n M_w)^{1/2}/M_{re}$ where M_{re} is the molar mass of a repeat unit, h is the Planck's constant, l_u is the projected length of one repeat unit in the chain direction, and q is the work of chain folding, $q = 2 a_o b_o \sigma_e$. All other parameters in the above two equations were defined earlier. Elimination of C_o from these two equations yields

$$n_L = 2\kappa\left(\frac{b_o k_B T}{h}\right)\left(\frac{a_o \Delta H \Delta T}{\sigma T_m}\right)\left(\frac{G_I^{\,o}}{n G_{II}^{\,o\,2}}\right)\exp(-q / k_B T) \tag{4.13}$$

This equation holds only at the temperature associated with the I/II regime transition. Thus, with G_j^o values available from the crystal growth rate data, n_L can be estimated, provided that κ is known. Two methods were introduced in the LH theory[24] to calculate the absolute substrate completion rate, g. When the expression of g obtained from the nucleation theory is equated to that derived from reptation theory, the quantity κ is obtained

$$\kappa = h \exp(Q_d^{\,*} / R T_o) \exp(q / k_B T) / \xi_o l^{*2} \tag{4.14}$$

where l^* is the initial lamellar thickness at the regime I/II transition temperature, and ξ_o is the friction coefficient at the reference temperature T_o, which can be obtained from independent studies. By a combination of $L = n_L a_o$ and Equations 4.13 and 4.14 yields the following expression for L,

$$L = \left(\frac{2a_o^{\,2} b_o k_B T \Delta H \Delta T}{\sigma \xi_o l^{*2} T_m} \right) \left(\frac{G_I^{\,o}}{n G_{II}^{\,o\,2}} \right) \exp\left(\frac{Q_d^{\,*}}{R T_o} \right) \tag{4.16}$$

So far, we have reviewed the procedure to follow the calculations of the substrate length for a given polymer, if it exhibits regime I and II behavior. Such calculations yield a value of 865Å for polyethylene. Such calculations were not performed for it-PP in the last chapter because it-PP only exhibits regime III and II crystallization behavior. Calculations of the substrate length for PEO are carried out below at the I/II regime transition temperature of 57.0°C.

A detailed study of the diffusion coefficient of PEO as a function of molecular weight and temperature was reported by Cheng et al.[26] Using these results, the diffusion coefficient for PEO at the reference temperature of 57°C can be obtained by extrapolation. The friction coefficient at the same reference temperature (57°C) is thus calculated to be 1.9×10^{-9} erg s cm^{-2}, which is within a factor of 3 of that of polyethylene (7.0×10^{-10} erg s cm^{-2} at 176°C).[24] With all the other input parameters listed in Table 4.5, the substrate length is calculated for the three PEO fractions and results are given in Table 4.5. For each PEO fraction, results are given using Equation 4.2 and U^* = 6270 J/mol, and Equation 4.3 and Q_d^* = 16 kJ/mol. σ_e values in the table are calculated from Equation 4.4 using K_g and T_m values in Table 4.3. The initial lamellar thickness was calculated based on Equation 4.7, l^* values with a symbol "$" at the beginning are results of the initial lamellar thickness by using δl instead of C_2 in Equation 4.7. In the case of polyethylene, C_2 rather than δl was used for estimations of the substrate length.[24] Using C_2 in equation 4.7, yields a value of ca. 10 Å for the substrate length of PEO lamellar crystals, which is clearly too small by nearly two orders of magnitude. Using δl in the calculation of the initial lamellar thickness leads to a substrate length in the vicinity of ca. 30 Å, which is still too small to be physically meaningful.

The possible origins of this discrepancy between theory and experiments are now discussed for PEO. (1) The activation energy for diffusion for most polymers increases slightly with increasing molecular weight and an asymptotic value is reached at intermediate to high molecular weights.[40,41] Though an abnormal situation for the activation energy for diffusion was reported for PEO,[26,27] calculations of the substrate length using the highest reported value of the activation energy of PEO, Q_d* = 29.3 kJ/mol and Equation 4.3, only increases the substrate length by about 10 percent. (2) The value of the friction coefficient was obtained indirectly by extrapolation, but the uncertainty is likely to be less than 100 percent.

Table 4.5. Calculations of the substrate length for PEO. U* refers to using Equation 4.2 and U* = 6270 J/mol; Q_d* refers to using Equation 4.3 and Q_d* = 16 kJ/mol (see text for details).

Parameter	PEO4		PEO5		PEO6	
	U*	Q_d*	U*	Q_d*	U*	Q_d*
M_n (g.mol)	23 000		56 300		105 000	
MWD	1.04		1.05		1.05	
a_o (nm)	0.462					
b_o (nm)	0.462					
ΔH_f (J/cm^3)	231					
σ (erg.cm^{-2})	11.4					
ξ_o	1.9×10^{-9} (erg.s.cm^{-2})					
T_m (°C)	80.5	78.2	81.5	80.3	83.8	81.2
$T_{transition\ I/II}$	57.3°C	57.3°C	58.0°C	56.3°C	56.9°C	56.8°C
G_I^o (μm/s)	9.09×10^{12}	5.27×10^{11}	4.95×10^{13}	5.85×10^{12}	3.61×10^{13}	1.32×10^{12}
G_{II}^o (μm/s)	5.67×10^{7}	1.71×10^{7}	8.16×10^{7}	3.68×10^{7}	6.91×10^{7}	1.66×10^{7}
σ_e (erg.cm^{-2})	78.4	61.3	88.3	76.0	99.3	77.6
l* (Å)	180	165	191	173	190	174
$^{\$}l$* (Å)	112	98	124	106	123	106
L (Å)	10.2	12.2	10.0	10.7	7.3	7.9
$^{\$}L$ (Å)	28.4	33.4	24.1	32.9	16.3	19.5

Furthermore, the value obtained is comparable to that reported for polyethylene, indicating no abnormality in the derivation of this value. (3) To make it similar to polyethylene, where CH_2 is take as the repeat unit, a bond which is an average over the three bonds (two C-O and 1 C-C) in one monomer of PEO is assumed to be the repeat unit. Thus the value of M_{re} is one third of the molar mass of PEO monomer (14.67 g/mol). If, on the other hand, the PEO monomer is taken as the repeat unit in the calculation, the substrate length is calculated to be three times large as before. (4) some researchers account for the transport of polymer segments across the melt/crystal interphase using the universal WLF parameters (U^* = 4120 cal/mol and $T_\infty = T_g - 51.6$K).[32,35] However, use of these parameters in the analysis of the temperature dependence of crystal growth rate and of the substrate length do not affect the results for PEO, (5) the scatter in the growth rate data leading to inaccuracy in the determination of the I/II regime transition temperature and the prefactors, (6) a revision of the LH theory may be necessary to yield a different chain length dependence of the spherulitic growth rate. In a recent publication, Snyder et al.[42] pointed out that a different treatment of the transport term should be used for the first and subsequent stems in the LH theory. Indeed, the deposition of the first stem is a local segmental process and the deposition of the following stems involves a reeling in effects and therefore the friction of a whole chain. If the deposition of the first stem is treated differently from that of subsequent stems, the prefactor in Equation 4.2 or 4.3 will have different chain length dependence.

4.5. Conclusions

The nonlinear HW analysis proposed in the second chapter was carried out in the case of PEO. The equilibrium melting temperature of PEO is found to be ca. 82±2°C, ca. 10 K higher than that obtained by the linear HW extrapolation. This study further confirmed that the linear HW extrapolation underestimates the equilibrium melting temperature and overestimates the thickening coefficient. However, the extent to which T_m was underestimated is much smaller in the case of PEO (10 K) than in the case of it-PP (25K), because PEO crystallizes at very low undercoolings and PEO crystals thicken more during isothermal crystallization. The fold surface free energy of PEO is found to be ca. 90 erg/cm^2 based on the nonlinear HW analysis. The temperature dependence of the initial lamellar thickness predicted for PEO is in excellent agreement with available morphological data on this polymer. Values obtained by the nonlinear HW analysis for both the equilibrium

melting temperature and the fold surface free energy of PEO crystals are consistent with those obtained from the temperature dependence of spherulitic growth rates of PEO. This latter study yields a value for T_m of ca. 82°C and a value of σ_e^1 ca. 88 erg/cm^2. It is therefore concluded that the temperature dependence of spherulitic growth rates is well accounted for by the LH secondary nucleation theory. A regime I/II transition was observed at ca. 57°C and the ratio (1.97) of the nucleation constants in regime I and II is close to the value of 2 predicted by the secondary nucleation theory, when the equilibrium melting temperature used in the LH analysis (80.6°C) is that obtained from the nonlinear HW method. The crystal growth rate data below 50°C were not included in the regime analysis because of two reasons. First a growth face change has been reported at this temperature and second very high growth rates (ca. > 10 μm/s) in this temperature range cast some doubt as to the exact temperature at the crystallization front. Finally, when experimental values of the growth rate prefactor are used to calculate the substrate length for PEO, unreasonably small values (ca. 10 – 30 Å) are obtained. This finding suggests that, a modification of the LH theory, such as that proposed by Snyder et al.,[42] may be necessary.

4.6. References

1. Wissler, G. E.; Crist, B.; *J. Polym. Sci. Polym. Phys. Ed*. **1980**, *18*, 1257.
2. Kovacs, A. J.; Gonthier, A. *Kolloid-Z u. Z. Polymere* **1972**, *250*, 530.
3. Buckley, C. P.; Kovacs, A. J. *Progr. Colloid & Polymer Sci*. **1975**, *58*, 44.
4. Buckley, C. P.; Kovacs, A. J. *Colloid & Polym. Sci*. **1976**, *254*, 695.
5. Kovacs, A. J.; Straupe, C.; Gonthier, A. J. *Polym. Sci. Polym. Symp*. **1977**, *59*, 31.
6. Allen R. C.; Mandelkern, L. *Polymer Bulletin* **1987**, *17*, 473.
7. Cheng, S. Z. D.; Zhang, A.; Chen, J.; Hegerer, D. P. *J. Polym. Sci. Polym Phys. Ed*. **1991**, *29*, 287.
8. Cheng, S. Z. D.; Chen, J.; Zhang, A.; Heberer, D. P. *J. Polym. Sci. Polym. Phys. Ed*. **1991**, *29*, 299.
9. Cheng, S. Z. D.; Chen, J. *J. Polym Sci. Polym. Phys. Ed*. **1991**, *29*, 311.
10. Cheng, S. Z. D.; Chen, J.; barley, J. S.; Zhang, A.; Habenschuss, A.; Zschack, P. R. *Macromolecules* **1992**, *25*, 1453.
11. Cheng, S. Z. D.; Chen, J.; Janimak, J. J. *Polymer*, **1990**, *31*, 1018.
12. Point, J. J.; Damman, P.; Janimak, J. J. *Polymer*, **1993**, *34*, 3771.
13. Marentette, J. M.; Brown, G. R. *Polymer*, **1998**, *39*, 1405.
14. Beech, D. R.; Booth, C. *Polymer Lett*. **1970**, *8*, 731.
15. Alfonso, G. C.; Russell, T. P. Macromolecules **1986**, *19*, 1143.
16. Floudas, G.; Tsitsilianis, C. *Macromolecules* **1997**, *30*, 4381.
17. Mandelkern L.; Stack, G. M. *Macromolecules* **1984**, *17*, 871.
18. Afifi-effat, A. M.; Hay, J. N. *J. Chem. Soc. Faraday Trans. II* **1972**, *68*, 656.
19. Flory, P. J.; Vrij, A. *J. Am. Chem. Soc.* **1963**, *85*, 3548.
20. Marand, H.; Xu, J.; Srinivas, S. *Macromolecules* **1998**, *31*, 8219.
21. Spegt, P. A.; Terrisse, J.; Gilg, B.; Skoulios, A. E. *Makromol. Chem*. **1967**, *107*, 29.
22. Hoffman, J. D.; Weeks, J. J. *J. Res. Natl. Bur. Stand. (U.S.)* **1962**, *A66*, 13.
23. Xu, J.; Marand, H.; Srivinas, S. *Macromolecules* **1998**, 31, 8230.
24. Hoffman, J. D.; Miller, R. L. *Polymer* **1997**, 38, 3151.
25. Alizadeh, A. Ph.D. Dissertation, Universidad Autonoma de Madrid, Madrid, 1997.
26. Cheng, S. Z. D.; Barley, J. S.; Von Meerwall, D. *J. Polym. Sci. Polym. Phys. Ed*. **1991**, *29*, 515.
27. Appel, M.; Fleischer, G. *Macromolecules*, **1993**, *26*, 5520.

28. Thomas, D. G.; Staveley, L. A. K. *J. Chem.Soc*. **1952**, 4569.
29. Hoffman, J. D.; Miller, R, L,; Marand, H.; Roitman, D. B. *Macromolecules* **1992**, *25*, 2221.
30. Roitman, D. B.; Marand, H.; Miller, R. L.; Hoffman, J. D. *J. Phys. Chem*. **1989**, *93*, 6919.
31. Talibuddin, S.; Runt, J.; Liu, L.; Chu, B. *Macromolecules* **1998**, 31, 1627.
32. Phillips, P. J.; Vatansever, N. *Macromolecules* **1987**, *20*, 2138.
33. Vasanthakumari, R.; Pennings, A. J. *Polymer* **1983**, *24*, 175.
34. Huang, J.; Lisowski, S.; Runt, J.; Hall, E. S.; Kean, R. T.; Buehler, N.; Lin, J. S. *Macromolecules* **1998**, *31*, 2593.
35. Lovinger, A. J.; Davis, D. D.; Padden, Jr.; F. J. *Polymer* **1985**, *26*, 1595.
36. Deslandes, Y.; Sabir, F.; Roovers, J. *Polymer*, **1991**, *32*, 1267.
37. Monasse, B.; Haudin, J. M. *Colloid & Polymer Science* **1985**, *263*, 822.
38. Cheng, S. Z. D.; Janimak, J. J.; Zhang, A.; Cheng, H. N. *Macromolecules* **1990**, *23*, 298.
39. Lauritzen, J. I. J. Appl. Phys. 1973, 44, 4353.
40. Von Meerwall, E.; Grigsby, J.; Tomich, D.; Van Antwerp, R. *J. Polym. Sci. Polym. Phys. Ed*. **1982**, *20*, 1037.
41. Pearson, D. S.; Ver Strate G.; Von Meerwall, E.; Schilling, F. C. *Macromolecules* **1987**, *20*, 1133.
42. Snyder, C. R.; Marand, H.; Mansfield, M. L. *Macromolecules* **1996**, *29*, 7508.

Chapter 5. The Effect of Structural and Topological Constraints on the Morphology, Melting and Crystallization Behavior of Ethylene/styrene Copolymers

5.1. Introduction

Primary crystallization of semicrystalline polymers from a free, unconstrained melt involves, sequentially, the formation of nuclei and the growth of lamellar structures. In the case of most homopolymers, lamellae can be organized into superstructures such as spherulites, axialites, quadrites or hedrites. Such superstructures are lost when a large concentration of defects is introduced into the backbone of a homopolymer because crystallization by chain folding is highly impeded by the presence of noncrystallizable defects, such as short chain branches or non-crystallizable comonomers.[1-4] A continuous morphological shift from spherulites with stacked lamellae at very low branch content, to thin lamellae with reduced lateral dimensions at higher branch content, and to bundle-like crystals at the highest branch contents has been recently reported in studies of ethylene/1-octene random copolymers.[1,2] The degree of crystallinity also continues to increase after completion of primary crystallization. This secondary crystallization takes place in the amorphous fraction constrained by primary crystals. While the kinetics of primary crystallization has been thoroughly studied and little controversy exists at the empirical level of experimental observations, detailed investigations of the secondary crystallization process are less numerous and have been rationalized by a variety of models. Lamellar thickening and increase in crystal perfection are by far the two most common models quoted for semi-flexible polymers (PE, it-PP, PEO, etc.), which exhibit a crystalline α_c relaxation.[5,6] For less flexible semicrystalline polymers (e.g. it-PS, PET, PEEK, PPS), for which the existence of an α_c relaxation has not been firmly established, secondary crystallization has been postulated to be associated with the formation of smaller lamellar structures between primary lamellae or within the inter-fibrillar regions.[7] When uncrystallizable comonomer units are introduced into a semi-flexible homopolymer, lamellar thickening or increase in crystal perfection are generally impeded. The formation of new chain-folded lamellar crystals between primary lamellae is also thought to be unlikely, especially at high undercoolings. Indeed, the topological constraints experienced by chain sections in interlamellar amorphous layers make

it difficult to envision how chain folding lamellar growth can proceed. In recent publications, Alizadeh et al.[8] and Marand et al.[9] proposed that secondary crystallization may be associated with the formation of fringed micellar crystals at high undercooling (high topological constraints) and mosaic block crystals at lower undercooling (lower topological constraints).

While the earliest reports of morphological investigations of semicrystalline polymers favored the fringed micelle model,[10,11] the pioneering work of Keller established that the basic morphological unit in solution crystallized polymers is the chain folded lamellar structure.[12] Subsequent morphological studies demonstrated that primary crystallization from a free, unconstrained melt also leads to chain folded lamellar structures. Although the fringed micelle model fails to represent the crystalline morphology resulting from primary crystallization, early studies of ethylene/vinylacetate random copolymers by Okui and Kawai[14,15] led to the proposal that fringed-micellar type may form during secondary crystallization. A similar proposal was later formulated by Chaturvedi[13] for trans-1,4-polyisoprene. These authors furthermore suggested that the coexistence of lamellar and fringed-micellar structures may be at the origin of the multiple melting behavior observed for these materials. These studies were apparently not recognized for a number of years and the multiple melting behavior of semicrystalline polymers has since either been accounted for on the basis of a melting-recrystallization-remelting process[16] or associated with a bimodal population of lamellae of different thicknesses.[17] It is only recently that the fringed micelle model was revived to explain the low endothermic transition of homogeneous ethylene/α-olefin copolymers.[8] In this latter study, the authors proposed that during cooling from the free, unconstrained melt the longest ethylene sequences crystallize first, leading to the formation of chain folded lamellar structures (primary crystallization), the shorter ethylene sequences crystallize subsequently from the residual amorphous fraction constrained by primary lamellar crystals resulting in the formation of fringed micellar structures (secondary crystallization). Significant differences in specific surface area and in environment at the time of melting between primary lamellar crystals and secondary fringed micellar crystals then provide a logical account for the differences in their melting behavior and in the location of their respective melting transitions. Isothermal crystallization leading to lamellar structures was found to be characterized by a nucleation-controlled growth process with

Avrami exponent in the range of 1 - 3, while crystallization at lower temperatures in the fringed micellar form was always characterized by Avrami exponent of 1/2. Similar Avrami exponents were reported by Okui and Kawai,[14] for the primary crystallization and by Schultz and Scott[18] for the secondary crystallization of linear polyethylene at high undercoolings. These latter authors furthermore concluded that the formation of secondary crystals is consistent with a one-dimensional, diffusion-controlled growth mechanism. We note that the deviation of the Avrami exponent from 3 is associated with the disappearance of the spherulitic superstructures at high comonomer content. Studies of ethylene/vinyl acetate[14] and ethylene/1-octene[8] random copolymers also demonstrated that, subsequent to isothermal crystallization, the low endotherm melting temperature increases linearly with the logarithm of crystallization time. While the latter authors tentatively explained this behavior by a decrease in the molar conformational entropy of the residual amorphous fractions as a result of secondary crystallization,[8] others have argued that the increase in melting temperature of secondary crystals with time is more consistent with an increase in their lateral dimensions. Similar studies of the secondary crystallization process have also been carried out and identical conclusions have been obtained with random copolymers of ethylene with 1-butene, 1-pentene, and 1-hexene in our laboratory.[19] Studies in our laboratory of secondary crystallization in semiflexible polymers such as poly(ether ether ketone), bisphenol A polycarbonate, isotactic polystyrene, nylon-6 and poly(ethylene terephthalate) suggest that the behavior exhibited by ethylene/1-octene copolymer may be universal.[9,20]

It is well established that the degree of crystallinity, the upper melting temperature and the average crystal thickness decrease systematically with an increase in the incorporation of α-olefin comonomers, but are independent of the n-alkyl branch size (if larger than a methyl group).[3] Thus, it is a logical conclusion that branches larger than the methyl group are excluded from the crystalline regions. It would be very interesting to contrast the behavior of copolymers exhibiting n-alkyl branches such as ethylene/1-octene copolymer with that of a copolymer having a different branch structure and bulkiness. Ethylene/styrene copolymers with phenyl side groups appear to be a good candidate for such a study. Copolymerization of ethylene and styrene was not successful using free radical or conventional Ziegler-Natta catalysts.[21,22] The use of metallocene-based single site catalysts made it possible to synthesize ethylene/styrene copolymers, where the styrene content can be varied from one to

eighty weight percent. Depending on composition, ethylene/styrene copolymers exhibit a wide range of properties intermediate between those of polyethylene and atactic polystyrene.[23] The present study deals with the secondary crystallization behavior of ethylene/styrene interpolymers synthesized using the INSITE™ technology at the Dow Chemical Company. The present study of this particular copolymer was further motivated by the observation that at the same comonomer mole fraction, the glass transition temperature (T_g) of ethylene/styrene copolymers is ca. 40K above that of ethylene/1-octene copolymers.[24]. Secondary crystallization of this material can then be observed near room temperature and should take place over longer time scales than for ethylene/α-olefin copolymers. Morphological studies by atomic force microscopy will also benefit from the lower compliance of these materials as compared to EO copolymers, which should provide better resolution of the fringed micellar structures, if these are indeed present.

5.2.Experimental

5.2.1. Materials

Six metallocene-based ethylene/styrene copolymers (trade name INDEX[25]) were used as received from Dow Chemical. The molecular characteristics provided by the manufacturer are shown in Table 5.1. Samples are hereafter referred to as ES-x, where the suffix is the mole percentage of styrene in the copolymers. All the ES copolymers have similar weight average

Table 5.1 The molecular characteristics of ethylene/styrene copolymers.

Sample ID	wt% Styrene	wt% at-PS	10^{-3} M_w (g.mol^{-1})	M_w/M_n	I_2
ES-1.9	6.8	0	160.2	2.3	1.0
ES-3.4	11.6	0	175.1	2.2	0.90
ES-5.1	17.7	1.3	164.6	3.5	0.91
ES-8.7	26.5	0.4	182.3	2.3	0.67
ES-11.6	33.0	0.3	208.9	2.2	0.62
ES-15.1	40.1	0.4	207	4.4	0.70

molecular weights (183±21K), and the polydispersity index is generally in the vicinity of 2.2 but was slightly higher for two of the samples. The quantity I_2 in the table refers to the melt index (ASTM). During preparation of the ethylene/styrene copolymers it is difficult to avoid the formation of a small fraction of at-PS homopolymer. The at-PS fraction, detailed in Table 5.1 was however generally very small in the samples investigated in this study.

5.2.2. Differential Scanning Calorimetry

Calorimetric experiments were performed in a Perkin Elmer DSC Model 7, using a dry nitrogen purge and a dry ice-isopropanol bath. Thin films (ca. 100μm) were prepared by melt pressing at ca. 150 psi and 170°C in a Carver laboratory hot press under dry nitrogen atmosphere and subsequent quenching in an ice-water mixture. Similar sample mass was used in all DSC studies in order to simplify the thermal lag corrections. Prior to crystallization all samples were kept in the melt state at 180°C for 2 minutes. DSC traces were recorded during cooling at different rates for studies of the crystallization process. A heating rate of 10K/min was employed for studies of the melting behavior subsequent to isothermal crystallization experiments. Temperature calibration of the DSC7 during cooling was carried out using the isotropic to nematic transition (136.0°C) of p-azoxyanisole. Temperature calibration during heating was performed using an indium sample sandwiched between two polymer films, to account for differences in thermal conductivity between polymers and metals. Finally, calibration of heat flow rates using a sapphire standard was performed to obtain the sample absolute heat capacity as a function of temperature.

5.2.3. Atomic Force Microscopy

Thin films (ca. 70μm) were melt pressed under the same conditions as described in the last section. Samples were re-melted in a Linkham heating stage to erase previous thermal and mechanical history and were subsequently slowly cooled to room temperature (CR = 1 K/min). All AFM experiments were conducted in a NanoScope III SPM instrument (Digital Instrument) operating in a tapping mode at room temperature.

5.3. Results

This section is organized in four parts. The first part focuses on the evolution of the degree of crystallinity during cooling from the melt at different rates. The second part is concerned with studies of the melting behavior after cooling at a constant rate or after quenching. In the third part, an investigation of the melting behavior subsequent to isothermal crystallization at different temperatures for various times is presented. The last part is concerned with morphological studies.

5.3.1. Evolution of the degree of crystallinity during cooling

The crystallization behavior of ES copolymers was first monitored in the DSC-7 during cooling from 180°C to –20°C at various rates (40, 20, 10, 5, 2.5 and 1 K/min). After thermal lag correction and sapphire calibration, the heat capacity is plotted against temperature for ES-0.0 (i.e. linear polyethylene), ES-3.4, ES-8.7 in Figure 5.1. The experimental heat capacities in the melt are found to coincide well with the theoretical heat capacities of ES copolymers, which are approximated by

$$C_p{}^l(\text{copolymer}) = \phi C_p{}^l(\text{PS}) + (1-\phi)C_p{}^l(\text{PE}) \qquad (5.1)$$

where l refers to the melt or liquid state, and ϕ is the weight fraction of styrene in the copolymer. Cp^l(PS) and Cp^l(PE) are the theoretical heat capacities of atactic polystyrene and polyethylene, respectively, obtained from the ATHAS data bank.[26] As elaborated upon later, this treatment is an approximation since the conformational entropy associated with the styrene units in the copolymer must differ from that inferred from pure at-PS, since styrene dyads do not exist in the copolymer.

ES copolymers crystallize over a much broader temperature range than linear polyethylene, and actually exhibit a relatively sharp crystallization exotherm at high temperature and a much broader exotherm at lower temperature. The temperature at maximum crystallization rate decreases at larger styrene content and exhibits a strong cooling rate dependence. Figure 5.2 shows the peak crystallization temperature versus comonomer content at 40 K/min and 1 K/min cooling rates.

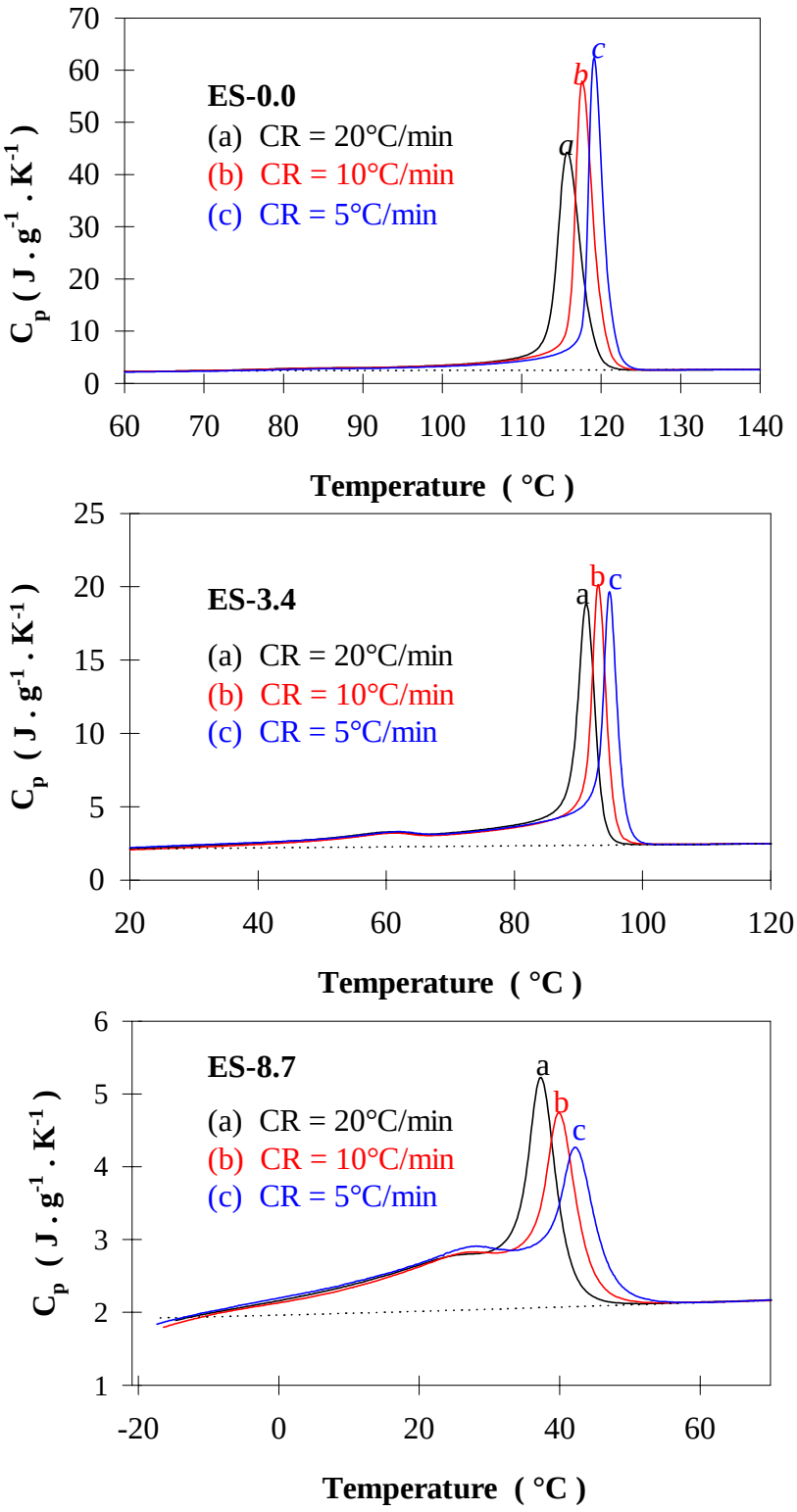

Figure 5.1. Heat capacity versus temperature during cooling at various rates for ES-0.0, ES-3.4 and ES-8.7.

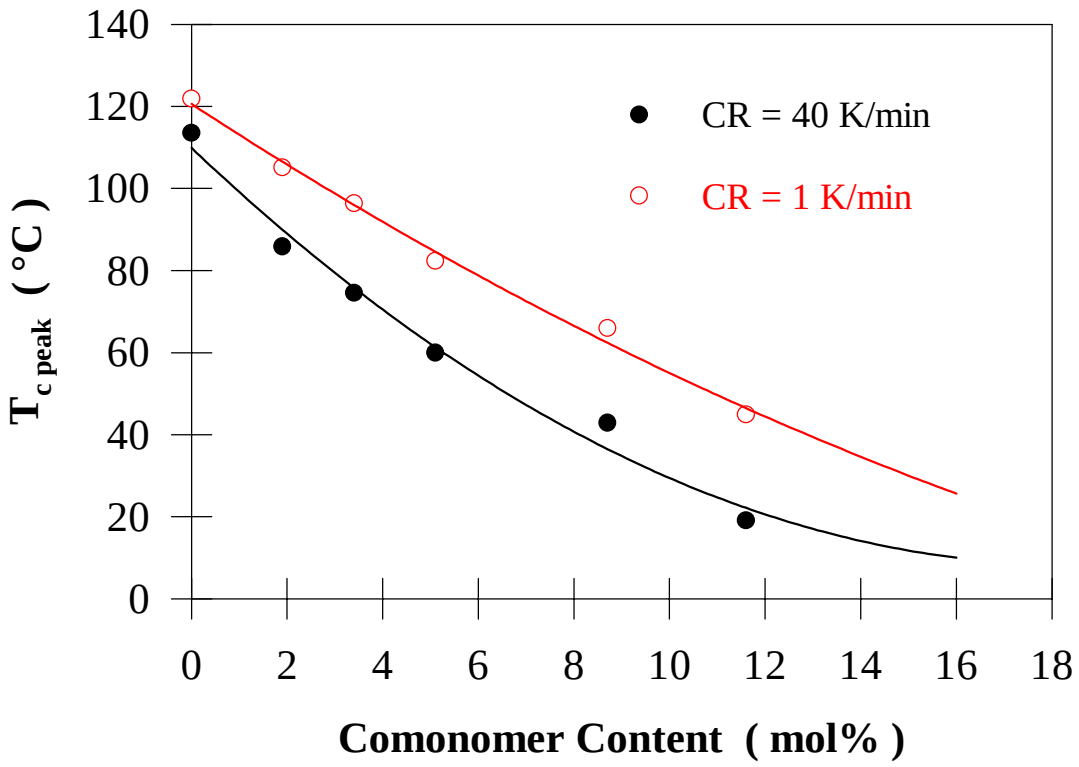

Figure 5.2. The peak crystallization temperature of ES copolymers versus the comonomer content at different cooling rates.

Based on the heat capacities of ES copolymers (Figure 5.1), the degree of crystallinity can be calculated as a function of temperature during cooling. It is first important to establish a correct heat capacity baseline for the ES copolymers. Two steps were taken in the calculation process. The first step is to take $C_p^{\,l}$ calculated for each copolymer from Equation 5.1 as the first heat capacity baseline. The degree of crystallinity as a function of temperature can then be calculated through Equation 5.2,

$$X_c(T) = \frac{-\int_{180}^{T}\left(C_p^{\exp}(T) - C_p^{l}(T)\right)dT}{\Delta H_f^0} \qquad (5.2)$$

where ΔH_f^o is the theoretical heat of fusion of the fully crystalline polyethylene at the equilibrium melting temperature. $C_p^{\,exp}$ is the apparent heat capacity obtained after calibration of the rate of heat flow. The second step is to establish a correct heat capacity baseline, $C_p^{\,bl}$ *(T)*, consistent with the degree of crystallinity at each temperature, X_c *(T)*:

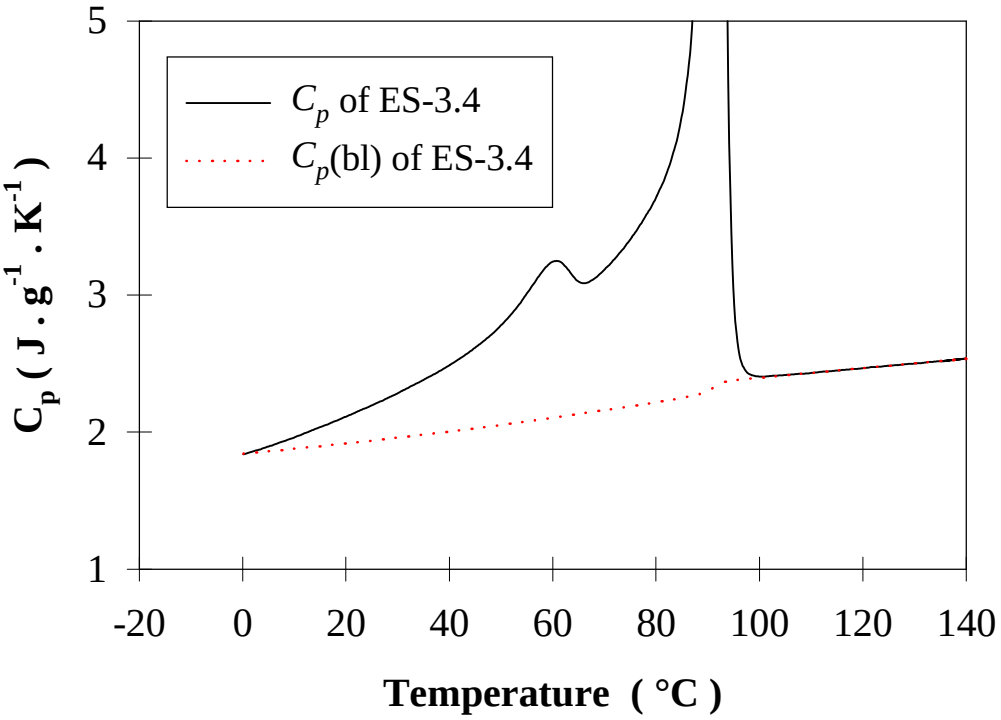

Figure 5.3. Heat capacity and the theoretical heat capacity baseline for ES-3.4 versus temperature.

$$C_p(bl) = \phi C_p^{\,l}(PS) + X_c C_p^{\,s}(PE) + (1 - \phi - X_c) C_p^{\,l}(PE) \tag{5.3}$$

where ϕ is the weight fraction of styrene in the amorphous fraction. The plots of original heat capacity and the second baseline against temperature are shown in Figure 5.3 for ES-3.4. The degree of crystallinity can then be recalculated through Equation 5.2 using the new heat capacity baseline. Repeating the same procedure using Equation 5.3 and Equation 5.2 leads to more accurate estimates of the degree of crystallinity and heat capacity baseline. This iterative process converges very quickly (after the second step). Finally, the resulting degree of crystallinity was divided by the weight fraction of ethylene in the ES copolymers to yield a normalized degree of crystallinity. The temperature dependence of the normalized degree of crystallinity for each ES copolymers and linear polyethylene is presented in Figure 5.4 at various cooling rates. Two important assumptions were made in the calculations of the

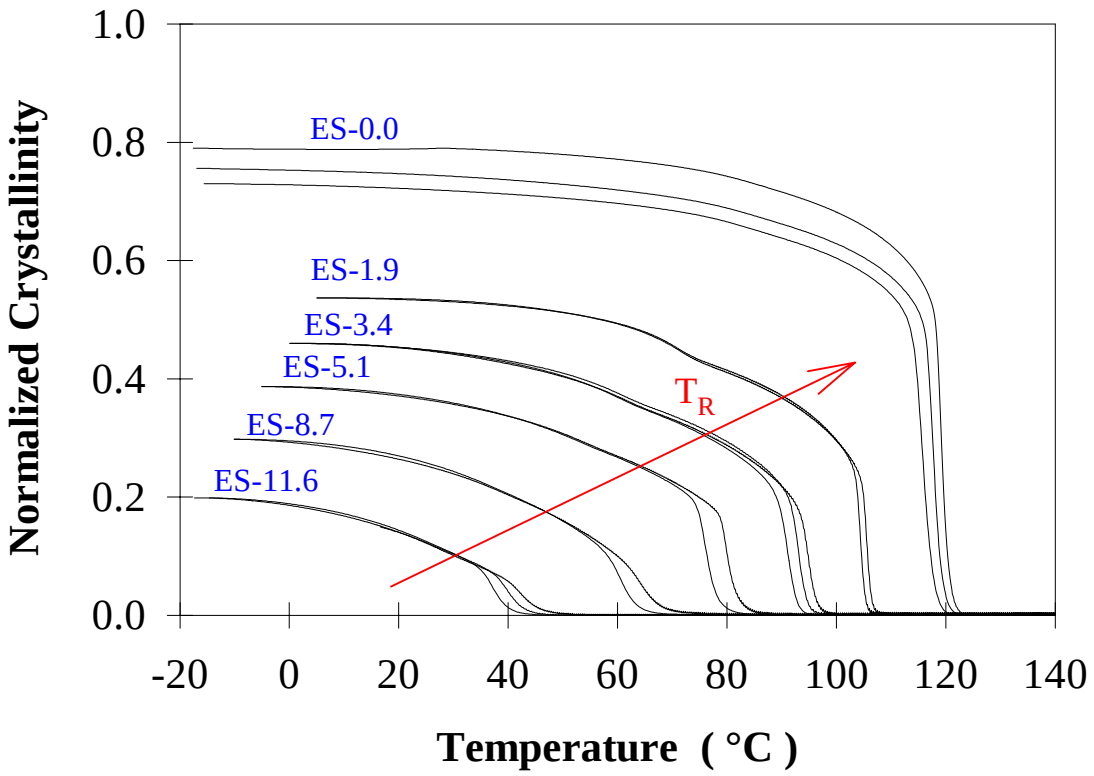

Figure 5.4. Evolution of the degree of crystallinity during cooling at various rates from the melt for linear polyethylene and ES copolymers. ES-1.9 (5 and 10 K/min), ES-5.1 and ES-8.7 (5 and 20 K/min), others (5, 10, 20 K/min).

crystallinity. First, the heat capacity per repeat unit for the styrene component in the ES copolymers is assumed to be identical to that in the polystyrene homopolymer. The coincidence of the experimental heat capacities of ES copolymers in the melt with the theoretical calculations shows that this assumption is reasonable. The second assumption relates to the use of the theoretical heat of fusion of fully crystalline linear polyethylene in Equation 5.2. This approximation leads to the underestimation of the degree of crystallinity because of three reasons addressed below. First, the theoretical heat of fusion decreases with temperature, and the experimental temperature range is far below the equilibrium melting temperature. Second, the appropriate theoretical heat of fusion for copolymer crystals should be lower than that used for linear polyethylene since the unit cell of the copolymers is

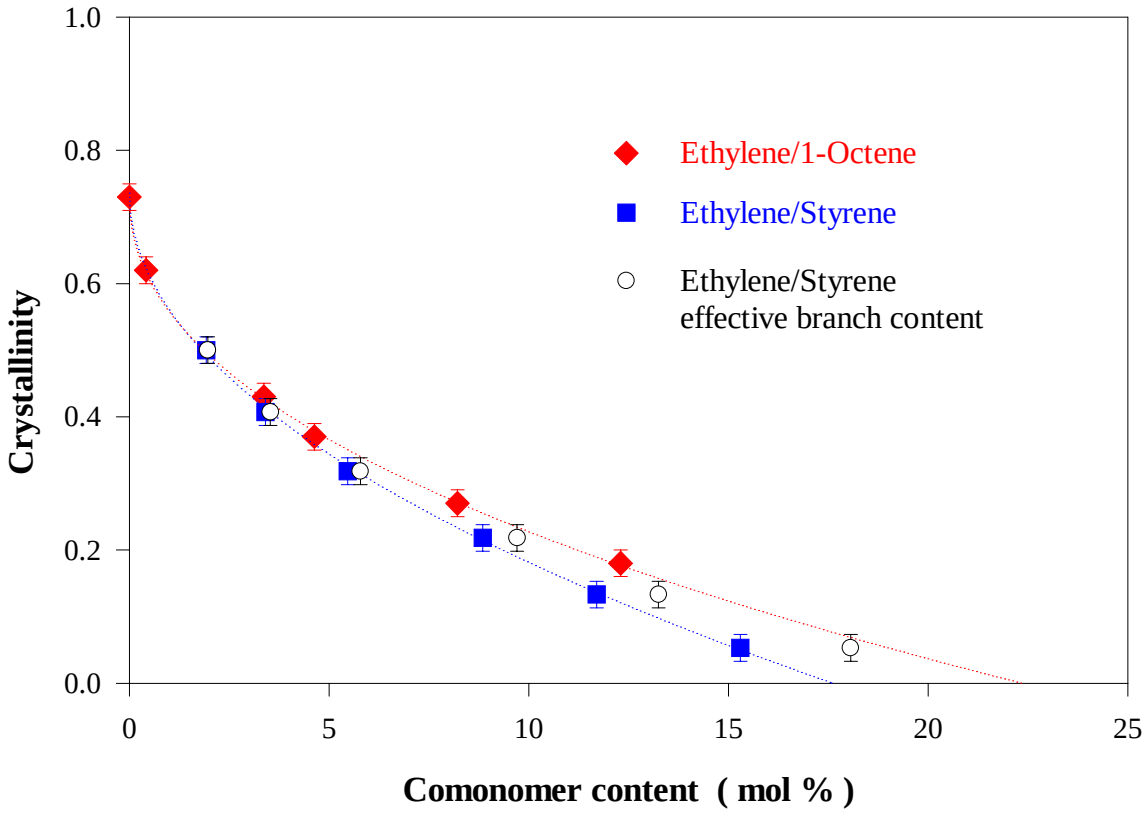

Figure 5.5. Normalized degree of crystallinity versus the comonomer content for the ES and EO copolymers. Data of EO copolymers were obtained from ref.8.

slightly dilated in comparison to that of linear polyethylene. This dilation is not the result of any incorporation of styrene comonomers in the crystal phase (see below) but arises as from interfacial stresses at lamellar surfaces due to lower adjacent reentry folding and steric repulsions between short branches.[27] Finally, crystallization of these copolymers is likely to lead to the formation of some hexagonal phase crystals for which the heat of fusion is expected to be smaller than that of the orthorhombic phase.[28] To our knowledge, corrections for these latter two factors cannot be carried out at the present time. The underestimation associated with the temperature dependence of the heat of fusion is less than ten percent of the measured crystallinity, based on calculations carried out in our laboratory. Since all estimations were carried out following the same procedure, the results presented here for different copolymers, although not leading to absolute degrees of crystallinity, can, however, be compared to each other on a relative basis.

Examination of Figure 5.4 indicates that the degree of crystallinity of ES copolymers increases steadily during cooling down to - 20°C. In contrast, the degree of crystallinity of linear polyethylene reaches a plateau in the vicinity of 60°C. The normalized degree of crystallinity of ES copolymers achieved at -20°C is plotted against the styrene mole percent in Figure 5.5. Also shown in this figure for comparison is the normalized degree of crystallinity of ethylene/1-octene copolymers.[8] At the same comonomer content, the crystallinity of ES copolymers is lower than that of EO copolymers, and the difference becomes more significant for larger comonomer contents.

Examination of Figure 5.4 suggests the existence of different crystallization mechanisms above and below a crossover temperature T_R. This cross over temperature decreases with an increase in the styrene content. Above T_R, the degree of crystallinity is strongly cooling rate dependent; while below T_R, the degree of crystallinity is cooling rate independent. In contrast to ES copolymers, the degree of crystallinity of linear polyethylene is cooling rate dependent throughout the temperature range. We also note that the fraction of the overall crystallinity that develops through the low temperature mechanism increases with styrene content. Identical observations were reported for ethylene/1-octene copolymers.

5.3.2. Melting behavior after cooling at a constant rate or quenching

In order to further explore the differences in crystallization mechanism below and above T_R for these ES copolymers, we recorded their heating scans at 10 K/min from –20 to 180°C immediately after cooling from the melt at 10 K/min. From this data, and using the method discussed above, the evolution of the degree of crystallinity during heating is obtained (Figure 5.6). A cooling-heating hysteresis is shown in the high temperature region above T_R. On the other hand, a reversible crystallization-melting behavior is observed in the low temperature region. Again, we note a difference in behavior between ES copolymers and the linear polyethylene. In the low temperature region, the crystallinity of linear polyethylene appears to remain constant, indicating that neither crystallization nor melting can detected.

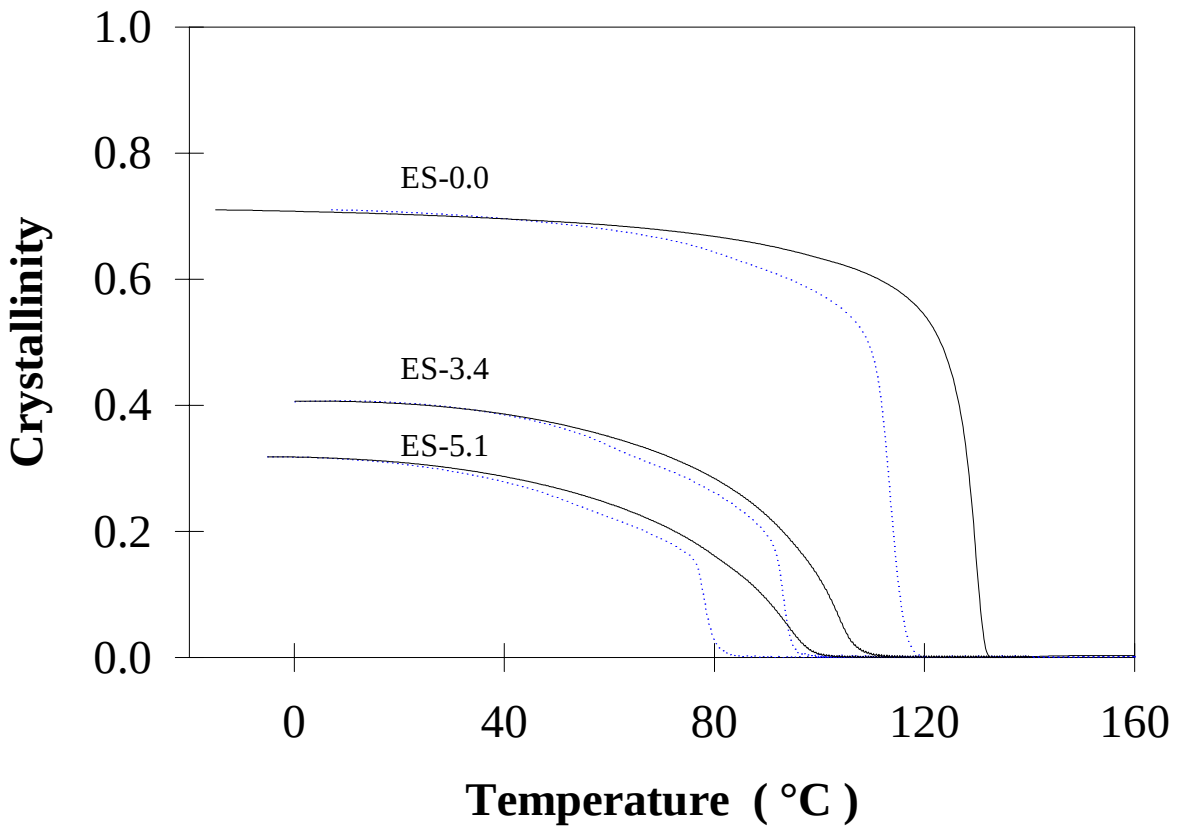

Figure 5.6. Degree of crystallinity versus temperature during cooling and heating cycle for ES-0.0, ES-3.4 and ES-5.1. Dotted line: cooling at 10 K/min, solid line: subsequent heating at 10 K/min.

The peak melting temperatures of ES copolymers, measured at a heating rate of 10 K/min after quenching from the melt are plotted against styrene content in Figure 5.7. Also shown for comparison are the melting temperatures of EO copolymers.[8] Melting temperatures of both ES and EO copolymers decrease with an increase in the styrene content. At the same comonomer content, ES copolymers exhibit a lower melting temperature than EO copolymers, the difference in melting temperature becoming larger with at higher styrene content.

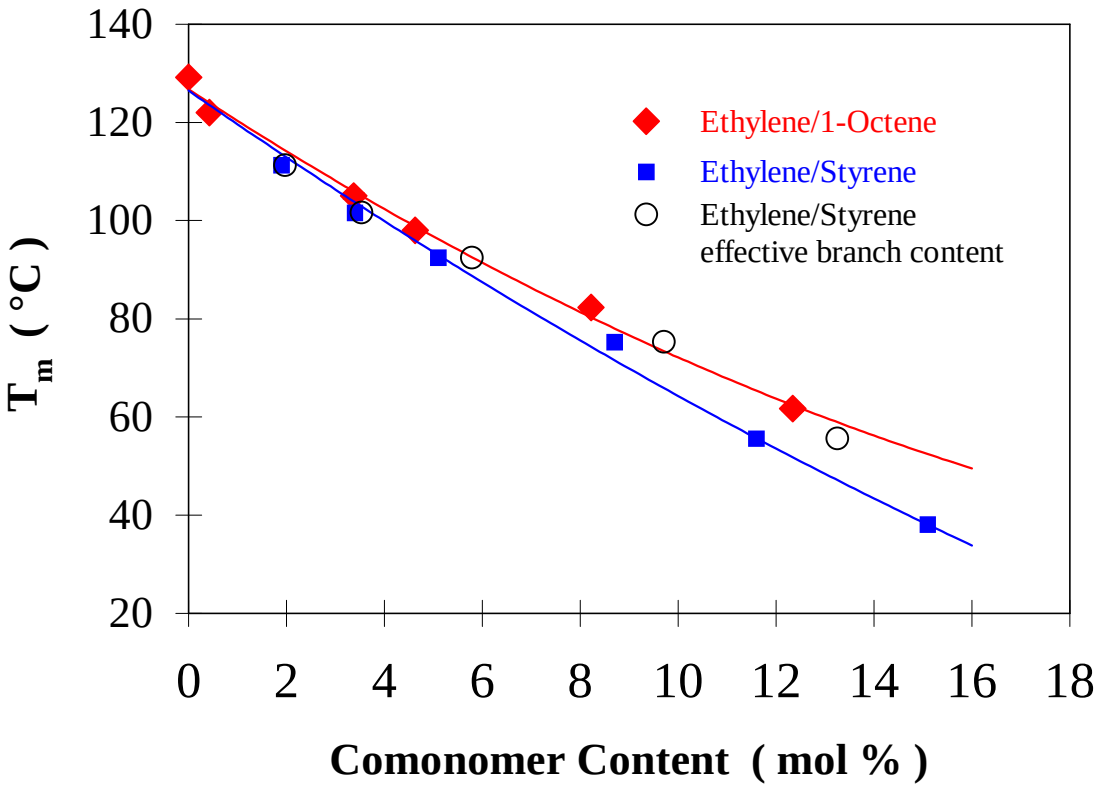

Figure 5.7. The apparent melting temperature versus the comonomer content for the ES and EO copolymers. Data of EO copolymers were obtained from ref.8.

The effect of heating rate on the melting behavior of the ES copolymers was also studied to investigate the possibility of crystal reorganization during heating. The heating scans after thermal lag correction are shown in Figure 5.8, for ES-3.4 and ES-5.1 for 5, 10 and 20 K/min. The lack of dependence of heating traces on heating rate implies that reorganization effects are insignificant during heating of ES copolymers in the range of heating rates employed.

5.3.3. Melting behavior after isothermal crystallization

In this section, isothermal crystallization kinetics will be investigated in the temperature regions below and above T_R (see Figure 5.4). Samples were quenched from the melt at 180°C to the desired crystallization temperature, T_x. After residing at T_x for a time interval, t_x, the

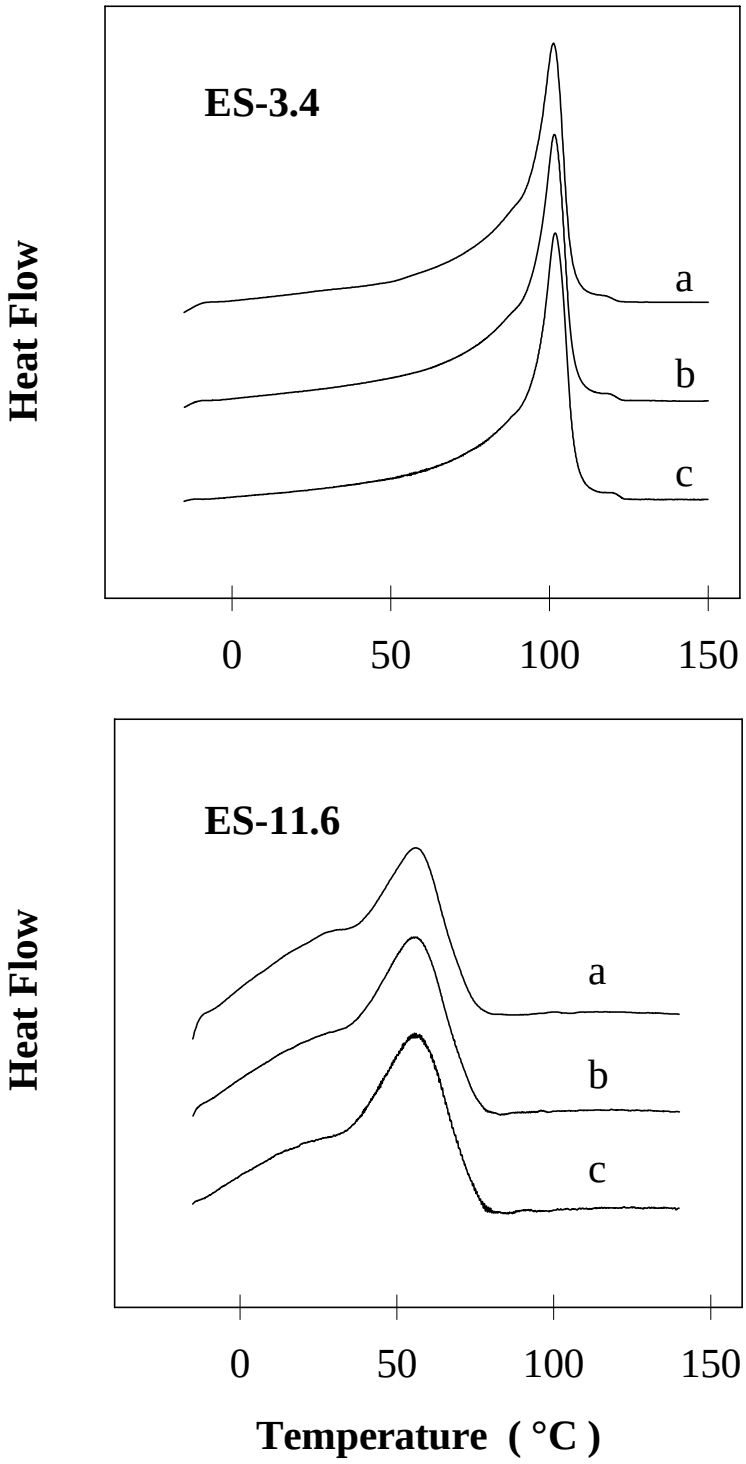

Figure 5.8. Heating scans at different rates for ES-3.4 and ES-11.6 after the samples were quenched from the melt. (a) 20 K/min, (b) 10 K/min, (c) 5 K/min.

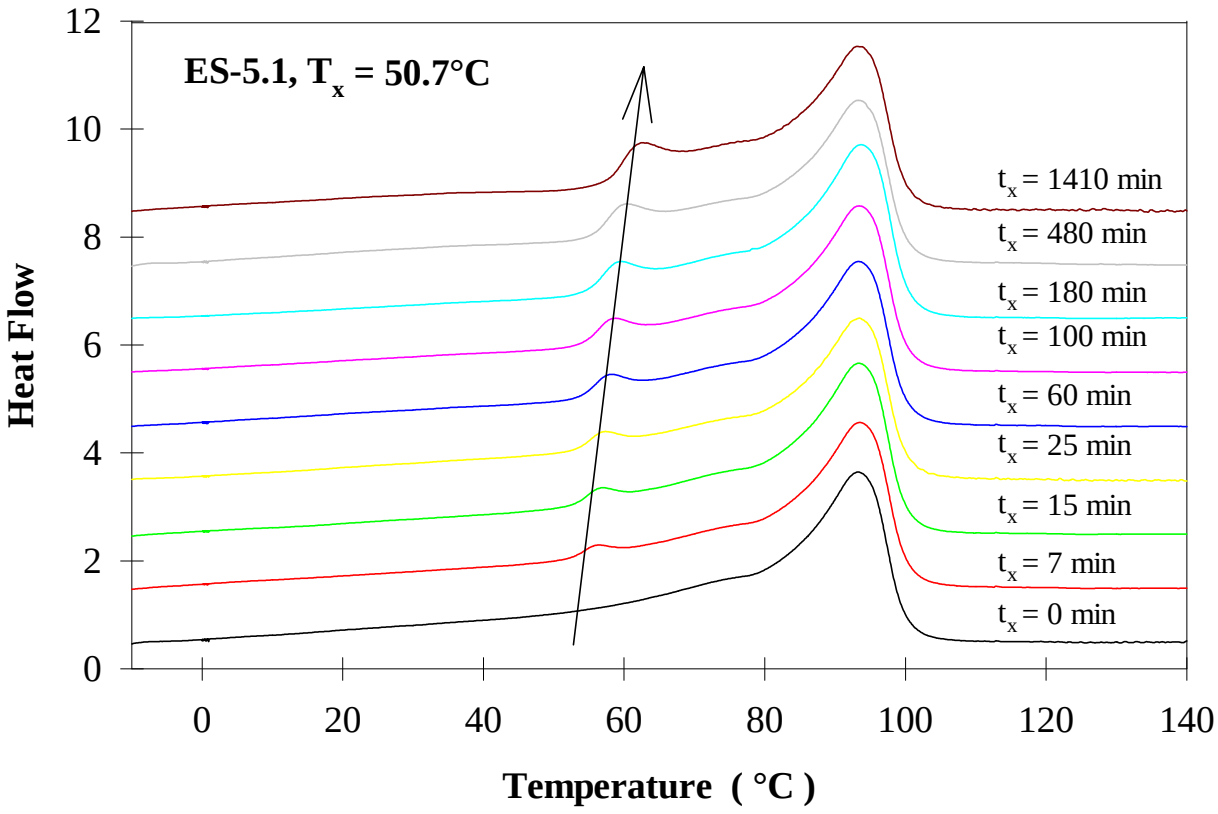

Figure 5.9. Evolution of the melting behavior for ES-5.1 after quenching from 180°C to 50.7°C, crystallization at 50.7°C for various times, and subsequent quenching to –20°C.

samples were further quenched to - 20°C and immediately reheated at a rate of 10 K/min from - 20°C to 180°C. Figure 5.9 shows the DSC traces of ES-5.1 crystallized for various times at 50.7°C, a temperature below T_R. Crystallization of ES-5.1 at 50.7° should be viewed as secondary crystallization because T_x = 50.7°C is far below the temperature at maximum crystallization rate for this polymer. Examination of Figure 5.9 indicates that isothermal secondary crystallization subsequent to primary crystallization during cooling results in a multiple melting behavior above the secondary crystallization temperature. The high endotherm melting temperature does not change with crystallization time, while the low endotherm shifts to higher temperature with increasing crystallization time. We also note that although the enthalpy of fusion associated with the low endotherm increases with crystallization time, the overall enthalpy of fusion remains constant.

In order to study the kinetics of secondary crystallization at T_x, the crystallization time dependence of the low endotherm enthalpy of fusion has to be evaluated. Two methods were employed for this estimation. The first method involves the deconvolution and fitting of the overall melting endotherm.[8] Four Gaussian peaks are used to obtain the best fit of the DSC trace associated with the quenched sample (t_x = 0 min, Figure 5.10a). Another Gaussian curve is added to fit the endotherm that appears after t_x slightly above the secondary crystallization temperature T_x (Figure 5.10b). One must be aware that peak fitting is a mathematical procedure without physical significance, and that the choice of peak shape to describe the various endotherms is arbitrary and only guided by the quality of the resulting fit. The low endotherm melting temperature and enthalpy of fusion are then obtained from the characteristics of this last Gaussian peak. The second method considered involves the direct subtraction of the DSC heating trace associated with the quenched sample (t_x = 0 min) from these obtained for samples crystallized for various times (t_x > 0 min). Results of this analysis are presented in Figure 5.11. Each trace exhibits a negative and a positive component. The area of the positive component (endotherm) increases with crystallization time as a result secondary crystallization at T_x. The negative component observed in the low temperature region is explained by the fact that melting at low temperatures is more significant for the quenched sample than for samples undergoing secondary crystallization at T_x. The observation that the magnitudes of the negative and positive contributions are identical and increase with secondary crystallization time first indicates that the total fraction of ethylene sequences which remain in the amorphous fraction after cooling to T_x and which would crystallize during further cooling to - 20°C is independent of residence time at T_x.. A longer residence time at T_x leads to a larger fraction of secondary crystals formed at T_x and a smaller fraction of crystals formed during cooling to -20°C. This is consistent with the fact that the total enthalpy of crystallization measured at -20°C does not depend on the crystallization time at T_x. To increase the accuracy of our estimation of the low endotherm enthalpy of fusion we therefore calculated the average of the areas associated with the negative and positive contributions. For a given crystallization time, the deconvolution and the subtraction methods yield values of the enthalpy of fusion for the low endotherm which differ by less than 5%.

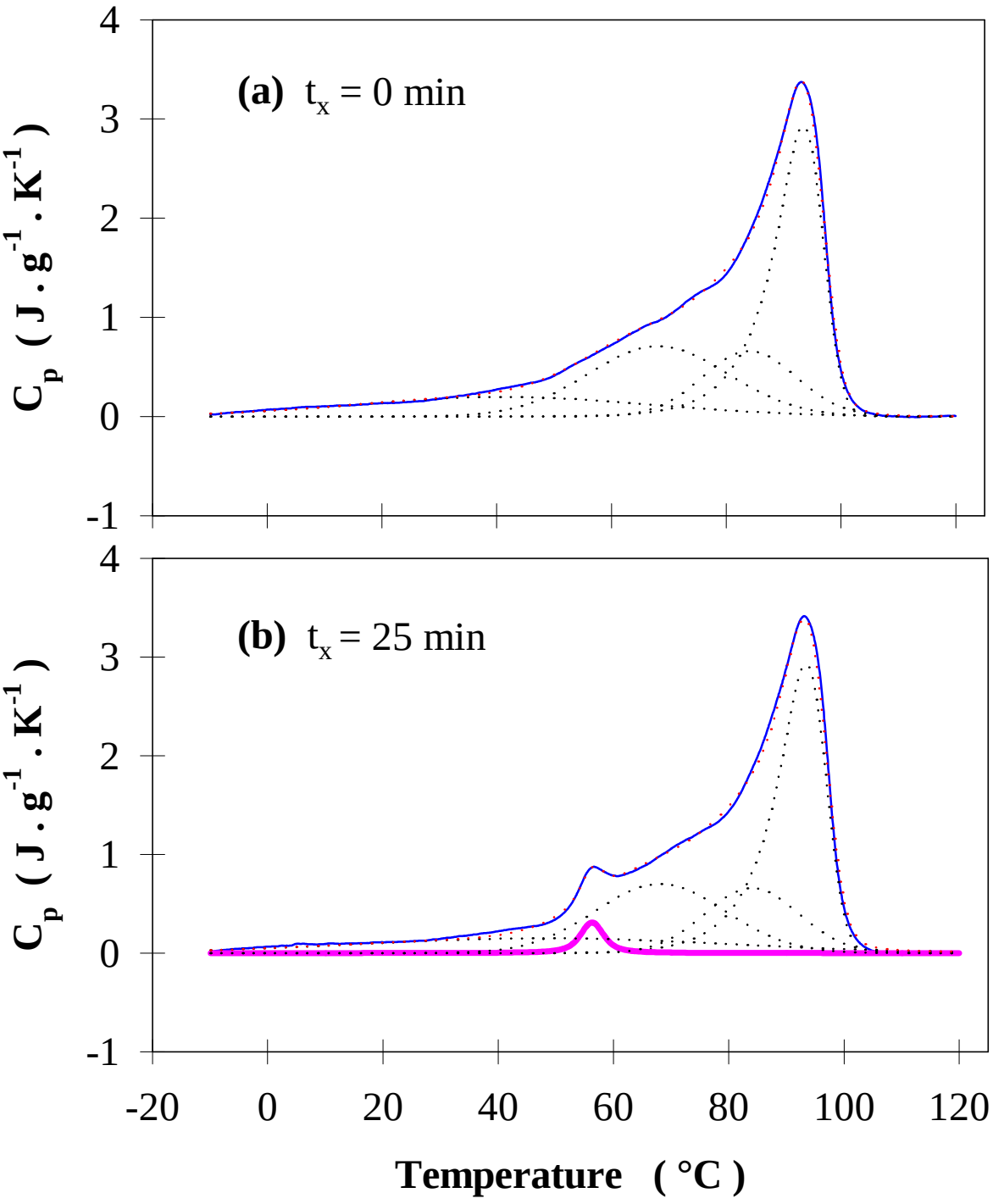

Figure 5.10. Peak-fitting process for ES-5.1 at 50.7°C, see text for details.

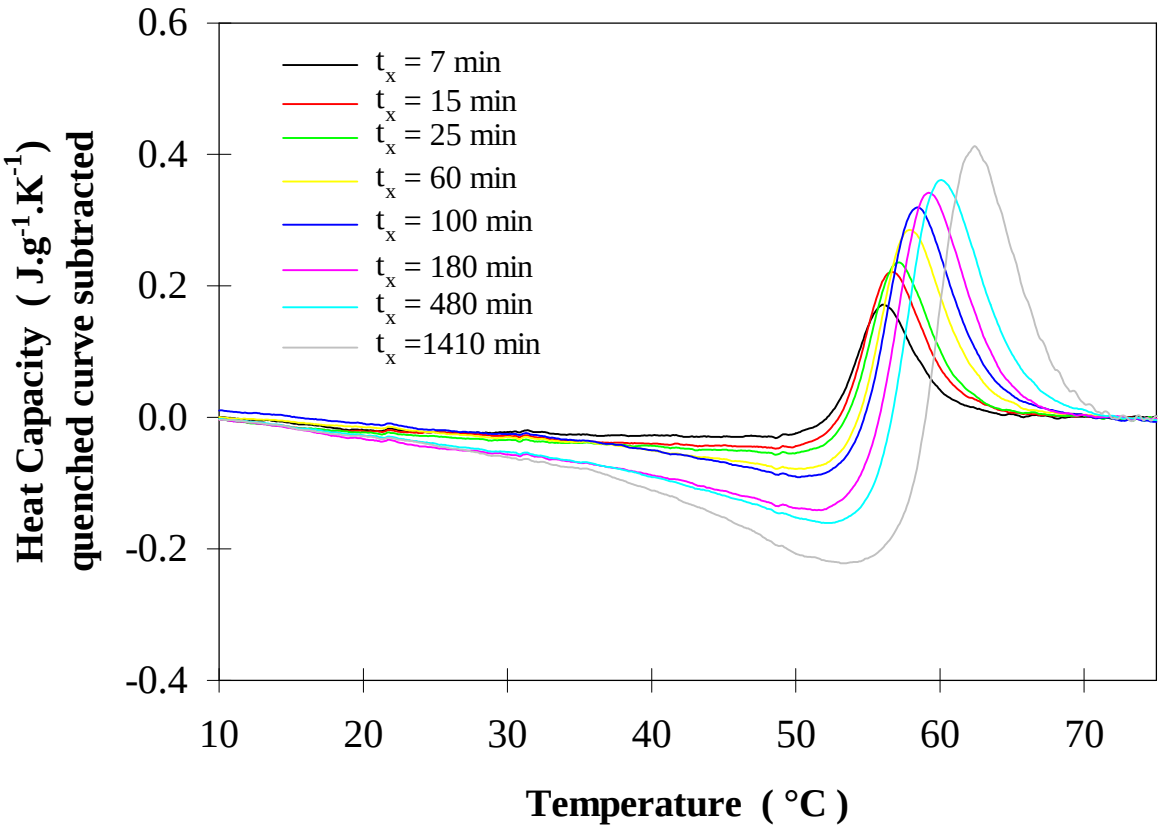

Figure 5.11. Melting traces for ES-5.1 after the samples were isothermally crystallized at 50.7°C for various times. The heating trace for the quenched sample was subtracted from that of each sample crystallized at 50.7°C.

The enthalpy of fusion associated with the low endotherm is plotted in Figure 5.12a as a function of crystallization time, in double logarithmic form. This data can then be analyzed with the Avrami equation, which at short times (or for low degree of crystallinity) can be written as:

$$\Delta H_f = kt^n \tag{5.4}$$

where ΔH_f is the enthalpy of fusion of crystals formed at T_x within the time t_x, k is the crystallization rate constant at that temperature, and n is the Avrami exponent, which describes the geometry and the mechanism of the crystal growth. Primary crystallization of homopolymers from the melt, where spherulitic superstructures form, often yields an Avrami

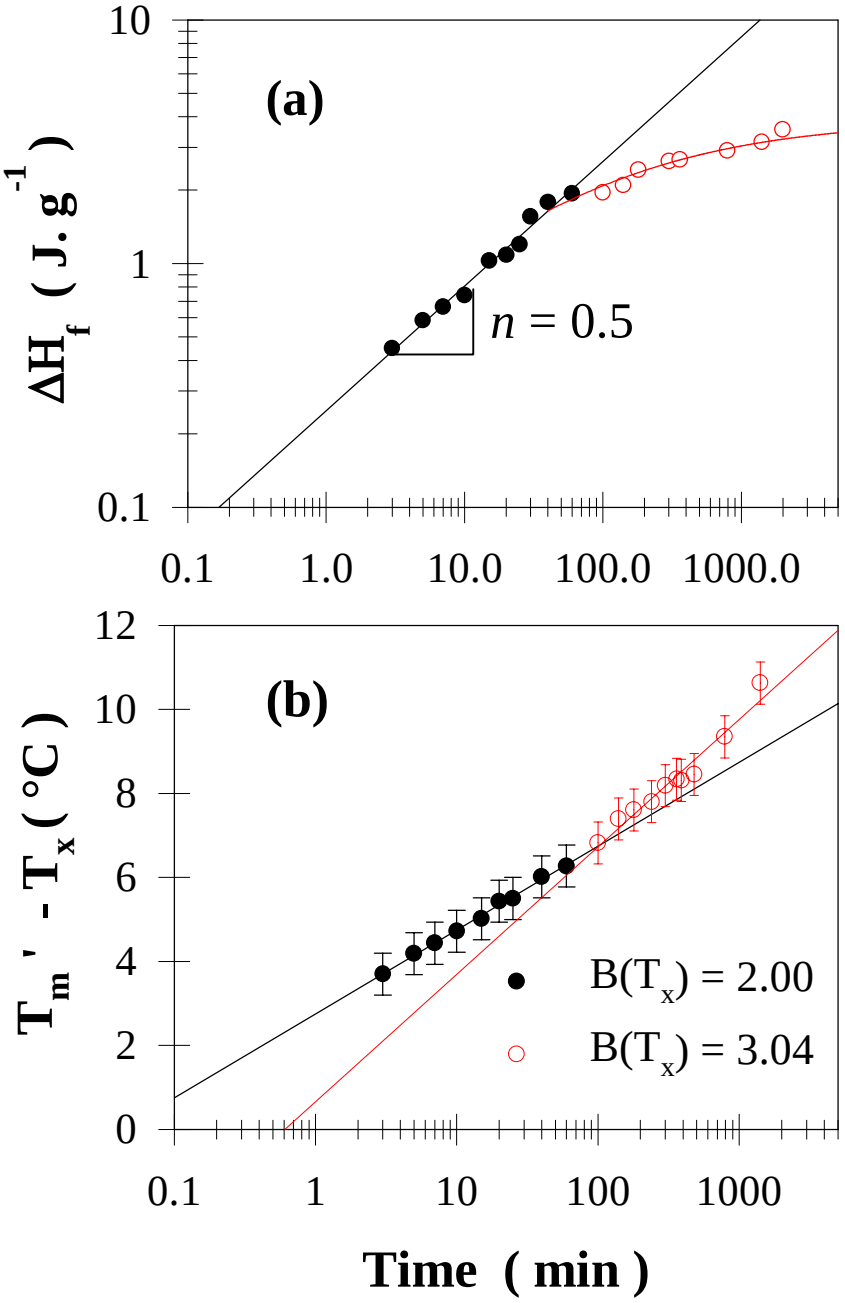

Figure 5.12. Evolution of the low endotherm characteristic For ES-5.1 after crystallization at 50.7°C for different times. (a) low endotherm heat of fusion, (b) low endotherm melting temperature.

exponent in the vicinity of 3. The initial Avrami exponent is therefore given by the slope of the plot shown in Figure 5.12a at short time in the secondary crystallization region. From this analysis, we conclude that an Avrami exponent of ½ is characteristic of the early stage of secondary crystallization of ES-5.1 at 50.7°C. The early stage of secondary crystallization is then defined by the range of crystallization times over which secondary crystallization is characterized by a constant Avrami exponent (here n = ½), while the late stage corresponds to time scale over which a deviation from the n = ½ law is observed.

Figure 5.12b shows the increase of the low endotherm melting temperature with logarithm of secondary crystallization time. Two regions can be defined in Figure 5.12b, which corresponds approximately with the early and late stages of secondary crystallization. In both early and late stages of the secondary crystallization, the peak melting temperature increases linearly although at different rates with the logarithm of secondary crystallization time:

$$T_m' - T_x = A(T_x) + B(T_x) * \log(t_x) \tag{5.5}$$

where $A(T_x)$ and $B(T_x)$ are the intercept and the slope, respectively. The magnitude of $B(T_x)$ at the early and late stages of secondary crystallization are show on the graph in Figure 5.12b. We recall that the early stage of secondary crystallization of EO copolymers was much shorter (ca. 15 minutes), so that differences in the magnitude of $B(T_x)$ for early and late stages of secondary crystallization could not be observed. Finally it is important to note that the low endotherm melting temperature extrapolates to the secondary crystallization temperature at very short times (i.e. a few seconds). This observation which was also made for EO copolymers and PEEK is consistent with the reversibility of the crystallization/melting phenomena for ES copolymers in the low temperature region ($T_x < T_R$) discussed in the context of Figure 5.6.

The effect of the crystallization temperature on the magnitude of $B(T_x)$ and n are now discussed. First, studies of the crystallization behavior at temperatures above T_R are reported for the case T_x = 90.4°C (see Figure 5.4). DSC heating traces of sample ES-5.1 after various crystallization times at 90.4°C are shown in Figure 5.13. Except for the quenched sample, two endotherms are observed. The upper endotherm is associated with the melting of

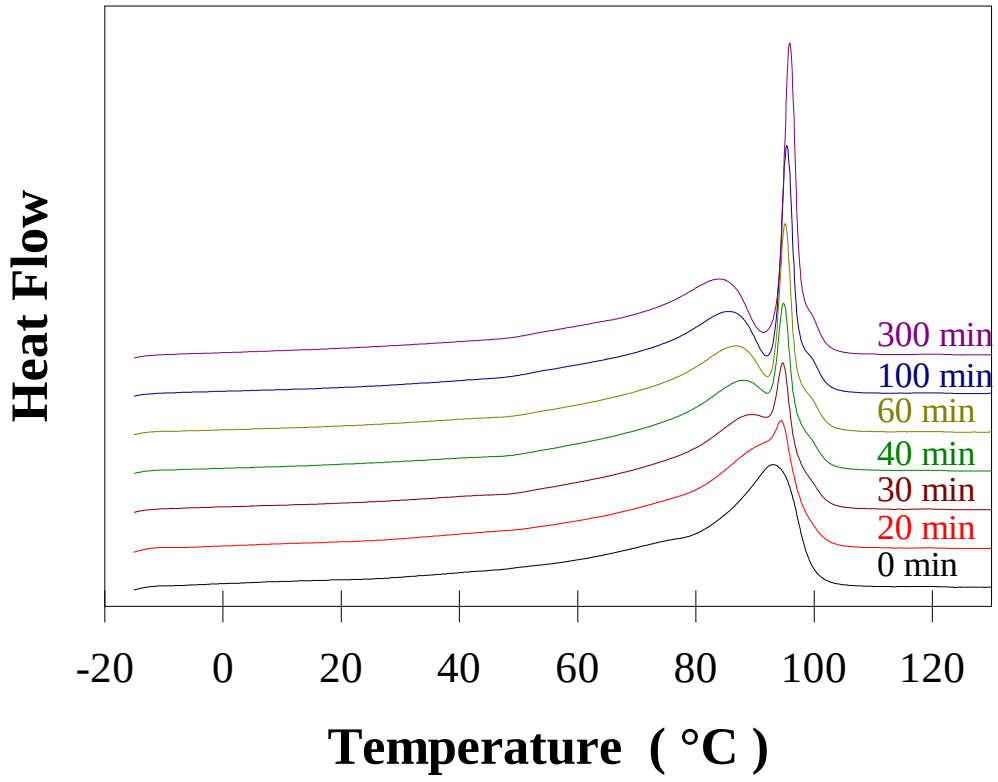

Figure 5.13. Evolution of the melting behavior for ES-5.1 after quenching from 180°C to 90.4°C, crystallization at 90.4°C for various times, and subsequent quenching to –20°C.

crystals formed at T_x = 90.4°C, while the broader endotherm corresponds to the melting formed during cooling subsequent to isothermal crystallization at T_x. Analysis of the higher endotherm was carried out as previously discussed and the results are shown in Figure 5.14. An Avrami exponent n = 1.11 is obtained for the early stage of crystallization. The rate of shift of the low endotherm to higher temperature, $B(T_x)$, is found to be 1.12, which is significantly lower than the value, 3.04 obtained for T_x = 50.7°C. It is very important to note that isothermal crystallization at any temperature $T_x > T_R$ (here T_x = 90.4°C) takes place in an environment initially devoid of any crystallinity (i.e. initially a free melt). In this case, the Avrami exponent corresponds to the initial stage of primary crystallization.

Results obtained from crystallization at other temperatures for ES-5.1 are shown in Figure 5.15, where $B(T_x)$ and n are plotted against the crystallization temperature, T_x. A crossover temperature, T^*, can then be defined as the temperature above which the Avrami

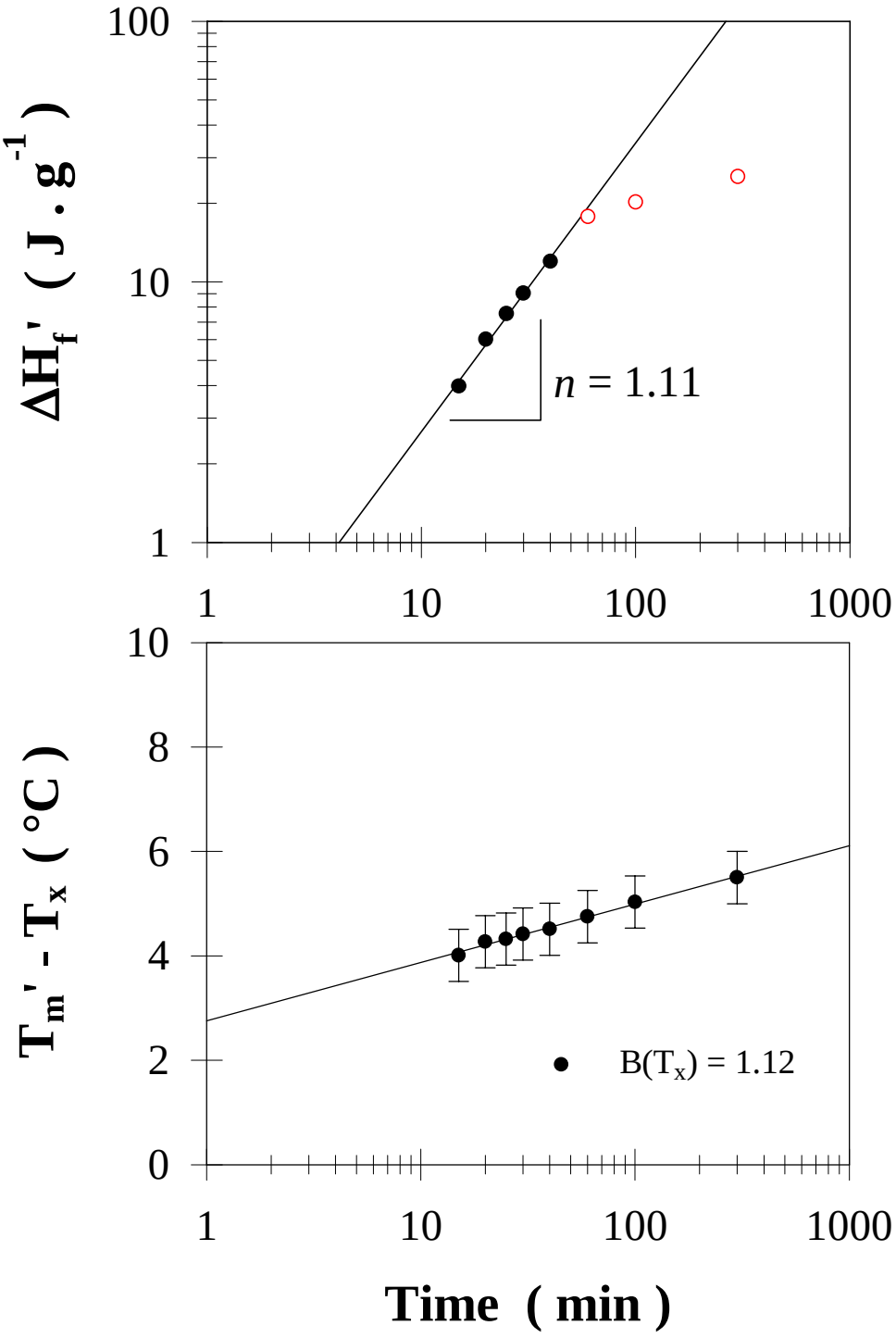

Figure 5.14. Evolution of the low endotherm characteristic For ES-5.1 after crystallization at 90.4°C for different times. (a) heat of fusion, (b) peak melting temperature.

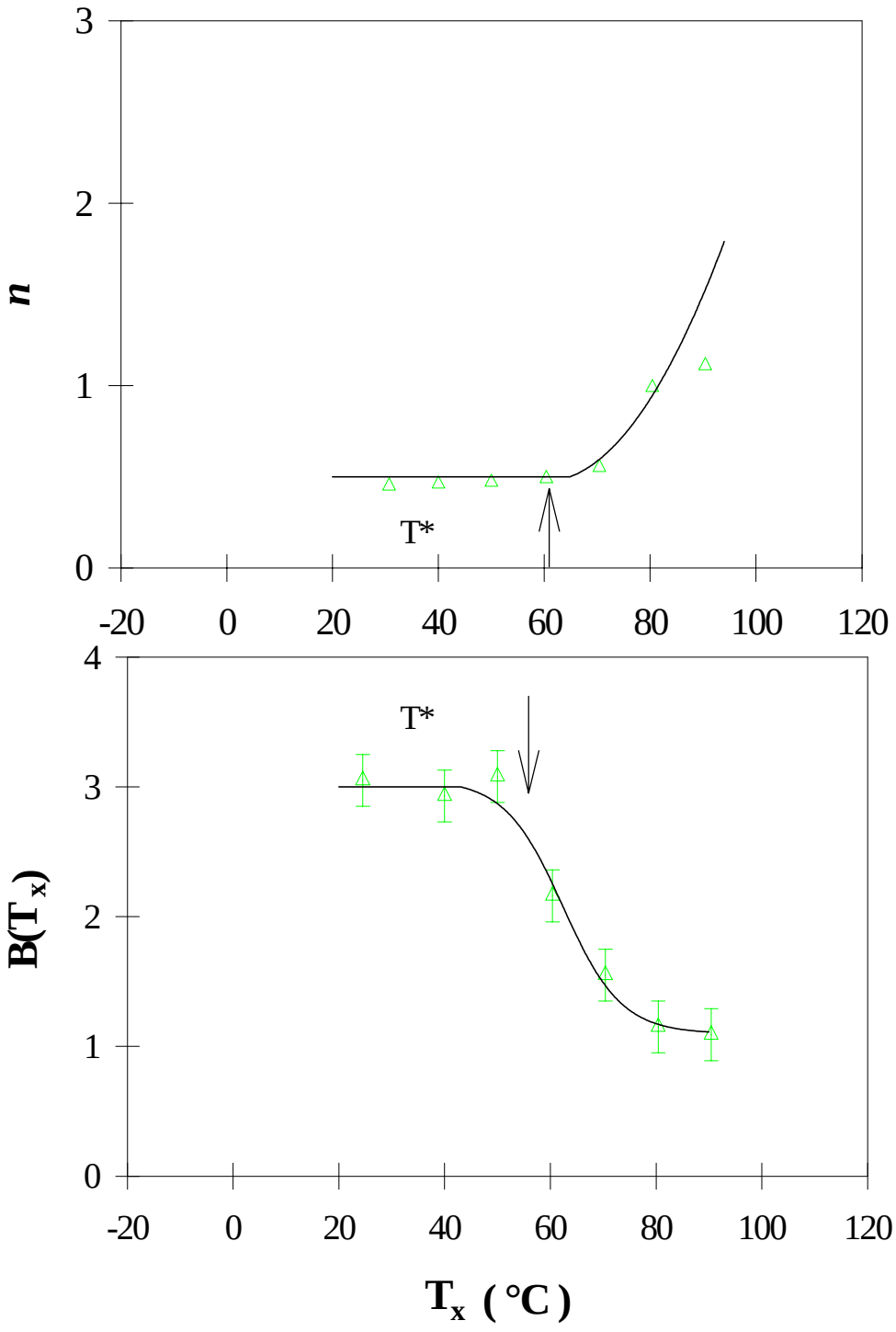

Figure 5.15. Crystallization temperature dependence of the endotherm temporal evolution for ES-5.1. Top is the Avrami exponent and bottom is the shifting rate of the peak melting temperature.

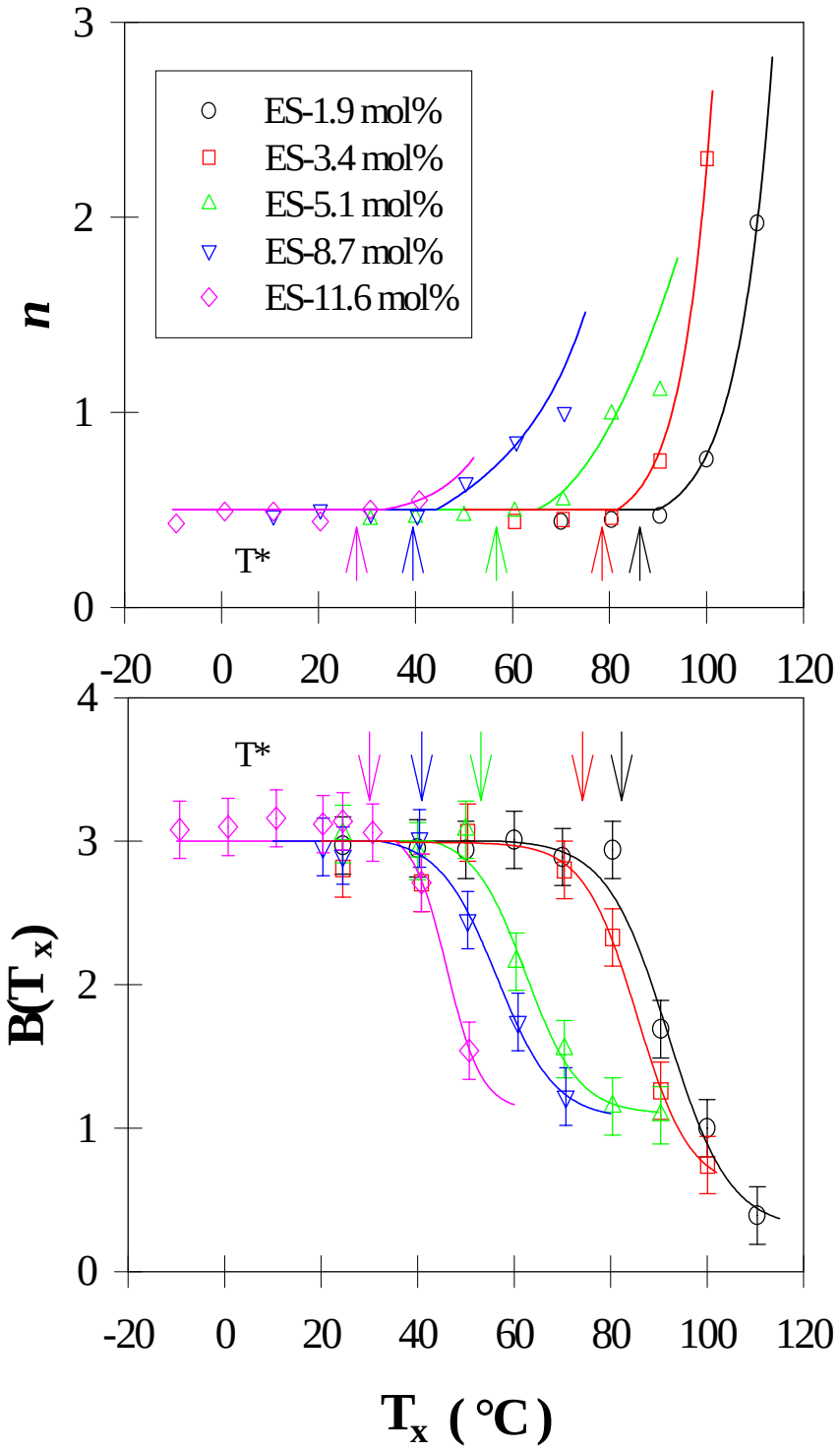

Figure 5.16. Crystallization temperature dependence of the endotherm temporal evolution for ES Copolymers. Top is the Avrami exponent and bottom is the shifting rate of the peak melting temperature.

exponent increases above ½ and $B(T_x)$ decreases below its low temperature plateau value. In the case of ES-5.1, T^* is found to be in the vicinity of 60°C.

Similar experiments were carried out for all other ES copolymers. Plots of n and $B(T_x)$ versus T_x are presented for these materials in Figure 5.16. All $B(T_x)$ values are associated with the late stage of crystallization. In both plots, a temperature T^* is observed for each ES copolymer, below which n and $B(T_x)$ are constant and respectively equal to ½ and 3.0, respectively. Deviation of n above ½ and of $B(T_x)$ below 3.0 are observed above T^*. For each copolymer, the temperatures T^* shown in Figure 5.16 and T_R shown in Figure 5.4 are remarkably similar to the temperature at maximum crystallization rate, $T_{c\ max}$, plotted in Figure 5.2. This indicates that isothermal crystallization at temperatures above T^* is a primary crystallization process, while isothermal crystallization at temperatures below T^* is a secondary crystallization process. Temperatures T^*, T_R and $T_{c\ max}$ decrease with an increase styrene content.

5.3.4. Morphology of ethylene/styrene copolymers

Atomic force micrographs of ES copolymers obtained in tapping mode are shown in Figure 5.17a-d. This series of micrographs indicates that as the styrene content increases, the thickness, the lateral dimensions and the regularity and extent of stacking of lamellar structures decrease. In the case of ES-15.1, only isolated, thin and short lamellar blocks are visible. Therefore, a continuous and significant degradation in the morphological features of lamellar structures occurs as the styrene content increases.

The morphology of ES-3.4 is shown at higher magnification in Figure 5.18. Periodically stacked lamellae, observed edge-on appear to coexist with very small crystalline entities, which are characterized by dimensions not exceeding a few nanometers in any direction. These very small crystals appear uniformly distributed along the lamellar structures but always reside in the direct vicinity of the lamellar surfaces. Similar bundle-like crystals or fringed micellar structures have been recently observed by Alizadeh et al.[8] and Minick et al.[16] in ethylene/1-octene copolymers.

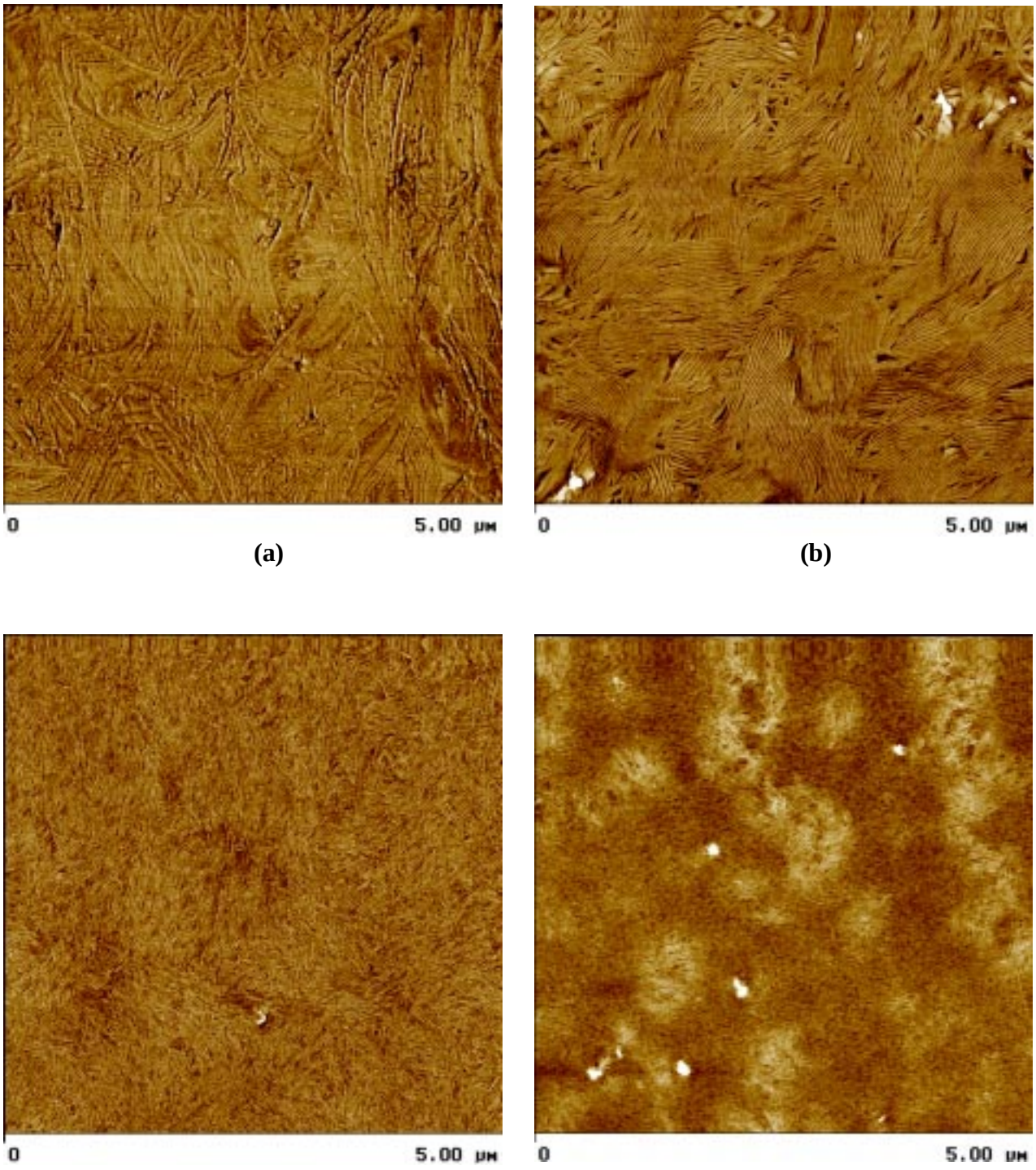

Figure 5.17. Atomic force micrographs in tapping mode (phase image) of (a) ES-0.0, (b) ES-3.4, (c) ES-8.7, and (d) ES-15.1. after crystallization during cooling from the melt at a rate of 1 K/min

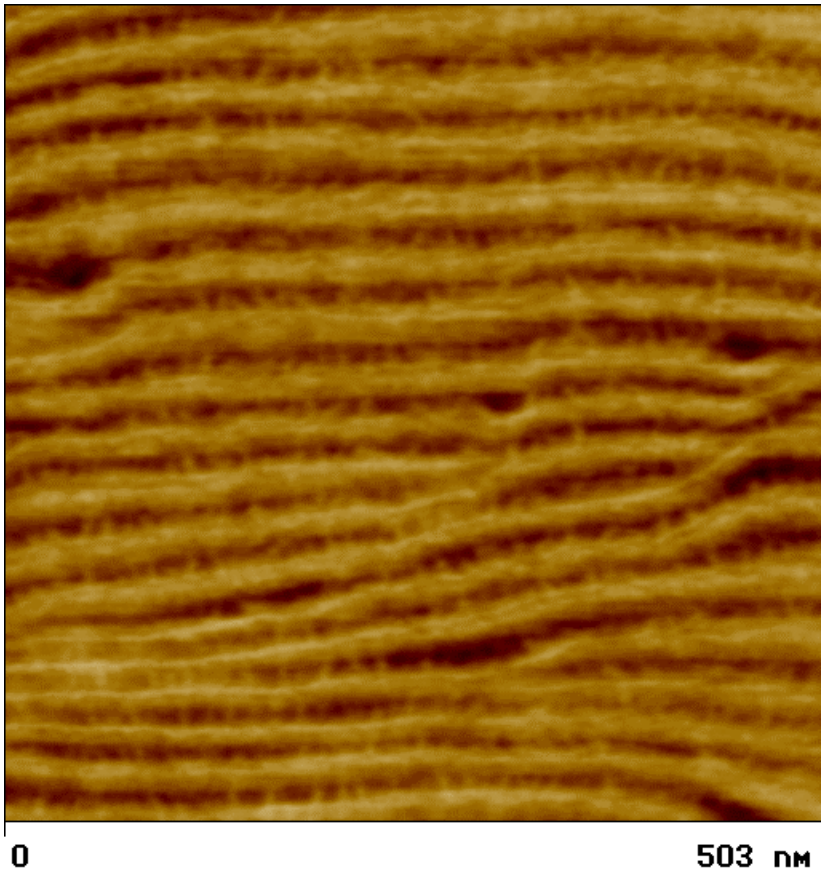

Figure 5.18. Atomic force micrograph in tapping mode of ES-3.4 after crystallization during cooling from the melt at a rate of 1 K/min.

5.4. Discussions

Ethylene/α-olefin copolymers have been under investigations for decades. The properties of ethylene copolymers depend strongly on the crystallizable sequence distribution along the polymer backbone.[1-4,29] Comparative analyses of results from earlier studies were rendered difficult by differences in the crystallizable sequence length distribution. For example, at 4.0 mol% branch content, a Ziegler-Natta based ethylene copolymer[29] exhibits an peak melting temperature of 126°C, ca. 20 K higher than the metallocene based random ethylene copolymers.[30] With the advent of metallocene-based catalysts in the early 1980's, the synthesis of random copolymers has now become possible. Furthermore, materials such as copolymers of ethylene and styrene, which could not be prepared by free radical method

or Ziegler-Natta catalyst,[21,22] can now be synthesized using these new geometry constrained catalysts. These new copolymers exhibit typical plastic properties at low styrene content (high crystallinity), elastomeric behavior at higher styrene content (low crystallinity), and glassy behavior at the highest styrene content (amorphous with T_g above room temperature).[23] It is furthermore of interest to compare the properties of ES copolymers with those of ethylene/α-olefin copolymers because the former copolymers have a phenyl group, quite different in chemical nature from the linear hexyl branch in EO copolymers. In the first part of this section, the morphology, crystallization and melting behavior of the ES copolymers are discussed and compared to those of the EO copolymers. The second part of the discussion section will focus on the secondary crystallization behavior of the ES copolymers.

5.4.1. Morphology, crystallization and melting behavior of the ethylene/styrene copolymers

It is well established that the melting temperature, the crystallinity and the lamellar thickness of random ethylene/α-olefin copolymers are depressed by the presence of short chain branches. It is also well known that these effects are independent of the alkyl branch size if the branch is larger than a methyl group.[3,8] Alizadeh et al. showed that random copolymers of ethylene with 1-butene, 1-pentene, 1-hexene and 1-octene exhibit the same melting temperature and normalized degree of crystallinity at the same comonomer mole fraction. One can conclude that short branches larger than methyl group are excluded from the crystals formed by the ethylene sequences. In a previous publication by this group,[8] properties of EO copolymers were also compared to those of hydrogenated poly(butadiene) (HPB), a model random ethylene copolymer system.[30] The identical decrease in the normalized degree of crystallinity and melting temperature with increasing branch content, imply that hexyl branches are approximately randomly distributed in the EO copolymers. In summary, metallocene-based (single site catalysts) ethylene/α-olefin copolymers can be considered to be random copolymers and branches of size larger than that the methyl group are excluded from the crystals. The properties of the ES copolymers are now compared to those of EO copolymers.

Figure 5.5 and 5.7 indicated that at the same comonomer content, the crystallinity and the melting temperature of ES copolymers are lower than those measured under similar conditions for EO copolymers. This difference appears to become more significant at higher styrene contents. This observation is at first surprising since any departure from a random sequence distribution toward a more blocky distribution should give rise to an increase in both crystallinity and melting point. NMR studies have, however, shown that there are no styrene-styrene dyads in ES copolymers.[31] Indeed, because of steric hindrance effects the addition of a styrene unit at the end of a growing chain is considerably slower than that of an ethylene unit. Therefore each styrene monomer (S) is always followed by an ethylene monomer (E) and ES copolymers should be viewed as random copolymers of ethylene (E) and ethylene-styrene (E-S) units. As a result, the styrene comonomer content should be replaced for all comparisons by the effective (ES) comonomer content. A simple calculation can be carried out to calculate the effective comonomer content (the content of E-S in the copolymer of E and E-S). Starting with an ES copolymer characterized by x moles E and y moles of S, the mole percent of S will be $100y/(x+y)$. If E-S is taken as the apparent comonomer, there are y mole E-S and $(x-y)$ mole E, and the mole percent of E-S is calculated to be $100y/x$. Thus, for ES copolymers, if the styrene content (S) is $100y/(x+y)$, the effective comonomer content (E-S) is $100y/x$, which is larger than $100y/(x+y)$. When the melting temperature of ES copolymers is plotted versus the effective comonomer content (Figure 5.7, open symbols), the same melting point depression is observed for EO and ES copolymers. Similarly, plotting the normalized degree of crystallinity versus the effective comonomer content for ES copolymers (Figure 5.5, open symbols) indicates similar behavior for EO and ES copolymers. Therefore, the ES copolymers can be considered to be random copolymers if the S-E dimer is taken as the comonomer.

Experimental results have shown that the degree of crystallinity and the melting temperature of random ethylene/α-olefin or ES copolymers are independent on the chemical nature of the branches if the branches are larger than the methyl group. This observation is consistent with the exclusion model proposed by Flory.[32] Although Flory's predictions are qualitatively consistent with experimental results, they are not quantitative as the predicted degree of crystallinity is far above the experimental value. The reason for this discrepancy lies in the fact that Flory's theory is based on a model of equilibrium crystallization,[32] while

actual crystallization processes are kinetically controlled. Although experimental results are consistent with the exclusion model, Helfand et al.[33] and Wendling et al.[34] proposed that inclusion of the comonomer in the crystal can not be avoided because it is a kinetically controlled process, namely, some comonomers will be trapped in the crystal. Since the extent of the comonomer inclusion in the crystalline regions is too small to lead to any effect on macroscopic copolymer properties, the exclusion model is considered for guidance in this study of the crystallization behavior of ES.

Random ethylene copolymers are expected to crystallize over a much broader temperature range than homopolymers because of the large distribution of crystallizable sequence lengths. Indeed, the upper temperature at which a crystal is stable is a function of the crystal thickness, which is directly controlled by the crystallizable sequence length. When copolymers are cooled from the melt, crystallization occurs approximately in the order of decreasing ethylene block length. Long ethylene sequences can crystallize into thick chain folded lamellae; thus they crystallize at high temperatures. Intermediate-size ethylene sequences form thinner lamellae at temperatures where the thinner lamellae can stay stable. Shorter ethylene sequences, which are not long enough to form chain folded crystals (the minimum length to fold is ca. 50 carbons), most likely form bundled-chain crystals without chain folding mechanism at low temperatures. Because of their small dimensions, these bundled-chain crystals, or fringed micelles, exhibit low thermal stability and can only exist at low temperatures. In view of the existence of crystals of different sizes it is therefore not surprising to observe a very broad melting range for these copolymers. Current work has demonstrated that the ES copolymers exhibit broader crystallization and melting peaks than linear polyethylene, and the width of the crystallization and melting peaks increases with the increase of the styrene content (Figure 5.1). Similar results have been documented in the literature[2,3,8] for ethylene/α-olefin copolymers, indicating that this is a general property of random ethylene copolymers.

When the styrene content increases, the average ethylene block length decreases dramatically, leading to the decrease in the temperature at maximum crystallization rate, the observed melting temperature, and the dimensions of the crystals formed, as shown in Figures 5.2, 5.7 and 5.17, respectively. The strong cooling rate dependence of the

temperature at maximum crystallization rate for each ES copolymer indicates that primary crystallization is a typical nucleation controlled process. Examination of the plot of normalized crystallinity versus temperature during cooling at various rates leads us to postulate the existence of temperature regions characterized by different crystallization mechanism (Figure 5.4, T_R is used to separate these two regions). In the high temperature region ($T_x > T_R$), where primary crystallization takes place, the evolution of the degree of crystallinity is dependent on the cooling rate. However, in the low temperature region ($T_x < T_R$), the evolution of the degree of crystallinity is independent of cooling rate. As is well known, the formation of lamellar crystals involves the nucleation and subsequent growth, a process very sensitive to cooling rate. Thus, we conclude that lamellar crystals are formed in the high temperature region, where the longest ethylene sequences can undergo chain folding. Using a similar line of reasoning we infer that crystallization in the low temperature region does not result in lamellar formation. Short ethylene sequences, which are not long enough to form folded chain crystals, can still crystallize by a bundling or local aggregation process to form small crystals at lower temperatures.[1] Studies of the evolution of the degree of crystallinity during consecutive cooling/heating cycles has provided supporting evidence for the proposed mechanism. The cooling-heating hysteresis observed in the high temperature region in Figure 5.6, is consistent with the nucleation controlled lamellar crystallization and with the usual difference between melting and crystallization temperatures. On the other hand, a reversible crystallization-melting behavior is shown in the low temperature region, implying that crystals formed in the low temperature region exhibit very low thermal stability (i.e they melt just above their formation temperature). No significant crystallization or melting is observed in the low temperature region in the case of linear polyethylene. This indicates that either the fraction of bundle-chain crystals is very small and cannot be detected or it is altogether absent. Crystallization in the low temperature region of the ES copolymers most likely involves the formation of the bundle-chain or fringed micellar crystals. Fringed micellar crystals show a reversible crystallization-melting behavior due to their small sizes, and exhibit no cooling rate dependence during the cooling process because their formation is instantaneous.

Although a similar crystallization behavior has been reported for EO copolymers,[8] these copolymers develop a higher degree of crystallinity during secondary crystallization than ES

copolymers. This difference in behavior is readily explained if we note that secondary crystallization in ES copolymers always takes place much closer to the glass transition temperature than was the case in EO copolymers. Figure 5.19 shows the glass transition temperatures of the ES and Co copolymers as a function of the comonomer content. Detailed studies of the kinetics of primary and secondary crystallization are presented in the next section to discuss the mechanism of secondary crystallization for ES copolymers.

5.4.2. Secondary crystallization of the ethylene/styrene copolymers

Since the nucleation and growth of secondary crystals cannot be observed in-situ in a time resolved fashion at the present time, a mechanistic description of the secondary crystallization process has to rely on bulk measurements of the evolution of the degree of crystallinity as a function of time and temperature. ES copolymers were isothermally crystallized at different temperatures for various times in a broad temperature range and subsequently cooled to low temperature. Heating of such samples always leads to the observation of multiple melting peaks when the isothermal crystallization takes place at low temperatures ($T_x < T_R$). A melting-recrystallization-remelting mechanism has been proposed to explain this behavior by Minick et al. in the case of the EO copolymers.[16] As is well known, this particular mechanism is a strong function of the heating rate.[35] Thus, a study of the heating rate dependence of the melting trace was carried out and the results were presented in Figure 5.8 for ES-3.4 and ES-11.6. The DSC melting traces corrected for thermal lag effects are independent of heating rate in the range employed (5, 10, 20 K/min), indicating that melting-recrystallization-remelting cannot explain multiple melting behavior in these copolymers. On the other hand, melting-recrystallization-remelting cannot be excluded if a very low heating rate (such as 1 K/min) is used. From a morphological point of view, crystals formed at high undercoolings are usually small and imperfect, and often have the tendency to undergo melting-recrystallization-remelting processes during heating. However, recrystallization is a kinetically controlled process and would be very hindered by the presence of the branches along the polymer backbone. For the heating rate of 10 K/min used to study the melting behavior of isothermally crystallized copolymers, we therefore anticipate that reorganization effects are very minor if at all present.

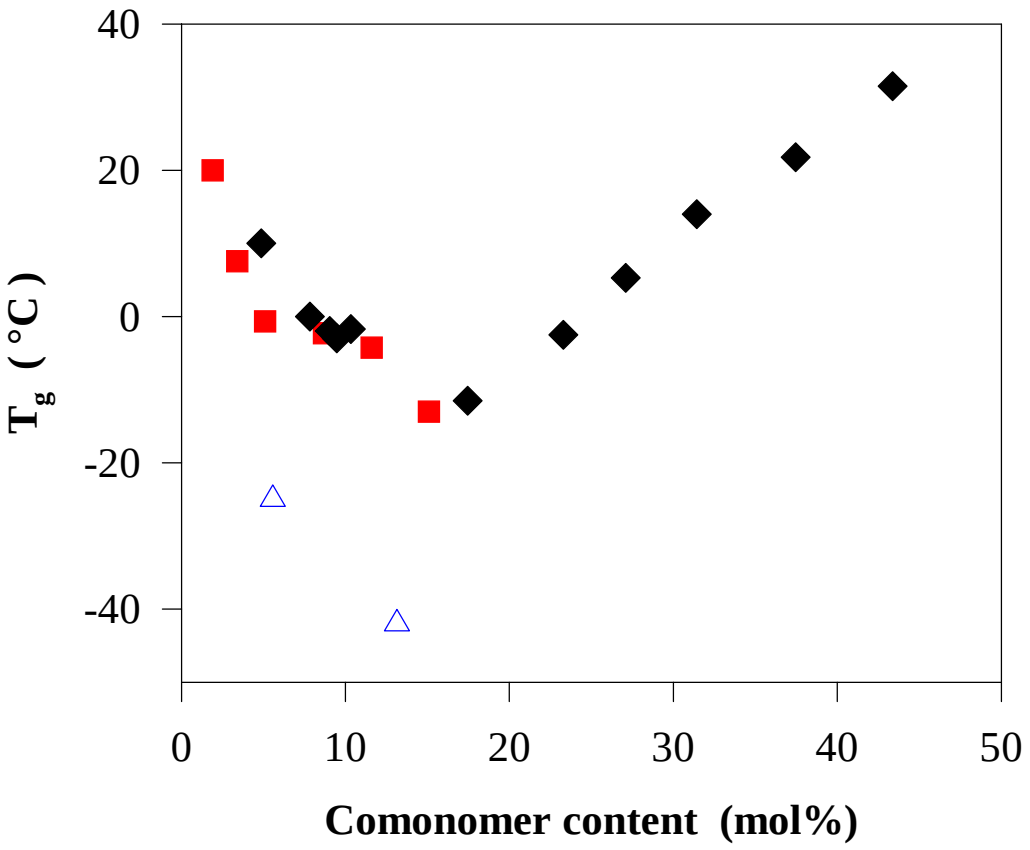

Figure 5.19. Glass transition temperatures of the ES and EO copolymers. Diamond: T_g of ES copolymers from ref. 23 and 24; open triangle: T_g of EO copolymers, data from ref. 24; rectangel: T_g of ES copolymers from this work, data obtained as the intercept of the experimental C_p curve with the calculated C_p baseline (Figure 5.3).

Therefore, it is safe to conclude that the multiple melting behavior of the ES copolymers is due to a bimodal population of crystals with different sizes, thus different stability. The high endotherm is associated with the melting of the lamellar crystals formed during the primary crystallization process.[8,13,14,17] The low endotherm is associated with the melting of secondary crystals formed at T_x ($T_x < T_R$). While Akpalu et al.[17] proposed that secondary crystals are thin lamellae, others describe secondary crystals are fringed-micellar, or bundle-chain crystals.[8,14] Kinetic studies of secondary crystallization will help shed some light on this issue because these two types of crystals exhibit different crystallization behavior.

Figure 5.9 shows the evolution of the melting trace with the crystallization time at 50.7°C for ES-5.1. The high endotherm position does not change with crystallization time, while the low endotherm increases in magnitude and shifts to higher temperatures with an increase in crystallization time. From Figure 5.12a, where the enthalpy of fusion of the low endotherm is plotted versus the crystallization time in a double log scale, a fast and linear increase was observed in the early stage of the crystallization time (ca. 100 minutes) with a slope, 0.5. A decrease in the rate of secondary crystallization is observed during the late stage of secondary crystallization. According to Equation 5.4, the slope value, 0.5, is the Avrami exponent of the isothermal crystallization at 50.7°C for ES-5.1. Such an Avrami exponent is consistent with a one-dimensional diffusion controlled growth. The same Avrami exponent was reported by Shultz and Scott in the study of the secondary crystallization of linear polyethylene at temperatures lower than the primary crystallization temperature.[18]

Figure 5.12b shows the evolution of the low endotherm melting temperature with the logarithm of crystallization time. The rate of shift of the low endotherm increases from 1.97, during the early stage of secondary crystallization to 3.04, in the late stage. It is also noted that the low endotherm melting temperature extrapolates to the crystallization temperature at very short crystallization time, i.e. a few seconds. This result is consistent with the reversible crystallization-melting behavior observed in Figure 5.6 at temperatures $T < T_R$. It is now logical to exclude the possibility that secondary crystals are thin lamellae, since many studies have shown that for lamellar systems the melting temperature at high undercoolings is significantly above the crystallization temperature. This fact derives from the consideration that for a lamella to grow at a finite rate, its thickness must be significantly larger (by an amount δl) than the minimum lamellar thickness[36-38] (for which $T_m = T_x$).

From the above discussion and considering that short crystallizable sequences do crystallize but cannot undergo chain folding, it is proposed that the morphology of secondary crystals formed at 50.7°C for ES-5.1 are of the fringed micellar type. Secondary crystallization in these copolymers always takes place from a topologically constrained melt because residual amorphous sequences are pinned at the crystal/liquid interface after primary crystallization. This pinning leads to a decrease in segmental mobility and is expected to prohibit further chain folding processes. At the early stage of secondary crystallization, it is

relatively easy for crystallizable sequences to diffuse toward one another to form bundle-chain crystals, or fringed micelles. As secondary crystallization proceeds, chain mobility in the amorphous fraction is reduced due to "crosslinking" of the amorphous chains by fringed micelles. This reduction in mobility could then explain the slowing down of secondary crystallization at the late stages. The increase in enthalpy of fusion with crystallization time would then be explained by an increase in the number of fringed micellar crystals formed during the secondary crystallization process.

There is however another possible explanation for the existence of two stages in the secondary crystallization process. The early stage may involve the rapid formation of fringed micellar structures from neighboring crystallizable sequences of the appropriate length and right conformation. The later stage may correspond to a further growth of these fringed micelles in directions perpendicular to the chain axis. An increase in secondary crystal size through further growth along directions perpendicular to the polymer chain axis could also explain the increase in melting temperature. Although one would anticipate such growth to be very limited, based on Gambler's ruin type concepts,[39] growth in a tapered fashion could certainly be envisioned. However, it is not clear how such a growth process can be reconciled with the two step crystallization experiments to be discussed next.

Now let us turn our attention to the origin of the shift of the melting temperature with the logarithm of crystallization time. Two possibilities can be considered: first, one can consider that during secondary crystallization existing crystals can become more perfect or increase in size; second, one can invoke the decrease in entropy of the residual constrained amorphous fraction as a result of secondary crystallization. A specific experiment was designed to investigate the first possibility. Isothermal crystallization of ES-5.1 was performed successively at two different temperatures, 60.7°C and 50.7°C. The residence time at 60.7°C was kept constant, while residence at 50.7°C was varied from 15 to 200 min. The sample was then quenched to -20°C, and the heating scan was recorded immediately at 10 K/min from -20°C to 180°C. The resulting DSC traces, shown in Figure 5.20, exhibit three endotherms. The high endotherm, which results from the melting of primary crystals formed during cooling to 60.7°C, is invariant. The intermediate endotherm associated with the

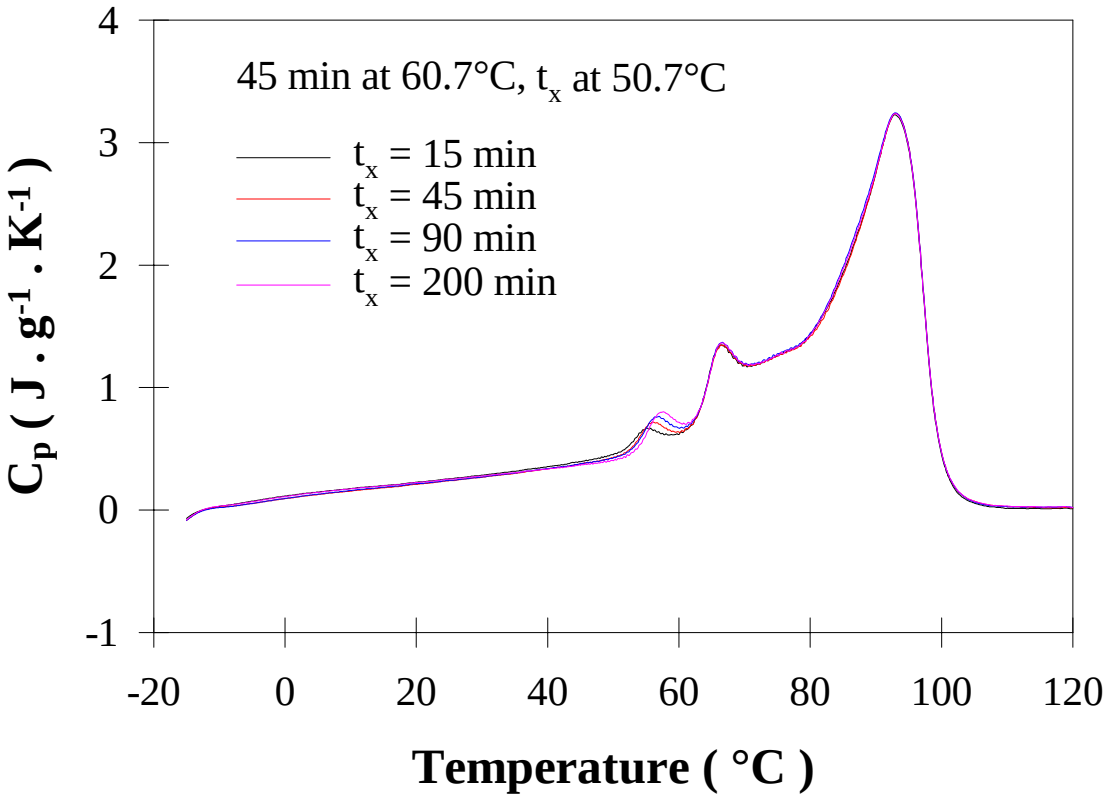

Figure 5.20. Heating traces from -10 to 180 °C at 10 K/min of ES-5.1 after samples were isothermally crystallized at 60.7°C for 45minutes and various times at 50.7°C (shown in plot by t_x).

melting of crystals formed at 60.7°C also remains constant, while the low endotherm associated with the melting of crystals formed at 50.7°C increases in magnitude and shifts to higher temperature with an increase in residence time at 50.7°C. This result suggests that the secondary crystals formed at 60.7°C do not change with residence time at 50.7°C, which is only 10 K below. If perfection or increase in size of all secondary crystals occurred, the intermediate endotherm would have shifted to higher temperatures. A logical conclusion is that the increase in perfection or size of secondary crystals during residence at temperature slightly below their formation temperature is insignificant. From a morphological point of view, it is recalled that the presence of branches at the surface of fringed-micellar crystals may hinder the segmental motion required for an increase in crystal perfection.

Similar shifts of the low endotherm to higher temperature with increasing crystallization time have been reported by Alizadeh et al. in the study of the EO copolymers.[8] The shift in the low endotherm melting temperature with logarithm of crystallization time, however, showed only one slope of magnitude in the vicinity of 3.0. For these materials an Avrami exponent of 0.5, was also shown to be characteristic of the early stage of secondary crystallization below T_R.

The origin of the difference in the evolution of the low endotherm melting temperature with time for EO and ES copolymers may be attributed to a variance in their glass transition temperatures and the relative extent of early and late secondary crystallization stages. At the same comonomer content, T_g for ES copolymers is ca. 40 K above that of EO copolymers (Figure 5.19). The early stage of secondary crystallization in ES copolymers, which exhibit the highest glass transition temperatures, appears to extend to longer crystallization times. While the time, t_d, associated with the completion of the early stage of secondary crystallization is only ca. 15 minutes for all EO copolymers, and it varies with styrene content in the ES copolymers. These characteristic times are given in Table 5.2 for each ES copolymer at various crystallization temperatures below the crossover temperature, T_R. A general trend observed in Table 5.2 indicates that t_d decreases with increasing styrene

Table 5.2. The time, t_d, for the early stage of the secondary crystallization for ES copolymers

ES-1.9	T_x (°C)	80.4		
	t_d (min)	60		
ES-3.4	T_x (°C)	60.4		
	t_d (min)	40		
ES-5.1	T_x (°C)	60.4	50.7	40.7
	t_d (min)	40	60	100
ES-8.7	T_x (°C)	30.8	20.4	10.7
	t_d (min)	20	20	25
ES-11.6	T_x (°C)	10.7	0.7	-9.3
	t_d (min)	15	15	30

content, reflecting the effect of the glass transition temperature on the rate of secondary crystallization in the ES copolymers. For each copolymer, t_d exhibits a significant increase at the highest undercoolings, where crystallization takes place in the direct vicinity of the glass transition temperature. Data for ES-1.9 and ES-3.4 are not available at very low T_x because the low endotherm enthalpy of fusion becomes less than 1 $J.g^{-1}$, which is close to the DSC detection limit.

Hence, for EO copolymers, the rate of shift, $B(T_x)$, of the low endotherm melting temperature with logarithm of crystallization time characterizes the late stage of secondary crystallization. Similar values of $B(T_x)$ (ca. 3.0) are observed for both EO and ES copolymer, during this late stage of secondary crystallization.

Let us now discuss the crystallization behavior of ES-5.1 at temperatures above T_R. When crystallization of this copolymer is carried out at 90.4°C, an Avrami exponent of 1.1, is obtained. The peak melting temperature of the endotherm resulting from crystallization at this temperature also increases linearly with the logarithm of crystallization time but the slope ($B(T_x)$ = 1.12) is now much lower than that for samples crystallized below T_R. Results are shown in Figure 5.14. Primary crystallization of linear polyethylene from a free melt usually yields an Avrami exponent in the vicinity of 3. The deviation of the Avrami exponent from 3 in the case of the ES copolymers is accounted by the fact that spherulitic superstructures are no longer formed. Similar results were obtained for all ES copolymers.

The Avrami exponent, n, and the rate of shift $B(T_x)$ of the endotherm in the late stage are plotted against the crystallization temperature. A transition temperature, T^*, can be assigned to each ES copolymer. When $T_x < T^*$, $B(T_x)$ and n of all the ES copolymers are constant with values of 3.0 ± 0.1 and 0.50 ± 0.05, respectively. The results indicate that secondary crystallization takes place in the temperature range, $T < T^*$. The same n value implies the same growth mechanism of the secondary crystals --- fringed micelles for all ES copolymers at $T < T^*$. When $T > T^*$, $B(T_x)$ starts to decrease and n starts to increase, respectively, above and below their low temperature values, implying a change in crystallization mechanism at

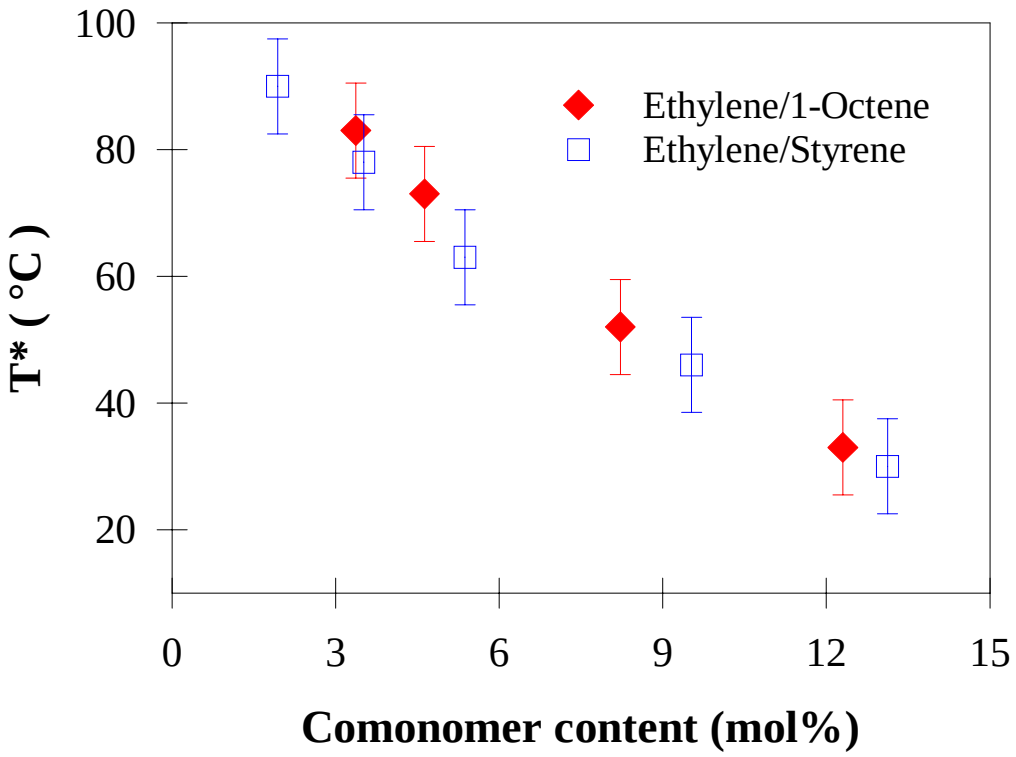

Figure 5.21. Variation of T^* versus the comonomer content for both EO and ES copolymers. The effective branch content was used for ES copolymers.

T^* or T_R (Figure 5.4). Primary crystallization occurs in the temperature range above T^*, and it is a typical nucleation controlled growth as mentioned in the last section. The fact that the T^* is within experimental uncertainty equal to T_R confirms that this crossover temperature separates the temperature ranges where primary and secondary crystallization are dominant. T^* decreases significantly with styrene content. Comparison of the evolution of T^* as a function of comonomer content for both the ES copolymers and the EO copolymers is shown in Figure 5.21, where the effective branch content was used for ES copolymers. The error bar was added to each T^* value to indicate that the transition from primary to the secondary crystallization temperature region is gradual. From Figure 5.21 it is concluded that the decrease in T^* with increasing branch content is identical for EO and ES copolymers.

5.5. Conclusions

Studies of ES copolymers made it possible to extend the structure/property relationship of random ethylene copolymers having linear short chain branches to these having cyclic branches. Considering the ES copolymers to be random copolymers of ethylene and ethylene-styrene, the apparent melting temperature, the crystallinity and the crossover temperature T^* are very similar to those characteristic of random ethylene/α-olefin copolymers for the same comonomer content.

From the crystallization studies of ES copolymers, it is concluded that, during cooling, long ethylene sequences crystallize first leading to lamellar structures in the primary crystallization process, and shorter ethylene sequences crystallize subsequently to form fringe-micelles in the secondary crystallization process. While the primary crystallization takes place from the free, unconstrained melt, secondary crystallization is believed to involve chain sequences pinned at primary crystal surfaces and takes place from a constrained amorphous fraction. Primary crystallization is a typical nucleation-controlled growth, and secondary crystallization can be described by a one-dimensional, diffusion-controlled growth. The small size of the fringed micellar structures is responsible for their reversible crystallization-melting behavior and the cooling rate independence of the degree crystallinity at low temperatures. The shift of the low endotherm to higher temperatures with crystallization time is tentatively explained by a decrease in the conformational entropy of the residual constrained amorphous fraction as a result of secondary crystallization, although the possible role of a slow increase in crystal dimensions during secondary crystallization needs to be further investigated.

The crystallization and melting behaviors of ES copolymers are very similar to those of EO copolymers and a similar crystallization mechanisms was proposed for EO copolymers in a previous publication by Alizadeh et al.[8] Differences between ES and EO copolymers only lie in the different time scales for secondary crystallization and are associated with a difference in their T_g values. A further consequence of the difference in T_g values between these two types of ethylene copolymers is the slightly lower degree of secondary crystallinity observed during cooling of ES copolymers as compared to EO copolymers.

5.6. References

1. Bensason, S.; Minick, J.; Moet, A.; Chum, S.; Hiltner, A.; Baer, E. *J. Polym. Sc., Polym. Phys. Ed.* **1996**, *34*, 1301.
2. Mathot, V. B. F.; Scherrenberg, R. L.; Pijpers, T. F. J. *Polymer* **1998,** 39, 4541.
3. Alamo, R.; Mandelkern, L. *Thermochimica Acta* **1994,** *238*, 155.
4. Voigt-Martin, I.; Alamo, R.; Mandelkern, L. *J. Polym. Sci., Polym. Phys. Ed*. **1986,** *24*, 1283
5. Boyd, R. H. *Polymer* **1985**, *26*, 1123.
6. Statton, W. O. *J. Appl. Phys*. **1961**, *32*, 2332.
7. Strobl, G. "The Physics of Polymers", **1996**, Springer-Verlag Berlin Heidelberg.
8. Alizadeh, A.; Richardson, L.; Xu, J.; McCartney, S.; Marand, H.; Cheung, Y. W., Chum, S. *Macromolecules* 1999, 32, 6221.
9. Marand, H.; Alizadeh, A.; Farmer, R.; Desai, R.; Velikov, V. submitted to *Macromolecules.*
10. Herrmann, K.; Gerngross, O. *Kautschuk* **1932**, *8*, 181.
11. Bryant, W. M. D. *J. Polym. Sc*. **1967**, *2*, 547.
12. Keller, A. *Philos. Mag*. **1957**, *2*, 1171.
13. Chaturvedi, P. N. *J. Mater. Sci. Lett.* **1992**, *11*, 1692.
14. Okui, N.; Kawai, T. *Die Makromolrkulare Chemie* **1972**, *154*, 161.
15. Okui, N.; Kawai, T. *Kobunshi Ronbunshu, Eng. Ed*. **1974**, *3*, 1325
16. Minick, J.; Moet, A.; Hiltner, A.; Baer, E.; Chum, P. M. *J. Appl. Polym. Sci*. **1995**, *58*, 1371.
17. Akpalu, Y.; Kielhorn, B. S.; Stein, R. S.; Russell, T. P.; Van Egmond, J.; Muthukumar, M. *Macromolecules* **1999**, *32*, 765.
18. Shultz, J. M.; Scott, P. D. *J. Polym. Sci. part A-2*, **1969**, *7*, 659.
19. Subramaniam, C.; Alizadeh, A.; Marand, H. manuscript in preparation.
20. Sohn S.; Alizadeh, A.; Marand, H. manuscript in preparation.
21. Aaltonen, P.; Seppala, J.; Matilainen, L. *Macromolecules* **1994**, 27, 3136.
22. Kissin, Y.; Goldfarb, Y.; Krentsel, B.; Uyliem, H. *Eur. Polym. J*. **1972**, *8*, 487.
23. Chen, H.; Guest, M.; Chum, S.; Hiltner, A.; Baer, E. *J. Appl. Polym. Sci*. **1988**, *70*, 109.
24. Chang, A.; Stepanov, E.V.; Guest, M.; Chum, S.; Hiltner, A.; Baer, E. *ANTEC*, **1998**, 1803

25. Fairley, P. *Chemical Week* **1998**, *December 23/30*, 12.
26. ATHAS data bank: http://funnelweb.utcc.utk.edu:/~athas/databank/intro.html.
27. Howard, P. R.; Crist, B. *J. Polym. Sci. Polym. Phys. Ed*. **1989**, *27*, 2269.
28. Androch, R.; Blackwell, J.; Chvalun, S. N.; Wunderlich, B. Macromolecules 1999, 32, 3735.
29. Mirabella, F. M.; Westphal, S. P.; Fernando, P.L.; Ford, E. A.; Williams, J. G. *J. Polym. Sci. Polym. Phys. Ed.* **1988**, *26*, 1995.
30. Crist, B.; Howard, P. R. *Macromolecules*, **1999**, *32*, 3057.
31. Suzuki, H.; Kimura, N.; Nishio, Y. *J. Thermo. Anal*. **1996**, *46*, 1011.
32. Flory, P. J. *Trans. Faraday. Soc*. **1955**, *51*, 848.
33. Helfand, E.; Lauritzen Jr, J. *Macromolecules* **1973**, *6*, 631.
34. Wendling, J.; Suter U. W. *Macromolecules* **1998**, *31*, 2516.
35. Wang, Z. D.; Hsiao, B. S.; Kampert, W. G. Polymer, 1999, 40, 4615.
36. Marand, H.; Xu, J.; Srinivas, S. *Macromolecules* **1998**, *31*, 8219.
37. Xu, J.; Srinivas, S.; Marand, H.; Agarwal, P. *Macromolecules* **1998**, *31*, 8230.
38. Hoffman, J. D.; Miller, R. L. **Polymer** *1997, 38,* 3151.
39. Guttman, C. M.; DiMarzio, E.; Hoffman, J. D. *Polymer* **1981**, *22*, 1466.

Chapter 6. General Conclusions and Future Studies

From Chapter 2 to Chapter 4, the application of the conventional HW linear extrapolation in the determination of the equilibrium melting temperatures for semicrystalline polymers has been critically reviewed. It is found that the linear HW approach always underestimates the equilibrium melting temperature and overestimate the thickening coefficient. A more rigorous, nonlinear analysis was proposed and was successfully applied to isotactic polypropylene and poly(ethylene oxide). As a result, the equilibrium melting temperature of it-PP is determined to be ca. 212°C, about 25K higher than the most frequently quoted T_m value in literature, and the equilibrium melting temperature of PEO is ca. 82 K, which is about 10 K higher than the literature value. The values of the equilibrium melting temperature and the fold surface free energy inferred from the nonlinear HW approach are consistent with those obtained from the analysis of the temperature dependence of the spherulitic growth rates. The predicted temperature dependence of the initial lamellar thickness matches well experimental results reported either in this dissertation (it-PP) or in the literature. The general applicability of the LH secondary nucleation theory was also addressed in the current work. With the exception of the prefactor, G_j^o, the LH theory stands well in both cases of it-PP and PEO. Different crystallization regimes were observed for both it-PP (regime II and III) and PEO (regime I and II). The ratios of the secondary nucleation constants in regime I to II (PEO) and in regime III to II (it-PP) are identical with the predictions from the LH theory, provided that the correct equilibrium melting temperature is adopted in the analysis of the temperature dependence of the spherulitic growth rates. However, calculations of the substrate length from the magnitude of G_j^o yield an unreasonably small value (ca. 10 Å) in the case of PEO, though similar calculations yield a substrate length, ca. 860 Å, for polyethylene. If the possibility that the inconsistent results from a large scatter in the PEO growth rate data or the use of incorrect input parameters in the calculations of L can be excluded, this inconsistency implies that a modification of the LH theory may be necessary. For instances, one may need to treat the deposition of the first stem and subsequent stems on the substrate in different ways, as suggested by Snyder et al..

The continuation of this project will cover the following three topics. First, a detailed and more accurate morphological study will be carried out to further examine the predictions arising from the nonlinear HW analysis. The predictions included (1) the relationship between the initial lamellar thickness and the crystallization temperature in the cases of it-PP and PEO, (2) the extent of lamellar thickening during isothermal crystallization in the case of it-PP is small, This goal can possibly be achieved by following in situ the isothermal crystallization process through microscopy like AFM or spectroscopy like Raman LAM. Second, the nonlinear HW analysis will be further applied to other polymers such as PLLA, s-PP, PS, PEEK, PPS and so on. An adjusted Gibbs-Thomson equation may be necessary to account for the small lateral dimensions of lamellar crystals in the case of semi-flexible polymers. It is also important to ascertain whether there is any recrystallization during the heating scans to find the observed melting temperatures prior to carrying out the nonlinear HW analysis. Third, more careful measurements of the crystal growth rates of PEO fractions as a function of crystallization temperature and molecular weight will be carried out. Regime analysis based on these data will be used to carry out a more rigorous test of the LH theory and probe the assumption in the LH theory that $G \propto n^{-1}$. Meanwhile, efforts will be put to develop a modification of the LH theory, which considers different chain length dependence for the deposition of the first and subsequent stems.

In Chapter 5, the effect of structural and topological constraints on the crystallization and melting behavior of ethylene/styrene copolymers was presented. During the cooling process, the longest ethylene sequences crystallize into chain-folded lamellar crystals (primary crystallization process) at relatively low undercoolings, while the shorter ethylene sequences form fringed micellar crystals without chain folding at relatively high undercoolings (secondary crystallization process). Kinetic studies of isothermal crystallization at various temperatures showed that crystallization into lamellar crystals is a nucleation controlled process, while the formation of fringed micelles is likely to be a diffusion-controlled growth process. The increase in the peak melting temperatures of secondary crystals with the logarithm of crystallization time is tentatively explained by a decrease in the molar conformational entropy of the remaining

amorphous fractions as a result of secondary crystallization. However, an increase in crystal dimension with time, which would lead to the same observation, cannot be rigorously ruled out. Quite similar crystallization behaviors were observed for ethylene/styrene and ethylene/1-octene copolymers, both exhibit very similar apparent melting temperatures and degrees of crystallinity for the same branch content, provided that the effective branch content is used for the ethylene/styrene copolymers. However, ethylene/styrene copolymers crystallize more slowly than the ethylene/1-octent copolymers in the secondary crystallization process because the crystallization temperatures are much closer to the glass transition temperature in the former case than that of the latter.

Vita

Jiannong Xu was born January 5, 1972 in Jiangsu, China. He entered Nanjing University in 1988. He received his bachelor degree of science in chemistry in 1992 and master degree of science studying quantum chemistry in 1995. Afterwards, he joined Dr. Marand's research group in the chemistry department at Virginia Polytechnic Institute and State University in pursuit of a Ph.D.